Development of Novel Oxidation Catalysts for Carbon Isotope Ratio Analysis

Thesis

UNRESTRICTED

Development of Novel Oxidation Catalysts for Carbon Isotope Ratio Analysis

by

Charles William Fomes

B.Sc. (Jt. Hons.) Nottingham 1995

A thesis submitted for the degree of

Doctor of Philosophy

August 2000

Planetary and Space Sciences Research Institute

The Open University

Abstract

The International Rosetta Mission is the name given to the European Space Agency's bold plan to perform in-situ analysis of a comet. One of the instruments on board, MODULUS, is a Gas Chromatograph – Mass Spectrometer that will use the concepts of chromatography and chemical oxidation to return data on chemical composition, and the carbon isotope ratios of the components of the comet. The requirements of the chromatographic columns and oxidation catalysts are severe. The issues of mass, power and stability at launch were concerns for the integration and functionality of the instrument at the comet surface.

The unique nature of the analysis system required that a laboratory analogue of the device to be designed and constructed, so that potential components could be tested using an instrument similar to MODULUS. Once developed, the laboratory system allowed performance testing of four chromatographic columns, as well as observing the effect of space qualification (vibration) testing of those columns. Results allowed recommendations of column choice to be passed to the MODULUS science team.

Traditionally, oxidation units for isotope ratio analysis consist of oxides of nickel and copper, which operate at high temperatures (800-1000°C) and therefore would draw large amounts of power if used on MODULUS. Compounds that potentially are more efficient were examined, created and tested (using the MODULUS laboratory analogue) for the replacement of such compounds. Oxides of rhodium, palladium and copper-chromium were found to preserve sample isotope integrity, oxidise efficiently, and work at far lower temperatures (<500°C) than the traditional materials.

As an application for techniques developed for MODULUS, a new method was created for analysis of $\delta^{13}C$ in terrestrial atmospheric CH_4. The method was tested using headspace samples of air from wetlands in Finland and Scotland. An experiment was devised to observe any $\delta^{13}C$ shift induced by the addition of sulphate to wetland soil and change in incubation temperature. No significant relationships between $\delta^{13}C$ of CH_4 and incubation conditions were found.

Acknowledgements

I would like to thank Geraint Morgan and Colin Pillinger for their supervision, inspiration and encouragement during the project duration. Thanks go to Simeon Barber and Anna Butterworth for reading early drafts of the thesis, and for pointing me in the right direction. I also appreciate the thorough examination by my examiners Ian Wright and Fred Goesmann. Acknowledgements go to PPARC for the funding for the project.

A number of people provided essential help for the completion of the project. Paul Wynn for the endless patience and help for metal oxide preparation (and Fred Vetel for letting me use his stuff). Frank Berry and Eleanor Crabbe for advice on what to make. Vincent Gauci provided the opportunity to do something completely new and exploratory. Justin Hargreaves for digging out all that useful background I missed. Sarah Bury and the rest of the Isogeochem people for getting me up (or down) to speed on our lab equipment. Thanks also go to those members of the PSRI who made the lab systems that little bit smoother - Andrew Morse, Jon Maynard, Ian Franchi, Mike Mucklow and Martin Miller were always at hand.

Cheers go to all the people from various courses over the years – PPARC's EE 2000, CRAC, LCIC, PSS, Alpbach, S102, and T271. Thanks go to all those who made life better in MK and for moral support. All the lunchtime crew - Barry, Liz, Sven, Jon, and Bob. All the people in PSRI and the Earthies from over the years, including Simon, Lee, Giles, Rob, Tubbs, Phil B, Phil H, Richard, Claire, Chris, Cheryl, Caroline, Victoria, Alan, and the guys at the Vicarage to count a few. Thanks to all those passing through 12th Street for making at a great place to live – Gav, Q, Rob, Vince, Bruce, Lee, not forgetting Tim and Kaz. I must also mention to the PGSS, both the organisers, and the followers without whom our Cellar Bar evenings would be drab (Hi Shara, Paul, Pete, Richard O, and the rest). And I must mention Anglia News.

Finally, thanks go to Nicola for putting up with me throughout, and for always pushing me to get to the finishing line.

Chapter 1

Chapter 2

Chapter 3

Chapter 4

Chapter 5

Chapter 6

Chapter 1

Chapter 2

Chapter 3

Chapter 4

Chapter 5

Chapter 6

1. INTRODUCTION

Among the many missions currently planned to visit comets, the most ambitious one is undoubtedly the Rosetta mission, to be launched in 2003. The most intensive analysis of a comet ever to be performed will include a unit separating from the main spacecraft, which will land on the comet surface. One experiment on board the lander is MODULUS, a gas chromatograph-mass spectrometer, specifically developed to identify and measure the concentration and the isotope ratios of light elements present in volatile cometary material. The mass spectrometer type is a quadrupole ion trap, a system not originally designed to measure isotope ratios of elements. To succeed on Rosetta, the device must be re-designed and tailored to the specific application.

This thesis addresses issues of the evaluation of chemical reactors and GC columns in the development stage of the MODULUS system. To perform evaluation of such components, standard laboratory instruments were required to emulate the MODULUS concept. The laboratory testing techniques created for MODULUS were also appropriate for an analysis system for isotopic analysis of terrestrial atmospheric CH_4.

1.1. Comets

Comets are celestial bodies that have inspired awe on their observable visits to the inner Solar System. On nearing the Sun, cometary matter can outgas, leaving a trail of material along the comet's path of travel. The relevance of comets in Solar System history is paramount; they are thought to be remnants from the early Solar System; material left over from the formation of the planets. Their ultimate origin, composition, nature and evolution are still debated; data collected from comets via telescopes and in-situ measurements have not given definite answers of the questions relating to formation of comets.

Comets are small irregular-shaped bodies with masses up to 10^{14} kg (Boice and Huebner, 1997), compared to planets (mass of Earth = 6×10^{24} kg) . Cometary orbits are highly elliptical, most with aphelia near Jupiter's orbit, and perihelia nearer to Earth's. Some orbits have aphelia beyond Neptune, giving comets long orbital periods, from hundreds to millions of years.

Comets comprise a solid nucleus (of the order of 1-10 km), and evolved material called the coma (of the order of 10^6 km), which is the only part of a comet observable from Earth. The nucleus of the comet persists after many orbits. The nuclear material is thought to be a conglomerate of frozen volatiles, grains of silicates and carbonaceous particles containing hydrocarbons (Whipple, 1950; Huebner, 1990). Water appears to be the major volatile species detected from spectral measurements, with CO and CO_2 being the next most abundant species. Measurements from one comet suggest both the density and albedo of the nucleus are low (Keller et al., 1987). Of the hydrocarbons, the specific heavy organic compounds have yet to be identified without inference or interpretation (Kissel and Krueger, 1987). Isotope ratios of various elements (including carbon) have also been measured remotely and in-situ (Vanysek, 1991), but the accuracy of the data is low compared to sample analysis.

Most comets are thought to exist in the Oort cloud, in an isotropic formation of up to 10^{13} comets lying at mean distances of the order of 50000 - 150000 AU from the Sun (Oort, 1950), rarely coming inwards to be observed. Gravitational perturbations from nearby stars can

influence the motion of these comets, sometimes propelling them towards the inner Solar System. No direct observations of these bodies can be made (not enough light is reflected), and the number of comets at this large distance was estimated from statistical analysis of detected comets' orbits by J. Oort. The hypothesis of the potential existence of an undiscovered planet was recently put forward from examination of the non-random distribution of aphelia of some long period comets (Murray, 1999). The suggestion was made that the potential planet's perturbations can influence comets within the Oort cloud to the inner Solar System.

Cometary orbital periods vary, and are defined as short- or long-period, with an arbitrary cut-off of 200 years. Long period comets spend most of their orbital period outside the orbit of Neptune. Short period comets are likely to have once been long-period comets which were subsequently drawn into shorter orbits through gravitational perturbation by Jupiter (and to a lesser extent Saturn). Comets lose more and more of their volatile components on each orbit of the sun, concentrating the total amount of refractory components. It has been postulated that some asteroids are the remnants of comets that have lost all their volatiles (Binzel et al., 1992). A coma of material emitted forms around the nucleus, and also a tail of material pointing away from the Sun formed by solar radiation pressure.

Scientists are interested in studying comets because they represent leftover material from the creation of the Solar System. The cometary composition is believed to be similar to the material present either in the parent interstellar cloud, or in the primordial solar nebula. The state of the material is thought to be the nearest match to the early Solar System. However, cometary matter will have been altered in the time since formation by thermal and/or stellar or solar radiative effects. Obviously, the surface of a comet's nucleus will have had more radiation exposure than material deeper within the comet. Therefore, chemical and morphological differences may be evident from samples in different parts of the nucleus.

Comets may also have been a provider of volatiles for the early Earth; the primitive hot Earth may have lost a significant proportion of any volatiles to space after formation, and may have

needed an additional supply to account for present conditions. It has been postulated that multiple impacts (or the matter from the tails) may have provided Earth with water and organic carbon-/nitrogen-containing compounds to Earth (Oro, 1961); mantle outgassing is the only other likely source of volatiles. It has even been suggested that comets may have harboured life, and may have seeded the early Earth (Hoyle and Wickramasinghe, 1986).

Knowledge of the composition of comets would help to answer the many questions regarding the origin of the Solar System. Analysis of a comet's nucleus would probably provide the greatest insight into their nature. There have been a number of missions launched to study comets, but encounters have been brief. Ambitious though it may seem, the Rosetta spacecraft intends to do more than any other previous cometary mission, and bring standard laboratory practices toward the nucleus.

1.1.1. Comet Missions: past and present

Of all the comets that have graced the skies, the most significant for humankind is Halley's comet. Its appearance approximately every 75 years has entitled it as the comet associated with people's history, appearing before the battle of Hastings, and also proving Edmond Halley's prediction of its appearance in 1758 (Sagan and Druyan, 1997).

Although three comets have been visited by spacecraft[1], Halley's comet is the most closely studied, as in 1986 it was visited by five explorers. All of the spacecraft (VEGA-1, VEGA-2, Sakigake, Susei and Giotto) were successful, and Giotto achieved closest approach to the nucleus (Newburn et al., 1991). The combined scientific results from the missions provided the first in-depth look at the nature of comets. The science return was great, although as is usual with missions such as these, more questions were raised than answers provided. However, all the missions were flybys, and therefore their encounters were brief.

[1] Comet Giacobini-Zinner was visited by NASA's International Cometary Explorer in 1985. Comet Grigg Skjellerup was visited by ESA's Giotto in 1989 (after the Halley encounter).

Giotto's camera observed the detail of the nucleus form, which was the first (visual) proof of a solid nucleus (Keller et al., 1987). It was found to be irregularly shaped, dark, cratered, and only a small proportion of the nucleus appeared to be active in material emission. Other detectors measured dust flux. Mass spectra revealed silicate particles (with Fe and Mg present), with high concentrations of organic material comprised of carbon, hydrogen, nitrogen and oxygen (designated as CHON[2] particles in the literature (Keller, 1990)). Some silicate samples contained no CHON particles. Other sensors measured aspects of the plasma and the coma.

Analyses of volatiles by mass spectrometry (MS) were performed by the Giotto and VEGA probes, although limited mass resolution resulted in ambiguity in the returned data. Giotto's Neutral Mass Spectrometer (NMS) was not able to determine the difference between ionic species of the same mass. Any of the species N_2, CO, or C_2H_4 could yield a response at a mass-to-charge ratio of 28 atomic mass units. This confusion is termed isobaric interference, and other similar identification problems were identified concerning the nature of the ionisation process in the NMS instrument (Huebner, 1990). The organic component was measured by a time-of-flight mass spectrometer (PUMA) on board Vega 1 (Kissel and Krueger, 1987). Molecular ion identification was confusing as the molecular fragmentation patterns were unknown. From interpretation and inference, the species detected include unsaturated and saturated hydrocarbons, aromatic hydrocarbons and nitrogen substituted cyclic compounds, but few oxygen-containing compounds were detected. Spectroscopy of the coma and nucleus also suffered limitations in identification of species. Low signal to noise ratios or inadequate spectral resolution generally caused imprecise identification of compounds.

Other cometary missions are presently under investigation or in flight. Stardust, a NASA mission launched in February 1999, will intercept (flyby of 150 km closest approach) comet Wild 2, in 2003. Onboard are collectors that will retain material from the comet's coma. The spacecraft will return the collectors to Earth for analysis by 2006. NASA's Deep Space 1, a

[2] A glossary and list of acronyms is included at the end of this thesis

mission primarily launched to test new technologies, has also been scheduled to flyby two comets, Wilson-Harrington and Borrelly, and gather information on the nucleus and coma of both bodies. Contour (Comet Nucleus Tour – launch date July 2002) is a NASA mission that over 5 years aims to encounter the three comets Encke, Schwassmann-Wachmann-3 and d'Arrest. Contour will take images and spectral data, and analyse the composition of cometary dust coming from each comet. The most unusual spacecraft planned for a comet approach is Deep Impact (NASA) which will attempt to launch a 500 kg impactor into the comet Tempel 1, while the main spacecraft observes the effects. The impactor will send close up images of the comet as it approaches the surface. Launch is timetabled for 1st January 2004 with the impact occurring on 4th July 2005. The ejecta produced after the impact will contain the pristine interior material from the comet, which may be observed via remote sensing. The crater created by the impact will also be studied.

The target for Contour, comet Encke, was the comet of study that drove Fred Whipple to put forward the 'icy conglomerate' model for comet nuclei (Whipple, 1950). He proposed that the nucleus "consists of a matrix of meteoric material with little structural strength, mixed with frozen gases – a true conglomerate... As the model comet nucleus approaches perihelion, the solar radiation will vaporise the ices near the surface. Meteoric material below some limiting threshold will blow away because of the low gravitational attraction of the nucleus, and will begin the formation of a meteor stream. Some of the largest particles may be removed by shocks, but the largest particles or matrix will remain on the surface, to produce an insulating layer. After a short time the loss of gas will be reduced materially by the insulation so provided". Whipple's model has since been extensively applied to other comets, not just Encke.

1.2. Rosetta

The European Space Agency's planned Rosetta mission will build on the successes of Giotto. The major limitation of all the spacecraft encounters with comet Halley, was that material was only detected from the coma, no measurements were made on the chemistry or morphology of

the nucleus, apart from spectroscopic data. Rosetta intends to land a science package on the nucleus, which should accurately determine its properties.

Following the success of Giotto, the European Space Agency examined the prospect of a cometary mission, and hence the Rosetta mission plan was created, and finally approved in 1993. Its prime objectives are to study the origin of comets, how they are related to interstellar matter, and to assess the implications of comets with regard to the formation of the Solar System. The study will be conducted on the nucleus and coma of comet 46P/Wirtanen, for a period of up to two years (Verdant and Schwehm, 1998). During the mission, a lander will be deployed to the surface of the comet, carrying instruments for in-situ analysis of the nucleus. This will be the first ever cometary landing, and will carry some risk (Kuhrt et al., 1997). The science goals of the mission include:

- Chemical, mineralogical and isotopic analysis of volatiles and refractories in the nucleus and coma. Interpretation will determine the relation between the volatiles and refractory materials.
- Observation of the onset of cometary activity (nucleus surface, inner coma) on approach to perihelion.
- Characterisation of the dynamics, morphology, and composition of the entire nucleus.

The Rosetta spacecraft will also flyby two asteroids (Ottawara, Siwa) before its encounter with Wirtanen. Remote sensing instruments will be used to study the respective asteroids during the flybys.

1.2.1. Comet Wirtanen (46P/Wirtanen)

The cometary target for Rosetta was discovered by Carl Wirtanen on the night of 15th January 1948 at Lick Observatory and was found to be a short period comet. Since its discovery two close approaches to Jupiter have changed the orbit of the comet so that its perihelion has changed from 1.63 to 1.03 AU, corresponding to a period of 5.46 years. Other parameters estimated from observations and models are collated in Table 1.1.

Table 1.1 Parameters estimated for comet 46P/Wirtanen. Source of data – Rosetta Nucleus Modelling Group meeting, September 1998

Parameter	Minimum	Typical	Maximum
Onset of activity	3.5 to 3.3 AU – brightness increasing strongly at 1.8 to 1.6 AU		
Mean diameter (m)	500	800	1500
Rotation period (hr)	3.5	7	days
Axes ratio a:b	1.09	1.74	2.6
Volume (m^3)	5.2×10^8	2.1×10^9	$1.4\ 10^{10}$
Surface area (m^2)	3.1×10^6	6×10^6	2.8×10^7
Nucleus bulk density (kg/m^3)	200	500	2000
Mass (kg)	1×10^{11}	1.1×10^{12}	2.8×10^{13}
Surface temperature (cover layer) (K)	≈150 (aphelion)	≤ 230 (3AU)	≤ 210 (perihelion)
albedo	0.02	0.04	0.14
acceleration due to gravity (m/s^2)	2.7×10^{-5}	1.1×10^{-4}	8.3×10^{-4}
Detected gaseous species	OH, CS, CN, C_3, C_2, H		
Flux (H_2O) (mol./s)	$(1 - 3) \times 10^{28}$ at 1.1 AU		

1.2.2. Rosetta operation

The Rosetta spacecraft is due to be launched on 21st January 2003 from Kourou, French Guyana, on board an Ariane 5 launch vehicle. Its mission plan is to reach comet Wirtanen by 2011, via a single martian gravity assist, and two Earth assists. On the way it will flyby two asteroids, notionally Ottawara and Siwa. On reaching the comet, the spacecraft will match its orbit to that of Wirtanen, over a period of one year, reducing the relative drift rate to 25 m/s. Near-nucleus operations start at the distance of 3.25 AU from the Sun, where the spacecraft will enter an orbit around the comet (at a typical distance of 60 comet radii), reducing the relative velocity to a few cm/s. Global mapping of the comet will then start, and after 30 days the surface science unit (the Rosetta lander) will be deployed. The orbiter will act as relay for the lander-Earth telecommunication transmissions. The mission has been timetabled to end at perihelion passage, on 10 July 2013.

1.2.3. MODULUS

One experiment onboard the lander will analyse the composition of the cometary material, and isotope ratios. It is known as MODULUS – Methods of determining and understanding light-

elements from unequivocal stable isotope compositions. MODULUS was originally planned to comprise two nearly identical instruments; Berenice (on the orbiter), and Ptolemy (on the lander). Unfortunately, Berenice was eventually cancelled because of resource and scheduling issues. The goals of MODULUS are to "establish the identity, abundance, and the isotopic compositions of major, minor, and trace constituents of the cometary nucleus and to employ these data to learn more about the processes responsible for the cometary phenomenon" (Wright and Pillinger, 1998).

The concept of MODULUS is based upon evolved gas analysis. Ptolemy will be given solid samples of the comet nucleus surface or sub-surface, and analyse the content by mass spectrometry. The instrument's detector is a gas chromatograph – isotope ratio – mass spectrometer (GCirMS). Samples are handled using a small vacuum system, and solid material will enter an oven (not part of Ptolemy) that can be step-heated to produce appropriate amounts of volatiles. The gas chromatograph will separate the volatile species generated from one and another. The mass spectrometer will then analyse these species as they elute from the columns. The cometary sample will be processed chemically within MODULUS, so the mass spectrometer will receive the sample material, in different processed forms. This method allows analysis of elemental isotope ratios within the sample; for example carbon isotopes can be measured once carbon-containing cometary material is converted to gaseous carbon dioxide.

Some of the isotope ratios of interest are $^{13}C/^{12}C$, $^{17}O/^{16}O$, $^{18}O/^{16}O$, $^{15}N/^{14}N$, and $^{2}H/^{1}H$. Isotope ratios are used to examine chemical changes that can occur within materials undergoing any physical process. These isotopes can be measured in a terrestrial laboratory from any samples containing these elements by using mass spectrometry. Using isotope ratio mass spectrometry (Chapter 4), minute (< 0.01%) variations in the ratios can be detected, and can be attributed to different processes. For instance, the $^{2}H/^{1}H$ ratio in terrestrial rainfall will vary according to condensation temperature, latitude and altitude (Dansgaard, 1964). Unfortunately, analysis systems common to laboratories cannot be readily transferred to space missions.

Commercial isotope ratio-mass spectrometers are heavy (>50 kg), use large amounts of power (in the order of kilowatts), and are large (>1 m^3). Automated sample preparation systems are often of the same scale. Although present systems need little operator control, maintenance requirements are high. Any space-bound analyser needs to be small, autonomous, efficient and return useful scientific data.

The MODULUS mass spectrometer/analyser is being developed by the Planetary and Space Sciences Research Institute (PSSRI) at the Open University, UK, in collaboration with the Space Science Department at Rutherford Appleton Laboratories, UK. Obviously it would be impossible to launch the same type of mass spectrometer as used in terrestrial laboratories, as the mass and size is comparable to the entirety of the Rosetta lander. Similar results must be obtained by different techniques. The primary difference is the development of a low-power, low-mass mass spectrometer known as an ion trap, and other components.

The precision in isotope ratio measurement of the ion trap is less than a standard laboratory instrument. However, by the use of novel mass spectrometer detection methods, the precision of the instrument can be improved so that a reasonable science return is achieved. A diagram of the current MODULUS system is shown in Figure 1.1. The full MODULUS operation is beyond the scope of this thesis, but a summary can be described as follows: samples from the comet are taken to a vacuum system, where they will be subjected to preparative chemistry (can be oxidation, fluorination or drying) and possibly gradual heating. The treated samples will then be transferred to one of four analytical channels, and finally the detector system. The specific treatments of the samples are the same as those used in terrestrial laboratories – e.g. for multi-oxygen isotope ratios, molecules must be converted to O_2 (Pillinger, 1997).

1.2.4. Payload

As previously stated, one cannot simply transfer an existing commercial instrument to a planetary explorer; the design must be adapted to survive the environmental constraints imposed by the spacecraft. As spacecraft operations will start at a great distance from the Sun,

solar cells will produce limited power (850W at 3.4 AU, 353W at 5.2 AU (Verdant and Schwehm, 1998)). All instruments must therefore maximise their power efficiency. Instruments must also have a limit on size and mass. Ptolemy has a mass limit of 4.5 kg, to contain everything from gas tanks and pressure regulators, to control electronics. Instruments must also be placed appropriately on the spacecraft in relation to other instruments. Interfering RF signals or excessive temperature should not be detectable by any neighbouring packages. All instruments must be structurally secure and be able to survive the rigours of launch.

All these limitations make the design, assembly and integration a complex task. This study addresses certain issues that may help MODULUS comply with these specifications.

It is imperative that the whole system is tested against possible damage during the launch of Rosetta. One particular problem is that part of the instrument relies on fragile components – Gas Chromatography (GC) columns. These are capillary tubes (<0.5 mm o.d.) that although flexible, can break under stress. Although they have been flown before (e.g. Cassini (Sternberg et al., 1999)) the choice of columns put forward for MODULUS includes a column known to be susceptible to vibration damage. If one of these columns were to break, or lose its capabilities on launch, many science goals of MODULUS would never be achieved.

Thankfully, the potential for assessing vibration damage is possible before launch. Part of this project includes using a vibration testing procedure that simulates an Ariane 5 launch, and assessing any damage caused to the fragile GC columns.

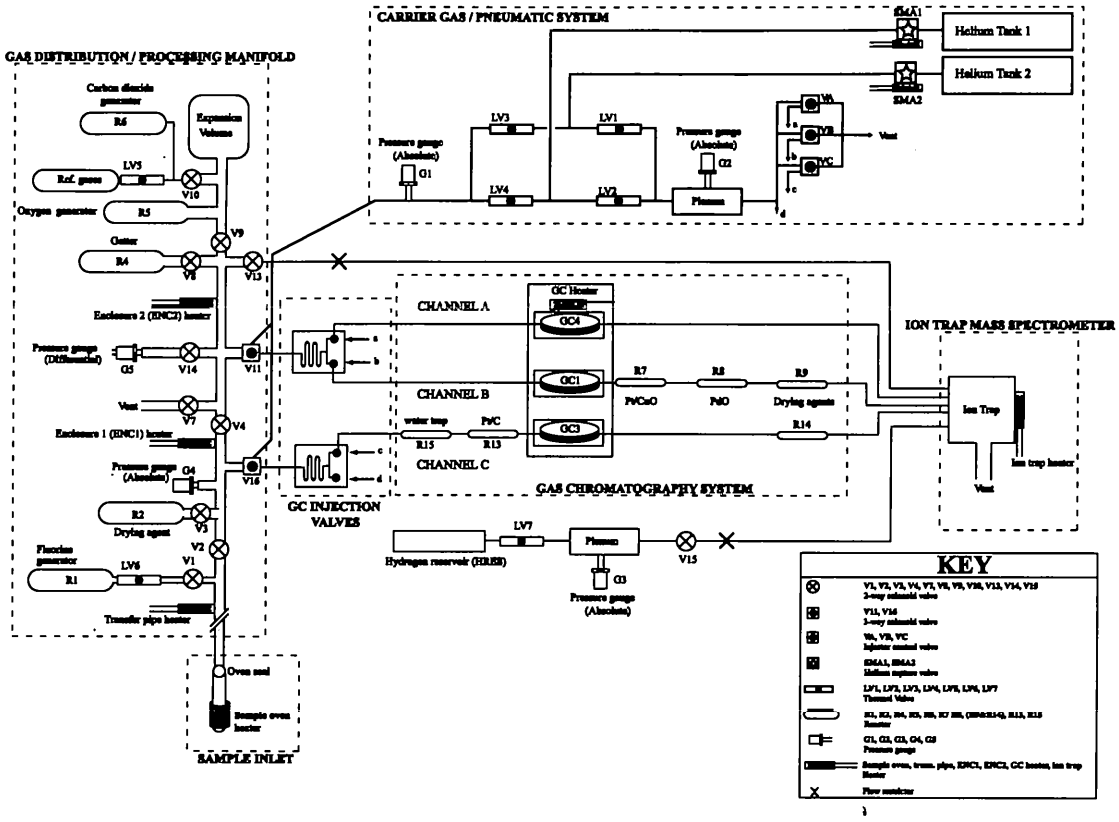

Figure 1.1 Configuration diagram of Ptolemy, showing vacuum sample manifold, GC combustion section and ion trap detector

The imposition of limited power constrains the amount and type of preparative chemistry that can be performed on the samples prior to analysis. The preparation samples for isotope analysis requires flow through vessels that heat milligrams of sample to a few hundred degrees. In the case of carbon isotopes, one procedure has a reaction vessel at 1100°C. Heating such a tube requires a relatively large amount of power (>4 W). To preserve energy and increase the lifetime of the instrument, investigations must be performed to ascertain whether the same reactions can occur at lower temperatures. The current planned number of samples that Ptolemy will analyse if between 20 and 50.

Increased instrumental lifetime will allow a greater number of samples to be processed. More data will allow Ptolemy to give higher precision isotope ratios of the material that constitute the comet. With greater precision, MODULUS' data can be applied to Solar System formation models, which potentially can ascertain the origin of comets.

To give the increased instrument capability that is desired, the chemical reactors must be made energy efficient. Instead of reactions occurring at 1150°C, novel catalytic materials may perform the same function at a considerably lower temperature. This thesis will explain the examination of materials that will provide this increased instrument lifetime, without sacrificing the science goals.

1.3. Isotopes

Different isotopes of an element have subtle differences in their chemistry. These differences make examination of isotopes useful environmental and chemical indicators. The isotopes have different atomic masses, causing variation in the energies of inter- and intra- atomic and molecular interactions. The origin of these interactions will be discussed

All of the chemical elements in the Periodic Table have more than one different form, or isotope, each with a different atomic mass. Atoms are comprised of atomic nuclei and electrons. The atomic nucleus contains protons (positively charged species) and neutrons (neutral species). The number of protons in a single nucleus defines what element the atom is. A similar number of neutrons to protons are required to provide energy balance within the atom[3]. However, some atoms of an element have the same number of protons, yet different numbers of neutrons (e.g. carbon - ^{12}C – has 6 neutrons, ^{13}C – has 7, ^{14}C – has 8). The addition of a neutron increases the atomic mass by one unit. Species with the same number of protons but differing numbers of neutrons are therefore defined as different *isotopes* of the same element. Some isotopes have unstable nuclei, and must decay by emitting energy and matter to achieve stability. In contrast to these *radioactive* nuclei (e.g. ^{14}C), others are *stable* and do not decay. Some radioactive isotopes decay at such a slow rate they are *effectively* stable (e.g. ^{144}Nd; $T_{1/2} = 2.1 \times 10^{15}$ years).

[3] The number of neutrons in an atom is in general greater than the protons, especially for heavier elements. Only the lightest elements have stable nuclei with equal numbers of protons & neutrons.

Different isotopes of an element have different natural abundances. The approximate terrestrial abundances of the isotopes of carbon, oxygen and hydrogen are shown in Table 2.3. The relative abundances are not fixed – small differences are found in nature, hence the ratio between the most abundant isotope and minor ones can vary. This is the effect of a process called isotopic fractionation, and it occurs because the physical properties of isotopes of an element are subtly different. Under physical processes such as evaporation, condensation or crystallisation, the reaction rate will be different for each isotope as a result of quantum mechanical effects. The mass difference between the isotopes has a small effect on the bond strengths between molecules. In general, bonds formed by lighter isotopes are weaker than bonds formed by their heavier counterparts (e.g. ^{13}C-X may be stronger ^{12}C-X). This implies that lighter isotopes will usually react more readily than heavier ones. If one considers evaporation, the molecules with lighter isotopes would enter the vapour phase faster than those with heavier isotopes, leading to enrichment of the lighter isotopes in the vapour phase. [In condensation, the lighter isotopes will show more resistance to forming intermolecular bonds, and hence stay in the vapour phase for longer.] Enrichment or depletion of one isotope compared to another during a physical or chemical process of two phases (or substances) is termed isotopic fractionation.

Chemical reactions act similarly to physical processes with respect to fractionation, but some reactions have rates sensitive to the atomic mass of the species involved; it is not *always* true that lighter molecules react quicker. At any point in a reaction (or some physical processes), the relative abundance of isotopes between reactant and product in a reaction can be described by the fractionation factor, α

$$\alpha_{A-B} = \frac{R_A}{R_B} \qquad (1.1)$$

where A and B are chemical compounds undergoing a reaction, and R (e.g. $^{13}R = {}^{13}C/{}^{12}C$) is the isotopic ratio of any two isotopes present in the compounds. The fractionation factor may

change during the course of a reaction until equilibrium is reached. Conservation of mass is applied, thus when a reaction completes the cumulative product has the same R as the substrate. Examination of the isotope ratio and its variation within a process can be related to the detailed mechanism of that process. For instance, in biological systems, different photosynthetic pathways lead to different degrees of fractionation of the isotope ratios of carbon (Hoefs, 1987).

1.3.1. Isotope ratios in comets

It is believed that comets contain the least processed material in the Solar System. However, many known comets have short periods that have had numerous orbits to process the material they contain. A more appropriate target for examination of pristine matter would be long period comets, but their orbits are prohibitive for feasible spacecraft interception as this would take many tens of years.

Measurement of isotope ratios can, and indeed have been performed by spectroscopic analysis of sunlight reflected by comets. Molecules with different isotopic compositions have slightly different properties caused by the mass difference. Any vibrational (or rotational) transition will have different energy due to the small difference in mass. The small mass difference results in a different wavelength for the same spectral feature in the molecule with a different isotopic composition (energy of a photon is proportional to its frequency). As the amplitude of the spectral feature is dependent on the source strength, the intensity ratio of a peak from say, ^{32}S and ^{34}S, would be equal to the ratio of the isotopes in the parent molecule. High resolution spectroscopy (in terrestrial laboratories) can sometimes even match the precision of isotope-ratio mass spectrometry (see Chapter 6).

Cometary spectra have been collected at various wavelengths from a few comets, including the Giotto flyby of comet Halley. From these spectra some isotope ratios have been published. In comparison with mass spectrometry, isotope ratios derived by spectroscopy are normally accompanied by relatively large errors of up to ± 30%. It should be noted that difficulty can exist in extracting isotope ratios from spectra, due to spectral interference or uncertainty in the

continuum measurement needed for calibration. A compendium of spectral results of carbon isotope ratios is shown in Figure 1.2.

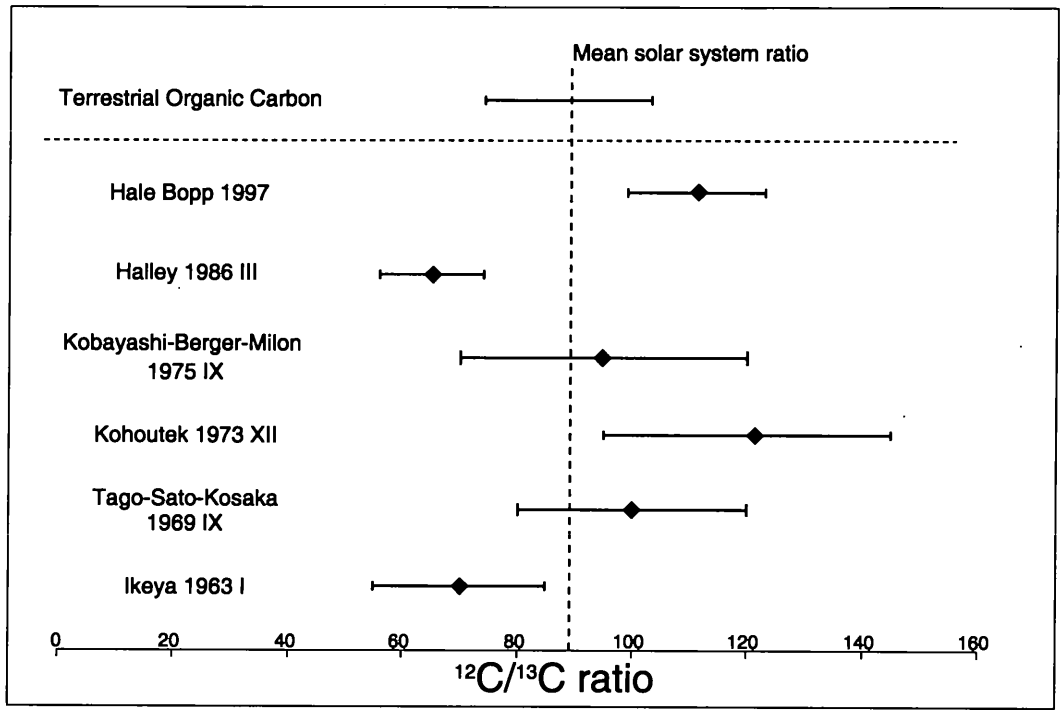

Figure 1.2 Carbon isotope ratio (and uncertainty) in cometary materials measured by spectroscopy of HCN or C_2 swan features (after (Vanysek, 1991)). The value for terrestrial organic carbon spans the range of isotope ratios found in natural materials

The data in Figure 1.2 for the Halley encounter were from remote sensing measurements of CN resulting in a carbon isotope ($^{12}C/^{13}C$) ratio of 65 ± 9, dissimilar from the terrestrial value of 89. Arguments have been proposed for a potential interstellar origin of comets based on the similarity between the comets and a diffuse interstellar medium value of $^{12}C/^{13}C = 43 \pm 4$ (Vanysek, 1991). Other arguments based on the similarity of UV spectra in many comets may suggest a common origin for all.

The Giotto payload also contained three magnetic mass spectrometers; the Neutral Mass Spectrometer (NMS), and the Ion Mass Spectrometer with two sensors. The data collected from mass spectrometry measurements from Giotto show inaccuracies even though they were collected in situ. Water was found to be the most abundant component, measuring 80% by number of molecules (see Table 1.2). Interpretation of NMS data has not been straightforward

due to isobaric interference, especially for carbon isotope ratio determination due to interference between ^{13}C and ^{12}CH at the same mass to charge ratio (Altwegg et al., 1999). Mass spectra have been interpreted to be near $^{12}C/^{13}C = 90$ from reliable data, which is consistent with the Solar System ratio. $^{18}O/^{16}O$ were measured from cometary water and was found to be close to the terrestrial value (1.8×10^{-3}). $^{2}H/^{1}H$ ratio has been determined to be $(3.08 \pm 0.3) \times 10^{-4}$ from measurements of the hydronium ion. This value shows the comet is twice as enriched in deuterium compared to sea water on Earth (1.5×10^{-4}) and also by a factor of 15 relative to the protosolar cloud (2.0×10^{-5}). The origin of the enrichment has been proposed to be due to chemical reactions at low temperatures (such as in interstellar molecular clouds).

Table 1.2 The concentration of various species detected by the NMS instrument on Giotto, normalised against the strength of the water signal (after (Altwegg et al., 1999))

Species	Source strength	Species	Source strength
H_2O	100%	CH_4	≤0.8%
CO	17%	CH_3OH	1.5%
H_2CO	3.8%	CH_2	0.27%
CO_2	3.5%	H_2S	0.15%
NH_3	1.5%	HCN	0.1%

Isotope ratios measured by spectroscopy will invariably give inconclusive results. The most useful bands for measuring the $^{12}C/^{13}C$ ratio are the absorption features of the CN bands and the C_2 swan band. These of course can only give detail about the parent molecule, not the entire carbon inventory. It is likely that the isotopic composition of the volatiles will be different to that of the refractory and CHON components, as their evolutionary history is likely to be different. The cometary dust can be regarded as material that pre-dates the entire solar nebula. The composition of dust should be preserved since growing in the interstellar medium, as only minor variations during grain temperature are expected in comet formation (Vanysek, 1991). In comparison, volatile components in comets are probably subject to processing and rearrangement.

1.3.2. Cometary unknowns

There are many open questions in cometary science. The origin of comets is not definite. Is their chemistry based on interstellar molecules? What were their formation and thermal evolution temperatures? The present theories of cometary growth cannot explain the low densities found. Which heavy organics are present, and what is their origin? Are comets the source of the terrestrial water?

It is likely that Rosetta will be unable to answer all the questions with certainty. It will however give insight on all the processes that can be feasibly studied.

1.3.3. Isotope ratios in atmospheric science

Among the many fields that isotope ratios can contribute to is the study of Earth's atmospheric system. As well as their concentration, isotope ratios in oxygen, nitrogen, carbon monoxide, ozone and almost all other species can be measured with isotope ratio mass spectrometers. Air samples are collected at source, and brought to the laboratory for analysis. The data of mixing ratio (concentration) and isotope ratio of species can be combined, and used in global circulation models to understand any possible climate change due to those species.

One trace compound linked to potential climate change is atmospheric methane (see Chapter 6). Numerous methods of isotope analysis exist for this compound, all with different sample size requirement, complexity, precision, and analysis time. All the current methods use GC columns to separate the atmospheric O_2 and N_2 from the CH_4 leading to long analysis time. If the dependence on chromatographic columns is removed, then sample analysis time is decreased, allowing more air samples to be analysed per day.

Using techniques developed for the MODULUS architecture, this thesis includes details on attempts to create a new, faster method for the analysis of atmospheric CH_4. As the science return from Rosetta would be beyond the timescale of this project, this application allowed true science to be tested on a related field.

1.4. Project outline

The prerequisite for testing of the catalytic reagents for MODULUS was that a laboratory analogue of MODULUS be constructed. A gas transfer manifold was assembled and connected to commercial GC and Ion Trap mass spectrometer systems, detailed in Chapter 2. Both of these units were vital for the work in subsequent chapters. Chapter 3 details the method for characterising the separation ability of the GC columns, and the effect of simulating an Ariane 5 launch on the columns. Any change in the properties of the columns after vibration testing was observed. One of the columns tested was subsequently used in the GC for the analysis of combustion ability of the reagents necessary for CO_2 conversion. This thesis is primarily concerned with carbon isotope measurement only, not oxygen or hydrogen. The techniques, results and recommended catalysts are specified in Chapter 4. As with the GC column testing, the laboratory analogue of MODULUS was used for evaluation of the compounds.

Once viable reagents had been assessed, further investigation required a commercial isotope ratio mass spectrometer. The reagents' ability to produce consistent carbon isotope ratio measurements of combusted CO and CH_4 were tested, and this forms the bulk of Chapter 5.

The inlet system of the isotope ratio mass spectrometer was adapted to allow gaseous sample analysis. An appropriate application for the instrument was carbon isotope ratio analysis of atmospheric methane. Traditional methods of methane analysis can take up to 1 hour for sample preparation and analysis. A new method developed to be appropriate for MODULUS, allowed the analysis time to drop to below 15 minutes and is detailed in Chapter 6. Development of the inlet system resulted in the ability to run air sample sizes on a scale of 300 ml, containing > 20 nmol of CH_4. Collaboration with Mr Vincent Gauci (Earth Sciences, Open University) allowed measurements of carbon isotope ratio from CH_4 emitted by methanogens of a soil sample in a closed system. The effect of variation in the isotope ratio with addition of sulphate to the soil was examined, exploring the relationship between the competing sulphate-reducing bacteria and methanogenic bacteria.

2. DEVELOPMENT OF GAS TRANSFER SYSTEMS TO ENABLE COMBUSTION TESTING ON SMALL SCALE CATALYSTS

2.1. Introduction

Commercial mass spectrometers are utilised for identification of compounds, but the methods of transferring samples to them can be non-trivial. This chapter details the design and assembly of a vacuum system to provide two mass spectrometers with the gaseous samples in a form suitable for analysis. To place the context of the assembly of the system, one must examine the development of the isotope ratio mass spectrometer and associated technologies.

In this chapter, the development background of the combined Gas Chromatograph-isotope ratio-Mass Spectrometer will be discussed. The principles of magnetic sector and ion trap mass spectrometry are detailed. Both mass spectrometer types were used during this project, and their calibration, sample handling, and operation procedures will be discussed.

2.2. The historical development of GCirMS and the associated sample introduction systems

2.2.1. Methods of isotope analysis for carbon compounds

There are numerous methods for isotopic analysis of samples containing carbon, most of which involve chemical pre-treatment. For example, solid materials often require the non-carbon content to be removed by wet chemistry methods. Some materials, especially biogenic ones, may contain enough carbon to combust to CO_2 directly, with little preparation needed except drying. The determination of the isotope ratios is usually undertaken by an isotope ratio mass spectrometer, which could be one of many flavours. Currently the most precise commercial system is a dual inlet system, but the simpler to use continuous-flow mass spectrometer gives accuracy and precision very close to dual inlet systems as well as consuming less sample (Brenna

et al., 1997). Other techniques include static-vacuum mass spectrometry (which needs much less sample) (Wright et al., 1983) and tunable-diode laser spectroscopy (Bergamaschi et al., 1994) (which needs considerably more). The ion trap mass spectrometer has yet to be used routinely for isotopic analysis. The type of mass spectrometer chosen determines the requirements of the analytical preparation system.

2.2.2. Traditional combustion reagents for carbon isotope analysis

Before the introduction of continuous flow isotope ratio mass spectrometry (CF-irMS), sample preparation had to be undertaken off-line (i.e. on a separate system to the mass spectrometer). Vacuum systems made from glass could be made to trap samples in quartz tubes, which could be then isolated and sealed by glassblowing torches. These sealed quartz tubes would then be attached to the vacuum system of the mass spectrometer inlet, and then cracked open, expanding the sample gas into the inlet system. Off-line combustion of organic matter is easily undertaken, by adding O_2 into a vacuum system and heating the relevant portion of the vacuum line with a tube furnace.

In many laboratories, including PSRI, copper (II) oxide (CuO) powder is placed in a part of the vacuum system separate to the sample; on heating, the oxide is partially reduced to Cu_2O liberating O_2 gas. On cooling, the reverse reaction can occur giving the effect of an O_2 pump. Copper oxide has been used as such for decades and is the most popular oxygen source used in sample combustion, as can be seen later in this chapter (Attendorn and Bowen, 1997). It does however, come with many problems: impurities (even when 99.9% pure) causing isotopic interference; some irreversibility with the cupric oxide reacting with O_2; high carbon content (disrupting carbon isotope measurement); and the high temperature of O_2 release (800°C). The nature of the compound actually accelerates the combustion of gaseous organics on the surface of the powder, hence acting as a catalyst as well as an O_2 source (PSRI internal study). CO_2 and H_2O produced in this way are then removed from the oxidiser cryogenically. The efficiency of the amount and physical form of CuO or other oxygen donor (Vandeputte et al., 1996), and the

effect of an additional catalyst e.g. Pt metal (PSRI internal study) have been studied. Other studies have concentrated on identifying the best oxidant for organic combustion, not for isotope research but for elemental analysis (Ma and Gutterson, 1976).

Different approaches of sample preparation are employed, depending on the final detector type. With the introduction of GCs coupled to Continuous-flow irMS (GC-irMS), most sample types do not need to be combusted off line. Adding a GC column in front of a mass spectrometer has been a fixture of organic analysis for many years. The fragmentation pattern detected in the spectrometer could be tied up to the chromatographic retention to give absolute identification of large molecules. For carbon isotope studies the breakthrough came when the effluent from the GC column could be combusted to CO_2 which would then enter the ion source of the MS at a time dictated by the chromatography (Matthews and Hayes, 1978). The irMS would then scan at m/z 44, 45 and 46 integrated over time, while an algorithm would apply the necessary corrections to give $\delta^{13}C$ and possibly $\delta^{18}O$ of each organic component in the original sample (see definition of $\delta^{13}C$ in 2.2.4). This combustion section was first applied to dual inlet mass spectrometers (Brenna et al., 1997) and later applied to continuous flow MS systems.

2.2.3. Dual Inlet Mass Spectrometers

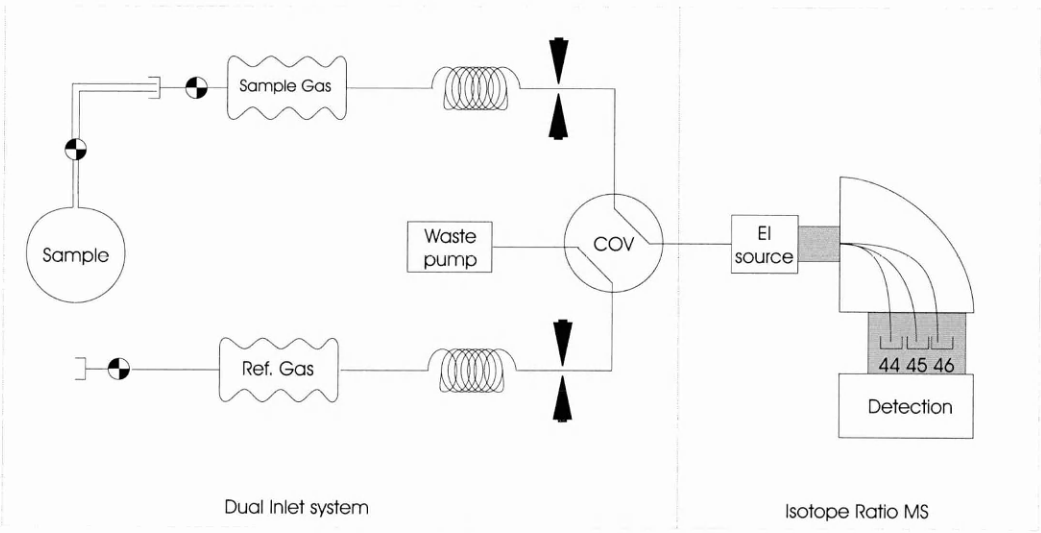

Figure 2.1 Schematic diagram of a dual inlet mass spectrometer inlet system with change over valve (COV) in sample analysis position. Detectors are set up to analyse CO_2. The reference gas (labelled Ref, in this case CO_2) is stored in a variable volume. The ionisation of gas is via electron impact (EI)

The high precision of a dual inlet mass spectrometer system is due to the rapid switching of a change-over valve between the reference gas flow and the sample gas flow. Both sample and reference gases must be expanded into variable volumes, both of which then have a continuous viscous flow through a capillary leak. Both of these flows must be matched, since the measured isotope ratio incurs a subtle, but detectable dependence on relative pressures in the ion source. The capillary dimensions are chosen so that no isotope fractionation occurs during the course of a measurement. The smallest sample size measurable is dictated by the viscous flow limitation. At lower pressures and so lower flow rates, molecular flow occurs and time-of-flight fractionation is seen. The waste pump is carefully set so that the flow into it matches the flow of the same gas to the electron impact ion source. There is no carrier gas in this system; pressures at the ion source are controlled by the capillary dimensions from the variable volume reservoirs, the design of the ion source, the vacuum pump of the mass spectrometer, and of course the pressure in the gas reservoir.

During a measurement, reference gas is bled into the source, while sample gas is bled into the waste pump. After an analysis time of up to 60 seconds the change-over valve is switched, sending the sample gas into the ion source, and the reference gas to the waste pump. Both the reference and sample gas both flow at a constant rate, as starting and stopping each flow results in fractionation. The valve is switched, and this cycle is repeated 6 to 10 times (Brenna et al., 1997). The mean of the results then give very precise isotope ratios, usually σ (standard deviation) of $\delta^{13}C$ is <0.1‰ for CO_2 analysis (see definition of $\delta^{13}C$ in section 2.2.4).

2.2.4. Isotope value nomenclature and calculation

The direct measurement of the carbon isotope ratio by mass spectrometry of carbon itself is rarely performed. In almost all laboratories undertaking carbon analysis, mass spectrometers are arranged to accept carbon dioxide gas, and measure the ratios of ion beams of mass-to-charge ratios 44, 45, and 46 a.m.u.. These ion beams are related to the carbon (and oxygen) isotope ratio of the CO_2 gas, and hence to the original sample.

The actual ratio of ^{13}C to ^{12}C is rarely reported. In the early development of such mass spectrometers, the variability performance made measuring the absolute isotope ratio difficult. In response, a new method of reporting isotope ratios was put forward by Urey (1948), and has been adopted by the isotope community. In the new scale, only the enrichment or depletion of the minor isotope compared to a reference substance is given. This variance is expressed as the term delta, generally measured in parts per thousand (per mil).

The general equation for any stable isotope system is given in the Equation (2.1). The reference material available for the mass spectrometer must be calibrated to an international standard reference. The term R is the abundance ratio of the minor to major isotope in any species, i.e. $R = {}^{A+n}X/{}^{A}X$. where X is the element, A the atomic number, and n the difference in atomic number between the minor and major isotopes.

$$\delta\,(‰) = \frac{R_{sam} - R_{ref}}{R_{ref}} \times 1000‰ \qquad (2.1)$$

In the case of CO_2, measurement of carbon isotope ratios are usually compared to the carbonate standard, Pee Dee Bellemnite (PDB). In Equation (2.1), the R value of carbon (^{13}R) is equal to the ratio of ^{13}C to ^{12}C (hence $^{13}R = {}^{13}C/{}^{12}C$), the natural abundance ratio of which is approximately 0.0112 (Mook, 1973).

$$\delta^{13}C = \frac{{}^{13}R_{sam} - {}^{13}R_{ref}}{{}^{13}R_{ref}} \times 1000‰ \qquad (2.2)$$

A subscript is usually added to the isotope label denoting to which standard the sample is measured against. For example, for the PDB standard, a carbon isotope ratio may be expressed as $\delta^{13}C_{PDB}$. The three stable isotopes of oxygen and two of carbon lead to a variety of possible molecular masses for a CO_2 molecule, as can be summarised in Table 2.1.

Table 2.1 Molecular masses of CO_2 comprising of all combinations of stable isotopes of carbon and oxygen

Atomic weight units of CO_2 species (a.m.u.)	Species
44	$^{12}C^{16}O^{16}O$
45	$^{13}C^{16}O^{16}O$, $^{12}C^{16}O^{17}O$, $^{12}C^{17}O^{16}O$
46	$^{13}C^{17}O^{16}O$, $^{13}C^{16}O^{17}O$, $^{12}C^{18}O^{16}O$, $^{12}C^{16}O^{18}O$, $^{12}C^{17}O^{17}O$
47	$^{13}C^{17}O^{17}O$, $^{13}C^{18}O^{16}O$, $^{13}C^{16}O^{18}O$, $^{12}C^{17}O^{18}O$, $^{12}C^{18}O^{17}O$,
48	$^{13}C^{17}O^{18}O$, $^{13}C^{18}O^{17}O$, $^{12}C^{18}O^{18}O$
49	$^{13}C^{18}O^{18}O$

Mass spectrometry measurement and correction

To discover the relative amounts of ^{13}C, ^{17}O and ^{18}O, it is not necessary to detect all the species that can possibly form from these isotopes. By detection of the ion beams at m/z 44, 45 and 46, one can derive simultaneous equations that (through assumptions) can be solved to give ^{13}C and ^{18}O abundance ratios, and ^{17}O by inference. Assumptions are necessary as unique solutions of three unknowns (isotope ratios) are requested from two ion-current ratios (45/44 and 46/44). From Table 2.1, it can be seen that m/z 45 has contributions from both ^{13}C and ^{17}O. In the reference standard PDB, about 6.5% of the m/z 45 ion beam is due to $^{12}C^{16}O^{17}O$ (Craig, 1957). It can also be seen that m/z 46 has contributions from ^{13}C, ^{17}O and ^{18}O. One assumption made to solve these linear equations was that the fractionation of the three stable isotopes of oxygen is linked by constant factors.

The continuous-flow instrument used for this thesis calculates delta values of isotopes similarly to other CF-irMS instruments. The start of a peak of flowing CO_2, is detected by control software (ISODAT, Finnigan Mat), by measuring the derivative of the m/z 44 trace over time, and comparing to slope thresholds (0.2 mV/sec) and size thresholds (0.005 mV). The data comprise points for each integration period, which can be selected in the software (in this case 0.25 sec). The exact peak start is set by the use of an algorithm comparing a 5-point linear regression at each point (Ricci et al., 1994). The baseline of an individual peak is taken as the

lowest point of twenty immediately preceding the peak start. Peak heights and areas are taken by subtracting the baseline from the peak.

Peak areas of all three isotopomers peaks are then normalised to the major peak, i.e. ratios of areas of m/z 45/44 and 46/44 are calculated. These ratios are then compared to the same parameters produced by introduction of reference gas into the mass spectrometer.

One effect normally present in GC-irMS is non-concurrence of the peak maxima of the m/z 44, 45 and 46 peaks. Under certain conditions, inverse isotope effects occur, where the peak for $^{13}CO_2$ precedes the peak for $^{12}CO_2$. The software corrects this by time-shifting the peaks to fit all the peak's maxima at the same time. As will be shown in Chapters 5 and 6 no GC will be connected to an irMS in any experiment, and this problem will be avoided.

2.2.5. Natural abundance of isotopes of carbon and oxygen

Any reference material used in isotope analysis must be calibrated to internationally agreed standards. These standards are distributed by the US National Institute of Standards and Technology, (NIST). For instance, the carbon international standard is the hypothetical V-PDB, superseding PDB due to material exhaustion. The material currently used by the isotope community for calibration is NBS-19, with a set $\delta^{13}C$ offset from V-PDB of +1.95‰.

Table 2.2 Standards for Carbon and oxygen isotope ratios and their absolute ratios

Standard	element	abundance ratio	δ ‰
V-PDB	$^{13}C/^{12}C$	0.0112372	0.00
Vienna-Peedee	$^{18}O/^{16}O$	2.067×10^{-6}	$+30.9_{SMOW}$
Bellemnite carbonate	$^{17}O/^{16}O$	380×10^{-6}	
V-SMOW	$^{18}O/^{16}O$	$(2005.20\pm0.45) \times 10^{-6}$	0.00
Vienna-Standard	$^{17}O/^{16}O$	$(379.9\pm0.8) \times 10^{-6}$	0.00
Mean Ocean Water	$^{2}H/^{1}H$	$(155.76\pm0.05) \times 10^{-6}$	0.00
NBS-19 calcite	$^{13}C/^{12}C$		$+1.95_{V\text{-}PDB}$
	$^{18}O/^{16}O$		$-2.20_{V\text{-}PDB}$ or $28.6_{V\text{-}SMOW}$

Table 2.3 Approximate natural abundance ratios of ^{13}C, ^{17}O and ^{18}O for all natural terrestrial materials.

Absolute isotope ratio	Natural abundance ratio
^{13}R	0.011
^{17}R	0.00038
^{18}R	0.021

2.2.6. Continuous flow and the use of combustion interfaces

The design of the original isotope mass spectrometer was of the dual inlet type, and is now approximately 50 years old. A more recent design (10 years) of irMS is the continuous flow mass spectrometer. Instead of the vacuum led viscous flow conditions for dual inlet mass spectrometry, a simpler method of flow matching was created. A helium stream could be attached to the sample gas system, and flow could be controlled via open-split interfaces or jet separators. The presence of helium solved the practical difficulties of viscous flow, and consequently very small samples could be carried to the source in the helium stream. Under dual inlet conditions, this size sample would be liable to molecular flow and thus isotopic fractionation. Gas injection systems common to GC systems were introduced, and an early application of the system was for $\delta^{13}C$ analysis of exhaled breath CO_2 (Schoeller and Klein, 1978). Without helium flow, the same analysis would need complex cryogenic trapping mechanisms, which would increase measurement times, complexity and failure rates. Of course the flow of the reference gas must still be of the same magnitude the flow of the He supply, and be stored in a variable volume system.

Compound Specific Isotope Analysis

The addition of a Gas Chromatograph before the mass spectrometer inlet system paved the way for rapid Compound Specific Isotope Analysis (CSIA). The $\delta^{13}C$ of individual compounds is potentially even more informative than the value of a complex mixture of compounds, as fractionation in different reaction paths can be measured. Before GCirMS, CSIA had to be performed using time consuming preparation methods to extract individual compounds using

many chemical techniques. Solvent extraction is one example, and is still a common method for pre-concentrating organic compounds of interest.

An in line combustion system linked to a GC column should convert carbonaceous compounds separated on the column to CO_2 with no isotopic fractionation, and high efficiency. The first such coupling,. (Sano et al., 1976), used a standard organic analysis mass spectrometer, and placed a pyrolysis unit (CuO, 60-80 mesh, 5 cm, 700°C) between the MS and the GC. Although described as a "pyrolysis" unit, it is more correct to say that the CuO actually acted as a combustion reactor. Combustion units (using CuO, $AgMnO_4$, V_2O_5) *had* been placed after GC systems before Sano's instrument, but only for quantitative elemental analysis (reviewed in Ma and Gutterson, 1976). The metabolites of aspirin were studied (by Sano) using ^{13}C labelled aspirin in human urine by examining the mass 44 and 45 peak areas and plotting their absolute ratio. This ratio would then translate to % of $^{12}CO_2$, and % of $^{13}CO_2$ present in the sample. Sano did not need precise isotope ratios (delta equivalent) as the initial compounds used labelled ^{13}C.

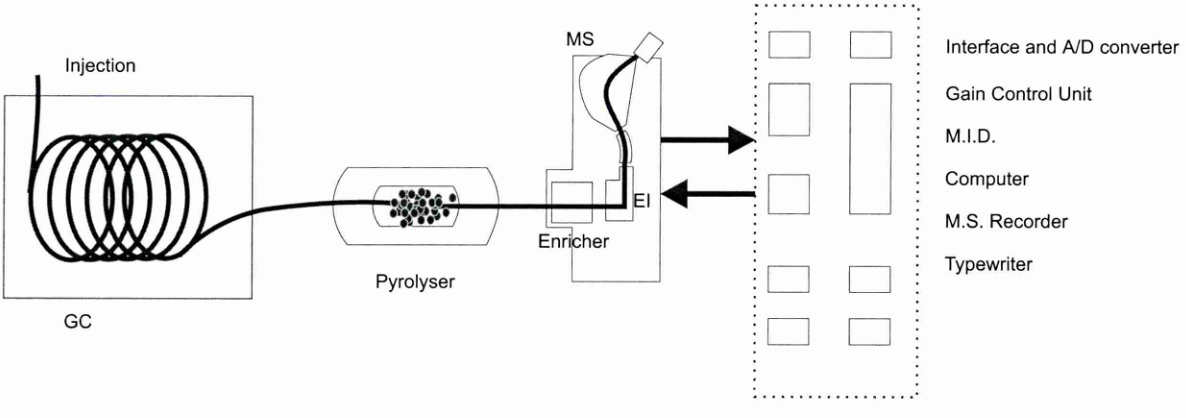

Figure 2.2 Schematic diagram of GC-oxidation MS as created by Sano et al. (1976), for the study of metabolites of aspirin. Note: M.I.D – multiple ion detector; A/D – analogue to digital; M.S. – mass spectrometer;

isotope-ratio-monitoring Gas Chromatography-Mass Spectrometry

Matthews and Hayes (1978) replaced the scan functions of The organic analysis mass spectrometer scan functions were replaced with functions more relevant to isotope ratio

measurements. A conventional magnetic sector mass spectrometer was tuned so the current amplification switched rapidly between a nominal value (for the major isotope) and 100 times that value (for the minor isotope). The combustion section consisted of a Vycor™ tube (4 mm i.d. x 30 cm) filled with CuO (60-100 mesh), heated to 750°C. The helium flow of 25 sccm (standard cubic centimetres per minute) maximum meant that higher temperatures were beyond the capabilities of their furnace. Other oxides were considered, namely cobalt (II, III) oxide and the thermal decomposition product of silver permanganate. However, due to the success of CuO within their initial testing regime (99.99% CH_4 combustion at 750°C, 15 sccm helium) no other catalysts were investigated.

The helium flow flushed combustion products downstream of the combustion tube, where a water trap (magnesium perchlorate) removed H_2O produced from combustion of organic components. A jet separator then allowed a controlled amount of the CO_2 into the ion source, whilst the remainder was pumped away. Another valve allowed unwanted GC effluent (solvent or other liquid carrier) to be directed away from the combustion unit. As with the system of Sano (1976), results were expressed in terms of absolute isotope ratios, but the samples studied were at natural abundance ratios. Therefore, instead of conversion to $\delta^{13}C$ in comparison to a reference, atom excess % (compared to an internal standard) was used as a comparative measure. The samples tested were mixed methyl esters (C_7 to C_{13}), and the absolute $^{13}C/^{12}C$ ratio of each GC-separated compound was given. A comparison was made between this new method of 'isotope-ratio-monitoring Gas Chromatography-Mass Spectrometry', and traditional sample combustion offline with transfer to a dual inlet mass spectrometer. In terms of delta notation (see 2.2.4), the method of Matthews & Hayes (1978) was able to be precise to ± σ=0.15‰ (1σ) for triplicate analyses - not as precise as a dedicated dual inlet machine with ± <0.10‰, but good enough for a great number of applications.

Barrie et al., (1984), underook the first coupling of a GC-combustion combination to a dual inlet isotope ratio mass spectrometer. Their combustion section comprised Co_3O_4 (0.125-0.200 mm dia.) at 700°C (300 mm x 0.5 mm quartz tube) followed by a trap (-80°C) for water removal. The mesh size of cobalt oxide was chosen as a compromise between flow rate and surface area. Instead of a jet separator, an open-split interface (section 2.2.7) was used to couple the CO_2 stream to the ion source. Two fused silica capillaries (one from the combustion unit, the other leading to the ion source) were surrounded by a constantly flushing helium cushion. Controlling the amount of the He purge gas would control the fraction of sample CO_2 to enter the ion source. Reference CO_2 was admitted to the system via a dual inlet changeover valve once the sample analysis was complete. The precision in $\delta^{13}C$ was better than ± 1.0‰ (1σ).

Atmospheric methane analysis

As an aside it should be noted that a method for the measurement of the $\delta^{13}C$ of atmospheric methane (CH_4) was also developed by Merritt et al., (1995). Their system used a sample (5 ml) of air, two cooled GC columns for volatile separation, CH_4 combustion, and then introduction into a viscous-flow dual inlet mass spectrometer. The combustion section comprised a NiO catalyst at 1150°C (see Chapter 5 and 6). The authors later changed the reactor unit and began a systematic examination of the problems with various combustion unit strategies (Merritt et al., 1995a). Tubing for the oxidant was 300 mm x 0.5 mm i.d. non-porous alumina, giving an internal volume of 50-70 µl. Three Ni wires (0.1 mm diameter, 200 mm long) and one Pt wire of the same dimensions were placed in the tube, centred, and oxidised (with O_2) in situ. Another tube was made in the same manner with copper instead of nickel. Oxygen was passed over the catalyst at 500°C for a few hours to re-oxidise spent catalyst.

Pt/NiO was shown to be the better oxidant for CH_4. The operating temperature of Pt/NiO had to be 1150°C or greater; otherwise the effects of carbon bound species on the NiO became

apparent. The formation of surface carbonates on various nickel surfaces had been previously reported in the literature (Behm and Brundle, 1991). Operating at 1050°C produced an offset in $\delta^{13}C$ of as much as –0.5‰ for the first few injections which decreased as more injections passed through the combustion unit. At higher temperatures, (> 1150°C) these effects were negligible. At lower temperatures the effects could be avoided by passing a bleed of O_2 gas with the carrier gas (0.1% O_2 in He) and equivalent results were observed. The NiO/Pt reactor has since been adopted by many methane isotope analysers and has become the standard method for on-line combustion, even finding itself in adapted commercial systems (e.g Brand, 1994).

2.2.7. The open split interface – enabling continuous flow MS

The sample introduction method of the open split interface was another vital technique to be developed for the GC-irMS system. Originally, combusted GC effluent would enter the ion source directly. While highly efficient (no sample is lost) and chromatographically inert, this caused problems when large solvent peaks entered the source and subjected the mass spectrometer to large quantities of unwanted gas, which would reduce filament lifetime (Ligon and Grade, 1991). Other problems included the exposure of the mass spectrometer system to atmosphere whenever a GC column needed changing. The organic GCMS community also encountered these problems and started to produce solutions for their GCMS systems, many of which could then be applied to isotope-ratio mass spectrometers.

A variety of early designs had the GC effluent capillary placed next to the capillary leading to the MS source (e.g. Arrendale et al., 1984). These early open split designs were housed within a steel or Pyrex™ tube, with an axial flow of He to prevent air entering the tube.

Other designs were promoted, one involving the crossing of the sample gas stream with a He flow at right angles in one union, effectively diluting the sample stream (Bourne and Croasmun, 1988). By varying the make-up He flow rate, sample could be purged (for solvent peaks) or diverted. Unfortunately changing the He flow also had an effect on the pressure of the gas

reaching the ion source (and changing chromatographic properties), ruining the benefit (source pressure invariance) that the interface was designed for.

A later design (Ligon and Grade, 1991) made use of the mechanical strength of fused silica capillaries. An actuator moved the MS source capillary up and down a glass or fused silica tube containing the GC effluent and He buffer capillaries, while one end of the tube was open to the atmosphere (Figure 2.3). Varying the height of travel of the actuator altered the proportion of sample entering the mass spectrometer.

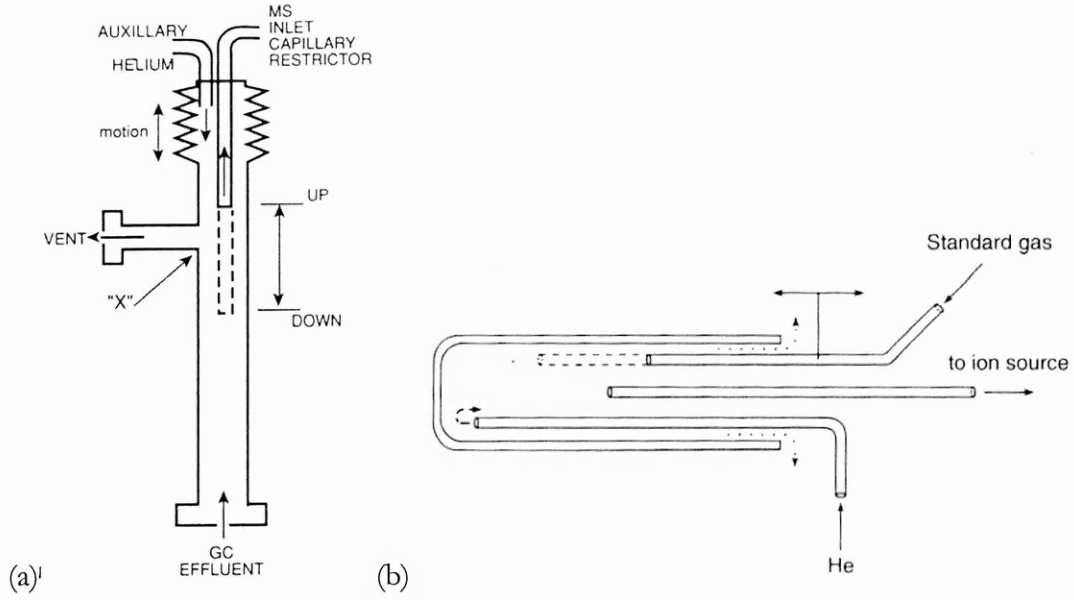

Figure 2.3 (a) Open split design by Ligon & Grade similar to that used in the Finnigan MAT GC interface II. (b) Open split design for reference gas admission to mass spectrometer. The Finnigan MAT GC Interface II has the ion source capillary that is actuated, not the reference gas. Fig source: (Platzner, 1997).

This design seemed to solve the expected problems associated with the direct coupling method, and other problems with primitive open-split interfaces such as source pressure variance, chromatographic resolution variances, solvent diversion, and the inconvenience of changing GC columns. By use of the open-split interface, the need for dual inlets to mass spectrometer sources (and changeover valves) was challenged. Mass spectrometer inlet design was simplified, and this paved the way for the development of the continuous flow mass spectrometer.

The first commercial system with coupling of a copper oxide reactor and open split interface to irMS instruments was produced in 1988 by Finnigan MAT and implemented in the GC Combustion Interface system supplied with their mass spectrometers. With these continuous flow instruments, the term Gas Chromatography-isotope ratio-Mass Spectrometry was applied (GCirMS). Figure 2.9 shows the inlet system (including open-split) found in the Finnigan MAT Delta C as used in this project.

For isotope ratio work, two open split interfaces are used, one for the sample stream, and one for the reference gas capillary. Both capillaries enter the source at one inlet, by means of a dual-hole graphite-vespel ferrule (in the case of the Delta C). The scheme of operation dictates the order and frequency of setting the open-split interfaces to sample gas (whether reference gas or real sample) or helium.

2.2.8. Water separation

During the complete combustion of hydrocarbons, CO_2 and H_2O will be evolved. Unless any further analysis of the water of combustion is necessary, it must be removed. The effect of admitting water on isotope ratio mass spectrometers is well known (e.g Leckrone and Hayes, 1998). Interactions between H_3O^+/H_2O and CO_2^+/CO_2 can result in protonation, where H_3O^+ reacts with $^{12}C^{16}O_2$ to form $H^{12}C^{16}O_2^+$ (and H_2O), which is isobaric with $^{13}C^{16}O_2^+$ (see Chapter 4). Drying agents must be employed to remove water of combustion as well as water from atmospheric leaks and even carrier gas supplies. A common drying agent is magnesium perchlorate, which is useful for pre-GC drying. Downstream of the GC and combustion reactor the addition of a large bore tube containing powder would degrade the chromatographic separation. Within the laboratory system as seen in Figure 2.9, a Nafion™ membrane dryer is used. The post column effluent reaches the tube of Nafion™ membrane, with a counter-current of dry He flow on the outside of the membrane which is housed within a quartz tube. Water then passes through the membrane and is removed, while sample CO_2 remains within the

membrane tube. This process does not produce significant fractionation and is used in many commercial irMS preparation systems (Brand, 1994).

2.3. Mass Spectrometry

2.3.1. Isotope ratio mass spectrometry

Although the history of the mass spectrometer goes far back, the operating principles have remained essentially the same for certain types of mass spectrometer. Sample gas is ionised within a vacuum chamber, and the ions are accelerated with an electric field. A magnetic field then separates these moving ions of differing mass. J.J. Thompson made the first detection of isotopes (resolving ^{20}Ne and ^{22}Ne) using a mass spectrograph, opening the field for other discoveries (Thompson, 1912). Aston improved on Thompson's work, eventually discovering 212 naturally occurring isotopes (Aston, 1919). Development of a (dual inlet) mass spectrometer specifically made to measure isotope ratios in gases was completed by Nier (1947). The design was taken further (McKinney et al., 1950), and since then all commercially available isotope ratio mass spectrometers work on the same principles, even though the technology behind all major components have been improved.

- Ionisation. Sample gas ionisation occurs via the interaction of low energy electrons, usually emitted by a hot filament. The energy of the electron needs to be greater than the first ionisation potential of the molecule. Different products can be formed within the electrons impact procedure, even negative ions through 'sticking' of the incoming electron, while sometimes the process can be repeated giving multiply charged negative ions. Multiple charge positive ions are also created. In most circumstances, the singly charged positive ions are used for the analysis.

- Beam formation and acceleration. An electric potential is applied to various plates in the ion source (repeller or drawout plates) with slits or holes (for beam collimation) in them allows ions to travel out of the ionisation chamber, to the entrance of the flight tube. High voltage (4 kV is common) is applied to other plates for acceleration toward the magnet. The ion

beam may have a minimised cross section to be on target, so further ion focussing is undertaken with electric immersion lenses.

- Magnetic Deflection. During acceleration, the ion beam enters a magnetic field which is applied perpendicular to it. When entering a magnetic field, a charged particle experiences the Lorentzian force, which is perpendicular to both the field and the velocity vector of the particle. This force will divert the particle into a circular path if the field is constant. The motion of the particle is defined by the equation:

$$\frac{M}{Z} = \frac{B^2 R^2}{2V} \tag{2.3}$$

where M is the mass of the ion, Z its charge, B the flux density of the magnetic field, R is the radius of circular path, and V is the accelerating voltage. Although the S.I. units of the M/Z expression is kgC^{-1}, in mass spectrometry the most used units are atomic mass units (a.m.u. = 1.66×10^{-27} kg) and the charge on a single electron (1.60×10^{-19} C). Thus, an ion with a single positive charge due to loss of an electron would have Z=1. If B and V remain constant, for singly charged ions, $M \propto R^2$. Emerging from the exit part of the magnetic field, different isotopes will have different trajectories, but will continue in a straight line as there is no magnetic field outside of the magnet. Some species in the ion beam are of higher or lower mass to the sample ions under investigation. These will also be deflected by the magnet, but not enough (or too much if lighter) to remain within the circular trajectory of the flight tube, and will collide with the inner wall, and will be discharged.

- Detection. The final process in mass spectrometer is interaction with a detector. Beams of ions from the magnet travel in non-parallel paths toward the detector unit. In gas isotope ratio systems each singly charged positive ion must be neutralised by the addition (or donation for negative ions) of one electron. The device used is a Faraday cup. The amount of ions received is measured indirectly through the equivalent property of the amount of electrical current passing, from the neutralisation process. The low current required to

neutralise the ion beam is put through a high gain amplifier, which contains a resistor of large resistance, and the voltage across this resistor is measured. Multiple Faraday collectors are usually placed in specific positions across the ion beam to collect sample ions at required trajectories. Voltages are then recorded for data analysis.

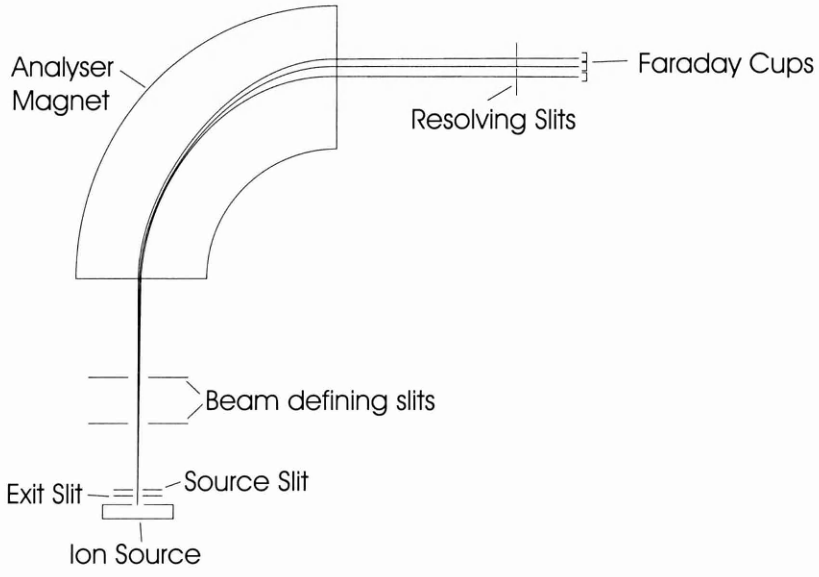

Figure 2.4 Schematic diagram of a generic isotope ratio mass spectrometer system

2.3.2. Ion Trap Mass Spectrometry

In Chapter 3 it is stated that the ion trap mass spectrometer has been used for many years as an analytical mass spectrometer. It would be surprising for some to learn that this MS is being modified to measure stable isotope ratios within MODULUS (Barber, 1998). Analytical mass spectrometers need much less sample than irMS systems, as the requirement to measure the minor isotope with the same clarity as the major is removed. Although described in the 1950s, the quadrupole ion trap first gained commercial success in the 1980s as the Finnigan MAT Ion Trap Detector™ for post-GC detection. In terms of sensitivity, ion traps are generally capable of working in the femtomole range, though the ton trap used throughout this thesis (Finnigan MAT ITD 700) would produce a usable mass spectrum from 5 nmol of CO_2. In comparison, a typical CO_2 injection on a continuous flow irMS would require 50 nmol.

Both the quadrupole mass filter and the quadrupole ion trap were developed in the 1950s (Paul and Steinwedel, 1956). The quadrupole ion trap consists of three electrodes arranged in such a manner that when radio-frequency (RF) fields and direct current (DC) potentials are applied to them, ions entering the space in between the electrodes may become trapped. In effect, ions in a range of mass to charge ratios (m/z) find stable elliptical orbits in three dimensions according to the RF and DC fields applied to the electrodes. Changing the fields causes ions of certain m/z to be unstable with respect to the trapping mechanism. These ions are then ejected axially from the ion trap and interact with an electron multiplier, which acts as the ion detector for this system. By ramping the amplitude of the RF field to specific values, ions of particular m/z are sequentially rendered unstable in the trap, reaching the electron multiplier at a certain time during the RF ramp. This timing of the RF ramp is crucial, as this related to the m/z of the ejected ions and hence a mass spectrum can be built up. The mass range can span 10 to 650 a.m.u, giving the ion trap a place in organic chemistry laboratories.

The ion trap is not as popular as the quadrupole mass filter ("quad") as a post-GC detector due to poorer quantitation and dynamic range. However, it has many advantages such as its size, sensitivity, and the ability for in-situ studies of ion-molecule reactions within the trap (Gevrey et al., 2000).

For the development of the mass spectrometer into an instrument suitable for isotope ratio detection, many parameters needed to be optimised. Work done in the PSSRI has taken the ion trap to give a precision of 5‰ in $\delta^{13}C$ of CO_2 (Barber, 1998). As a working spaceflight model was not available during the course of the laboratory investigation, a commercial analogue of the Ion Trap was used to test the MODULUS configuration for quantitative analysis.

So far it has been shown that both the types of mass spectrometers (isotope ratio and ion trap) encountered during this project have specific uses, and one model of each type was available for the duration of the project. MODULUS comprises a GC-ion trap system with a combustion unit post-column (Figure 3.9). This approach has not been used for this project, as to study the

combustion catalyst itself requires a system geared to analysing the gases combusted, or quantity uncombusted. Therefore for this project, the combustion unit is upstream of the column in the GC-ion trap system. Both MS systems require measured amounts of test gases to pass over the catalysts at elevated temperatures. It would be useful for both of the mass spectrometers to have the same common gas inlet system. A block diagram of the proposed arrangement is shown in Figure 2.5. The decision was taken that a vacuum manifold with 6-port valves would transfer the gases from a vacuum system to a flowing carrier gas. The carrier gas (helium) then would transport the gases over the catalysts and to the mass spectrometers for detection.

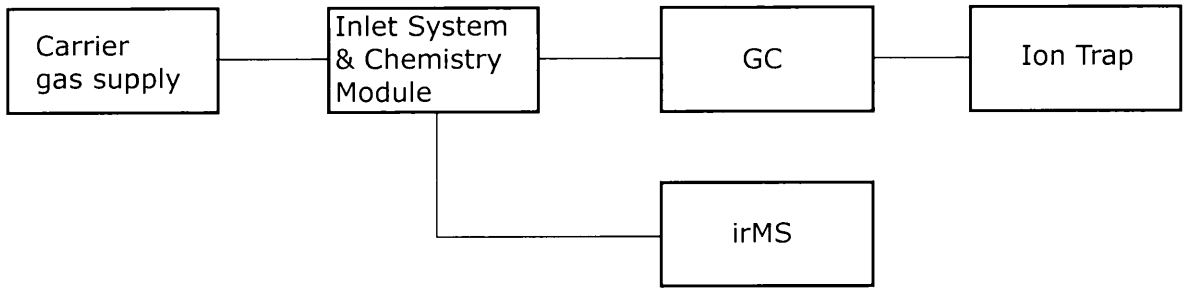

Figure 2.5 Simplified block diagram showing arrangement of instrument configuration

2.4. The gas transfer manifold

Early catalyst investigations were underway by the author using the irMS before the ion trap was installed into the laboratory. For these early experiments the inlet system used a flowing helium supply to mix with the test gases in closed vessels. It was noted that using this approach on the Ion Trap as well would be less controllable than creating a custom-made common vacuum inlet system for both the irMS and the GC-ITD. Other advantages to having a common inlet system include:

- gas pressures can be easily measured
- test gases can be stored in volumes
- other gases can be tested by attaching lecture bottles to the vacuum system.
- sample preparation time is minimal

The vacuum manifold was assembled by the Open University S&T Workshops, and was designed by the author and Geraint Morgan (PSSRI). It comprised ¼" stainless steel pipework,

with welded sections to make the 3-way and 4-way pipe unions. A schematic of the system is shown in Figure 2.6. The vacuum system was attached to both rotary and turbomolecular pumps via different valves. The rotary pump (Edwards High Vacuum Pump 2) was also used as a backing pump for the turbomolecular pump (Balzers 56 l/s). A Penning gauge (Edwards – range 10^{-2} – 10^{-7} mbar) was placed between the turbomolecular pump and the vacuum manifold. The pumping system was protected by a trip circuit (designed and built in-house) which closed valves if pressures rose above a given value (typically 10^{-2} mbar).

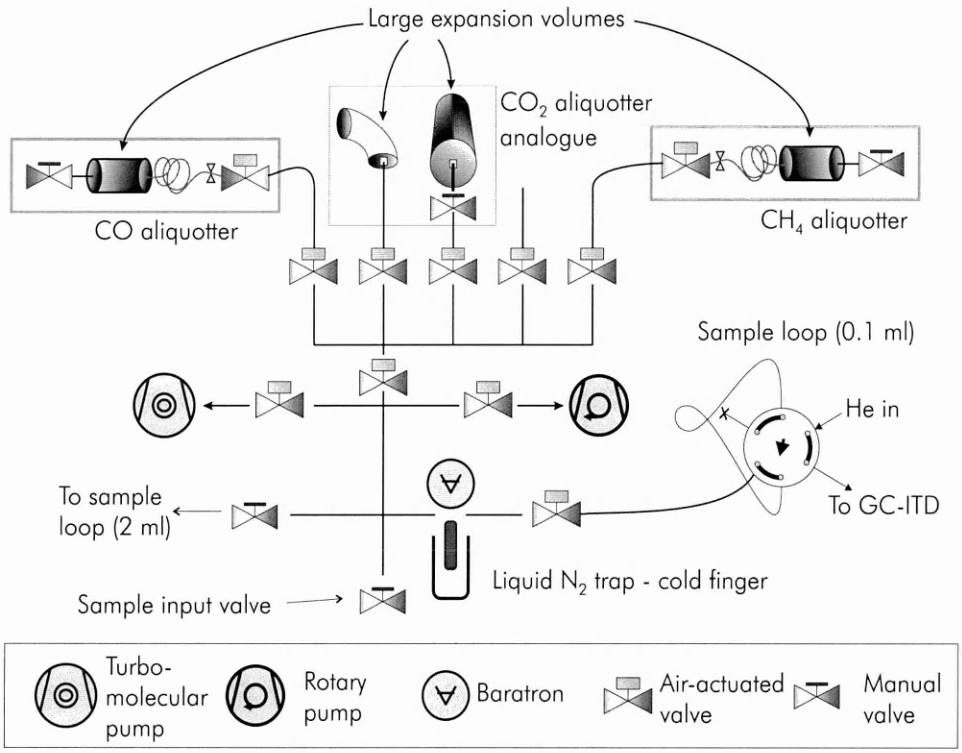

Figure 2.6 Schematic diagram of vacuum inlet system for Ion Trap and isotope ratio mass spectrometers. The six-port valve is seen on the right of the diagram.

The manifold comprised a mixture of manual and air-actuated valves to transfer gases selectively between parts of the vacuum line. Manually switchable valves (Nupro, SS-4H) allowed the connection of external glass or steel vessels via ¼" Swagelok™ fittings. The air-actuated valves (Nupro, SS-4BK) were also connected to the pipework by Swagelok™ connectors. Some portions of the line included VCR fittings, e.g. connection the turbomolecular pump. A cold

finger allowed the condensation of gas mixtures required during some experiments. A 0-10 torr, Baratron (MKS Instruments) allowed the measurement of gas pressure within the manifold.

2.4.1. Manifold valve system

The air –actuated valves required a system of compressed air supply to be available. The system can be seen in Figure 2.7.

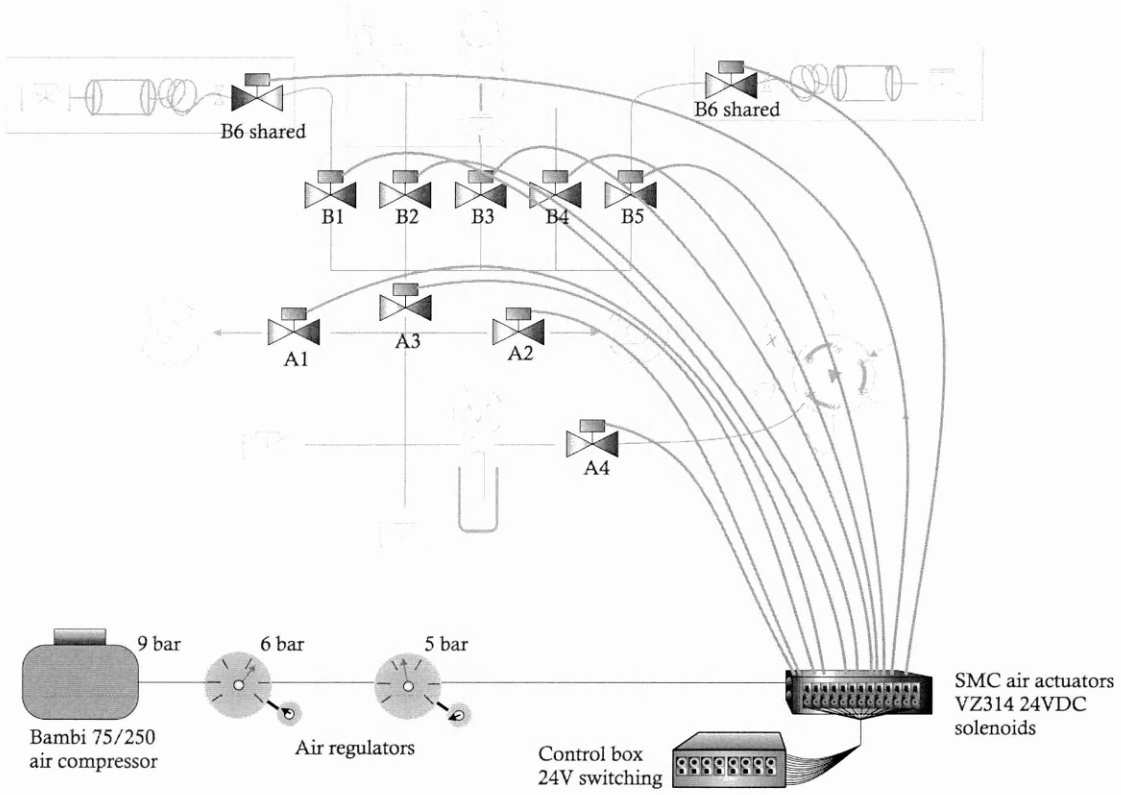

Figure 2.7 Arrangement for switching of air actuated valves, by means of a compressed air system

As the supply of air was also used by other instruments in the laboratory, shut-off regulators were attached at points which allowed isolation of the section for use on the vacuum line. Actuation with the Nupro SS-4BK valves occurs at 3-4 bar, therefore the final regulator was set to 5 bar. A 24V control box (designed and built in-house) allowed the control of individual solenoid air actuators (SMC Pneumatics).

2.4.2. Gas storage and transfer

CO and CH_4 were contained in storage units of a type described by Butterworth (1997), and shown as the CO or CH_4 aliquotter in Figure 2.6. Each of these consisted of a large volume (~700 cm^3) filled to a pressure of the order of 2.5 bar (absolute) from an appropriate lecture bottle. A metal capillary (30 cm, $^1/_{16}$") attached to the large volume bled the contents into a normally closed, air-actuated valve. This results in the small volume of the capillary and the connector to the valve, containing a small amount of the CH_4 or CO gas at the same pressure. Opening this valve into the evacuated manifold delivered gas to the sample loop. This relatively constant bleed rate from the large vessel dictated the quantity of gas available for expansion. If a large amount was required, then the valve to the manifold could be opened and the gas bled into it for the time required.

For CO_2 gas the delivery system was different due to cost constraints. Two large (~1 l each) steel vessels were attached to the manifold via air-actuated valves. A manual valve was placed on one of the vessels, which was filled to 3 bar with CO_2. The other vessel was used as an intermediary storage for the CO_2 expansion from the high pressure vessel.

Transferring the one of the test gases to the flowing helium carrier stream of the analytical systems was accomplished by using 6-port 2-way valves (Valco, NLV). Figure 2.8 shows how the valve was modified from conventional usage with two flowing systems to act as an interface between a static and a flowing system. One valve position Figure 2.8 (a) allows a closed loop to be connected to the vacuum line, while helium flows uninterrupted to the mass spectrometer system. In this position test gas can be loaded into the closed loop. The amount of gas could be calibrated by measuring the pressure and by knowing the volume of the loop. The Valco valve could then be switched (Figure 2.8 (b)), bringing the loop in-line with the gas flow and injecting the sample into the path of carrier gas flow. The test gas would then be transported toward either of the mass spectrometers by the helium carrier gas.

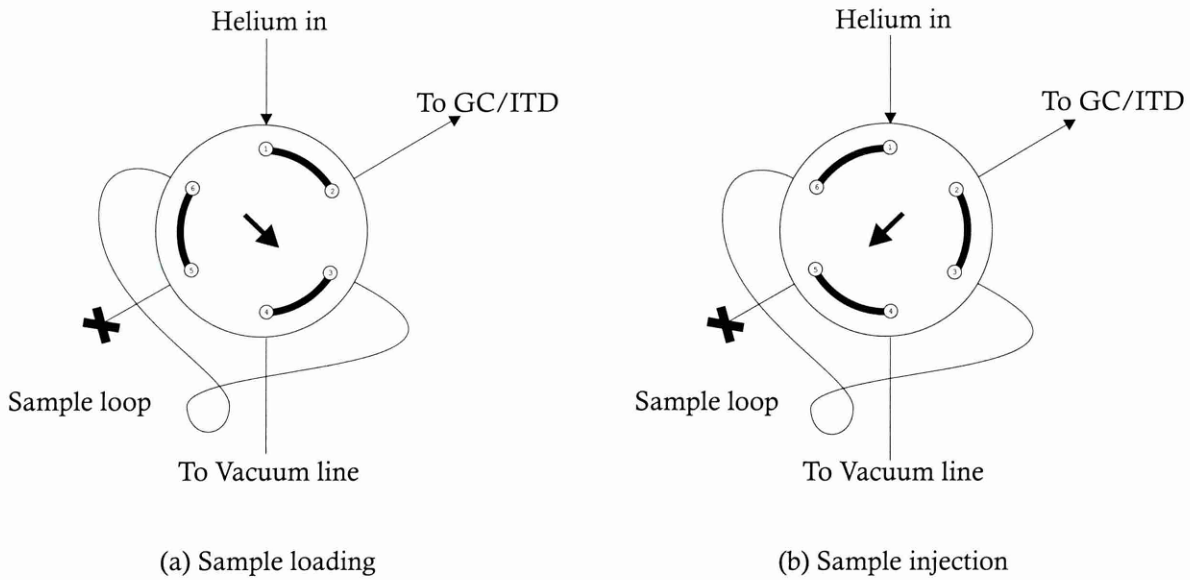

Figure 2.8 Valco valve arrangement to switch between vacuum and flowing gas streams. (a) shows the sample inject position and (b) shows the sample load position. The sample loop was either 0.1ml and $1/16$" (mass spectrometer) or 2.0ml $1/8$" (ion trap)

Once the test gas has been flushed out of the loop, the loop remained filled with helium. As the valve was turned into its original loading position, this helium was expanded into the manifold and pumped away.

This attachment to the 6-port valve to the manifold was allowed to be easily removable, as an identical Valco valve also was able to be attached to the manifold at the same point, giving a choice of sample loop size. However, this second Valco valve was used to transfer 300 ml of air for atmospheric methane analyses (Chapter 6).

2.4.3. Isotope ratio mass spectrometer interface

Chapters 5 & 6 use the isotope ratio mass spectrometer using different sample introduction systems. Each has different configurations for analysing the analytes in question. However, both configurations were set up to analyse CO_2 that had been cryogenically trapped in a small loop on another Valco valve. After heating, the CO_2 is transported by helium to a water separator, and an open split inlet before heading to the ion source. This is shown in Figure 2.9.

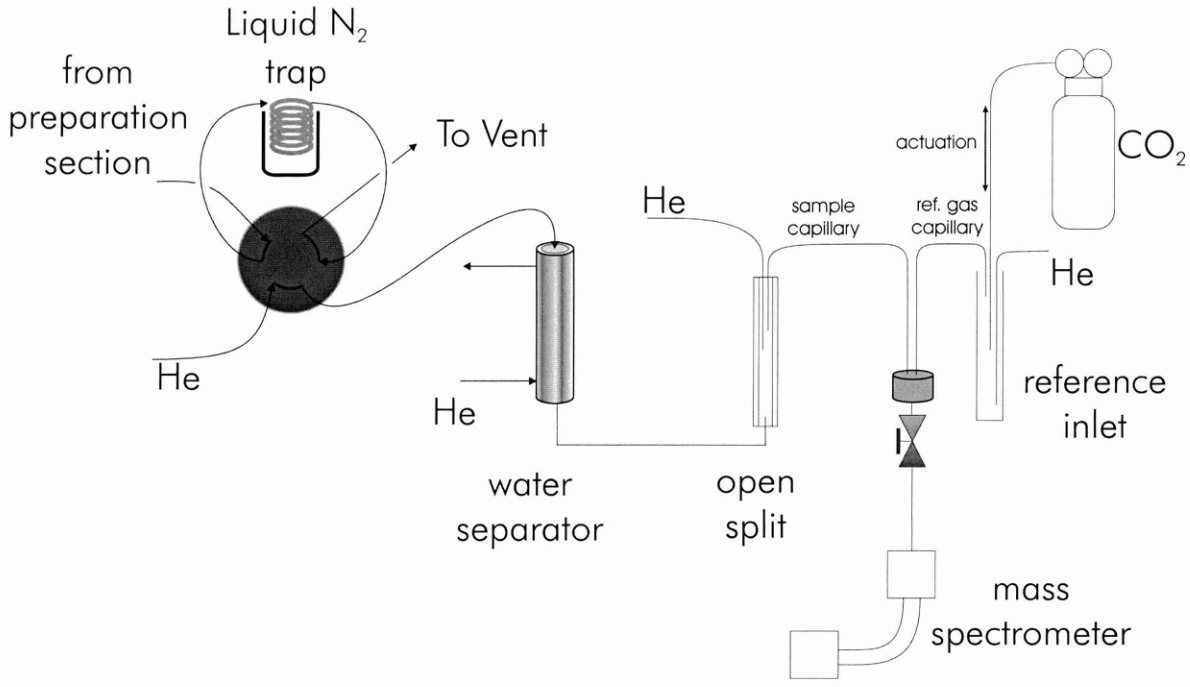

Figure 2.9 Schematic diagram of the Delta C GC interface II inlet system

It can be seen from Figure 2.9 that two capillaries (sample and reference) enter the ion source of the mass spectrometer. The reference gas inlet allows the controlled admission of He and CO_2 to flow into the source. This is accomplished by using an open split with two capillaries flowing gas into a tube closed on one end, and one capillary leading to the source. The helium capillary resides at the bottom of the tube, while the reference capillary resides half way up the tube. Flowing helium prevents air from entering the capillary. The mixture is controlled by vertical actuation of the position of the incoming CO_2 capillary. Moving the CO_2 capillary to the bottom of the tube results in CO_2 entering the reference capillary, and hence the ion source. Raising the position vents CO_2 to atmosphere.

2.4.4. Methodology of irMS use

In order to derive a $\delta^{13}C$ value of an unknown sample, the ratios of ion beams (m/z 44-46) always have to be compared to beams of a reference with known isotopic ratios. The switching of the Valco valve in Figure 2.6 makes it possible to have one single injection per chromatogram. To calibrate the reference gas to measure this peak, a method was devised to

admit reference CO_2 for 20 seconds, twice, before the sample peak. This can be seen in Figure 2.10.

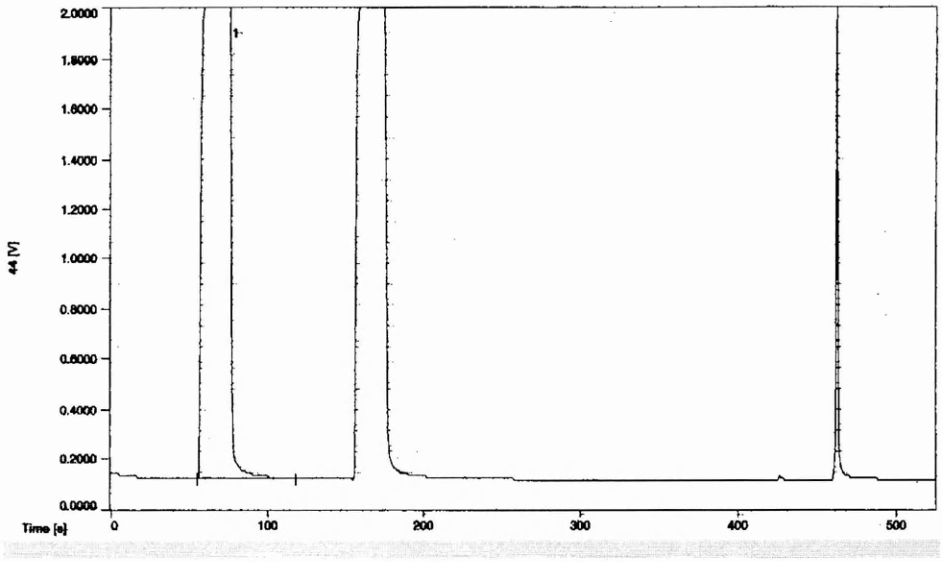

Figure 2.10 Typical chromatogram trace from the irMS. The first two wide peaks are reference gas (and are off scale), and the final peak is the sample.

The precision of the instrument at any one time can be calculated by performing a method known as a "zero-enrichment". This method usually involves repeated admissions of reference gas to the mass spectrometer, where statistical analysis of the calculated δ values gives a measurement of the precision. The sequence used in this project injected pulses of CO_2 reference gas consecutively to the ion source 8 (i.e. N=8) times for 20 seconds with a gap of 40 seconds between pulses. When the run is complete and delta values are calculated by comparing pulse N against pulse N+1, the latter set to be "zero" (i.e. a fixed isotope ratio set by the user in the software). An alternative method was to vary the pulse width of the reference gas. The first pair of peaks were set at 20 seconds each, the next pair 15, 10, 5 and the last pair 2 seconds. Any effect on $\delta^{13}C$ with peak width is then apparent. Typical results from both zero-enrichment methods are seen in Figure 2.11. Figure 2.11 (a) shows the variation in the $\delta^{13}C$ and $\delta^{18}O$ measurements is lower when CO_2 pulses are 20 seconds wide, and more deviation in δ is seen from shorter pulses.

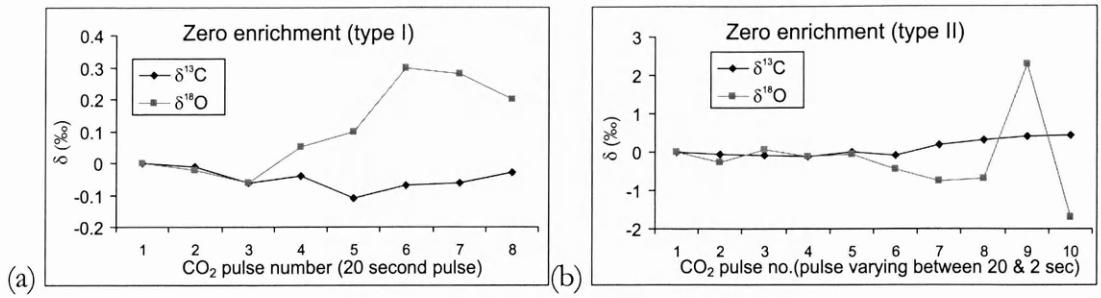

Figure 2.11 (a) Typical results from a single zero enrichment run of 8 peaks, 20 seconds each. (b) Typical results from zero enrichment of 10 peaks with reference gas between 20 and 2 seconds wide.

As can be seen from the first method of typical zero enrichment in Figure 2.11 (a), $\delta^{13}C$ is returned with much lower spread than $\delta^{18}O$. All of the 8 injections of CO_2 yielded $\delta^{13}C$ results within $\pm$ 0.1 ‰, where as the results of $\delta^{18}O$ were within $\pm$ 0.3 ‰. These values of precision were typical for the instrument when all components were functioning well. Figure 2.11 (b) also shows the results of the 10 CO_2 injections using the second zero-enrichment method. It can be seen that as the injections of CO_2 get shorter in time (with the later peaks), the precision of $\delta^{13}C$ and $\delta^{18}O$ decreases to over $\pm$ 0.5 ‰.

The shape of the CO_2 peak is controlled by the sublimation of sample CO_2 trapped under liquid N_2 at 77K, upstream of the inlet system. The heating of the loop is simply ambient heating from removal of the liquid N_2; no additional heating is applied to the loop. The heating rate then defines the sharpness of the peak. The peak width is an important parameter in the calculation of isotope values.

2.5. Mass Spectrometer Calibration

2.5.1. Calibration of the isotope ratio mass spectrometer

Quantitative calibration of mass spectrometers usually entails measuring the peaks from known amounts of CO_2 and comparing the detected peak areas. Complications arise when blank levels of CO_2 were detectable. Blanks can be quantified by injecting an empty sample loop. Minimising the blank can occupy some time when building transfer systems. Air (which includes CO_2) can enter a vacuum system if joints are not sealed to their best ability.

Swagelok™ joints can over time loosen and need tightening. This also holds true with connections to Valco valves and other connections (e.g. dead volume GC connections). $\delta^{13}C$ and $\delta^{18}O$ can be reported for blanks which may be useful if the amount is significant, and corrections applied to sample isotope ratios, using mass balance. For most of the experiments in the thesis the sample:blank ratio was >25 and often >100. Once blank sources were identified and removed, actual calibration could occur. A typical calibration sequence using CO_2 on the mass spectrometer can be seen in Figure 2.12 (a) where peak area is compared to amount of injected CO_2.

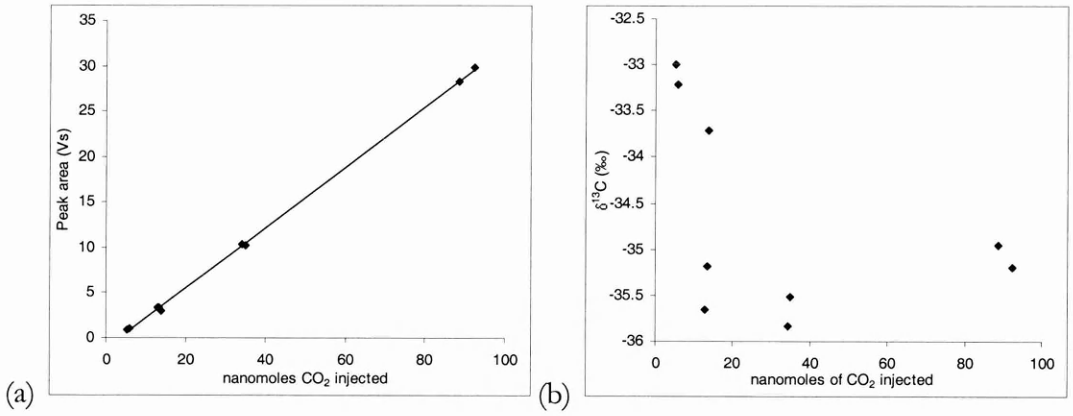

Figure 2.12 (a) Typical quantity calibration of CO_2 injections. (b) $\delta^{13}C$ of CO_2 injected in (a)

Observation of $\delta^{13}C$ results also show the reproducibility of the instrument. It can be seen from the injection series in Figure 2.12 (b) that greatest reproducibility in $\delta^{13}C$ occurs with the largest sizes and the smallest sizes of CO_2 injection. However, the difference of 2‰ in $\delta^{13}C$ from small sized injections was one factor that made larger (>20 nmol) injections preferable. This effect was also seen in subsequent calibration tests.

The calibration process was performed on several occasions over the project period. Although always linear, there was some variation in the gradient of the calibration line. Some problems were traced to the open-split interface. On inspection, the capillaries exact position in the split

could vary, producing no significant change in CO_2 yield, but a variability of up to 2‰ in $\delta^{13}C$ in open-split tests (Baker, 1997).

2.5.2. Methodology of Ion Trap mass spectrometer use

As with the irMS system, a gas sample is loaded into the loop on a Valco valve attached to a vacuum system. The 0.1 ml sample (Figure 2.8) loop is then pulsed and the gas is then transported to the gas chromatograph, which is coupled to the ion trap mass spectrometer. Two test procedures used the ion trap: the GC testing process (Chapter 3) and the catalyst evaluation process (Chapter 4). An entire run can last up to 10 minutes, depending on flow characteristics of the catalyst, or the GC column installed. At the end of the process the Valco valve is switched, and the carrier gas pumped away, ready for the next sample. More details of the process for the individual tests are described in the relevant chapters.

2.5.3. Calibration of Ion Trap mass spectrometer

A similar calibration procedure to the irMS was attempted for the Ion Trap. Measured amounts of various gases were injected to the GC-ITD system peak and areas recorded. Peak areas were compared with injection amount and the correlation noted. Initial indication from gas injections led to the thought that the detector was behaving linearly. More data were collected and are shown in Figure 2.13. The difference in the sensitivity of the instrument to differing amounts of gas was then discovered. There appear to be two effects: loss of sensitivity at larger injections, and difference in response from different species.

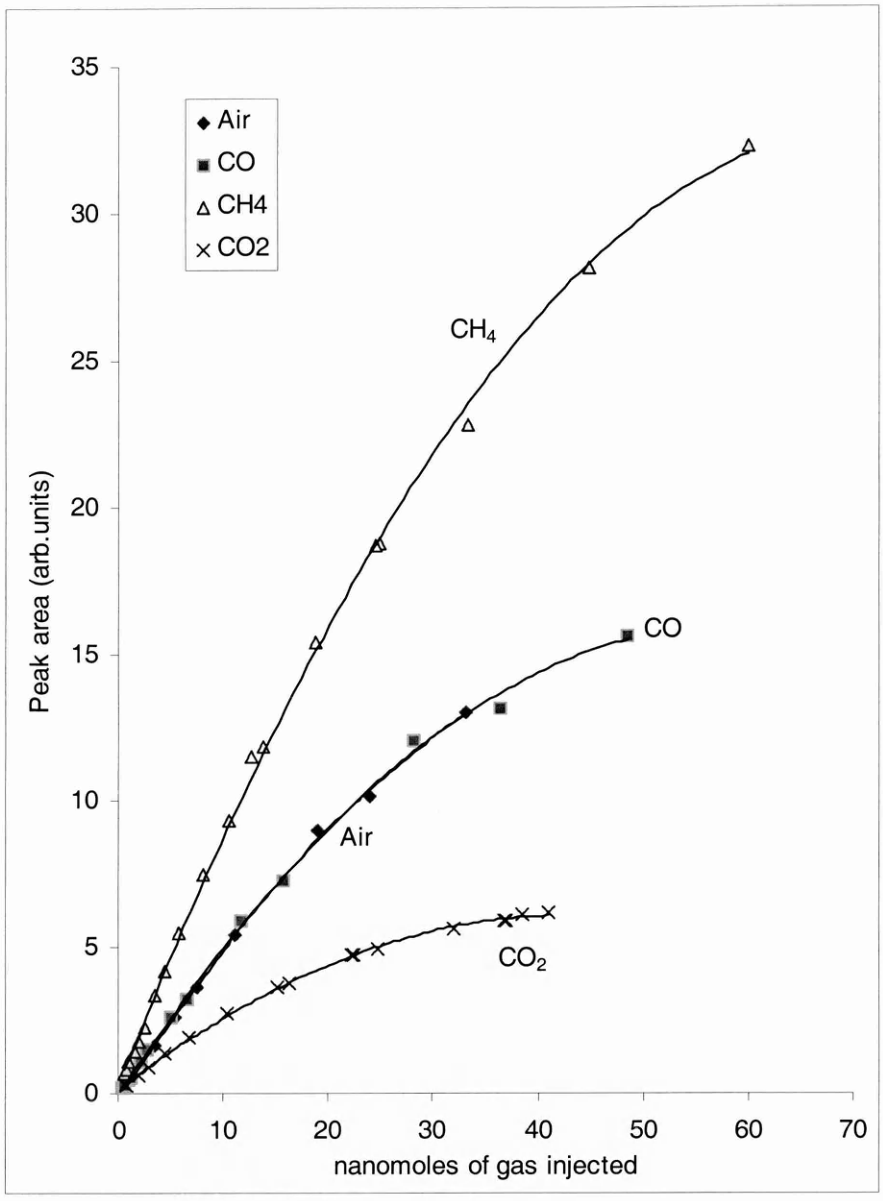

Figure 2.13 Quantity calibration of various gases on the Ion Trap, including 2nd order polynomials calculated for trendlines for the data series. Trendlines for air and CO appear to overlap. [The peak area for air was calculated as the total number of ions between m/z 28-32]

Loss of sensitivity

Increasing the amount of material injected into the trap does not result in a linear increase in peak area. One problem is due to space charge, and in effect limits the dynamic detection range of the mass spectrometer. As more and more material in the trap is positively ionised, ion-ion repulsion becomes an important factor (Yost et al., 1987). This repulsion can also distort the RF fields operating in the trap, and hence cause the trap to behave non-ideally. The detector can be saturated (as can be seen in the CO_2 plot in Figure 2.13) when the ion density reaches a certain

limit. The solution employed in commercial instruments is to vary the ionisation time to for each microscan, and is termed AGC (Automatic Gain Control).

With AGC, as the amount of material detected increases, the ionisation time is reduced to limit the number of ions formed. A correction must then be applied to account for the reduced ionisation time. Using AGC can allow a linear response over 6 magnitudes (Yost et al., 1987). Although this feature was available for the commercial Ion Trap used in this thesis, the additional artefacts in the spectrum caused confusion. For example, once atmospheric leaks had been minimised, switching on the AGC function resulted in very large CO_2 and N_2 backgrounds, precisely the type of molecule the experiment was designed to detect. Thus, throughout experiments in this work, the AGC was off. As can be seen from Figure 2.13, the loss of sensitivity is most pronounced during large gas injections. At lower injection pressures, the curvature showing loss of response is less visible, and the linearity appears to be good (Figure 2.14).

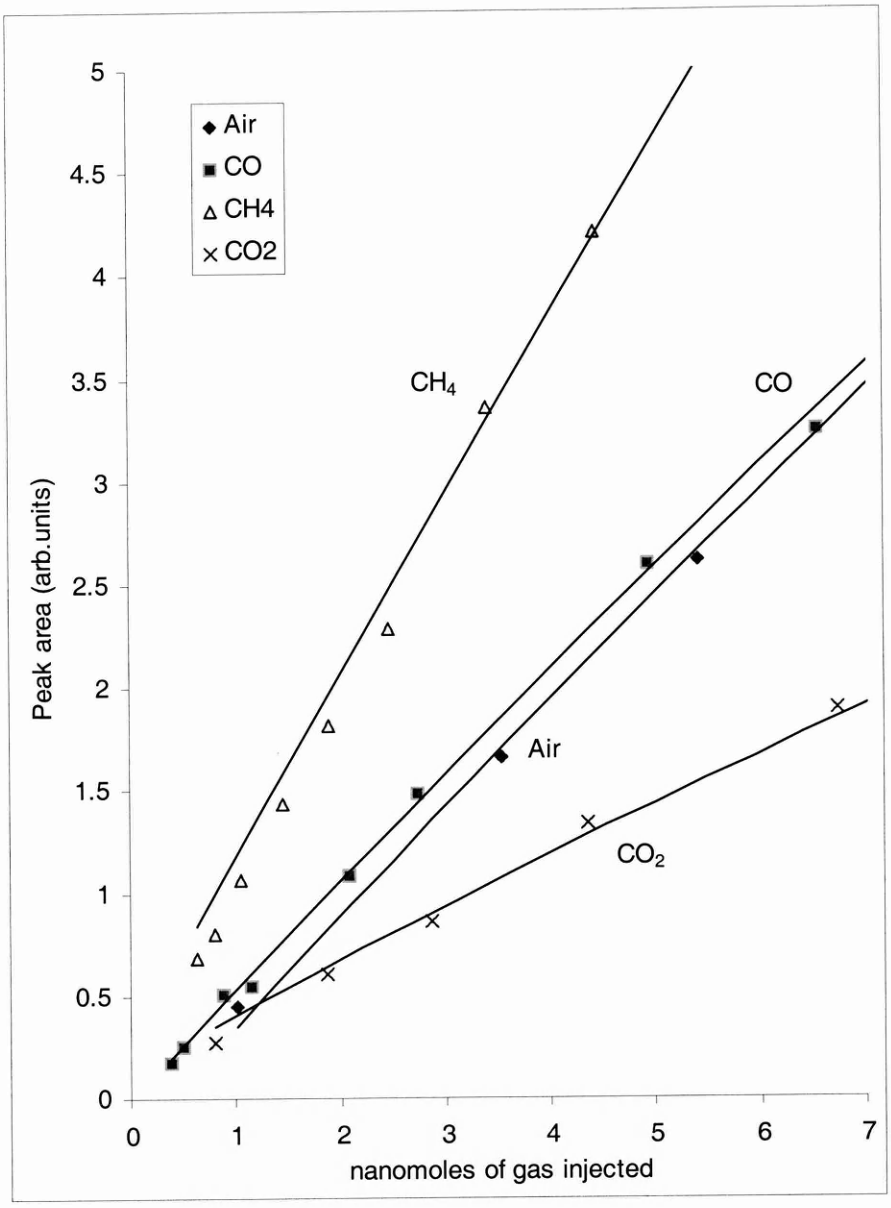

Figure 2.14 Same quantity calibration experiment as Figure 2.13, but only showing lower pressure injections. Trendlines are based on the complete dataset as in Figure 2.13, not this subset

Mass-dependent response

The other effect in Figure 2.13 shows a difference in response from different ions. Lighter ions appear to produce a stronger signal than heavier ones. One can see that CO (m/z 28) and air (78% m/z 28) appear to have a very similar response. This effect has its roots in the manner of the Ion Trap storage system. During a scan, a voltage is applied to store the ions within the trap. This voltage increases at a set rate, and at certain voltages, ions of a particular mass unit are rendered unstable within the trap. These unstable ions are ejected, and interact with the

detector. It is the time that species are stored in the trap which defines the mass selectivity. As the voltage increases, ions of greater mass become unstable and are then ejected. The time involved in the ramping decrees that higher mass ions exist and are trapped for a longer period of time. This allows greater potential for higher mass ions to incur ion-molecule reactions. Protonation from H_3O^+ may occur, producing a CO_2H^+ ion of mass 45, although this was rarely seen. It is more likely that the reaction is charge transfer: $CO_2^+ + H_2O \rightarrow CO_2 + H_2O^+$. Water, of which some may be ionised by the EI process, will always be present in the ITD system, leading to the reaction above, the net result of which is the removal of CO_2^+ (m/z 44) from the trap over time. This can be seen in Figure 2.15, where a CO_2 coming out of a GC column coincides with an increase the background water quantity. This evidence of the reaction above.

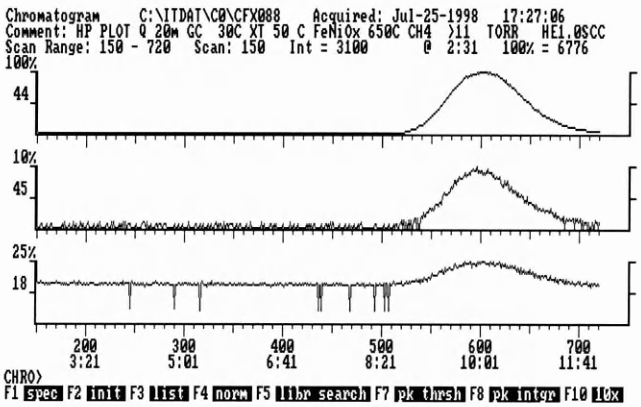

Figure 2.15 Ion Trap chromatograms showing three ions: m/z 44 (CO_2), m/z 45 (CO_2), and m/z 18 (H_2O). Note the increase in m/z 18 concurrent with CO_2. Also the m/z 45 shows 10% of m/z 44 height, which is due to tailing of the 44 peak to 45, and the production of CO_2H^+.

Another possible explanation for the lack of response in high-mass ions is the influence of storage mass (Barber, 1998), but this is beyond the scope of this thesis.

As with the isotope ratio mass spectrometer, the sensitivity of the instrument changed with use. Unlike the irMS where the sensitivity changed by no more than 20%, the ITD had variations spanning an order of magnitude, largely due to the response of the electron multiplier. To make sure the ITD was working efficiently, self-testing and calibration software was run. The consequence of the irreproducibility in the ITD was quantitative comparisons of peak areas

taken at different times may be invalid. However, the ITD's major use was in the comparison of the *relative* amounts of CO_2 and uncombusted material (Chapter 4), and in the chronological separation of volatile compounds (Chapter 3), and there were experiments carried over short time intervals during which the sensitivity remained constant.

3. GAS CHROMATOGRAPHY AND SPACE QUALIFICATION

3.1. Introduction

It is mandatory for any instrument on board a spacecraft to be tested against possible failure. A principal source of failure tends to be when the object is undergoing the mechanical stresses of launch. This chapter details the methods whereby such tests were carried out on various individual elements of the MODULUS system. The concept of gas chromatography (GC) will be discussed. The commercial vibration table used for the mechanical testing will be shown, as will the laboratory system for analysing the behaviour of the gas chromatography columns. The recommendations to the MODULUS design team from data gathered by the experiments are given at the end of the chapter.

3.1.1. Qualification requirements for Rosetta

Any spacecraft, whether manned or unmanned, will undergo stresses under the harsh conditions a launch vehicle must impose for the acceleration to escape velocity. Delicate instrumentation in terrestrial laboratories rarely undergo these stresses, hence the adaptation of the GC-MS for space use must explore the question of mechanical stability. The extreme vibration on the launch can potentially cause havoc with capillary columns, valves, mechanical structure, cabling and any material join. The questions this experiment will address are:

1. whether a capillary column could mechanically survive launch

2. whether gas will still flow as normal through the capillary

3. whether the retention characteristics of the column have been impaired

4. which column(s) are appropriate for the chosen application in MODULUS

In addition to survivability with respect to launch, there are many more parameters for qualification, for instance radiation, thermal and electrical properties must also be tested. Similar components present in other space missions may have already been space qualified, and hence may not need as thorough tests. For example, NASA's Cassini mission contains a GC-quadrupole mass spectrometer system for the analysis of composition of Saturn's system (e.g. Sternberg et al., 1999). The GCMS system is known to be in excess of 17 kg, and uses between 40 and 70 W, which is almost an order of magnitude greater than MODULUS. Discussions with the MODULUS team have indicated that no components within the science portion of the Cassini mission are utilised on MODULUS.

At the time of writing, there are no published data for space qualification or vibration testing of capillary columns.

3.1.2. Survey of gas chromatography - mass spectrometry in space

Although GCs and MSs are very often linked in terrestrial laboratories, their space heritage is less obvious. Many planetary explorers have previously flown GCs with non mass-specific detectors. Similarly, many probes have had mass spectrometers containing an inlet system that directly admitted the sample to the ion source, with no chromatographic separation. In many cases this would lead to confusion in the mass spectra, where isobaric species are interfering. Nevertheless, in some cases enough was known about the gas mixture that this confusion could be minimised.

Early manned spacecraft flights required the analysis of the build up of potential toxic gases in the closed systems of the capsules themselves. Gas Chromatography was first used in space in these systems, and also later used to examine and test systems which reportedly removed these mixtures from the closed cabin atmosphere (Toliver and Morris, 1966). The first use of GC on board a probe destined for another Solar System body were those used in the Viking landers in 1976. Later utilisation was on the Pioneer Venus mission in 1978, which had GC columns and

mass spectrometers, but not linked to each other. Later Soviet missions to Venus (Venera and Vega) also carried GC systems.

The only coupling of GC columns to mass spectrometer inlets have been in the Viking Landers (Biemann et al., 1977) and the Cassini-Huygens mission (Sternberg et al., 1999) launched in 1997. Within a few years (at the time of writing) Rosetta's MODULUS (and COSAC and CHARGE instruments (Raulin et al., 1999)) will join these two missions in having GC-MS systems although configurations, and target compounds, will be different.

Viking had two experiments that contained GC units: the GC-MS experiment and the Gas Exchange experiment. Viking's goal was to identify the compounds present in the atmosphere on Mars and evolved compounds from pyrolised or heated soil. The mass spectrometer was of sector type, using H_2 as a carrier gas through the packed 2 m column (Biemann et al., 1977). As organic analysis was the major investigation, the stationary phase[4] (polymetaphenoxylene on 2,6-diphenyl-*p*-phenylene oxide, or poly MPE-Tenax) enabled separation of alcohols, hydrocarbons and amines. The choice of stationary phase also maximised the separation of water and CO_2 from organic compounds, and was designed to be mechanically and thermally compatible with space flight. Scanning by the MS was undertaken every 10 seconds, with a mass range m/z 10-220 and a resolution near 200. Temperature programming was required so that the volume of data recorded was minimised, as little tape recorder space was available. The column was held at 50°C for 10 min and ramped to 200°C at 8.3°C/min, and held at this temperature to the end of the analysis. The holding period could be switched between 18, 36 or 54 minutes. No organic compounds of martian origin were found at detection limits of ppm.

The scanning mass spectrometer also had an inlet to allow sampling of the Martian atmosphere directly, as an ion pump was present to maintain vacuum. Valves opened from the atmosphere into a sample chamber, where optional scrubbers in separate cavities could remove two problematic compounds (Owen et al., 1977). Magnesium perchlorate was used to remove

[4] Material that enables separation of compounds. See 3.2.1 for details.

water, while carbon monoxide was oxidised to CO_2, and absorbed by LiOH which also removed ambient CO_2. The removal of CO was to eliminate the risk of isobaric interference when analysing for the presence of nitrogen. Results from the instruments showed the atmosphere being made up primarily of CO_2 (95%), with N_2, Ar, O_2, CO and H_2O as minor constituents, while trace compounds included Ne, Kr, Xe and O_3 (Owen et al., 1977). Thanks to this instrument, the correlation between Martian atmosphere and glass inclusions within SNC meteorites gave evidence that these meteorites must have had Mars as the parent body (Bogard and Johnson (1983), Becker and Pepin, ((1984)). This has sparked debate whether the organic compounds and microscopic fossil-like features found in the Martian meteorite ALH84001 could have been formed from biogenic processes on the Martian surface (McKay et al., 1996). Another view is that they could have originated from contamination while on Earth (Becker et al., 1997).

Viking's other GC unit was part of the Gas-Exchange eXperiment (GEX) (Oyama and Berdhal, 1977). The purpose of this experiment was to examine if any changes occurred in the concentration of metabolic gases above a soil sample. The soil was treated with a nutrient solution or was incubated with humidity. Any terrestrial microbial activity would of course metabolise the nutrients and produce waste gases. The gas detection system involved coupling two packed columns (containing Porapak Q) with a thermal conductivity detector (including one gas stream as reference for the Thermal Conductivity Detector, or T.C.D.) with helium as carrier gas. Operating conditions were set to 13.5 ml/min at 24°C, giving rise to good separation of permanent gases: H_2, N_2, O_2, Kr, CO_2, CH_4. The experiment found that N_2, CO_2, O_2, and Ar were evolved on addition of water (with and without nutrient) to the soil samples. Oxygen evolution was associated with decomposition of superoxides (of Group I & II elements) within the soil. N_2, CO_2, and Ar were thought to originate from soil desorption caused by water vapour. Subsequent CO_2 evolution from recharges were thought to be form oxidation of organics present in the nutrient by Fe_2O_3 in the soil.

During December 1978 many probes, US and Soviet, entered the Venus atmosphere. Five mass spectrometers and two GC systems were sent to study the upper atmosphere and the lower atmosphere including the surface. Mass spectrometry of the upper atmosphere was carried out on the US Pioneer probes, where the atmosphere directly entered the ion source of the MS unit (Hoffman and Hodges, 1980). The relative pressure was low enough for this to work efficiently (in the region of 0.1 bar). In the lower atmosphere this was not possible as atmospheric pressure increased up to 100 bar. The pressure drop required (up to 10 orders of magnitude) for the MS was provided by a leak, so that samples entered the ion source at manageable 10^{-5} mbar region (the MS was actively pumped). Pioneer's GC system consisted of packed GC columns with Porapak N and poly-divinyl benzene respectively as the stationary phases (Oyama et al., 1980). The instrument was a modified version of that flown on the Viking's GEX, and used helium as a carrier gas. The detector was a T.C.D. and the mode of operation was isothermal at two temperatures; 18 and 62°C. The system was able to inject the atmosphere and sample it directly. The Venusian atmosphere was constantly purged through a sample loop attached to a valve arrangement similar to a 6-port system. Hence switching the valve caused sample gas to enter the column, similar to the MODULUS laboratory analogue described in this chapter. Again, using this column arrangement allowed the separation of permanent gases.

The Soviet Venera probes contained both GC instruments and mass spectrometers. The GC instrument was called Sigma, in which 3 packed columns were placed, each contained a polysorb molecular sieve stationary phase (Gelman et al., 1980). These could be placed in series or parallel depending on the mode of operation, and were used isothermally at 70°C. The detector used was a Neon Ionization detector. The results from Pioneer's and Venera's mass spectrometers and GC systems were broadly comparable, all giving N_2 (2.5-4.5%) as the next major species in the CO_2 atmosphere, with minor constituents of He, Ar, O_2, CO, SO_2, H_2O, Ne and Kr also being detected. Technology used in this experiment was later modified for the Vega mission in 1985, where again 3 columns were packed with Porapak QS + N and Porapak

T (Mukhin et al., 1987). The detectors on Sigma-3 were a helium ionisation detector, a T.C.D. and two electron capture detectors (E.C.D.) in parallel.

With this being the current complement of planetary explorer's GC instruments, it will be interesting to see the results from Cassini-Huygens as it has the first ever capillary column used in planetary exploration. Cassini's GC-MS system carries three columns; a carbon molecular sieve packed column for the analysis of volatiles, a capillary column for light hydrocarbons up to C_3, and a second capillary column for heavier hydrocarbons and nitriles (Sternberg et al., 1999). A packed column was chosen over the more standard PLOT (Porous layer open tubular) capillary column for the analysis of volatiles, probably due to the thinking at the time that PLOT columns were not suitable in space due to poor mechanical stability. Any vibrations can loosen the particles (even handling in terrestrial laboratories) present in the columns, and hence block gas flow and cause retention characteristics to be compromised.

For GC-MS units in future missions the choice of column type and phase is now limited by other means. A packed column would need greater head pressure for comparable (to a capillary column) chromatographic separation, a longer analysis time per sample. MODULUS could not use any packed columns as carrier gas pressure would need to be greater or equal to the maximum supplied by the tank regulator. Flow rates also need to be greater for optimum separation (of the order of 20 ml/min), leading to the selection of a different detector, as ion traps cannot trap effectively at such flow rates.

3.2. The theory behind Gas Chromatography

A mixture of chemical species can be separated by an array of techniques; some require a chemical change of the compounds and others utilise purely physical processes. Chromatography is the method whereby a mixture of components can be separated by distributing these analytes between two phases, one mobile and the other static. The *mobile* phase (e.g. a solvent) moves in one direction in contact across the *stationary* phase. The mobile phase can be any fluid, whereas the stationary phase can be a solid, liquid or even a gel. In gas

chromatography, the mobile phase is known as the carrier gas, and is usually hydrogen, helium or nitrogen. This section explains the nature of the separation process, and illustrates the ability for chromatography to be fundamental in analytical science.

3.2.1. Partitioning of components

To demonstrate the separation process, one can imagine a mixture of two compounds entering a GC column in one ideal pulse. Consider the situation when component *A*, which does not interact with the column coating and a second component *B*, which does. Both *A* and *B* are forced through the column by the carrier gas. The relative concentrations of these components at certain times across the column can be shown by the simplified view in Figure 3.1.

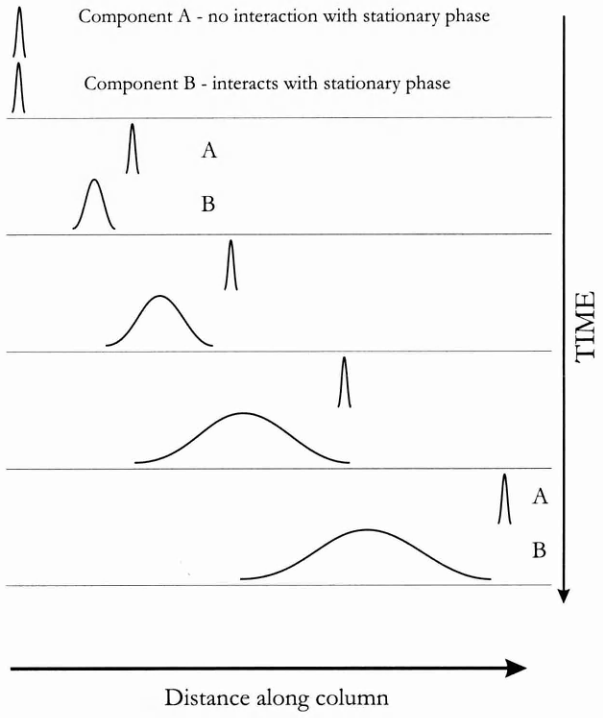

Figure 3.1 Schematic representation of the partitioning between mobile and stationary phase, with two differently interacting components

Component *A*, as it travels nearly same speed as the carrier gas, shows its concentration as a gaussian across a portion of the column. The gaussian shape is due to diffusion of the gas pulse while travelling. Component *B*, having an interaction with the stationary phase, spends a portion of its time in the phase. Its concentration profile along the length is also a gaussian

curve, but its width is far greater. When eluted, this results in a greater temporal width compared to the peak of component *A*. On examination of peak maxima, one finds they are at different points along the column, giving rise to separation. The degree of separation varies with a number of parameters, including column temperature, carrier gas flow rate, and stationary phase material.

The interaction between analytes and the stationary phase is a process called *partitioning*. Each component's molecules passing through a capillary column will adsorb on to, and desorb from, the stationary phase repeatedly. While in the mobile phase the components travel mostly at the same velocity, but with some small variation. When in the stationary phase, the molecules are motionless with respect to the column. All the solutes spend an equal amount of time in the mobile phase, but different solutes can spend different amounts of time in the stationary phase. Those species highly attracted to the stationary phase (strongly retained) will spend a longer time in the column than those that have a lower attraction (weakly retained) will. The weakly retained compounds will come out of the column (elute) earlier than the strongly retained compounds.

The degree of interaction between the analyte and stationary phase can be expressed in terms of the *partition coefficient*, K, as the ratio between the equilibrium concentrations of a solute in the stationary and mobile phase during the partitioning process:

$$K = \frac{c_S}{c_M} \tag{3.1}$$

where c_S and c_M are the equilibrium concentrations in the stationary and mobile phases respectively. The value of K is dependent on the temperature and the stationary phase itself. A higher value of K implies a greater affinity for the solute with that specific phase at a specific temperature. On sending a mixture of analytes through a GC column differences in physical (including isotopic differences) and chemical properties of the components result in each having a different value of K, giving rise to separation from each other.

3.2.2. Retention and resolution

In general analytical chemistry, one tries to aim for the sharpest peak possible in the GC chromatogram, so that closely eluting peaks appear distinctly with no overlap. This maximises the signal to noise ratio, and increases the potential of detection of minor components.

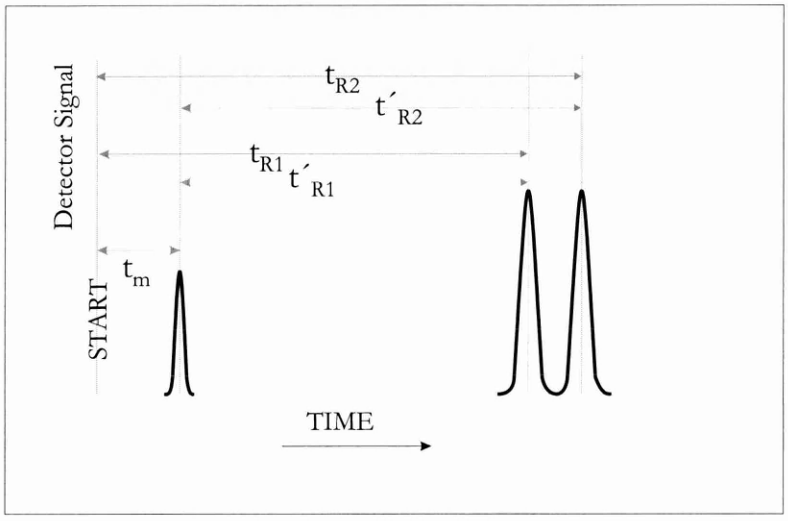

Figure 3.2 A typical chromatogram, with one non-interacting component, and two differently interacting components

In Figure 3.2, a hypothetical mixture of three components is injected onto a GC column simultaneously. Two of the components interact with the column, and one does not. The component that elutes first did not interact with the stationary phase, is not retained, hence it has a partition coefficient of zero. Little peak broadening is observed with this compound as a result of transport down the column. The two other peaks elute sometime later and are separate (each having different values of K), and are perfectly *resolved*, i.e. it can be seen that the end of the first peak and the start of the second do not overlap. The time taken for each peak's maxima to elute from the column is termed the *retention time*. The retention time of a compound is measured and can lead to identification of the individual species when non-specific detectors (e.g. flame ionisation detector, or F.I.D.) are used.

Another measure of retention is to calculate what fraction of time a compound spends in the *stationary* phase of the column. This is termed the Retention Factor (k). To calculate this factor, one needs to know how much time components spend in the *mobile* phase. This time is the

same for all compounds, as they all travel at the same rate as the carrier gas, and is termed the *gas hold up* time. In Figure 3.1, this is the time taken for the first peak (t_m) to elute. In many columns methane is used due to its insolubility in the stationary phases used for organic analyses[5]. The retention times of two retained peaks are described as t_{R1} and t_{R2}. The time differences between each peak and the unretained peak (t_m) are then defined as t'_{R1} and t'_{R2}. The retention factor, k, is therefore given by:

$$k = \frac{t_R - t_M}{t_M} = \frac{t'_R}{t_M} \tag{3.2}$$

The retention factor gives relative information on a peak's retention, not absolute information. Other retention measures (e.g. retention indices) can be created but are beyond the scope of this thesis.

The separation of any two peaks can also be measured. Due to the width of peaks it is possible (and common) that two peaks may be separated, but not *resolved*, i.e. the peaks may still overlap. The absolute separation is the time difference between two peak maxima, in the above example this is (t_{R2} - t_{R1}). A relative amount of separation can also be described as the separation factor, α;

$$\alpha = \frac{k_2}{k_1} \tag{3.3}$$

where k_2 and k_1 are the retention factors of the first and second peak respectively.

Two peaks can be said to be completely resolved if there is baseline separation between them. Resolution (R) can be measured by;

$$R = 2\left(\frac{t_{R2} - t_{R1}}{w_{b1} + w_{b2}}\right) \tag{3.4}$$

[5] Unfortunately for volatile gas analysis columns, methane *is* retained; and even noble gases have some retention. This means any measure of t_m to be an estimate

where w_{b1} and w_{b2} are the width of the first and second peaks (in units of time) at the base of the peak respectively. A resolution of 1.5 or greater would imply there was baseline separation of the two peaks. Any lower value would imply peak overlap. This would introduce errors if one used integrated area as a method to determine relative amounts. It is of paramount importance for stable isotope mass spectrometry that peaks do not overlap.

Other measures of peak separation are also used. Percent resolution (%) is calculated as the ratio of the valley height to the total peak height. One can also measure the dispersion of the peak from the statistical nature of the Gaussian peak shape. Resolution of 1.5 would be equal to 6σ where σ is the standard deviation of a Gaussian distribution.

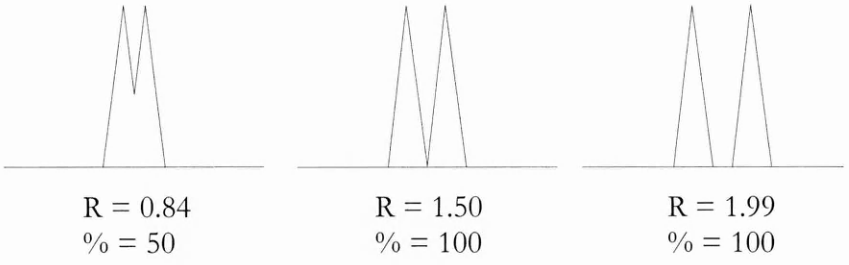

Figure 3.3 An illustration of peak resolution in terms of R, and percent resolution, from the overlap of two identical peaks with different retention times. R = peak resolution, % = percent resolution

3.2.3. Column efficiency

As stated previously, it is almost always advantageous to have sharp peaks when compounds elute from capillary columns. A column that produces sharper peaks (under identical conditions) is said to be more efficient for a particular analyte. The efficiency of a column can be measured in terms of the number of *theoretical plates*. The concept of the theoretical plates is made in comparison to distillation columns, where a column with more (physical) plates present produce fractions with better separation of closely boiling substances. The number of theoretical plates in the column (N) can be calculated from a peak's retention time (t_R) and standard deviation (σ) from the equation:

$$N = \left(\frac{t_R}{\sigma}\right)^2 = 16\left(\frac{t_R}{w_b}\right)^2 \qquad (3.5)$$

The smaller the width of a peak, the smaller the standard deviation, leading to a higher value of N. The value of N does not take into account the gas hold up time. For peaks with a small retention factor, the value of N will be high, although the retention by the column was small. For these peaks, the *effective* number of theoretical plates can be used, N_{eff}. This is calculated in the same way as in equation 3.5, but t_R' is substituted for t_R. The total number of plates in a column is dependent on the length of the column, so a measurement independent of column length is useful. This concept is called the *plate height*, and is the equivalent to the distance along the column occupied by one theoretical plate, and is calculated by,

$$H = \frac{L}{N} \qquad (3.6)$$

where L is the length of the column. A smaller number for H, implies a higher number of N, therefore sharper peaks.

3.3. Gas Chromatography in practice

For Gas Chromatography, two types of stationary phase are used; packed columns and wall coated capillary columns. Packed columns are short (order of 1 m) lengths of $^1/_4$-$^1/_8$ inch steel or glass tubing containing a solid which can continuously absorb and desorb gases passed over it. Zeolites are common materials for this purpose. Capillary columns are longer lengths (10 to 30 m) of fine, flexible fused silica (or deactivated stainless steel) tubes with diameters of <1 mm. Capillary columns contain similar materials for the separation of the gases, but these must be bonded to the inside of the silica tube resulting in a very fine layer of material. Recently, manufacturers have created capillary columns that now contain packed material instead of a bonded compound. These columns have particularly high number of theoretical plates but require very high head pressures for operation which are out of the scope for MODULUS.

GCs are rarely used in isolation; rather a detector is usually connected to the outlet which records the time taken for the components of a sample to emerge. Many GCs are connected to non-mass selective (and inexpensive) detectors e.g. Flame-Ionisation Detector (F.I.D.) and Electron-Capture Detector (E.C.D.), which measure retention time vs. signal strength. Identification of individual compounds is done by comparing chromatograms to reference ones made under similar, if not identical conditions, with known standard mixtures. This may cause problems, as some interpretation (or even re-calibration) maybe needed if a sample was analysed under non-standard conditions. Alternatively, mass spectrometers can give detailed mass spectra to show the molecular weight of sample compounds. Isotope Ratio Mass Spectrometry (irMS) cannot alone give identification of compounds as preparative chemistry changes the chemical composition of a species to a specific target analyte e.g. combustion of organic matter to CO_2 in carbon isotope analyses. If necessary, Ion Traps or quadrupole mass spectrometers can sample a part of the gas stream entering an irMS, which can then give additional identification of the original sample compounds. Alternatively, a small portion of the original sample would be analysed independently by GCMS, then a larger portion by irMS.

3.3.1. Stationary phase types

Today's most common stationary phases for capillary columns are polysiloxanes with a variety of functional groups. These are optimised for high molecular weight hydrocarbon analyses, which is the most widespread GC application. Common functional groups utilised are methyl, phenyl and cyanopropyl groups. MODULUS requires volatile gas separation, which needs a different type of phase. Volatile gas separations can be undertaken by molecular sieves or zeolites, or alumina-based columns. These phases act as adsorbents and are given the title of PLOT (Porous Layer Open Tube) columns. The term open-tube designates an open-tubed capillary as opposed to packed capillary column. A porous layer is etched on or in the column before adding the coat of polymer. The porous layer itself also acts as a stationary phase, since particle size and shape can increase the selectivity of specific compounds. Due to the etching process, PLOT columns are percieved to be structurally weak, and manufacturers request that

on installation of such a column into a GC system, no mechanical stress, strain or vibration is applied to the column.

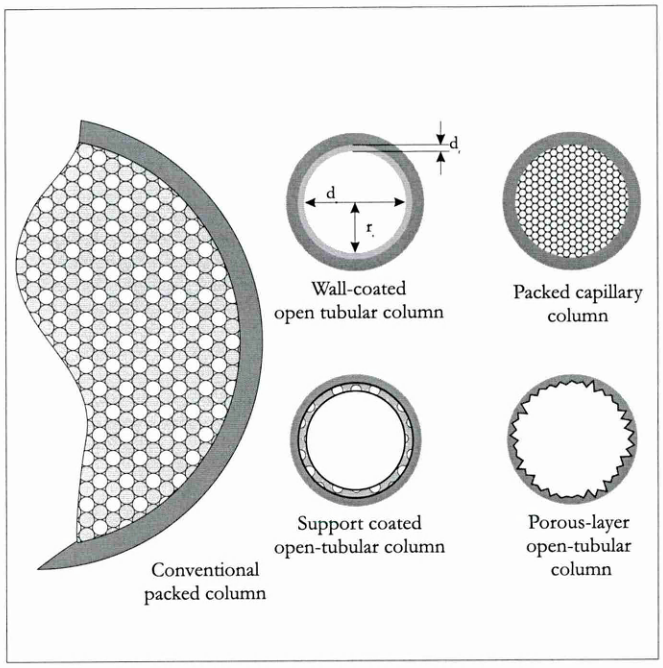

Figure 3.4 Types of open-tubular columns with size comparison to a packed column. Open tubular columns have a diameter near 1mm, while packed columns generally have a diameter of 3-10mm.

Other types of columns include Wall-Coated Open-Tube (WCOT) which are the most common. A thin film of the phase, usually polysiloxane based, is coated onto the inside of the column wall. The film thickness will have an impact on the retention capability, as a thicker film gives a larger total volume for the distribution of solute, which would make an analyte take more time for equilibration. Columns with thicker films would also result in longer retention times per analyte, but decrease the column efficiency. Films are generally <1 μm thick, as thicker films are unstable with respect to forming droplets.

Packed capillary columns are the capillary equivalent to packed glass or steel columns, and display similar properties. Flow dynamics of gas within these columns is different due to obstructions within the flow path. These columns are not yet widely commercially available, and are currently used as a research tool (e.g. Shariff et al., 1996). Support coated open-tubular columns are so-called as instead of a thin film of stationary phase, a support is finely dispersed

onto the column wall. Similarly to PLOT types this gives greater phase volume and stability is improved.

3.3.2. Pressure drop and gas velocity

In order that any gas may flow, there must be a pressure drop along the length of the column. The conditions of gas flow are controlled by the difference in absolute pressure between the entrance and the exit of the column. A greater pressure drop along the column creates an increase in the average flow rate of the carrier gas. A faster flow rate reduces the time taken for components to elute, but this has a drawback; the components may not have spent enough time in the stationary phase to achieve separation and resolution. Conversely, if a flow rate is so low that molecular diffusion then dominates, peaks appear to be very wide, and resolution is lost. Therefore, it follows that there must be an optimum flow rate for the carrier gas, to maximise the efficiency of the column. The optimum velocity is dependent on the solute, carrier gas, column temperature, dimensions, and stationary phase.

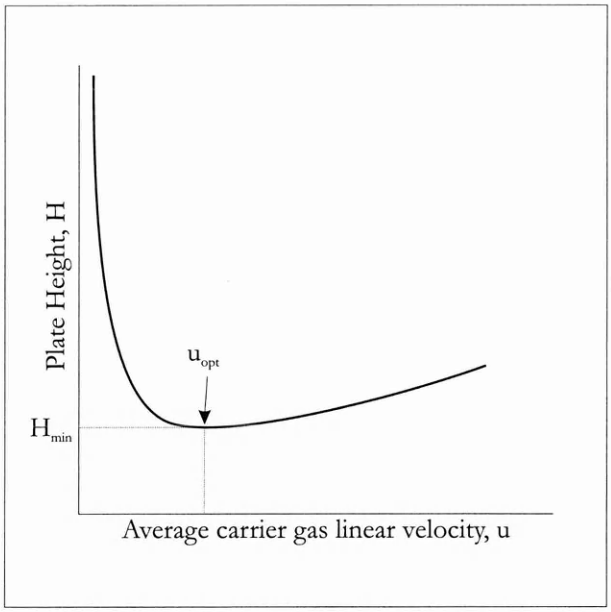

Figure 3.5 Curve of plate height vs. average (idealised) carrier gas velocity along the column (known as the Van Deemter plot). The minimum plate height corresponds to the most efficient flow rate of the column. H can be expressed in mm, and u in cm/s

From Figure 3.5, plate height is shown against carrier gas velocity. The lower the plate height is, the more efficient the column is, such that the minimum value corresponds to the optimal carrier gas velocity. Plate height is calculated in theory by use of the Golay equation:

$$H = \frac{B}{\bar{u}} + C \cdot \bar{u} \tag{3.7}$$

where $\bar{u}$ is the carrier gas average velocity, and B and C represent the contributions from longitudinal gas-gas diffusion and resistance-to-mass transfer, respectively. Both of these processes lead to band broadening in open-tubular columns. The values of the terms B and C are affected by the physico-chemical properties of the solute, the carrier gas and the stationary phase. The discussion of the equations describing these terms is beyond the scope of this thesis.

In practise, the carrier gas linear velocity is set to be 1.5 to 2 times the optimum velocity, since little efficiency is lost but time is saved in the analysis. An added advantage is that if the velocity is set to above the optimum, any minor variation in velocity (e.g. as a result of temperature programming) will not result in loss of separation. The gradient of the curve in Figure 3.5 implies that below the optimum velocity separation will be impaired. Different carrier gases have different Van Deemter curves (as seen in Figure 3.6), with H2 having the greatest efficiency at the highest flow rate. Unfortunately, H2 comes with safety considerations making it unsuitable for MODULUS.

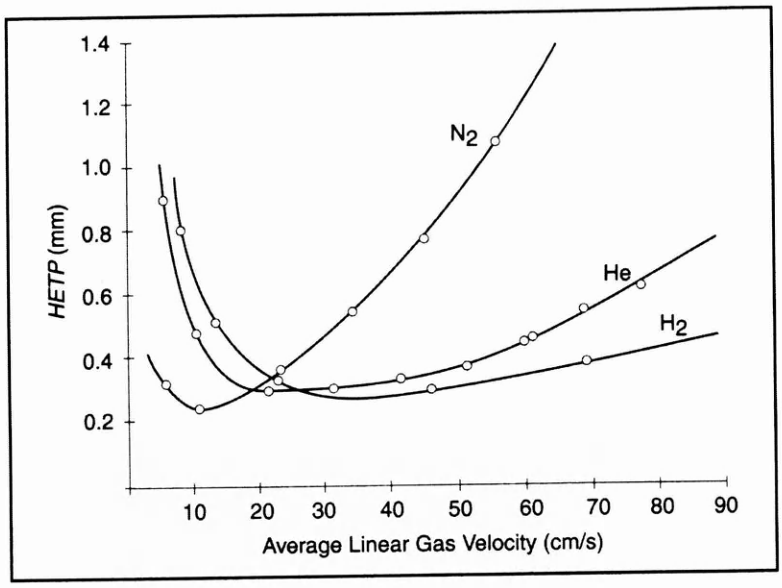

Figure 3.6 Van Deemter plots for N_2, H_2, He for n-heptadecane at 175°C. Column used: 25m x 0.25mm i.d., 0.4μm OV-101 methylsilicone on fused silica. Source: Hinshaw and Ettre (1994)

The pressure drop across a column is defined as the pressure difference between the entrance and exit of the column. Carrier gas pressure is set via a regulator upstream of the column. At the exit of the column is a detector, of which most types (e.g. F.I.D. and T.C.D.) are at atmospheric pressure. Mass spectrometers are a special case, as the column exit reaches into a chamber at vacuum. Therefore in both cases, the exit pressure is fixed, and one can only *control* the pressure *drop* by adjusting the head pressure of the carrier gas supply.

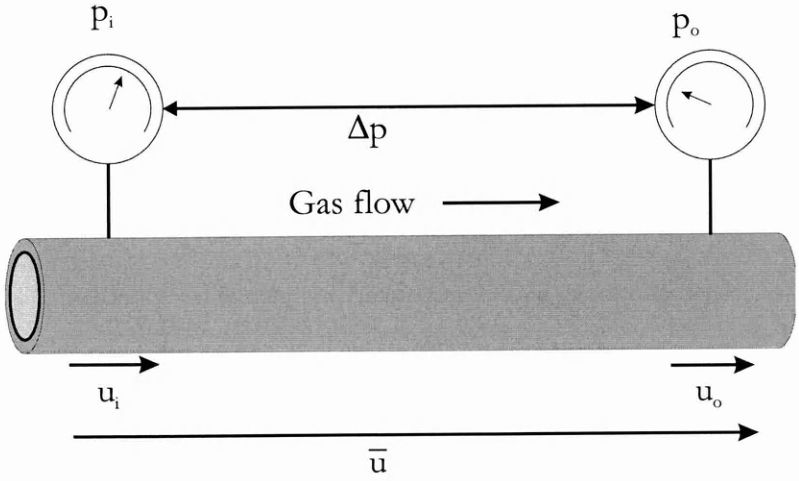

Figure 3.7 Illustration of the pressure drop along an open-tubular column, where p_i is inlet pressure, p_o is outlet pressure, Δp is pressure drop, u_i is inlet velocity, u_o outlet velocity, and u (barred) is mean velocity.

Table 3.1 Pressure terms and descriptions

Term	Symbol	Description
Inlet pressure	p_i	Absolute column inlet pressure
Ambient pressure	p_a	Absolute atmospheric pressure
Outlet pressure	p_o	Absolute column outlet pressure; T.C.D. $p_o=p_a$, MS p_o=zero
Pressure drop	Δp	Drop across column $\Delta p= p_i-p_o$
Relative pressure	P	Inlet pressure relative to outlet; $P=p_i/p_o$

On the GC Ion trap system (Figure 3.9), there was a mass flow controller, set to 1 standard c.c. per minute (sccm), and a clockface gauge located downstream, to measure pressure at the head of the column. As p_o in the Ion Trap Detector is near zero (10^{-3} mbar) there was another requirement that the inlet pressure of the column must be greater than 1 bar (otherwise there is great potential for air to leak into the column inlet). To minimise atmospheric leaks the inlet pressure (and hence gas flow rate) had to be increased, such that the GC columns properties were being measured to the right of the Van Deemter curve. It was not possible to use the columns at the optimal velocity.

3.3.3. Column Conditioning

Before first use, and whenever a column had been unused for some time, it required conditioning. A typical conditioning process involves gradually heating the column (with carrier gas flowing through) to its maximum operating temperature (typically 300°C), and holding that temperature for a few hours, then cooling to room temperature gradually. This process minimises the baseline signal due to column bleed at the detector. All the columns were conditioned prior to testing.

3.4. Laboratory procedures

3.4.1. Experiment summary

The analogue of the MODULUS sample analysis system (as introduced in Chapter 2) consists of a GC oven (Varian 3400) coupled via a standard transfer line to a commercial Ion Trap detector (Finnigan MAT ITD 700). The overall experiment is described in greater detail in section 3.4.3.

Several columns were shortlisted to be tested for the four properties as mentioned in section 3.1.1. Instead of using a full size 30 m columns, 10 m portions were used, to examine if separations could be affected with these shorter columns, potentially saving space and mass for the spacecraft instrument. A gas mixture (Alltech) containing CO_2, CH_4, CO, N_2, O_2, H_2 and He was injected using a 6-port valve, with the ITD measuring elution time and peak separation. Isothermal injections were repeated at various temperatures, ranging from -30° to +30°C. Sub-ambient temperatures were attained by using a liquid nitrogen cryogenic facility fitted to the GC oven.

Better separation of components mean the column is of greater benefit to MODULUS. Separation of components without requiring cooling to -30°C is also an advantage as this extends the useful lifetime of the mission. The testing temperature range mirrors the expected operation temperature. The separation of CO_2 and CH_4 is crucial for isotope ratio measurements by the MODULUS ion trap. Also required is the separation of N_2 and CO, both of which have the same molecular mass.

Once GC retention was determined, the columns were vibration tested to simulate an Ariane V launch. On return, columns were re-conditioned and the above procedure was repeated to note any change in retention behaviour.

3.4.2. Vibration Experiment details

The vibration facility available to MODULUS was based at the Rutherford Appleton Laboratory (RAL) in Oxfordshire, UK. RAL are partners in the MODULUS programme.

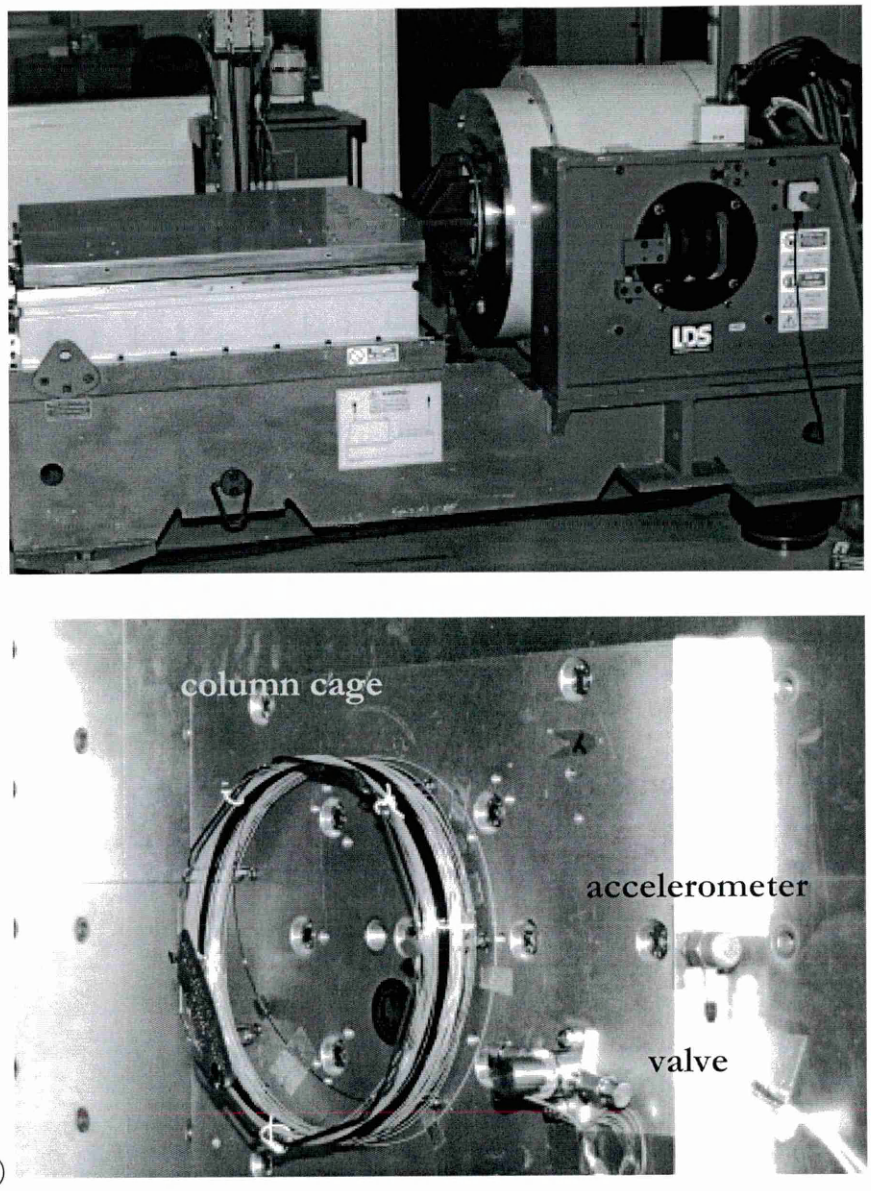

Figure 3.8 (a) the vibration unit placed for vibration in the x-direction, (b) the GC columns on a column cage mounted on the baseplate

The columns were mounted on an aluminium baseplate (approx 50x30x3 cm) which was bolted to the vibration table. A capillary column cage (Finnigan MAT, diameter 20 cm) was used to hold two columns at once and was screwed to the baseplate, on which other MODULUS components (valves) were also attached. An accelerometer (Endevco type 7254A-100) was used to feedback to the control equipment to measure instantaneous acceleration. Two separate sweeps were used, a sinusoidal acceleration[6] peaking at 20g and a random noise sweep, set to 20 g r.m.s. with a peak of 60 g. Frequencies ranged from 5 to 150 Hz for the sine sweep and 20

[6] The term g used here is in reference to multiples of Earth's acceleration due to gravity

to 2000 Hz in the random test. Maximum travel of the unit was 20.5 mm. Both sweeps were repeated a further two times as the baseplate was re-oriented so vibration occurred in each of the three spatial dimensions. These test specifications are given in ESA document RO-EST-RS-3002/EID A, Issue: Draft 2. The vibration test was referenced as AIV-98-055-VIB (RAL internal report).

3.4.3. Laboratory analogue of MODULUS

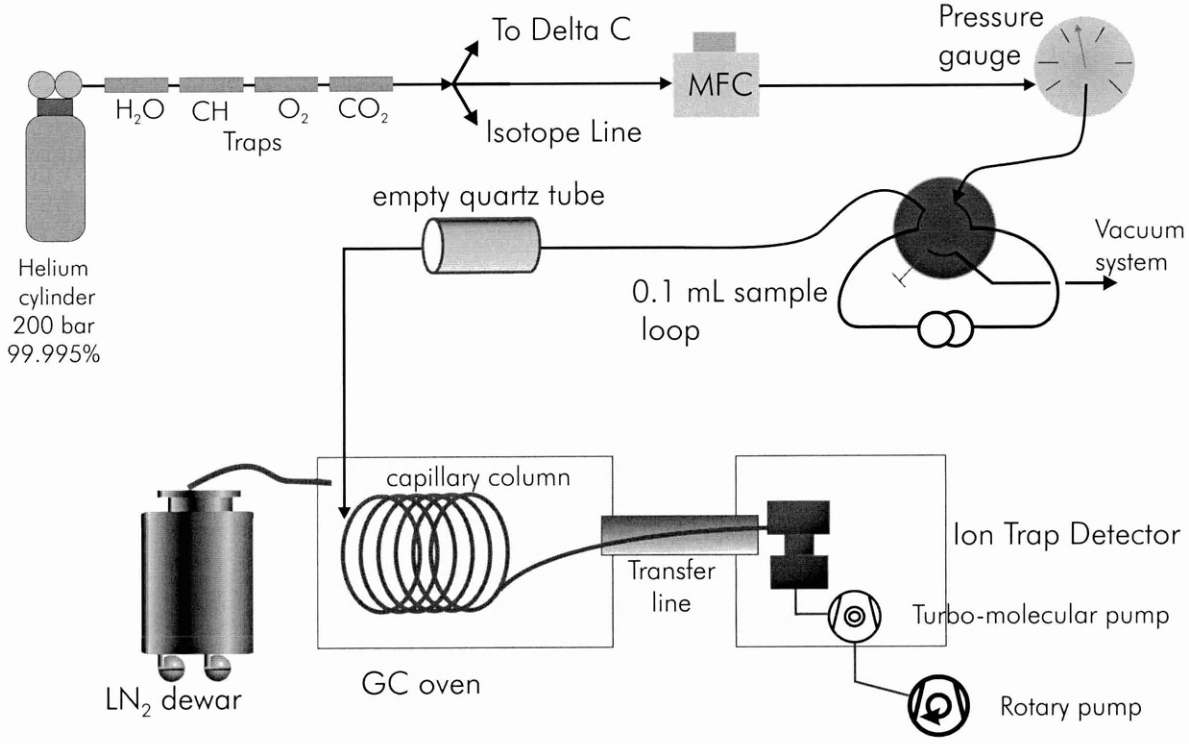

Figure 3.9 Schematic diagram of the GC, Ion Trap and injection system used for chromatographic column testing

A schematic representation of the GC-ITD system is shown in Figure 3.9. The helium cylinder (200 bar, 99.995% purity) was set to 4 bar on the outlet of the regulator. Downstream, there were 4 carrier gas purifiers, comprising of a water trap, a hydrocarbon trap, an oxygen trap (all from Alltech) and finally a CO_2 trap/getter (GC50 - SAES). Flowing purified helium was split into 3 paths via the use of Swagelok™ T-pieces (North London Valves {NLV}), 2 of which supplied gas to the isotope mass spectrometer system (sample and reference gas flows independent). A mass flow controller (Aalborg) could set a helium flow of between 0-10 sccm. A pressure gauge (zeroed at 1bar) was placed inline at this point. Further downstream was the

sample loop, a 6-port 2-way Valco switching valve connected to a vacuum line (Figure 2.5) where sample introduction took place.

Switching the Valco valve forced carrier gas through a 0.1 ml sample loop (Figure 2.7), carrying the gas mixture towards the GC. The junction between $^1/_{16}$" stainless steel tubing to <1 mm diameter fused silica capillary was made by a SGE zero dead volume union.

A transfer line connected the column exiting the gas chromatograph to the Ion Trap inlet. The capillary column passed through the heated transfer line, to a rubber seal on the edge of the Ion trap inlet. For accurate positioning of the end of the column inside the Ion Trap source, the GC end of the column needed 431 mm of column inside of the transfer line. Graphite Vespel ferrules (Scientific Glassware Equipment, Australia) made sure that once the nut was tightened the position was held until the column was removed. Inaccurate positioning of the column end reduces the efficiency of the electron-impact ionisation process, and had an effect on the performance of the ion trap.

A pressurised liquid N_2 dewar supplied a cryogen to cool the GC column to sub-ambient temperatures. A cryogenic on-off valve linked to the GC oven thermometer controlled the entry of N_2. Only a few minutes were required for the oven to cool to -30°C.

A Compaq 386 PC was attached to Finnigan MAT ITD 700 mass spectrometer, which contained the DOS-based Ion Trap Data System software. A description of the operation and features of ion trap mass spectrometry is presented in Chapter 2. Details relating to the operation of the Finnigan MAT ITD 700 and its ITMS software are given in Chapter 4.

3.4.4. Procedure

Each GC column was installed into the GC-ITD system in turn. The retention times of each component in the volatile gas mixture was recorded. The temperature of the GC column was varied between +30°C and -30°C and the dependence of retention time with temperature was noted. Each run was carried out isothermally. Each column was then vibration tested and

returned. The columns were re-installed into the GC-ITD and the gas injections were repeated over the same temperature range. The temperature of the transfer line linking the GC to the ITD was set to 50°C.

For GC tests the gas used was Scotty Mix 234 (Alltech) containing the following: 5% CH_4, 5% CO_2, 5% CO, 5% N_2, 5% O_2, 4% H_2, with helium making up the balance. The steel vacuum system allowed introduction of controlled quantities of gas into the manifold, where they were expanded to fill the sample injection loop of the Valco valve (see Chapter 2).

Before the 6-port Valco valve was switched, the data system on the Ion Trap was arranged to acquire spectral data and made ready for introduction of the sample. At injection, data collection was started, and the pressure of the gas in the sample loop was noted. In general, the 6-port valve was not switched back until the whole of the sample had been eluted and the peaks measured, as potential disruptions in the gas flow were found to impair peak shapes. As is shown in Chapter 5 this was particularly relevant when working with larger volumes.

Data were acquired by setting the ITD software to perform a full mass scan, from 10 to 90 a.m.u., with no minimum data threshold. Data collection was set to 2 scans per second, a frequency which was found to give sufficient definition of peaks without using excessive quantities of computer memory. The acquisition was stopped when the slowest component of the original mixture was eluted and detected.

Four columns were selected and tested:

- Hewlett-Packard PLOT Q
- Chrompack SilicaPLOT
- J&W Scientific CarbonPLOT
- Restek Molsieve 5A PLOT

Although all the columns were PLOT types, the Restek Molsieve column had molecular sieve 5A as the column coating, whilst the other 3 had the polymers in each of the columns' stationary phases (all different). Peak retention times were measured for the individual components in the

test gas mixture. The Ion Trap was unable to detect hydrogen and helium, but all the other components of the test matrix were detected.

3.5. Chromatography results

Results were collated to compare the behaviour of each column before and after vibration. Retention characteristics are also noted. A summary of the aims of the chapter and the associated results are shown in Table 3.2. A more detailed breakdown of the performance of the columns is given in the subsequent sections.

Table 3.2 Summary of all retention data gathered for the four columns tested. All results of characteristics shown are common for both before and after vibration testing

Characteristic	HP PLOT Q	Chrompak Silica PLOT	J&W Carbo-PLOT	Restek Molsieve PLOT
Physically survive vibration test	✔	✔	✔	✔
Gas able to flow through column post-vibration	✔	✔	✔	✔
CH_4 – CO_2 separated and resolved at 30°C	✔	✔	✔	no CO_2
CH_4 – N_2 separated and resolved at 30°C	✖	✖	✖	✔
CH_4 – N_2 separated and resolved at -30°C	just	✖	✔	✔
Volatile gas mixture: 5% N_2, 5% O_2, 5% CO, 5% CO_2, 5% CH_4, 4% H_2 (undetectable in ITD), 71% helium by volume. (Scotty mix 234)				
Vacuum injection system, using Varian 3400 GC and Finnigan MAT ITD 700 detector. 10 nanomole nominal injection size				

3.5.1. Hewlett-Packard HP PLOT Q (10 m, 0.32 mm i.d. column)

The retention times of CH_4, CO, CO_2, and N_2 over the required temperature range are shown in Figure 3.10. Figure 3.10 (a) shows the retention times determined before vibration, while Figure 3.10 (b) shows the retention times after vibration and reconditioning. On examination, no

discernible difference in retention times is notable, hence vibration caused no significant performance change. Peak widths were also similar before and after retention. No change was noted for the head pressure required for 1 sccm of He flow, which suggests that the stationary phase remained intact.

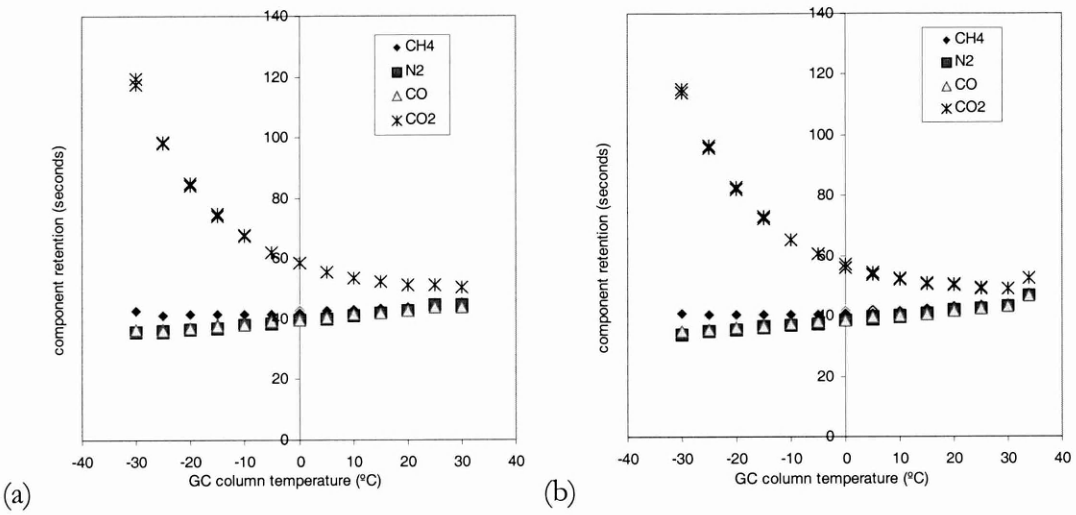

Figure 3.10 Retention characteristics for HP PLOT Q column (a) before vibration testing, (b) after vibration testing

As with all the columns tested, the retention time of most components changed with temperature. Carbon dioxide exhibited the longest retention time on this column, eluting last. It can be seen from Figure 3.10 (a) that the elution time of CO_2 varies from 50 seconds at +30°C to 120 seconds at -30°C. The elution time of N_2/CO decreased from 44 to 36 seconds as column temperature varied from +30°C to -30°C. The separation of CH_4 from N_2/CO is not apparent until a column temperature of -10°C, and is only just complete at -30°C. At 30°C, only two peaks were visible in the chromatogram (Figure 3.11 (a)).

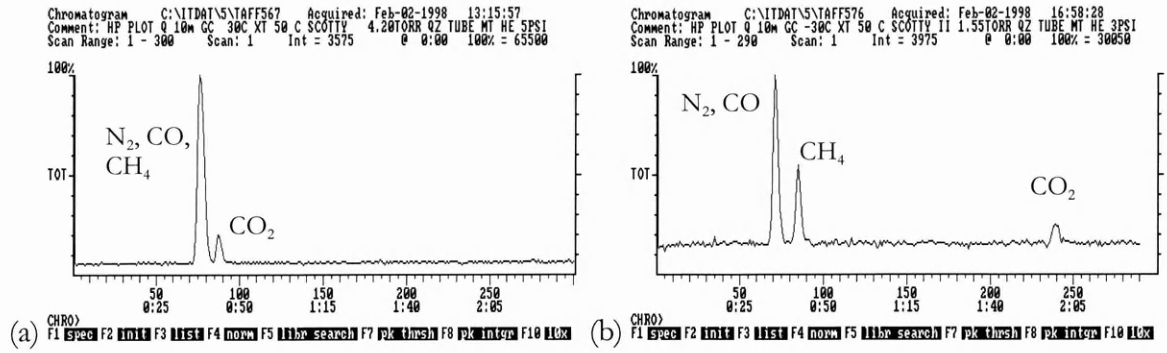

Figure 3.11 Chromatogram of HP PLOT Q before vibration at (a) 30°C and (b) -30°C

On decreasing temperature, the average velocity of the gas in the column increases, giving rise to shorter retention times for most components. However, cooling GC columns resulted in longer elution times, and greater separation, for components that interact with the stationary phase which in the case of CH_4 and CO_2 offsets the increase in the linear velocity. Of the unretained compounds, there was not a large change in the retention time with temperature from -30°C to +30°C.

At lower temperatures, the CO_2 peak eluted later and the CH_4 peak was distinct from the other components (Figure 3.11 (a)). Although the same molar quantity of CH_4 and CO_2 were inserted, the CO_2 peak is much smaller, illustrating a characteristic of the Ion Trap to be more sensitive to lower mass ions, as detailed in Chapter 2. The retention times of the compounds can be used to produce the separation factor (see 3.2.2) between CO_2 and CH_4, which is shown in Figure 3.12. The gas hold up time was taken to be the retention time of N_2. The figure shows no significant difference in the relative retention before or after the vibration.

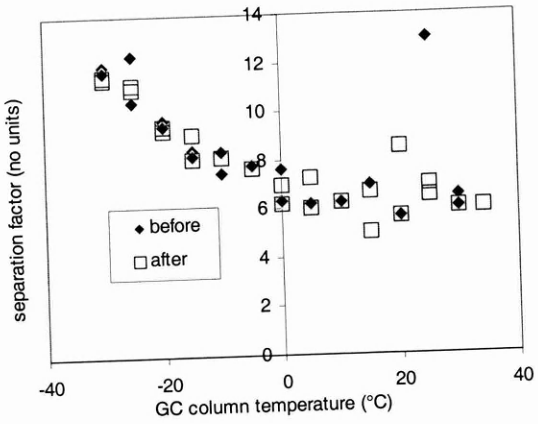

Figure 3.12 $\alpha(CO_2 - CH_4)$ with column temperature before and after vibration.

3.5.2. Chrompack SilicaPLOT (10 m, 0.32 mm i.d. column)

This column showed a unique retention capability for CO_2. As with the HP PLOT Q, CO_2 was retained while other components co-eluted at +30°C. Once cooled, the CO_2 elution time increased dramatically, but no other components were separated or resolved

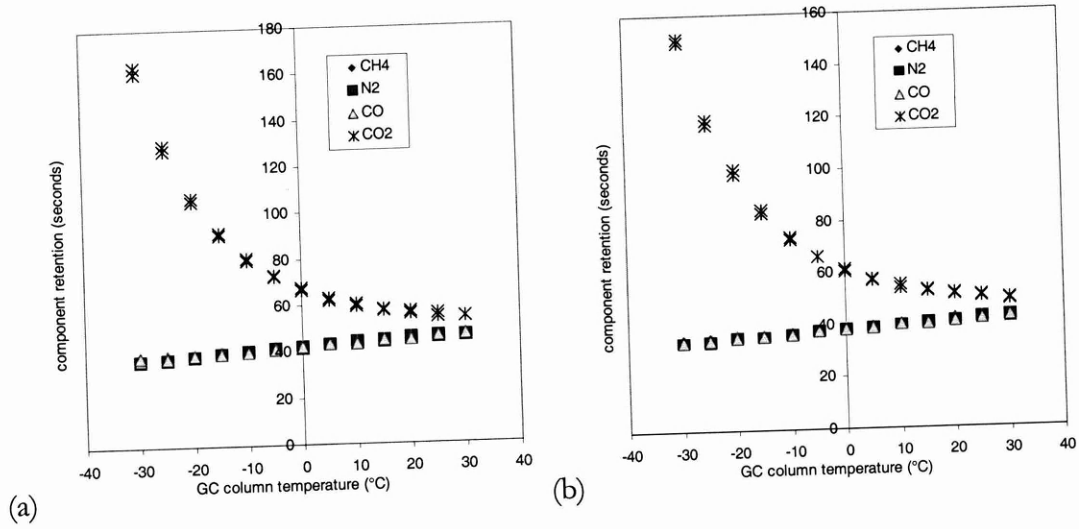

Figure 3.13 Retention characteristics for SilicaPLOT column (a) before vibration testing, (b) after vibration testing. CH_4 shared the same retention time as N_2

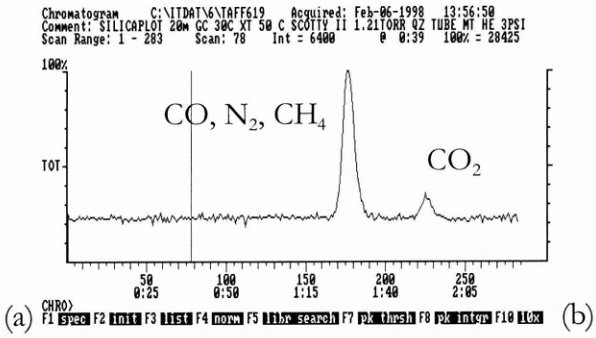

Figure 3.14 Chromatogram of SilicaPLOT at 30°C (before vibration)

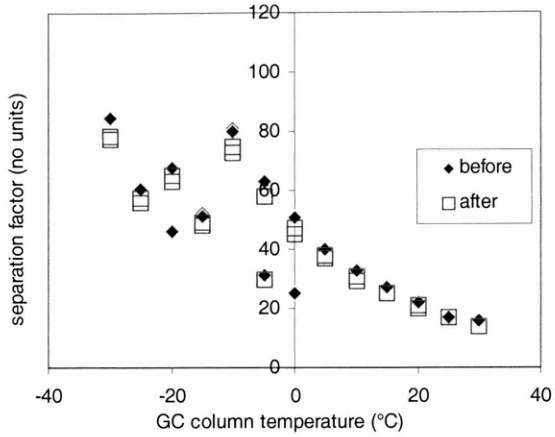

Figure 3.15 $\alpha(CO_2 - CH_4)$ with column temperature before and after vibration.

There was little significant change in the retention characteristics of the column after undertaking the vibration test. Although the retention times for most components decreased slightly, the separation factor between CH_4 and CO_2 (Figure 3.15) did not change significantly after the vibration test.

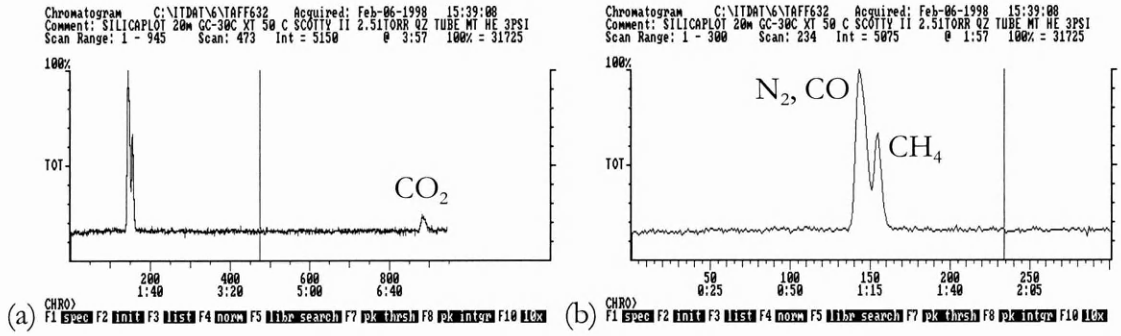

Figure 3.16 Chromatogram of SilicaPLOT after vibration at -30°C (a) the full chromatogram showing the large retention of CO_2, (b) the early part of (a) enlarged to show partial methane resolution

At -30°C the CO_2 eluted far later, 6 minutes after the other components. However, the CH_4 and the $N_2/O_2/CO$ peak was not resolved as seen in Figure 3.16

3.5.3. J&W Scientific CarbonPLOT (10 m, 0.32 mm i.d. column)

The CarbonPLOT column was generally similar in performance to the HP PLOT Q column, although it achieved greater separation of CH_4 from N_2 and CO +30°C. Once cooled to -30°C

the methane peak was quite distinct from the $CO/N_2/O_2$ peak (Figure 3.17). Compared to the HP PLOT Q column, CH_4 eluted with much greater separation, with 6σ resolution (between CH_4 and $CO/N_2/O_2$) occurring at -10°C. Based on the criteria of relative component separation, vibration did not affect the CarbonPLOT column performance, as shown in Figure 3.18.

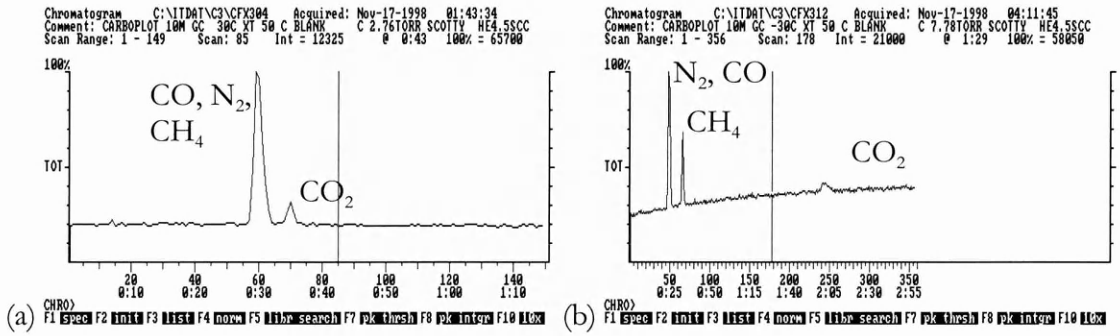

Figure 3.17 (a) Chromatogram of CarbonPLOT at 30°C showing separation of CO_2, (b) Chromatogram of CarbonPLOT at -30°C showing the separation of CH_4 and CO_2. Note the increase in the background, due to the change in viscosity of the carrier gas. Lower viscosity requires less pressure difference (Δp) needed to produce the same flow rate, and hence atmospheric air encounters less resistance to the column-ITD interface

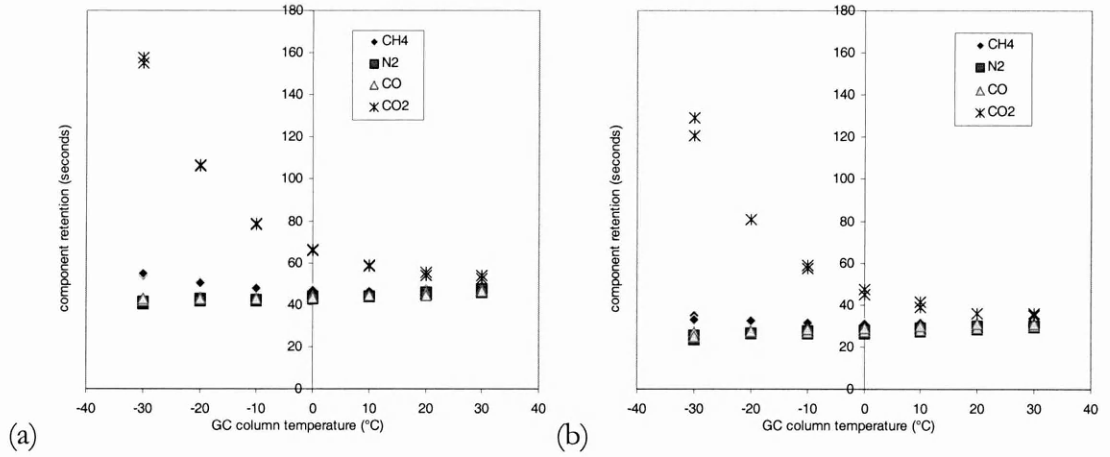

Figure 3.18 Retention characteristics for CarbonPLOT column (a) before vibration testing, (b) after vibration testing

It should be noted that the relative separation was not changed significantly despite the decrease in retention times during the re-testing experiment. As shown in Figure 3.19, the change in relative separation of $CO_2 - CH_4$, α, is very small compared to the change in retention time. A

small increase in α is seen at low temperatures after-vibration. On comparison of α of CO_2 – CH_4 with that of the HP PLOT column (Figure 3.12), the relative separation of both columns is similar. However, Figure 3.19 does not indicate the increased ability for methane resolution using CarbonPLOT. During the re-testing of the column, a large air background was noticed. Increasing the mass flow to greater than the 1 sccm optimum was the only way of increasing the column head pressure to a point such that the air leak was minimised. This eventually occurred at 4.5 sccm, giving a pressure of 2psi at room temperature. A month after these tests were conducted the Ion Trap was given a thorough component clean, was re-assembled and this problem did not re-occur. This is not related to the increase in background at seen at low column temperatures (as seen in Figure 3.17 (b))

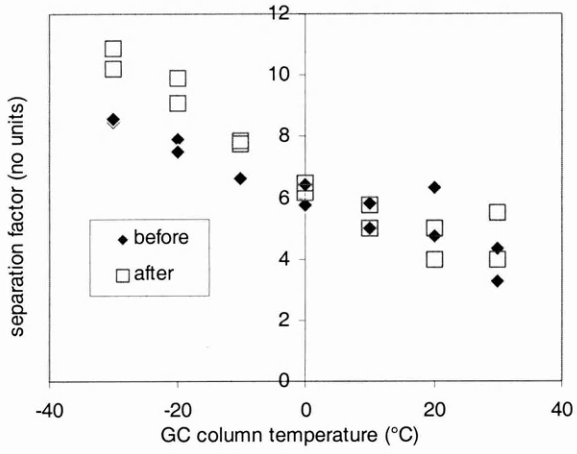

Figure 3.19 α(CO_2 – CH_4) with column temperature before and after vibration

3.5.4. Restek Corporation Molsieve 5A PLOT (15 m, 0.32 mm i.d. column)

This column had a molecular sieve as the stationary phase, and therefore exhibited different properties to other PLOT columns. An initial injection of the gas mixture was made after installation (GC at 70°C), and revealed the chromatogram in Figure 3.20 (a).

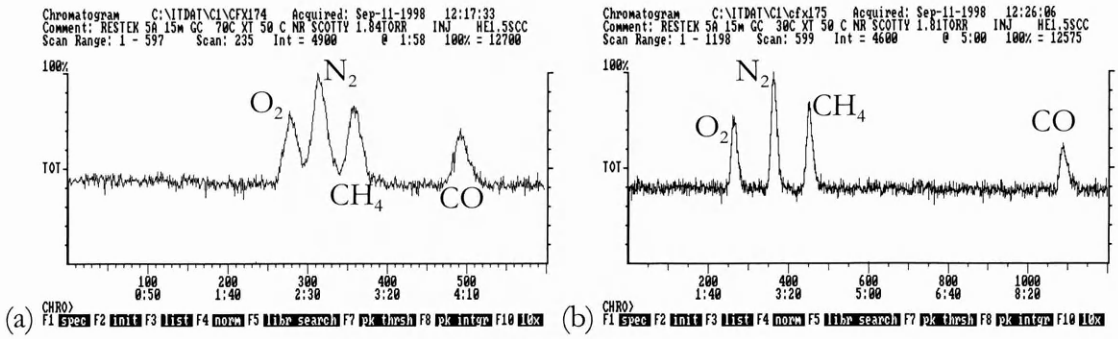

Figure 3.20 Chromatogram of test gas over Molsieve 5A column at (a) 70°C showing separation of CO, CH_4, O, N_2 but with low resolution (b) at 30°C showing the separation of CH_4 and CO, N_2, O_2 with each peak resolved

At 70°C, the O_2, N_2, and CH_4 peaks were not resolved at the 6σ level. At 30°C these peaks were separate and resolved. One noticeable feature is that CO_2 was chemisorbed on the column. As shown in Chapter 5, molecular sieves are used to remove contaminants from gas streams, of which Molsieve 5A is used to trap CO_2 at room temperature. Using the Molsieve 5A column (at 30°C), CO and N_2 were not co-eluted, hence the isotopic composition of CO and N_2 could potentially be measured separately with no isobaric interference from N_2. The retention time of CO was far greater than that of all the other components (Figure 3.20). Because of this, its retention time was not shown as the separation was guaranteed within the temperature range of interest. Carbon isotope ratio measurement of hydrocarbons on MODULUS would be impossible if this column was the only one installed. The combustion of the hydrocarbons would result in CO_2, which would never be eluted by the column. The retention times of the components before and after vibration are shown in Figure 3.22.

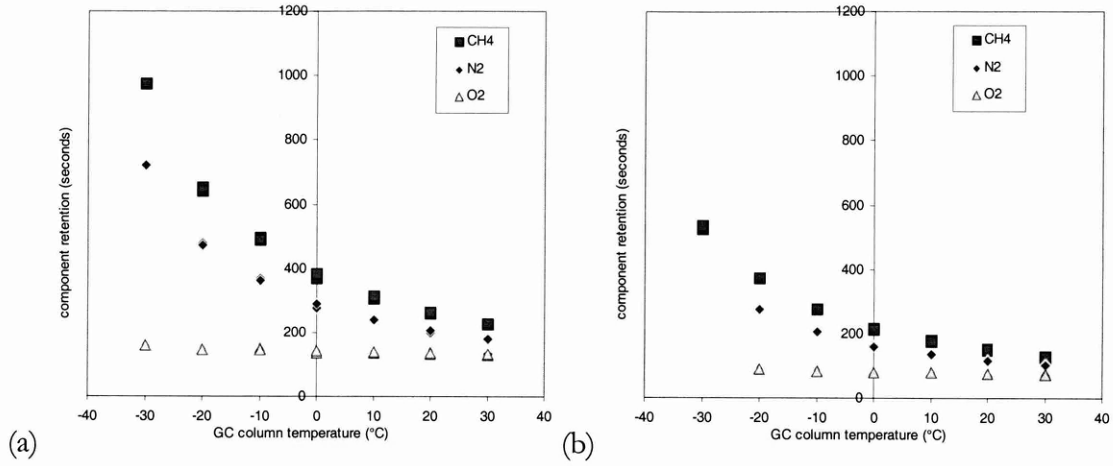

Figure 3.21 Retention characteristics for Molsieve 5A column (a) before vibration testing, (b) after vibration testing

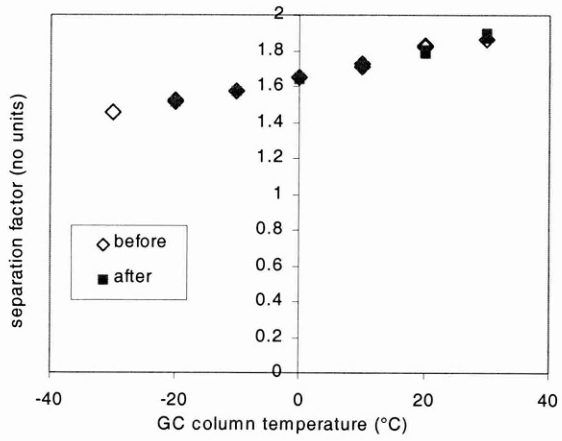

Figure 3.22 α (CH_4 – N_2) over the temperature range before and after vibration.

It can be seen from Figure 3.21 (a) and (b) that the retention times of all components have decreased after vibration. Figure 3.22 shows the separation factor between CH_4 and N_2, with O_2 treated to be the unretained compound, as opposed to N_2 in the other experiments. Unlike the $\alpha(CH_4\text{-}CO_2)$ from the other columns, the separation factor between the two compounds on this column decreased slightly with temperature. Despite the change in retention times in the column re-test experiment, the relative separation of CH_4 – N_2 was equal (within error) before and after the vibration.

3.5.5. Effective column efficiency for CH_4

Ion trap chromatograms were analysed to provide the column efficiency for the elution of methane. The effective number of theoretical plates can be derived from the retention time of the methane peak widths, and the gas hold up time. In this case, the gas hold up time was taken as the retention time for N_2 (or in the case of the Molsieve column, O_2). The values of N_{eff} indicate the column's ability to elute sharp peaks and the amount of retention of that compound (see 3.2.3).

Table 3.3 Effective number of theoretical plates (N_{eff}) for CH_4 through all four columns at both temperature extremes. Adjusted retention time was calculated with N_2 or O_2.

Column	temperature	N_{eff} (CH_4) before vibration	N_{eff} (CH_4) after vibration
SilicaPLOT	30°C	0.3	0.0
	-30°C	1.7	4
HP PLOT Q	30°C	0.7	1
	-30°C	64	64
J&W CarbonPLOT	30°C	0.85	1.7
	-30°C	96	231
Molsieve 5A	30°C	441	1230
	-20°C	11258	5258

Table 3.3 shows that the highest methane separation is provided by the Molsieve 5A column, which is also seen in Figure 3.22. Of the three traditional PLOT columns, the data shows that no column separates CH_4 from N_2 significantly at 30°C, whilst at the lowest temperature measured, -30°C, J&W's CarbonPLOT is shown to have the greatest efficiency for methane retention.

3.6. Conclusions and Recommendations from Vibration testing.

Structurally, no column was adversely affected by the vibration. All columns behaved well after being subjected to these mechanical stresses. No column was broken, and all allowed gas to flow through once re-installed after vibration. This was in contrast to conventional thought on the structural integrity of PLOT columns. Whether column reconditioning will occur after years

of dormancy in space has yet to be decided, although conditioning has been timelined in certain operational modes. A possible difficulty is the column configuration on the final assembled unit. The column will have to be wrapped to its smallest diameter without breaking. Column cages for laboratory use are around 15-20 cm in diameter, whereas requirement for MODULUS may need the column wrapped around a steel ring less than 10 cm in diameter. This will cause greater mechanical stress on the system, and increase the likelihood of vibration damage.

As is known from laboratory use of GCs, certain procedures must be applied for best chromatographic results. The same must apply to GCs on board space missions. Of course, the correct column must be chosen for the desired application. The tests described in Chapter 3 highlighted some difficulties the GC-ITD system might face in terms of getting the best performance from the hardware.

In terms of GC performance, the Molsieve 5A column gave the greatest number of discrete peaks test gas mixture (CH_4, N_2, O_2, and CO could all be analysed quantitatively). The problem encountered with the use of the Molsieve column was the CO_2 trapping effect. This limits its potential use to analytical channels not designed for carbon isotope analysis. The other columns all separated CO_2 from the bulk of the other test gases. The CarbonPLOT column also managed to have discrete (6σ) separation of CH_4 from CO at -10°C, which better than the HP PLOT Q column could give at that temperature.

There have been recent developments in capillary technology such that these stationary phases are now available in steel (capillary) columns. These columns are of the same dimensions of fused silica but are much more flexible, and potentially have greater strength. The breakthrough to create these columns was the perfection of a process to de-activate the inner surface of the steel tube, so that the stationary phase can be applied to the surface.

Table 3.4 Collated separation data for CO, CO_2, CH_4, N_2, O_2 over the capillary columns tested. Compounds in square brackets emerge in one peak.

Separations	Column at 30°C	Column at -30°C
HP PLOT Q	[CH_4/CO/N_2/O_2] CO_2	[CO/N_2/O_2] CH_4 (just) CO_2
SilicaPLOT	[CH_4/CO/N_2/O_2] CO_2	[CO/N_2/O_2/part CH_4] CO_2
CarbonPLOT	[CH_4/CO/N_2/O_2] CO_2	[CO/N_2/O_2] CH_4 (6σ at -10°C) CO_2
Molsieve 5A PLOT	O_2 N_2 CH_4 CO no CO_2	O_2 N_2 CH_4 CO no CO_2

From examination of the data, CarbonPLOT has the advantages for the carbon isotope analysis channel. Its N_2 - CH_4 separation is the greatest of all columns tested. Molsieve 5A could be used for an alternative qualitative channel, if CO_2 analysis was not required. *NB.* The effect of water on the columns was not investigated due to the difficulty of introducing a wet sample into the vacuum system. This should be investigated once a full model of MODULUS is built.

4. OXIDATION OF CARBON COMPOUNDS FOR ISOTOPE ANALYSIS USING METAL OXIDES AS OXIDANT

4.1. Introduction

In stable isotope chemistry, measurements of $\delta^{13}C$ and $\delta^{18}O$ are used as tools to show thermal history, processes, environment, and reaction history. Miniaturising a laboratory that also analyses samples in this way is the challenge facing the MODULUS designers. This chapter investigates if alternatives to the standard laboratory methods can be applied utilised for MODULUS. Combustion reactions are required for conversion of organic components to CO_2 for carbon analysis, and the standard reagents are not necessarily the most appropriate for the assembly of MODULUS. Many alternatives are presented in this chapter.

The MODULUS sampling strategy will focus on cometary volatiles, so expected species include CO_2, and CO and minor CH_4 (see Chapter 1). Other organic compounds are also expected, requiring the instrument to be sensitive in the ppm range. For the purpose of this study the analysis of CO and CH_4 were chosen as test gases for the performance evaluation of reagents. As shown in Table 1.2, CO and CO_2 carry the majority of the carbon, with CH_4 and other carbonaceous compounds having much lower concentrations. Carbon monoxide requires mild oxidative conditions for its conversion to CO_2. In contrast, methane needs far more extreme conditions for oxidation.

The goals of the experiments in this chapter are to discover the most appropriate chemical oxidants for the conversion of either pure carbon monoxide or methane to carbon dioxide gas. Many potential oxidants were investigated, which was performed using the same system as the gas separation tests in Chapter 3. In general, the lower the temperature required for the

complete oxidation of CO and CH_4, the greater the power saving experienced by the MODULUS instruments once cometary sampling is underway.

To understand the necessary chemical reaction schemes and how the combustion system works, one must examine the many facets of catalysis. The method of combustion of cometary volatiles in the proposed MODULUS configuration is slightly different from the normal continuous flow oxidation system which is not limited by temperature or reagent quantitiy. Therefore it would be prudent to examine the processes that lead to the catalysed combustion reaction.

4.2. Surface and Combustion Science

The combustion of cometary volatiles by MODULUS for carbon isotope analysis can only be simulated correctly by using a mixture containing all the compounds likely to be sampled from the nucleus of comet Wirtanen. As these are not known precisely, other species must be used to measure the combustion ability of the oxides. Methane is a hydrocarbon that requires very high temperatures for complete oxidation to CO_2. Carbon monoxide requires far lower temperatures for the same combustion process. As both of these species represent extremes in oxidation chemistry, they therefore provide useful window to investigate the entire phenomenon. CO and CH_4 were hence chosen as gases with which to test combustion properties of suitable catalysts.

One major difference to the combustion of both these gases in the irMS system as opposed to industrial systems (for pollution control) is the absence of gaseous oxygen. Commercial catalytic systems have been created for the abatement of CH_4 and CO from combustion engine exhaust gases and other systems, where incomplete combustion of hydrocarbons can produce these gases. Generally, a stream of gases passes over a catalyst bed, before reaching an exhaust. However, almost invariably there will be O_2 gas from air in the stream with the gases to be combusted. The catalyst then provides a surface so that the oxygen can react with the hydrocarbon to produce CO_2 and H_2O.

The accepted definition of a catalyst is that it is a substance that increases the rate at which a chemical system approaches equilibrium, without being consumed in the process, although (in practice, a catalyst can be consumed during a reaction, by many processes). The equilibrium point (defined by thermodynamics) of the reaction in question is unchanged by the catalyst's presence. The potential energy of the reactants and products are the same whether a catalyst is present or not, therefore the enthalpy change is identical.

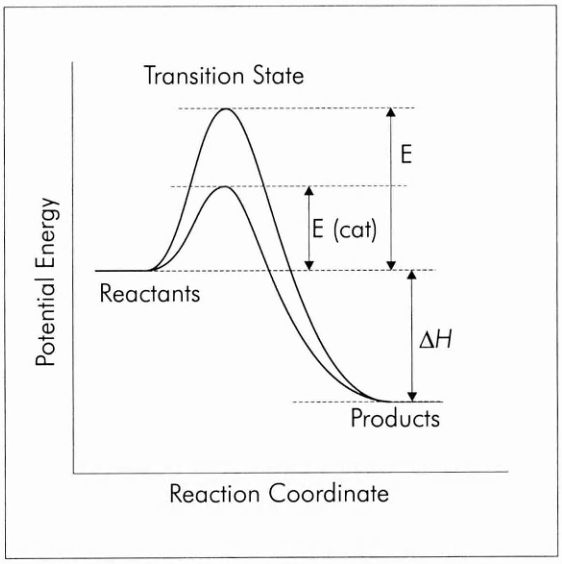

Figure 4.1 Potential energy versus reaction co-ordinate of a reaction, showing activation energy of catalysed and uncatalysed reaction.

Most chemical reactions need some energy to proceed, even if they are exothermic. An intermediate step (the transition state) requires additional energy (the activation energy) for the system if the reaction is to occur. In the case of a catalysed reaction, the only function of the catalyst is to lower the activation energy. Thus the rate of reaction at a given temperature is increased, or conversely the temperature at which the reaction can proceed is decreased. Catalysts can be divided into two categories; heterogeneous and homogenous. Homogenous catalysts reside in the same phase (exclusively liquid or gaseous) as the reactants, while heterogeneous catalysts reside in a different phase (exclusively liquid or solid) and the catalytic action usually proceeds on the phase boundary surface.

This work concentrates only on the reaction of gaseous compounds with solid catalysts. However, two differences are present in these experiments that make it unlike classical catalyst studies. First, the reaction does not occur statically - only a short time is available for the reaction to achieve completion. Second, the oxidation reaction must occur without the presence of gaseous oxygen. Although these differences imply that the quantification of equilibrium and kinetics may be difficult, classical catalytic studies can still derive the probable reaction mechanism.

4.2.1. Adsorption

The process that permits gas-solid catalysed reactions to take place is adsorption. The phenomenon of adsorption which allows the catalytic action to occur, is the ability of gaseous molecules to "adhere" to a solid surface. Species can be adsorbed by two processes; physisorption (physical adsorption) or chemisorption (chemical adsorption). Physisorption occurs due to the electrostatic attraction of species to the surface by their permanent dipole moments, or by slight fluctuations in electron density. Neither the surface or the adsorbate are substantially altered chemically during physisorption. The bonds formed are weak, with no activation energy needed for adsorption, and it is generally a low temperature event. Chemisorption on the other hand, is far more energy intensive. If one considers the atoms at a uniform surface, the regular formation of the solid is broken, and each of the atoms on the surface possesses one or more free valencies. The number of neighbouring atoms around a surface atom is less than those in the bulk solid. Depending on the bonding and orientation of the surface, this leads to a net force acting inwards. These free valencies are available for interaction with adsorbates, where the electronic rearrangement can be regarded as a chemical reaction. The bonds formed during chemisorption are strong, and small activation energy is required for the adsorption. Chemisorption of molecules forms the major pathway for heterogeneous catalysis.

Let us consider the oxidation of carbon monoxide with O_2 on platinum, in a closed system. The total reaction can be expressed as:

$$CO_{(g)} + \frac{1}{2} O_{2(g)} \rightarrow CO_{2(g)} \quad (4.1)$$

The reaction is energetically favourable, (ΔH = -282 kJ mol^{-1}) but only takes place at high temperatures without a catalyst present. Addition of platinum will allow the reaction to occur at the surface of the metal, by two possible methods. In the Langmuir-Hinshelwood mechanism, a "carbon monoxide atom may condense on a surface of platinum and an oxygen atom can condense by the side of it, and then the two can interact" (Langmuir, 1922). In the Eley-Rideal mechanism, an oxygen atom can be adsorbed on the surface, and a carbon monoxide molecule can combine with it during collision. It is known that this particular reaction (in equation 4.1) follows the Langmuir-Hinshelwood mechanism (Engel and Ertl, 1982).

Oxygen can be adsorbed onto solid surfaces as three different species. A weakly held molecular form ($O_{2,ad}$) may be present at low temperatures. This molecular form is the precursor for the most dominant form, chemisorbed atomic oxygen (O_{ad}). At room temperatures and above (typical catalytic temperatures) $O_{2,ad}$ is almost undetectable, implying the rate of the disassociation is fast. The atomic oxygen species plays the active role in any catalytic oxidation reaction. The third type of adsorbed oxygen is found at high temperatures, and is designated as a sub-surface oxide, and may be formed at over 500K if the gas is oxygen rich. This has reduced reactivity compared to the chemisorbed species and is considered to play only a minor role in the kinetics and mechanism of the reaction, which proceeds as follows;

$$O_2 + \square \leftrightharpoons O_{2,ad} \rightarrow 2O_{ad} \quad (4.2)$$

$$CO + \square \leftrightharpoons CO_{ad} \quad (4.3)$$

$$CO_{ad} + O_{ad} \rightarrow CO_2 + 2\square \quad (4.4)$$

where □ signifies an active site available on the surface. This reaction mechanism follows the Langmuir-Hinshelwood (LH) model. The Eley-Rideal (ER) reaction scheme would replace the last reaction with the following two potential reactions.

$$CO \text{ (gas or physisorbed)} + O_{ad} \rightarrow CO_2 + \square \quad (4.5)$$

$$2CO_{ad} + O_2 \rightarrow 2CO_2 + 2\square \quad (4.6)$$

The last reaction is unlikely to occur. A surface saturated with CO_{ad} exposed to $O_{2(g)}$ will not form CO_2. The chemisorbed atomic oxygen is necessary for the oxidation. The reaction has been found to proceed along the LH path, as the surface lifetime of the CO_{ad} species is long enough for reaction to take place. The physisorbed CO species in the ER path will have a short time available for the reaction to occur. The potential energy diagram for the reaction is shown in Figure 4.2.

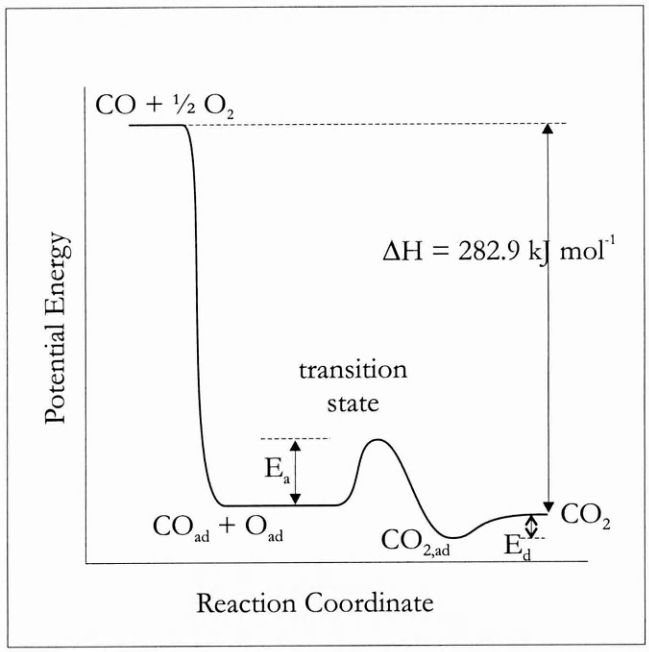

Figure 4.2 Reaction sequence between CO and O over a platinum surface. E_d signifies energy of desorption, and E_a signifies energy of adsorption

This reaction sequence illustrates the energy changes associated with the catalytic oxidation of CO on a metal catalyst. Other catalysts that can be used in this reaction include Pt, Rh, Pd, and Ru. A similar reaction sequence can occur on the oxides of base metals (e.g. copper oxide).

Oxidation can proceed through the variation of the transition metal's oxidation state. Many oxidation/reduction cycles of the top layers of the oxide facilitate this.

4.2.2. Metal Oxides

Like metals, metal oxides also show potential for catalytic reactions. Many reactions such as dehydrogenation and dehydration can occur on the surfaces of various oxides. Obviously, the surface properties of such oxides dictate the type of reaction to be catalysed. The surface characteristics of metals are relatively easily measured. By contrast, oxides have two components, metal cation and oxide anion. These species do not necessarily have the relative amounts fixed in different crystal planes. Most oxides active in catalysis are complex mixtures of oxides, making it difficult to obtain accurate surface information.

Oxides can be classed as semiconductors or insulators, according to their electrical conductivity. Insulating oxides (such as SiO_2, Al_2O_3) have stoichiometric oxygen ratios and are generally inactive in catalysis (although they can be used as bases for catalysts - see section 4.2.3). Oxides which have greater bulk conductivity can be classed as semiconductors (such as ZnO, NiO) and have higher conductivity due to their departure from the precise stoichiometry. Semiconductors have the attribute that their conductivity increases with temperature. The non-stoichiometry of the oxides can be examined by the effect of the mobility of oxygen ions in the lattice. On heating the oxides in air, some lose oxygen from the lattice and become oxygen deficient (n-type, such as TiO_2). Others gain oxygen from the air once heated, becoming enriched (p-type, such as CoO). Expressed chemically, some metal cations in p-type oxides, can increase their oxidation state to accommodate the extra oxygen. Similarly, in n-type semiconductors a lower available oxidation state in the metal is needed (which may include the zero-valent state).

Certain oxides can then act as an oxygen pump; in a closed system, n-type oxides once heated can lose O_2 and on cooling can re-adsorb that O_2. In stable isotope laboratories Copper (II) oxide is the reagent of choice. In their deficient state, the oxides can adsorb as much O_2 as is needed for the stoichiometry to be restored, and metal cation oxidation states are maximised.

Once an oxide has reached perfect stoichiometry it will be unable to chemisorb any more oxygen. In copper (II) oxide, the oxygen pump effect occurs via the copper (I) oxidation state:

$$2\ Cu(II)O \leftrightharpoons Cu_2(I)O + \tfrac{1}{2}\ O_2 \qquad (4.7)$$

Other oxides such as zinc (II) oxide also show this behaviour. Oxides which show ability to store large amounts of oxygen per unit mass are often considered for three-way catalysts where multiple metal oxides are mixed and each component plays a different role in the reaction system. This approach is common in many catalysts including those used to condition automobile exhaust emissions.

4.2.3. Insulating oxides

As stated previously, insulating oxides are almost inactive in catalysis. Their metal cations cannot be oxidised or reduced. They cannot chemisorb oxygen, carbon monoxide or hydrogen. However, reactions with polar molecules can occur. The oxides of alumina or silica are normally covered with a layer of chemisorbed water from exposure to the atmosphere. Industrially, catalysts are often made from mixtures of many components. Along with the active phase, a promoter may be present. This phase may not be catalytically active, but it increases the efficiency of the active phase, for example by making the active phase more resistant to poisonous species. The final component is the support, usually made from an insulating oxide.

Supports perform several functions, and in general contain most of the mass of a commercial catalyst. One of its roles is to provide a large surface area for the active phase. Combining a small concentration of active phase with a support can still produce a catalyst that retains much of the functionality of the active phase alone. For instance platinum (by mass less than 5%) supported in alumina can provide the same catalytic activity during hydrocarbon combustion one from pure platinum powder. The support also allows the catalyst to be cast into a variety of forms for industrial use, form pellets to extrudates. Although the supports are intended to be inactive for the catalysis, often they can participate in the reaction sequence.

4.2.4. Pulse-flow reactors

Many different types of reaction vessels are used in industrial processes and research laboratories. Static systems utilise reactions occurring in a closed volume, where the reaction can be examined by noting the concentrations of the reactants, intermediates, and products. In such a scheme reaction kinetics and rates are often straightforward to calculate. In dynamic systems gaseous reactants can flow through a bed of catalyst particles (continuous flow reactor) and out through an exhaust. The flow rate of the gases dictate the amount of time spent in the catalyst reactor. The degree of conversion increases along the catalyst bed.

Variations on these two types of reactor are possible. For instance, a continuous flow reactor can reconnect the exhaust and inlet, and then cycle the gas mixture through the catalyst until a desired conversion is reached. This system is termed the recirculating gas reactor, and its operation exhibits features of both static and dynamic modes. Another variation is the pulse-flow reactor, in which one reactant flows continuously, whilst a pulse of second reactant is admitted upstream of the reactor.

The pulse-flow type reactor is used in some analytical systems for the oxidation of organic material for carbon isotope analysis (Merritt et al., 1995a). Other commercial systems use an adaptation of the pulse-flow reactor, where effluent from a GC system is combusted but without a continuous flow of oxygen. In this case combustion relies on oxygen being supplied from the metal oxide. Clearly in such a configuration, the oxide will reduce to such a point that all available oxygen has been exhausted from the catalyst. Re-oxidation of the metal oxide can be performed by adding flowing O_2 instead of the carrier gas. Both the lattice and the surface should be saturated with oxygen species by this oxidation procedure. Chemisorbed oxygen reacts much faster than bulk oxygen. The mobility of oxide ions within the lattice should dictate the quantity of organic material converted before the oxide is spent. Where lattice oxides are highly mobile, migration to the surface allows oxidation to continue after all chemisorbed oxygen is exhausted.

Under dynamic conditions but with no flowing oxygen gas, the oxidation of CO will proceed along a different path to that described in section 4.2.1. The reaction scheme is more likely to compose of the following:

$$CO + \square \rightarrow CO_{ad} \quad (4.8)$$

$$O^{2-} + \square \rightarrow O_{ad} + 2e^{-} \quad (4.9)$$

$$2e^{-} + M^{2+} \rightarrow M \quad (4.10)$$

$$CO_{ad} + O_{ad} \rightarrow CO_2 + 2\square \quad (4.11)$$

where O^{2-} is the oxide ion of the metal surface. The complete reaction of all CO (or CH_4) implies that all incoming reactant must be chemisorbed onto the surface of the catalyst, for a time period long enough for reaction to take place. Chemisorption of CO may be followed by desorption without reaction, followed by re-adsorption on another site. In general, the likelihood of complete reaction of an incoming CO or CH_4 molecule increases with the reactor temperature, as the activation energy of the transition state is more likely to be overcome.

Other reaction sequences have been proposed for the oxidation of carbon monoxide on supported gold catalysts in a continuous flow system (Tsubota et al., 1993). CO is reversibly adsorbed on gold particles and partly migrates to support oxides, where it reacts with adsorbed oxygen. This forms a bidentate carbonate species[7], which decomposes to CO_2.

4.2.5. Catalyst preparation methods

The preparation of some of the catalysts used in this study were performed in the laboratories of the Chemistry Department at the Open University, by the author and Mr. Paul Wynn (PhD student in Chemistry Department). Different chemical techniques were employed in the preparation, although most mixtures used the co-precipitation technique. In this technique a metal salt is dissolved, and the support powder is added to the solution. On the addition of a

[7] A structure formed between a carbonate ion with a surface, with bonding via two oxygen atoms

base such as Na_2CO_3 or NH_4OH a precipitate forms (depending on the precipitation pH), as the metal hydroxide bonds to the support. The powder is then dried, and calcined.

Care has to be taken with the base added. A common base for co-precipitation of combustion catalysts is Na_2CO_3, which could potentially leave some carbon on the catalyst. In this project, the purpose of the catalyst is to combust CO and CH_4 to CO_2, and any carbon within the catalyst is likely to change the isotope ratio of the combusted CO_2. Such contamination must therefore be avoided, and NH_4OH was used as the base in the majority of compounds preparations.

Calcination of a dried precipitate usually implies heating to over 400°C in air for a few hours. During heating, the mixture loses any bonded H_2O or CO_2, and generates the surface for the active phase whilst the hydroxides decompose into stable oxides.

Another method used for the preparation of some catalysts was wetness impregnation. Here an aqueous solution of a metal salt was added to the anhydrous support material. Only a small amount of solution was required, so that the solid support remained a paste. Removal of the solvent by evaporation left a precursor of the active phase within the pores of the support material. Again, the mixture needed to be calcined for the active phase to be formed.

The final method used for catalyst preparation was direct heating. In this case two metal oxide powders were mixed, placed in a furnace and heated. Calcination is unnecessary for these mixtures. The final product was a mixed metal oxide.

4.3. Catalysts for the analysis of carbon isotopic composition

4.3.1. CO and CH_4 oxidation on metal oxides –History

Horacek et al., (1960) tested many materials for their oxidation ability by passing 4% CH_4 in O_2 over a selection of compounds. The lowest temperature of total conversion to CO_2 + H_2O was measured. In the gas phase, the reaction scheme is as such:

$$CH_{4\,(g)} + 2O_{2\,(g)} \rightarrow CO_{2\,(g)} + 2H_2O_{\,(g)} \qquad (4.12)$$

and is energetically favourable (ΔH = -802 kJ mol^{-1}). Table 4.1, summarises the successful oxides Horacek et al. (1960) found under their testing regime. Other oxides tested gave incomplete combustion even at 650°C.

Table 4.1 Minimum temperature for complete conversion of CH_4 (4% in O_2) for various oxides

Catalyst	Min temperature (°C) of $CH_4 \rightarrow CO_2$
Co_3O_4	311 to 345 depending on preparation
Co_2O_3 + Ag	350
Fe_2O_3 + Ag	362
CuO (fine powder)	370
Fe_2O_3	375
$Zn(MnO_4)_2$ ◘	391
MnO_2	394
NiO	396 to 401 depending on preparation
NH_4MnO_4 ◘	412
MnO_2 + Ag	418
Co_3O_4 on asbestos	430
MnO_2 from Nitrate	453
Co_3O_4 on pumice	464
Cr_2O_3	480
$AgMnO_4$ ◘	487
Pt on asbestos	506
◘ refers to the thermal decomposition product of the compound as the catalyst	

There is a marked difference between NiO acting at about 400°C (Table 4.1) and the NiO/Pt reactor used by Merritt et al., (1995a) which required 1150°C for perfect combustion. The operating conditions (including quantity of reagents and CH_4/O_2 ratio) therefore have a marked impact on the minimum temperature of combustion.

Pechanec, (1973) took the work further and measured similar materials, and in addition measured surface areas of the oxides in question. This study found a direct correlation between the degree of surface area and combustion temperature of CH_4. Normalising to 10 m^2/g surface area he categorised the combustion temperature into five groups as given in Table 4.2. Obviously the first two groups are of high potential interest for MODULUS.

Table 4.2 Minimum temperature of complete conversion of CH_4 (4% in O_2) for various oxides, but normalised to 10 m^2/g surface area (Pechanec, 1973)

Minimum combustion temperature (°C) normalised to 10 m^2/g surface area	Reagent
300-400	Ru, Co_3O_4, Rh, Ir, Pt
400-500	Ag, CuO, Cr_2O_3, NiO, CdO, Mn_3O_4, PdO, Fe_2O_3
500-600	Many other 4/5 d-block, lanthanide and actinide oxides
600-700	MgO, PbO, V_2O_5, MoO_3, CeO_2, ZrO_2, TiO_2, Sc_2O_3, Au
Over 700	Nb_2O_5, Ta_2O_5, GeO_2, WO_3, BeO, Al_2O_3, SiO_2

The lowest temperature group contains metals, not oxides, confirming that heterogeneous catalysis will occur with both CH_4 and O_2 in the gas phase as discussed in 4.2.1.

Other studies, for example Kainz and Horwatitsch, (1960) confirmed the influence of surface area - for copper oxide a marked difference was found in the combustion of methane with O_2, with variation in surface area and grain size (Figure 4.3).

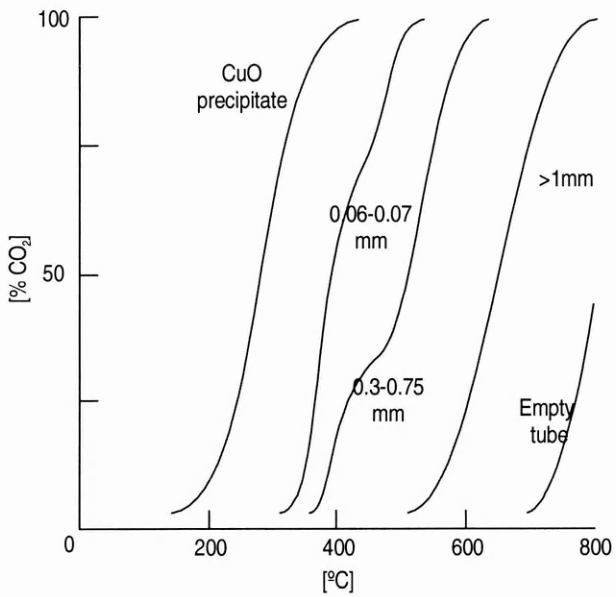

Figure 4.3 Combustion curves for methane combustion (with O_2) by different forms of CuO, with different grain sizes of powder (Kainz and Horwatitsch, 1960)

Kainz and Horwatitsch (1961) found that for combustion of CH_4 within a partial O_2 atmosphere one could build an order of combustion ability: Co_3O_4 > MnO_2 > NiO > CuO >

Cr_2O_3 > CeO_2. In another experiment a hindering CO_2 partial pressure was present in addition to the oxygen pressure and different oxides performed best: MnO_2 > CuO > Co_3O_4 > Fe_2O_3 > NiO.

From these studies one can presume that those metal oxides that performed well under oxygen-rich conditions, are maybe versatile enough to work under the MODULUS regime. The testing of these oxides were considered first in this investigation.

CO oxidation has also generated interest in the industrial sector. Any combustion engine will produce small amounts of CO and uncombusted hydrocarbons. This is especially common in automotive engines. For these applications, a standard catalyst system has been adopted with variable success. Generally, Pt deposited in small quantities on γ-Al_2O_3 will combust most unburnt hydrocarbons and CO at temperatures below 400°C (Heck and Farrauto, 1995). Again this is with O_2 in gas phase, the amounts depending on engine burning conditions. Other applications have driven more novel metal-on-metal-oxide catalysts. Previously considered inactive in combustion catalysis, gold supported on metal oxides has been accepted as the most recent research advance for this application (Haruta et al., 1996). These gold compounds are remarkably active; they will combust CO at temperatures as low as -70°C. Other non-precious metal oxides have also had use in CO-only applications. Copper-manganese oxides have demonstrated many successes (Hutchings et al., 1998). $CuMn_2O_4$ is known as hopcalite, and has often been traditionally employed in respiratory protection systems, for environments where the ambient CO concentration is hazardous to health (e.g. mines).

Again, compounds that work well for CO conversion may exhibit good combustion properties for other hydrocarbons. Hence these compounds also have been tested in this chapter.

4.3.2. Methodology of experiment

MODULUS has been designed to analyse the isotopic composition of cometary volatiles. Designing instrumentation for space exploration has numerous problems, not least remaining within mass and power budgets. For the purpose of oxidation the goals for the catalyst are that:

- All the sample gas is combusted
- The catalyst does not retain sample on surface
- The catalyst is stable at elevated temperatures
- High storage capacity of oxidative agent
- No isotopic fractionation induced during combustion

The test regime for investigating the suitability of selected reagents was as follows: the oxide was placed in a quartz tube upstream of the commercial GC-ITD system described in Chapter 2. A pulse of CO was passed over the oxide at various temperatures. If combusted to CO_2 completely, the furnace temperature was lowered and injection pulses were repeated until some CO remained. If only CO or a mixture of CO and CO_2 was eluted, the operating temperature was increased and the CO injection repeated until complete combustion was encountered again. Evaluation of the isotopic effects associated with different catalysts is discussed in Chapter 5 where suitable catalysts identified in Chapter 4 were subjected to more stringent tests.

There were a number of other issues that needed to be considered with some of the oxides. For instance, gas flow problems occurred with some reagents, producing unusable peak shapes (i.e. very broad or with severe tailing) in the Ion Trap Detector. Other effects include the decomposition (reduction) of the oxides, releasing O_2 into the mass spectrometer, while reducing the oxide itself. Once a minimum combustion temperature had been found for CO, the same investigation could be undertaken for CH_4. Successful CH_4 conversion was rare with most metal oxides, even if they were competent at CO combustion. The use of CO and CH_4 as test gases for combustion was designed to emulate the carbon compounds that require the least and most effort to combust to CO_2. The test regime is summarised in Figure 4.4. *NB.* The combustion efficiency of a catalyst at a particular temperature is not fixed, as it depends on many factors such as reactant amount, flow dynamics, active site availability, and ion mobility.

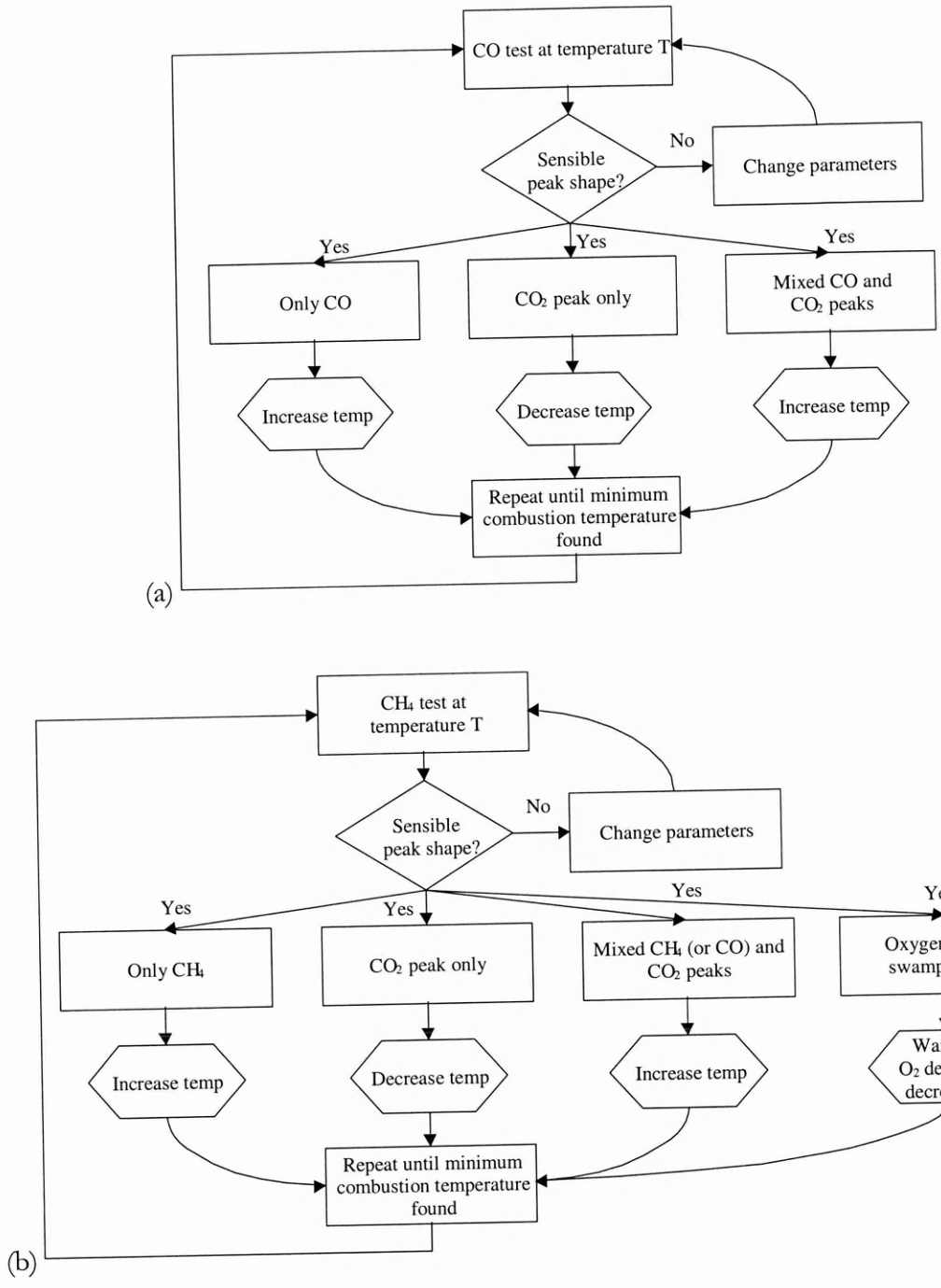

Figure 4.4 Flow chart showing the testing system for the evaluation of the in-line combustion process for (a) CO, and (b) CH_4

4.3.3. Further evaluation of the properties of the catalysts: isotopic analysis

The initial testing process on the GC-ITD system is shown in Figure 4.4. After evaluation of the combustion properties, some samples were chosen to be tested in the irMS system, as seen in Chapter 5. Here the isotopic integrity of the combustion process were investigated. Using the irMS system, samples were again exposed to high temperatures to combust CH_4 or CO. Peak sizes of CO_2 and isotopic composition of carbon and oxygen were measured. Due to the

change in operating conditions between the GC-ITD system and the irMS system, the minimum temperature of combustion of the compounds may not match between the two systems. The irMS system requires a higher carrier flow rate, and also greater amount of material for analysis.

4.3.4. Apparatus

The GC-ITD system (Figure 4.5) was almost identical to that used in the GC chromatography tests described in Chapter 3. Samples of CH_4 or CO (typically 1-50 nmol) was injected into the flowing GC-ITD system. The test gas travelled as a pulse (slowly widening through diffusion) at the rate of the carrier gas mass flow setting. The gas then passed through a quartz tube containing the oxide being tested ("catalyst reactor" in Figure 4.5).

This reactor was heated by a tube furnace (150 mm long, 40 mm o.d.) controlled electronically (Eurotherm 842 PID) using a R-type thermocouple (Pt/Pt-Rh wires). The maximum temperature of the system was 1075°C. The controller allowed the temperature of the reagent to be ramped at a constant rate both when heated and cooled, and this function was used in the Temperature Programmed Desorption (TPD) experiments as described in section 4.3.7.

The contact time of reactant gas to solid catalyst was of the order of seconds, therefore any reaction upon the surface would have had to have occured quickly. Carbon dioxide, and unbunrt CO or CH_4 then passed as a pulse to the start of the GC column. The GC columns used in the experiments were HP PLOT Q (20 m, 0.32 mm i.d., 20 μm film) or J&W Scientific CarboPLOT (20 m, 0.32 mm i.d., 1.5 μm film) columns. Retention characteristics of both of these columns can be found in Chapter 3. The columns were always used isothermally (usually 30°C). The ITD was set to collect all spectra including background (from 10 to 90 a.m.u.). Data collection was set to integrate at a rate of 2 scans per second.

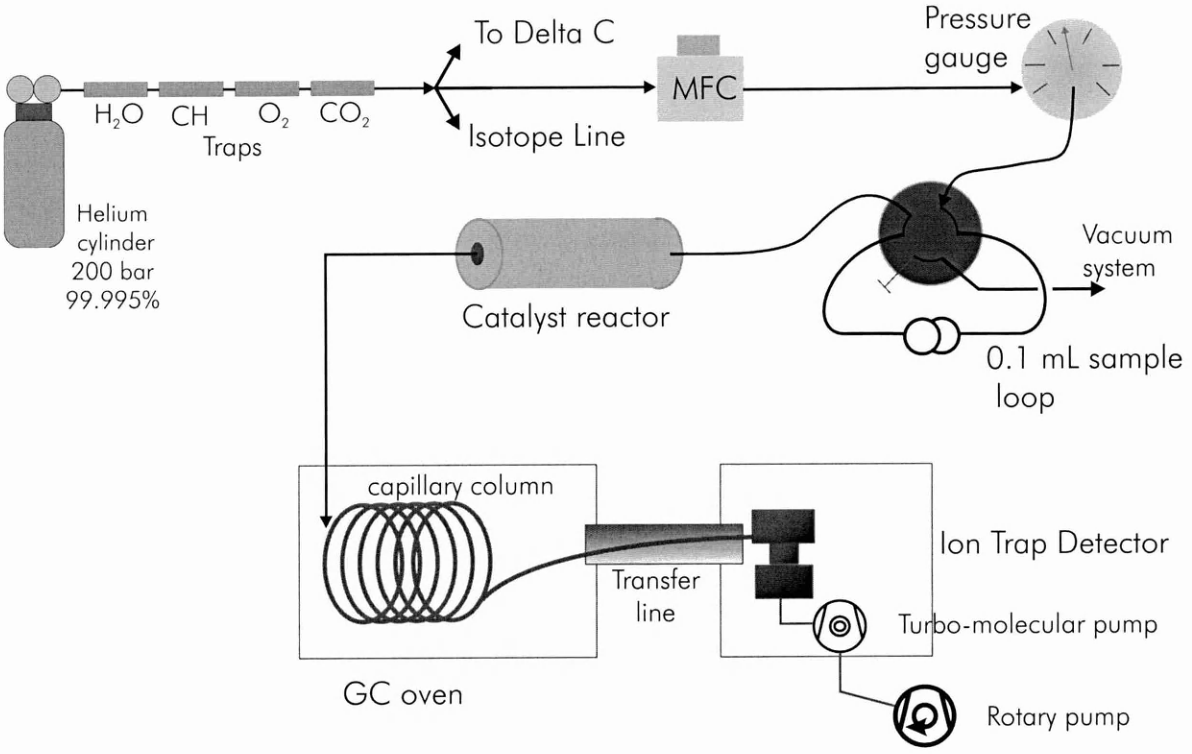

Figure 4.5 GC-ITD and sample injection arrangement for the catalyst combustion tests

Once an oxide sample had been evaluated, it was then removed from the system and a replacement quartz tube containing another sample was placed in the furnace. If the oxide was to be investigated further, it was tested using the irMS system as detailed in Chapter 5.

4.3.5. Sample preparation issues

Metal oxides were used either as received from suppliers, or made in laboratory. Drying of powders was only deemed necessary if the sample was exposed to wet chemicals in preparation. If a powder was too coarse grained, it was ground in a mortar and pestle, although particle size was not measured. Powders were then placed in the quartz tube (Multi-Lab), 3 mm o.d. and 1 mm i.d. approximately 200 mm in length. To prevent the powder from migrating out of the reactor, a plug was made from silica wool and inserted into the tube, approximately two-thirds of the way in. It was found that by forcing it in the long path, the wool compressed more and was unlikely to move axially along the tube.

Admitting sample powder to the tube was not without problems. The 1 mm orifice of the tube effectively prevented the use of a funnel. The only method that worked was placing the tube on a workbench on some aluminium foil, heaping a small amount of sample at the tube mouth, and spooning powder into the tube with a microspatula. This would usually allow powder to enter to within 2-5 mm inside the tube, depending on dryness. By carefully inserting a tungsten wire (0.8 mm diam.) the powder could be forced to reach the silica wool plug. By repeating the process one could place on average 0.1g of powder into the tube. The precise amount was measured by weighing the tube before and after loading. Contamination was avoided by the use of solvent cleaned utensils and foil surfaces.

It was noted that the tube furnace only provides its maximum temperature to its central 5 or 6 cm along its length. Although a small proportion of the powders may have been outside the maximum heated region, the overall performance of these oxides were assumed not to have changed significantly.

4.3.6. Installation of reactors

The union between the $^1/_{16}$" pipework (used between the injection valve and the ITD) and 3 mm quartz sample tube was made by $^1/_8$" PTFE ferrules, joined with a Swagelok™ nut and union (NLV). During installation the ion trap was turned off, and the helium flow was reduced to zero, and the system was left so that the head pressure of the column was only a few psi above atmospheric pressure. The tube was installed with the silica wool plug located downstream of the sample oxide. After attachment flowing helium eventually forced tout any air present and was pumped away. The amount of air in the system rendered the Ion Trap useless until the air and associated water vapour had been pumped and background had returned to usable levels. In practice this took from a couple of hours to leaving the system overnight to settle. A schematic of the installation arrangement can be seen in Figure 4.6.

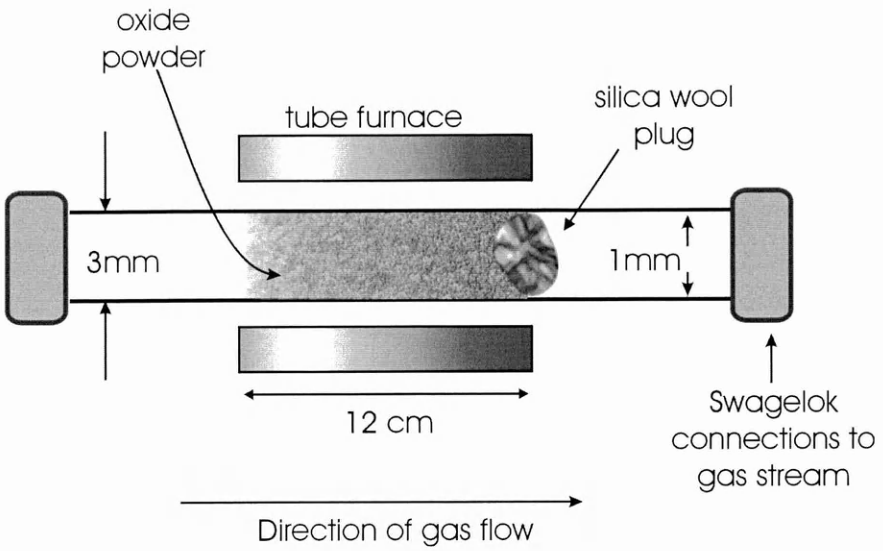

Figure 4.6 Schematic cross-section diagram to show the arrangement of the powder, plug and tube furnace for each sample tested.

4.3.7. Temperature Programmed Desorption (TPD) Experiments

Before the initial combustion testing, each sample was subjected to desorption testing. The Ion Trap was set to collect mass spectral data at a lower recording rate (0.5 scan/second) than combustion testing, with a mass range of 10-90 a.m.u. With only helium passing through, the furnace was set to heat the catalyst from room temperature to 400°C with a ramp rate of 20°C per minute. This slow increase in temperature gave information on the species physi- and chemisorbed onto the surface of the oxide. A series of compounds reach the ITD at different times, corresponding to their release temperatures and their chromatography.

Unless the powders had been pre-dried, most contained a large quantity of water from exposure to the atmosphere. Water release generally peaked and then decayed very slowly, after the sample had reached 400°C. CO_2 was the other major species detected. The pattern of CO_2 release was highly dependant on sample, but there would always be a peak release at a particular temperature. Other species released showed the chemical history of the sample, e.g. an oxide formed from a metal chloride, usually evolved HCl. On occasions, the amount of material released was too great for the Ion Trap to measure, and so it was not possible to access what was released.

Oxygen release was also observed during the heating of many oxides, either due to decomposition of the oxide into a more reduced form, or from oxygen sorbed onto the surface. This effect could prove beneficial in an anoxic environment, such as in the proximity oxygen requiring catalyst. Mixing a material that emits O_2 at certain temperatures with a catalyst that needs O_2 to work is standard practice in industrial catalyst design. For instance, three way catalysts used in automobile exhaust systems use cerium oxide or MnO_x as an oxygen storage unit[8] (Terribile et al., 1998; Chang and McCarty, 1996). Some of the experiments in this chapter have attempted to find if this approach is successful in a GC-ir-ITD[9] system such as MODULUS.

Analysis of relative amounts of volatile release from TPD traces (for example, Figure 4.7), can be done by examination of the baseline. At the start of the test (on the left side of the trace), the material is at room (or other low) temperature and release of gases is almost always insignificant. Therefore, at this temperature this is the baseline signal detected by the ion trap. As the oxide is heated, volatiles are released, and the increase above baseline can be seen as signal rises over time.

[8] Throughout this thesis the term O_x is used when the oxygen stoichiometry in a metal oxide is unknown. (NO_x signifies multiple nitrogen oxides)

[9] Gas Chromatograph - isotope ratio – Ion Trap Detector

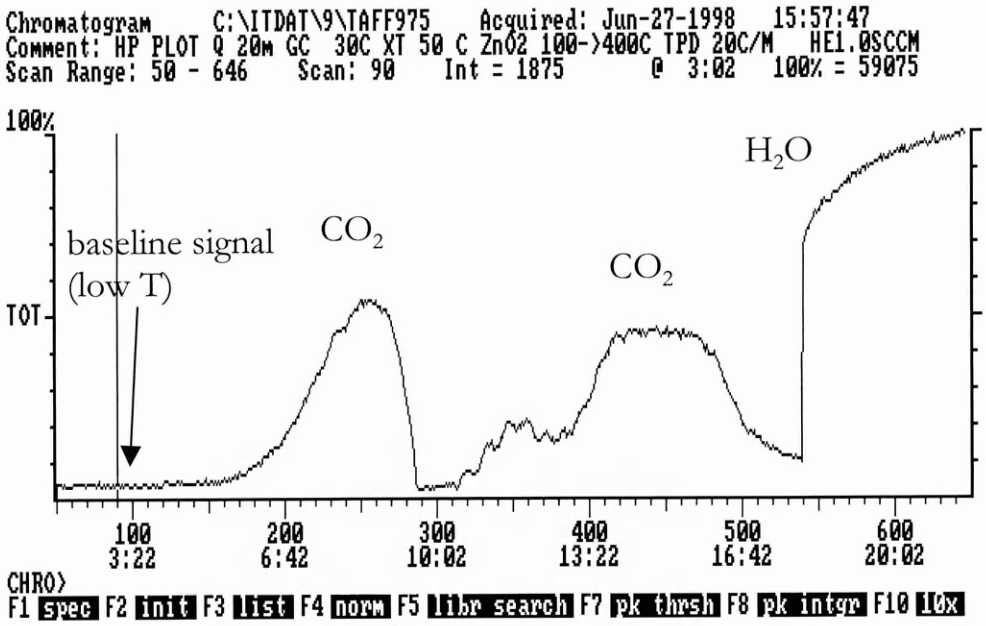

Figure 4.7 Temperature programmed desorption of ZnO_2 from 20°C to 400°C (ramped) with releases of CO_2 and H_2O detected by the ITD

4.3.8. Test gas injection

Once the amounts of background water and CO_2 detected by the Ion Trap were low, the catalyst was ready to be tested. The usable detection limits of the Finnigan MAT Ion Trap equated to less than one nanomole of CO_2, but this was dependent on the width of the peak. At the other end of the scale it was found that a sharp (<30 s) peak would not saturate the detector if it was less than 100 nmoles. In practice, the admission of a maximum of 60 nmoles was chosen for good peak size, (which necessitated the use of a 0.1 ml sample loop).

The first combustion test involved injecting pure CO over the sample. A gas aliquot of order of 3 torr was used; the Valco valve was switched and the ITD was set to measure spectra. The chromatogram was recorded until the final eluent was measured. The 6-port valve was then switched back from the inject position to the load position, filling the vacuum unit with the helium in the loop, which needed removal.

4.3.9. Effect of water in the Ion Trap

Various phenomena were seen if the amount of water in the Ion Trap built up to high levels. These can be demonstrated by examining Figure 4.7, displaying a temperature programmed desorption run with ZnO_2.

The first two major peaks are CO_2 evolved from the solid. The final surge is at mass 19 – from water undergoing self-protonation, and only appears to occur at high water levels in the ion trap (Barber, 1998). In general, protonation occurs when a singly charged ion reacts with a neutral water molecule that transfers a H atom (i.e. uncharged) to the ion, therefore increasing its atomic mass by 1 unit. For isotope ratio measurements it is crucial that this is minimised. The more water present in the trap, the more water is detected at mass 19, not 18. Protonation also occurred with other compounds e.g. $^{12}CO_2^+$ (m/z 44) to $^{12}CO_2H^+$ (m/z 45).

Self-protonation of water is visible (in the same chromatographic run) in Figure 4.8, where mass 18 shows increased levels at the time of CO_2 release peaks (on Figure 4.7) and a spike at the point where water approaches. At the later part of the chromatogram, where water is detected at mass 19 (the bottom chromatogram), mass 18 shows no more signal than background. The reason for the delay of the water surge could be attributed to both the sample oxide's water retention, and the effect of the GC column. Released water can interact with column coatings, to such an extent that retention behaviour is altered. In such cases columns need to be heated to at least 100°C to ensure the vapour is mobile and eluted out of the column. The water surge detected may be the result of overflow of water/water vapour, after the column's stationary phase has been saturated.

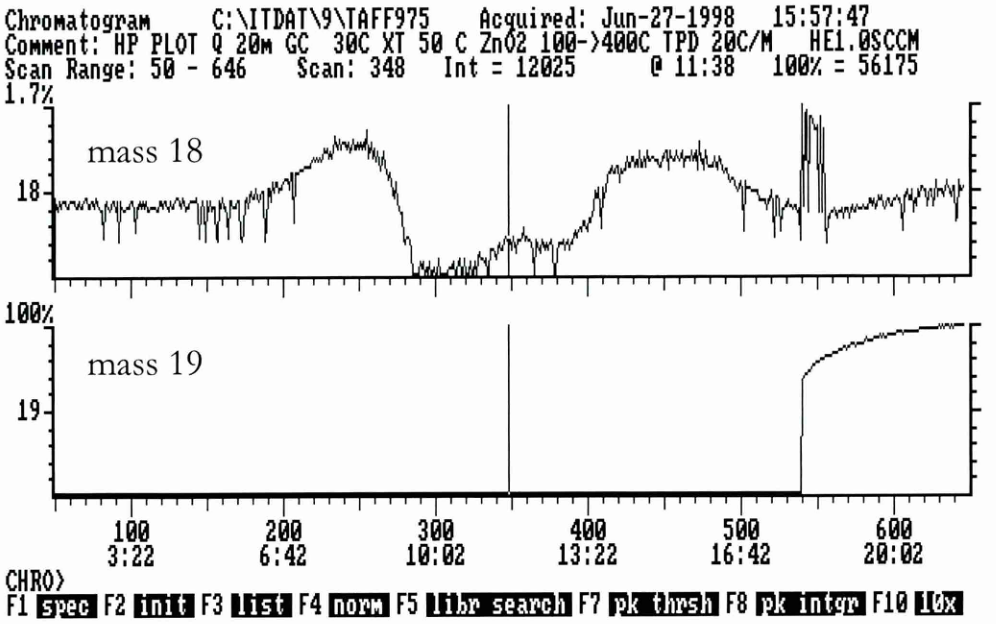

Figure 4.8 Same trace as Figure 4.7 but showing only the amounts of material detected at m/z 18 & 19

4.3.10. Format of chromatogram output from Ion Trap Detector

The Total Ion Chromatogram (TIC) shows the detected amounts of combusted and uncombusted gases, as well as gases released by the sample. By re-displaying the chromatogram, to show the ions specific to the species, it can show to what extent conversion has taken place. Calibration is difficult, due to the non-linear relationship between peak height and the amount of injected compound (see discussion in Chapter 2), but the retention time, and secondary ions can be used for additional identification.

Table 4.3 Major and minor ions detected in the ion trap after admission of selected species

Species	m/z of major peaks	m/z of minor peaks
CO	28	12 & 16
CO_2	44	16, 32, some 12
CH_4	16 & 15, self reacting, 17 & 29	
N_2	28	14
O_2	32	16

The relative intensities of the peaks from different gases can vary due to many parameters including the amount of gas or ion-molecule reactions. This is in contrast to quadrupole mass

spectrometers where cracking patters are more predictable, as ion-molecule reactions are less frequent due to the immediate extraction of ions from the ion source. Each chromatogram is comprised of individual mass spectra recorded over set time intervals between a certain mass range. Figure 4.9 shows a mass spectrum of carbon monoxide.

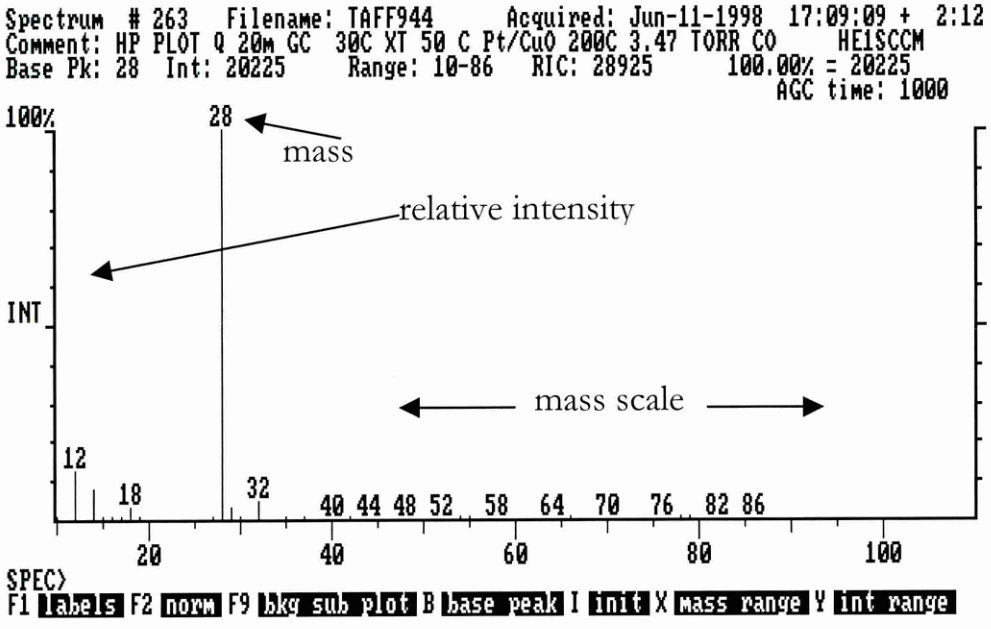

Figure 4.9 Instantaneous mass spectrum from 10-100 a.m.u., with CO detected as seen by the presence of m/z 28 & 12. Note the peak height is given as relative intensity normalised to 100% for the highest peak

Peak areas in chromatograms can be calculated from manually setting starting and end peak points on the Total Ion Chromatogram. These can be used to show relative amounts of CO/CH_4 and CO_2 for combustion efficiency. Unfortunately because of the non-linear response, this can only give an indication of the efficiency, and not an accurate value. Attempts were made at producing calibration curves, and were shown in Chapter 2.

By altering the display of the chromatograms within the ITDS software, the variation of individual ions versus time can be displayed. Figure 4.10 is an example of a CO partial oxidation displaying the total ion count. The first peak shows the CO and the second peak is CO_2. The standard display produced by the Ion Trap software is the total ion count during every scan (in

this case 2 scans/sec). This display does not give mass information of peaks, just retention time only, much like an F.I.D. or other non mass-selective detector.

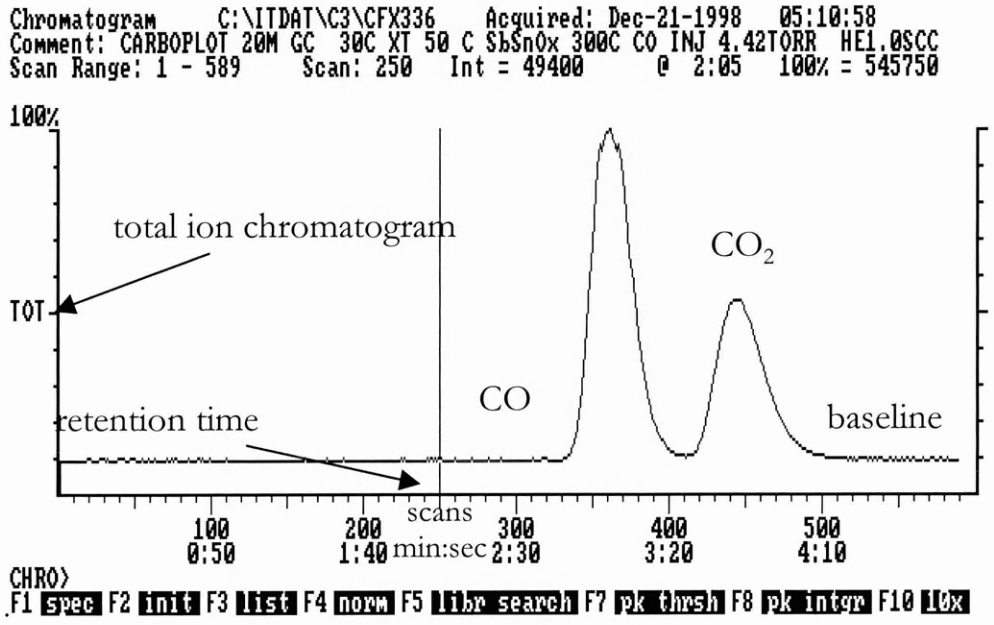

Figure 4.10 Total Ion Chromatogram (TIC) of an injection of CO over $SbSnO_x$ at 300°C.

The display shown in Figure 4.10 is the Total Ion Chromatogram (TIC) which is simply the sum of all the ions measured per scan interval. It can be seen from Figure 4.11 that distinct peak shapes are not always possible. The shoulder of this peak is CO_2 but is not distinct from the CH_4 of injection.

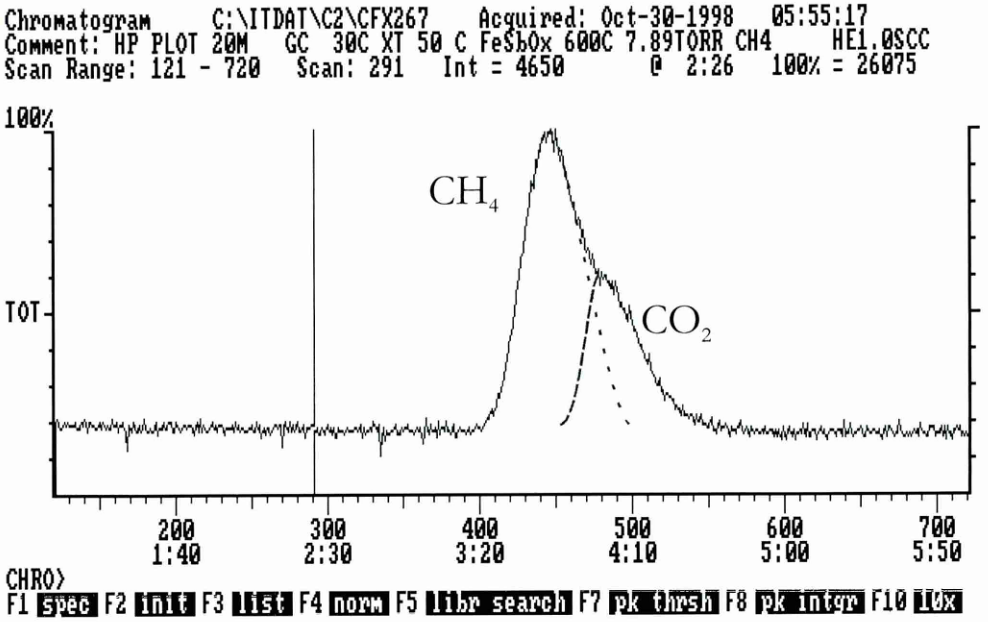

Figure 4.11 TIC of CH_4 injection over $FeSbO_x$ showing CH_4 and CO_2 peaks separated but not resolved. The additional curves show approximate position of individual peaks

One function of the ITD software is to show up to three individual ions (or mass ranges) simultaneously. Individual ions can be traced and the retention times measured, and secondary ions can identify the original sample material. In Figure 4.12 the trace shown in Figure 4.11 was changed to display the chromatograms of masses 15 and 44 only. From these traces, separation, relative peak intensity, and peak areas can be measured. For the purposes of this thesis, combustion efficiency (in %) is defined as the peak area of CO_2 divided by the sum of the peak areas of CO_2 and the uncombusted CO or CH_4.

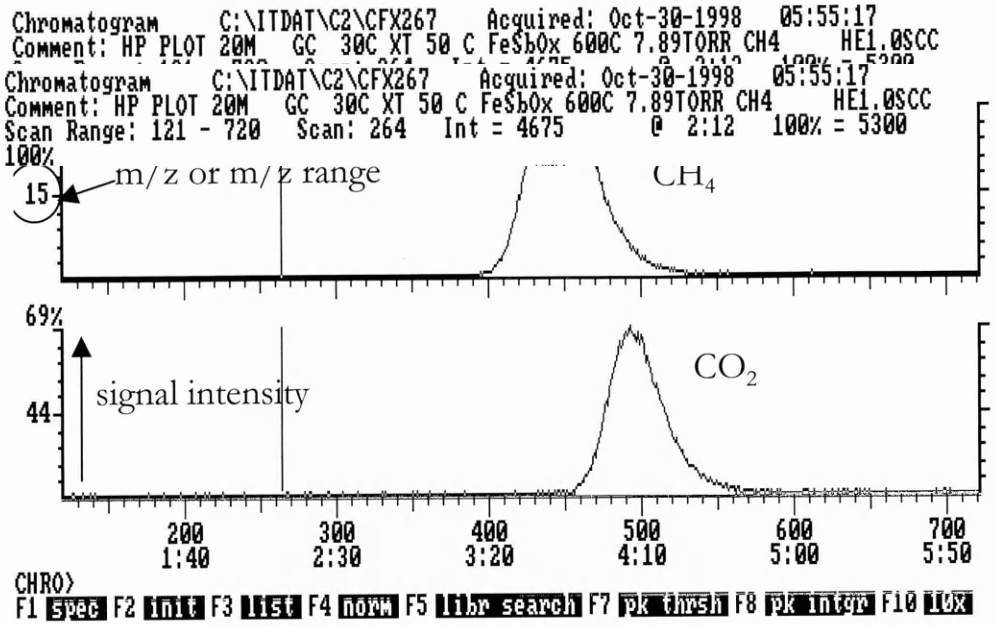

Figure 4.12 Same chromatogram as shown in Figure 4.11 but with software displaying only m/z 15 and 44

Using this display, the relative peak height can be used as an indication of combustion efficiency. Again, this response is not perfectly linear, and is dependent on the sensitivity of the ion trap for each species (number of ions detected from molecules admitted).

A useful function of the ITD was its ability to show the real-time detection of a certain mass range. This function allowed the ability to see the amount of material entering the detector without the need to set up chromatogram recording. During TPD and oxygen release events this allowed observation of emissions which could potentially render the filament inoperative or detector saturation. The measurement displayed by the ITD was counts/sec, where saturation level is equivalent to 4000 counts/sec. Typical clean background levels were of order 50-200 counts/sec.

4.4. Samples - Wire based catalysts

Commercial systems use a ceramic tube containing either oxidised copper wire, or oxidised nickel wire, with or without additional platinum as catalysts for use in carbon isotope analysis of methane and other organic molecules. Thus copper was considered to be a suitable starting point.

These experiments were undertaken without measured helium flow, as the mass flow controller was not procured at the time of the experiment, and thus flow was not measurable. The pressure of helium was set at 5 psi (measured upstream of the column) for every test for reproducibility.

4.4.1. Copper

Copper oxide in various forms has been the most common of all combustion reagents for isotope analysis. Oxidised wire form is known not to be as efficient at combustion as fine powder form (Kainz and Horwatitsch, 1960). Copper wire, oxidised in situ, has only been reported as used for chromatographic work – the low dead volume involved does not degrade the peak shapes. As explained previously in this chapter, Matthews et al. (1978) had used CuO wire form ground to a certain mesh size. Other groups used the powder as supplied - Sano et al. (1976) used CuO (60-80 mesh) powder. The research led to commercial systems having copper wire oxidised in situ for isotope ratio work (Merritt et al., 1995a).

The first combustion experiments attempted using the GC-ITD system were with oxidised copper wire. 0.4 grams of copper wire (0.25 mm diam., 99.99%, Goodfellows) was inserted into a 175 mm long quartz tube of 3 mm o.d. and 1 mm i.d. The outlet of a regulated O_2 cylinder was connected to the tube when installed into the tube furnace. O_2 flow rate was set to 4 ml/min and the furnace temperature was set to 400°C. After 2 hours, the furnace was left to cool to room temperature with a purging flow of O_2. Only when the temperature had dropped sufficiently was the O_2 flow turned off and He flow restored.

To verify this, a different column had to be installed, and the HP PLOT Q was chosen. This column was one of two used in this Chapter, the other being the J&W CarboPLOT column. At ambient temperatures, there was no substantial (in terms of peak width variations) retention difference between the two columns, and they were both considered interchangeable. On this occasion the copper wire was re-oxidised at 900°C for 3 hours and cooled as previously. The

oxide was then temperature ramped to 400°C in flowing He. Water and a small amount of CO_2 were evolved, but surprisingly the O_2 baseline fell (Figure 4.13).

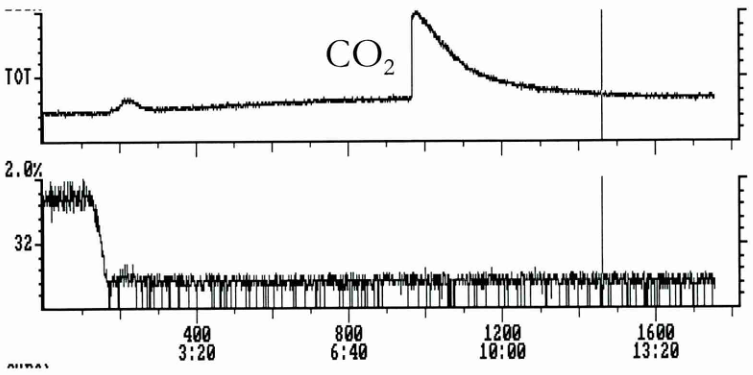

Figure 4.13 TPD of CuO with HP PLOT Q column installed showing TIC and m/z 32

Instead of O_2 being released by the oxide at this temperature, it appeared that any oxygen in the gas stream flowing over the copper oxide was adsorbed onto the surface. This effect was subsequently seen to occur with many oxides tested. Quantitative testing of combustion could only be achieved once a pressure gauge and gas aliqotter delivery/store system was constructed.

For the CuO reactor, CO combustion was complete at 290°C. However, increasing the amount of gas injected resulted in incomplete combustion (i.e. a small CO peak present in the chromatogram). Increasing the temperature and repeating the large injection gave the required temperature for a maximum measurable sample size. If the sample size was less than 2 nanomoles, 245°C would be enough for complete combustion (Figure 4.14 (a)). Nevertheless, a 60 nmol injection needed a temperature of 420°C for no residual CO to be detected (Figure 4.14 (b)), under the conditions of the experiment.

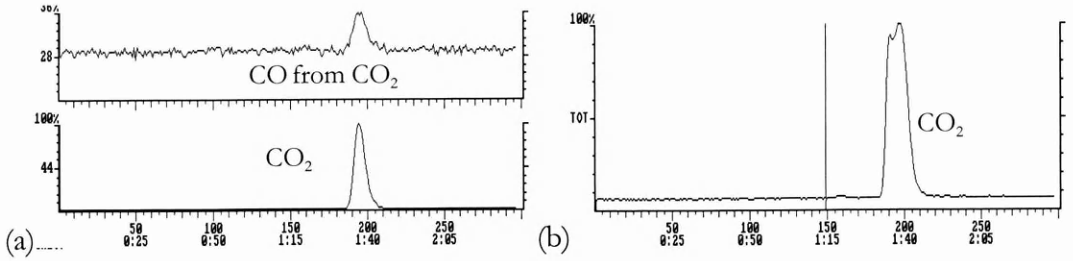

Figure 4.14 Chromatographic traces of (a) m/z 28 & 44 of small sample size of CO - injection at 245°C, (b) total ion chromatogram of 60 nmol of CO - injection at 420°C

Methane was also injected over the reactor, and even at high temperatures, complete combustion did not occur. At 1150°C only 95% combustion was observed for large (~30 nmol) CH_4 injections (Figure 4.15).

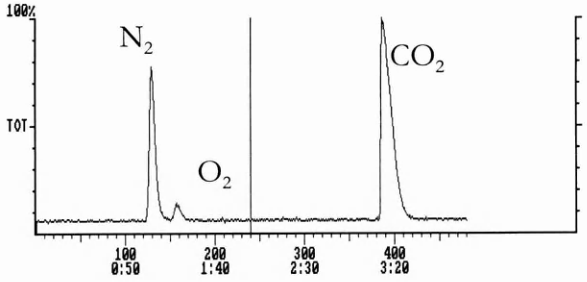

Figure 4.15 CH_4 combustion at 1150°C with air peaks present. This chromatogram shows the air peaks (from a loose fitting on the 6-port valve) before the CH_4 peak

4.4.2. Molybdenum

Pechanec (1973) found that MoO_3 was moderately active with respect to methane oxidation (with O_2). Furthermore, an investigation into oxygen isotope exchange with MoO_3, (Iizuka, 1994) used CO for the experiment, which oxidised well at 500°C. Herein three pieces of Mo wire (Goodfellows, 15 cm long, 0.5 mm diam, 99.95% purity, 0.7g total) were placed in a standard quartz tube, which was heated to 450°C and oxidised in an O_2 stream. TPD showed an increase in background levels but no individual ionic peaks (Figure 4.16 (a)). At 400°C there was no sign of any conversion of either CO or of CH_4 (Figure 4.16 (b)). Higher temperatures were attempted after the addition of Pt wires to the sample (see section 4.4.3)

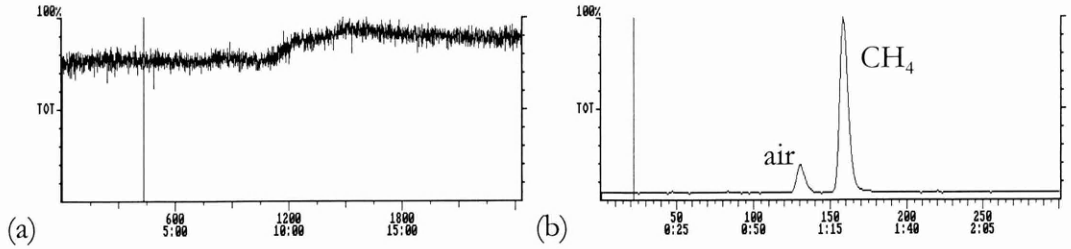

Figure 4.16 (a) TPD of oxidised Mo wire (b) CH_4 injection at 400°C. The first peak is from an air leak, and the second the uncombusted CH_4

4.4.3. Molybenum/Platinum

Merritt et al., (1995a) found that combining Pt and Cu wires led to more reproducible isotope values. Platinum wire was added to the molybdenum wire sample used in section 4.4.2. The tube was re-oxidised to 650°C in 6 ml/min O_2 flow. TPD to 400°C evolved small amounts of water only. Best combustion observed was with CO at 500°C (Figure 4.17 (a)), with a 30% conversion. At 600°C, no CO_2 was observed after a <5 nmol CH_4 injection (Figure 4.17 (b)).

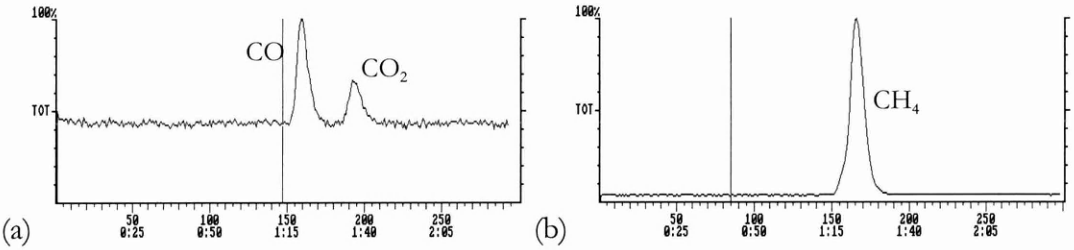

Figure 4.17 (a) Partial CO oxidation at 500°C, (b) CH_4 injection at 600°C, with no conversion observed

4.4.4. Nickel/Platinum

Oxidised nickel/platinum was used in the seminal work of Merritt et al. (1995a), and is also used in the commercially available Combustion Interface sold by Finnigan MAT. This sample was expected to give the most reproducible combustion at high temperatures. A combination of approximately 20 nickel wires (0.125 mm diam, 150 mm length) and two Pt wires (0.25 mm diam) were oxidised to 1150°C. The high temperature was assumed to be necessary as the operating temperature may be that high. The TPD result showed oxygen baseline dropping, but

no other gas was evolved (Figure 4.18 (a)). At 400°C CO oxidation was efficient, with 93% conversion. Complete combustion not achieved at 400°C as there always seemed to be residual CO. For complete conversion, 500°C was necessary (Figure 4.18 (b)). CH_4 conversion was more reliable at 700°C, with 25 nmol injections giving 100% CO_2 (Figure 4.18 (c)). Water production was evident, as some injections produced a water surge, [H_2O possibly held in the GC column (Figure 4.18 (d))]. It may be possible that the water may have interfered with the combustion process as the subsequent combustions were incomplete at the same conditions. The incomplete combustion may also have been due to the oxidative ability of the NiO having been depleted.

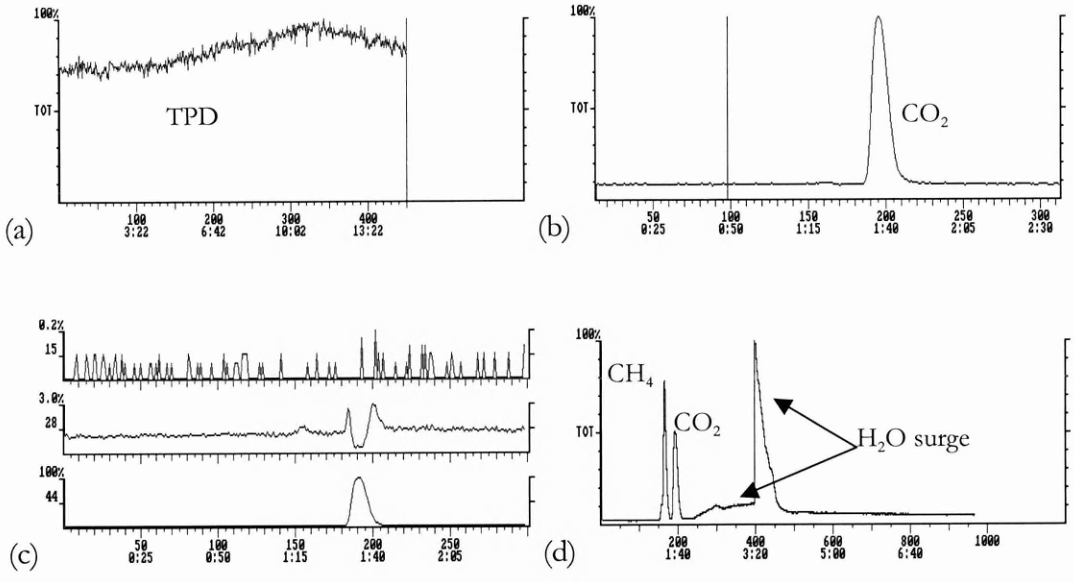

Figure 4.18 (a) TPD of NiO/Pt, (b) CO oxidation at 500°C, (c) CH_4 oxidation, with no remaining methane present at 700°C, (d) CH_4 oxidation at 700°C with water surge entering ITD

A second quartz tube was filled with nickel and platinum, but the length of the wires in the tube was decreased to 25 mm (more compatible with MODULUS). The same oxidation conditions were applied. With CH_4 injections (over the whole size range) at 600°C, partial oxidation to a mixture of CO and CO_2 was seen. On increasing the temperature to 900°C, injections larger than 30 nmol were not completely converted to CO_2 (Figure 4.19). The greatest conversion for injections of this size was 97% CO_2 and 3% CO at 900°C. Therefore, the reduction in the

quantity of catalyst material in this second sample lowered the amount of CH_4 or CO that it could combust.

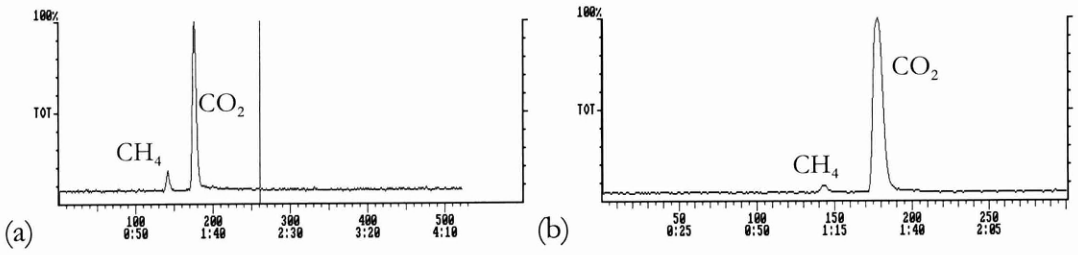

Figure 4.19 Experiments using a short NiO reactor, i.e. more appropriate for MODULUS (a) CH_4 oxidation at 700°C, (b) and at 900°C

4.4.5. Copper/Platinum

A copper analogue of the small scale nickel/platinum reactor was created. This sample (25 mm length wires) was oxidised at 800°C. Small (<10 nmol) CO injections were 100% combusted at 400°C. CH_4 injections never reached complete conversion to CO_2, even at 1000°C. At best, both CO_2 and CH_4 peaks were of comparable peak area. Increasing the temperature caused the CuO to act as an oxygen source, preventing the use of the Ion Trap. Figure 4.20 shows a CO injection of 1.2 nmol, and a CH_4 injection (10 nmol) at 1000°C.

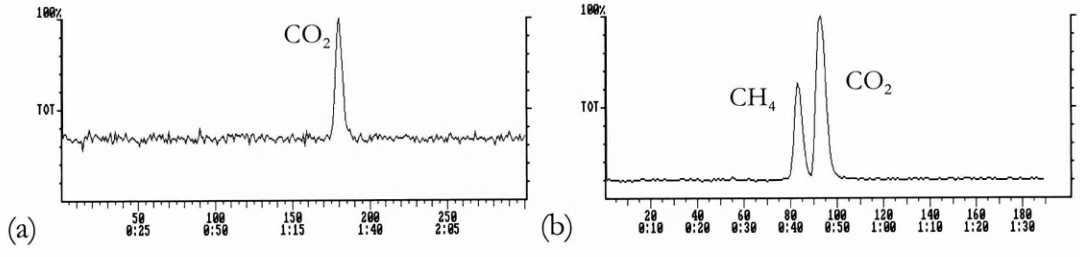

Figure 4.20 (a) 1.2 nmol of CO over Cu/Pt oxidised wire at 400°C, (b) 10 nmol CH_4 injection at 1000°C

4.4.6. Silver

Silver metal was found by Pechanec (1973) to have as good an oxidative catalytic ability as CuO and Cr_2O_3 in O_2. Other silver compounds (silver-manganese oxide mixtures) are also known for their combustion quality (Gardner et al., 1991). A quartz tube containing silver wire (0.25 g) was

oxidised to 400°C. No visible change was seen on the wire after oxidation. So clearly using silver wire may not have been the most efficient manner of using Ag_2O. TPD released some O_2 and CO_2. CO injections always showed incomplete combustion, with the highest conversion being 50% at 700°C (Figure 4.21 (a)). Injections of CH_4 showed no signs of conversion even at 900°C (Figure 4.21 (b)).

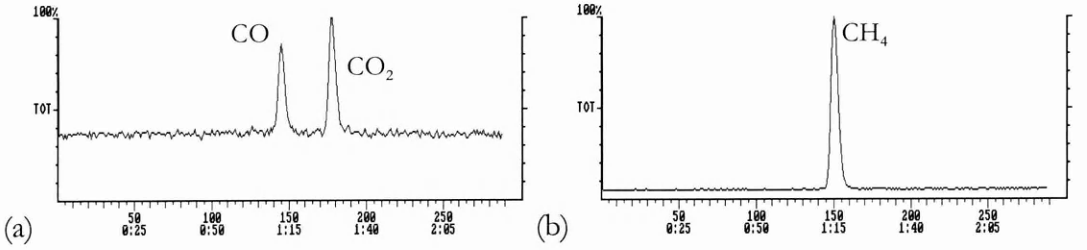

Figure 4.21 (a) partial CO oxidation over Ag oxidised wire at 700°C, (b) CH_4 injection at 700°C showing no oxidation

4.4.7. Conclusions from wire tests

From the above tests a summary can be drawn of the results from the oxidised wire samples. No wire performed well enough to completely oxidise methane, even at high temperatures.

Table 4.4 Summary of combustion data from CO and CH_4 injections over various heated oxidised wires All injections were with pure CO and CH_4, injection range (for all materials) 2 – 50 nanomoles (approx.)

Material	Combustion efficiency	
	CO	CH_4
Copper	CO 100% at 420°C	CH_4 95% at 1150°C
Molybdenum/Platinum	CO 30% at 500°C	CH_4 0% at 600°C
Nickel/Platinum (large)	CO 100% at 500°C	CH_4 100% at 700°C
Nickel/Platinum (small)	untested	CH_4 97% at 900°C
Copper/Platinum	CO 100% 400°C	CH_4 50% at 1000°C
Silver	CO 50% at 700°C	CH_4 0% at 900°C

No oxidised metal wire was capable of 100% conversion of methane to CO_2. Since nickel/platinum achieved the best combustion results for methane combustion, it was selected as one system to investigate further (Chapter 5). Nickel/platinum, copper, and copper/platinum were also the only successful reagents for carbon monoxide conversion.

4.5. Powders – Active Reagents

Powders generally have greater surface area than oxidised wires. An increase in surface area will almost always cause an increase in the activity of the reagent. In total, 31 different compounds were analysed, of which some had multiple preparations. The following section details the properties of each compound, including their ability to combust CO and CH_4, and any effects seen on heating the compounds, such as emission of volatile compounds. Other effects observed were the complete absence of any peak (CO, CH_4 *or* CO_2) implying that the oxide had adsorbed the compound (or the combustion product) onto its surface.

Data for the grain/particle size distribution for the powders was unavailable for almost all samples. The approximate mass of reagent used in each sample was 0.1 g. Between 10 – 13 cm of reagent were loaded in each of the quartz sample tubes, the process of installation being described in section 4.3.5.

The collated results from the following section is shown in 4.7.

4.5.1. Palladium sponge (Oxidised)

Palladium oxide has been shown to be active in methane oxidation. Pechanec (1973) found that PdO was able to combust CH_4 at 420°C in the presence of O_2. More detailed investigation of the PdO system has been performed by Farrauto et al., (1992). If PdO is supported on alumina, the mixture enhances oxygen adsorption, lowering activation energy for methane oxidation below 650°C, in comparison to PdO. Farrauto et al. (1992), reported that oxidation does not take place above 650°C. This is because at high temperature PdO reduces partially, to palladium-oxygen species dispersed on bulk palladium, but cooling does not re-adsorb the oxygen until 650°C or lower is attained. Significant hysteresis is apparent, showing that at least two distinct palladium/oxygen species are present.

Palladium sponge (from Aldrich), a light grey, finely powdered form of the metal, required oxidation prior to use. A total of 0.10 g of metal was used. Oxidation was achieved with 6

ml/min O_2 flow at 400°C. Its appearance changed to a red/light brown powder. TPD detected releases of CO_2, N_2 and O_2 (Figure 4.22 (a)). The oxygen release was relatively slow in decaying.

Combustion of CO occurred easily at low temperatures. At 400°C, all CO injected was converted to CO_2. As the temperature was lowered, CO conversion was still 100%. The minimum combustion temperature was found to be 200°C (Figure 4.22 (b)). Even at 30°C, a large CO injection (20 nmol) gave 10% conversion. Large (>25 nmol) injections were completely oxidised at 200°C

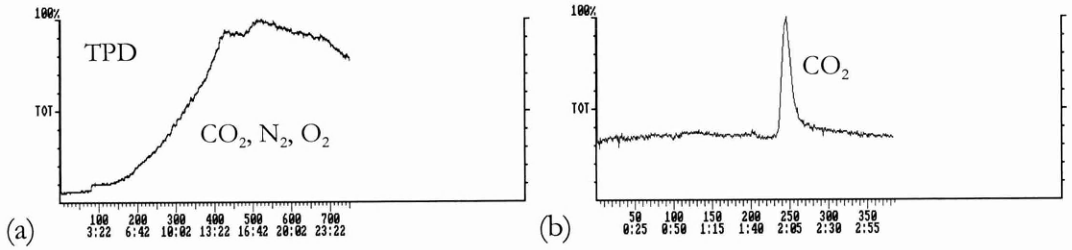

Figure 4.22 (a) TPD of oxidised Pd sponge, with CO_2, N_2, and O_2 releases, (b) 10 nmol CO oxidation at 200°C showing complete conversion

No reconditioning was performed. Large injections of CH_4 were fully converted to CO_2 at temperatures of 450°C or higher (Figure 4.23 (a)). After lowering the temperature to 400°C, some CH_4 was evident in the chromatogram if the injection was greater than 10 nmol (Figure 4.23 (b)).

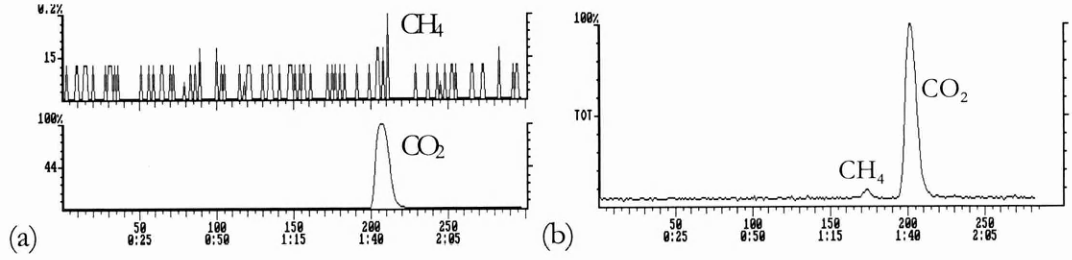

Figure 4.23 (a) CH_4 oxidation over PdO (sponge) at 450°C showing complete conversion, (b) incomplete conversion of CH_4 at 400°C

The repeatability of the injections were tested with 4 more CH_4 injections at 450°C over a range of injection sizes(3.3 to 44 nmol), and all gave 100% conversion to CO_2.

4.5.2. Nickel (II) Oxide

Nickel oxide had been shown by Pechanec (1973) to combust CH_4 successfully at 460°C. Its combustion potency was found to be hampered in a CO_2 atmosphere (Kainz and Horwatitsch, 1960). Nickel oxide powder (0.066 g) was used as received from Aldrich (99.95%). TPD revealed water and CO_2 evolution (Figure 4.24 (a)). Injecting CH_4 over the oxide at 700°C, gave partial combustion to CO_2, depending on the amount injected (8 – 44 nmol) (Figure 4.24 (b)). Increasing to higher temperatures resulted in a release of CO_2, which did not decay significantly after leaving for 12 hrs.

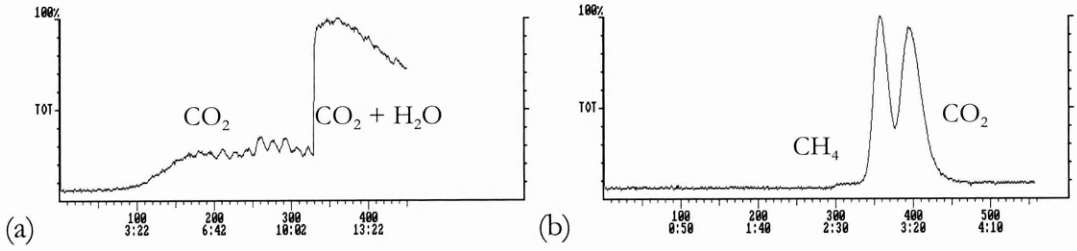

Figure 4.24 (a) TPD of NiO with CO_2 and H_2O releases, (b) (45 nmol) CH_4 injection at 700°C showing partial conversion

4.5.3. Cerium (IV) Oxide

Cerium oxide is known to be multi-functional in oxidation catalysis. The oxide was shown to combust CH_4 at temperatures between 600 and 700°C by Pechanec (1973), placing it among the higher temperature oxides tested. Ceria (CeO_2) has also been known to act as an oxidation promoter in catalysts comprised of precious metals on ceria-alumina mixtures (Yao, 1984). Its use in three-way catalysts as an Oxygen Storage Component (OSC) has resulted in CeO_2 being placed in automotive catalysts, to eliminate HC, NO_x, and CO from exhaust gas. Mixing with other metals to form $(Ce,Zr)O_2$ solid solutions for example, increases the storage capacity further (Cuif et al., 1997). Cerium oxide has also played the role of an active surface phase once

supported on alumina for CH_4 oxidation (Haneda et al., 1994). This oxygen storage is due to the partial reduction of Ce(IV) to Ce(III):

$$xCO + CeO_2 \rightarrow xCO_2 + CeO_{2-x} \quad (4.13)$$

and the reverse: $\frac{1}{2}xO_2 + CeO_{2-x} \rightarrow CeO_2$ (4.14)

The yellow powder was used as received from Aldrich (0.11g purity 99.95%, particle size <5μm). TPD from this compound revealed a large amounts of water and CO_2 were evolved (Figure 4.25 (a)). A second TPD run was attempted, from 400°C to 800°C at the same ramping rate. More CO_2 was evolved (Figure 4.25 (b)). (The container label actually noted that the compound absorbs CO_2 from the atmosphere.) The compound was left at this high temperature for 2 days, and on return there was still a measurable m/z 44 background.

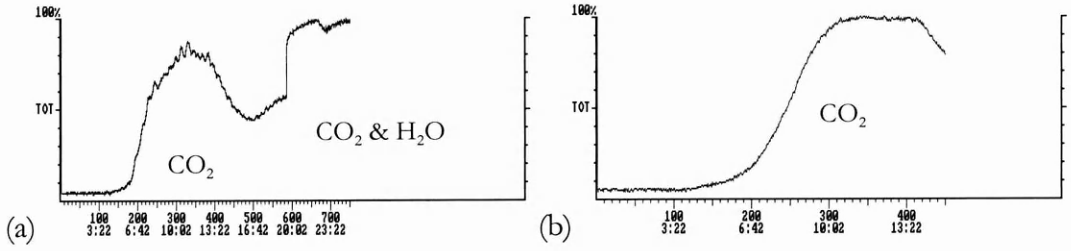

Figure 4.25 (a) TPD from CeO_2 with CO_2 and water releases, (b) ramped heating from 400 to 600°C revealing CO_2 emission

When CH_4 was injected at 900°C, CO_2 peak shapes were wide, asymmetrical and decayed very slowly (Figure 4.26 (a)). Reducing the temperature to 650°C increased the peak symmetry, but no combustion of CH_4 was observed (Figure 4.26 (b)).

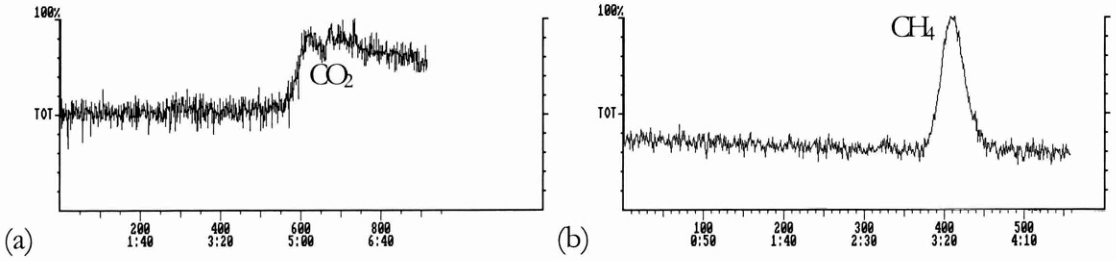

Figure 4.26 (a) CH_4 injection at 900°C, showing wide CO_2 peak, (b) CH_4 injection at 650°C with no oxidation observed

The sample was removed, re-oxidised with flowing O_2 and re-installed in the ITD system. Some CO_2 was seen to be evolved on heating to 400°C. Heating to 900°C, where previously good combustion was marred by peak tailing, revealed the combustion to be good. Perfect CO_2 peak shapes were seen, with no remaining CH_4 in the chromatograms. The re-oxidation process probably regenerated active sites for oxidation or removed contaminants hindering the oxidation process.

4.5.4. Cobalt (II, III) Oxide

Co_3O_4 has been used previously as a combustion catalyst in isotope ratio mass spectrometry (Barrie et al., 1984) and was compared with NiO and CuO by Merritt et al., (1995a). Ebel, (1973) showed it to have greater combustion properties than MnO_2, NiO, CuO, and Cr_2O_3 when used with O_2 gas. Horacek et al., (1960) found Co_3O_4 to have the lowest temperature of CH_4 combustion, at 311°C, of any other oxide tested. This oxide has been widely used in elemental analysis thanks to its combustion properties (Ma and Gutterson, 1976).

Co_3O_4 (0.052 g) was supplied by Aldrich. TPD (from 20 to 600°C) results showed a large amount of water evolved (Figure 4.27 (a)). Initial CH_4 injections at 600°C showed small peaks eluted; methane was combusted to CO_2, but the peak size was much smaller than expected (Figure 4.27 (b)). At 500°C, 100% CH_4 conversion was observed for loads of less than 10 nmol, while larger (30 nmol) injections resulted in over 97% conversion. A notable CO_2 background was present. On heating Co_3O_4 to 900°C a large amount of O_2 evolved, with a release rate 8 times as much as at 850°C. O_2 release dropped to background levels at 800°C.

It was during the analysis of this compound that the commercial mass flow controller was installed. On repeating the injections, a set flow rate of 1 sccm gave 14psi column head pressure. Interestingly, CH_4 injections at 750°C resulted in good CO_2 peaks, but with a small (<1%) amount of CH_4 remaining (Figure 4.27 (c)). Reducing the temperature to 600°C, resulted in incomplete combustion (Figure 4.27 (d)).

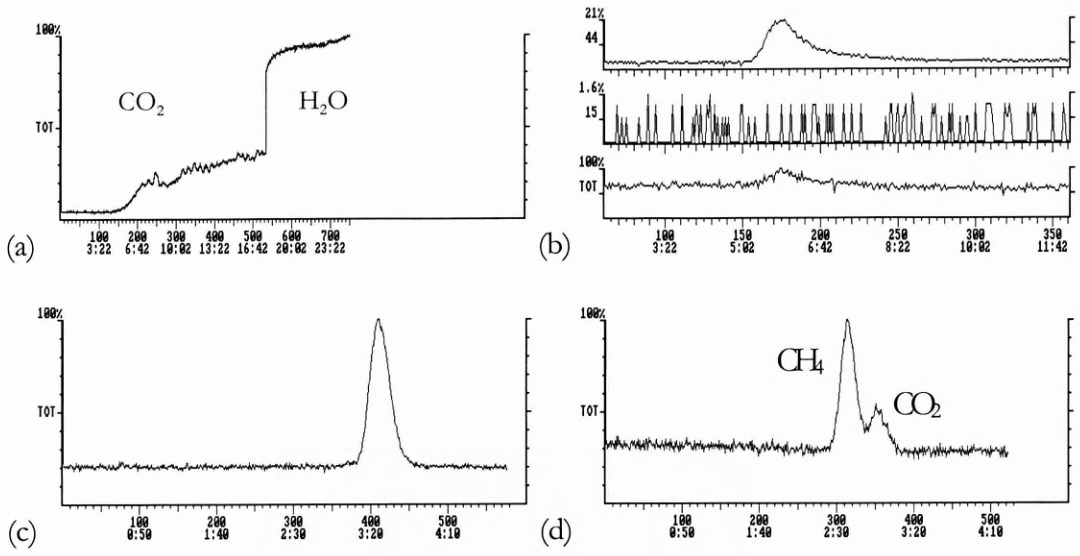

Figure 4.27 (a) TPD of Co_3O_4 to 600°C with H_2O and CO_2 release, (b) CH_4 injection at 600°C over Co_3O_4 showing complete combustion, (c) near complete combustion of CH_4 at 750°C, (d) incomplete combustion of CH_4 at 600°C

Carbon monoxide conversion was tested at 600°C, and resulted in 100% conversion to CO_2. Combustion to 100% was noted (by the complete loss of reagent) at lower temperatures down to 100°C, but expected peak sizes of CO_2 reduced dramatically once the temperature was lowered below 300°C (Figure 4.28).

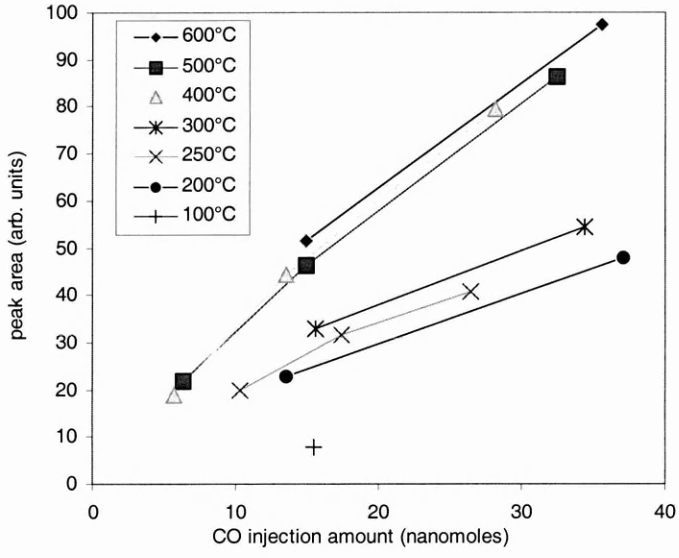

Figure 4.28 Peak area versus CO injection amount for various temperatures of Co_3O_4. Higher temperatures give consistently better oxidation

Quantitative conversion is observed when the amount of sample injected over an oxidant is proportional to the amount of CO_2 detected by the mass spectrometer. If the detected amount is not linear, or if the slope of a line formed by the relationship is lower than expected, then incomplete conversion has taken place (or in some cases CO_2 may be retained). Figure 4.28 shows that at 300°C and below there is a drop from the line presented by the higher temperature combustion. This could suggest either CO was physisorbed by the Co_3O_4 surface on contact, or CO_2 being formed on the surface, but a portion of CO_2 was not desorbed. In all likelihood, isotopic fractionation is occurring in this process. Temperatures of 400°C and above show no significant loss of CO_2, so CO is 100% converted. Therefore, it would be anticipated that at 400°C isotopic integrity of carbon should be preserved.

4.5.5. Manganese Oxide

Manganese oxide has also been used as a combustion agent in elemental analysis equipment (Ma and Gutterson 1976). Horacek (1960), found its methane combustion temperature to be 453°C under the conditions employed. (Kainz and Horwatitsch, (1960) showed the superiority of MnO_2 over Co_3O_4 when used in a closed atmosphere containing CO_2 or O_2 partial pressures. MnO_2 also showed the capability to be an oxygen storage component (OSC) when supported on $LaAlO_3$ with a noble metal added for activity (Chang and McCarty, 1996). It has also been used as a support for gold in testing low-temperature CO oxidants (Hoflund et al., 1995).

According to the supplier, the melting point of this oxide was 535°C. In order to explore this oxide (0.081 g used) was heated to 550°C, and was seen to emit a large quantity of O_2, peaking at 1000 counts/s before decaying to 100 counts/s after 10 minutes. Injections of CH_4 at 550°C, found combustion to be no greater than 50%. At 400°C, testing CH_4 combustion resulted in no detectable CO_2. CO oxidation was measured at 400°C, and combustion was 100% at this temperature (Figure 4.29 (a)). Using the oxide at 300°C also resulted in 100% combustion of

CO. At 200°C, CO was not fully combusted, with large injections producing only 95% combustion (Figure 4.29 (b)).

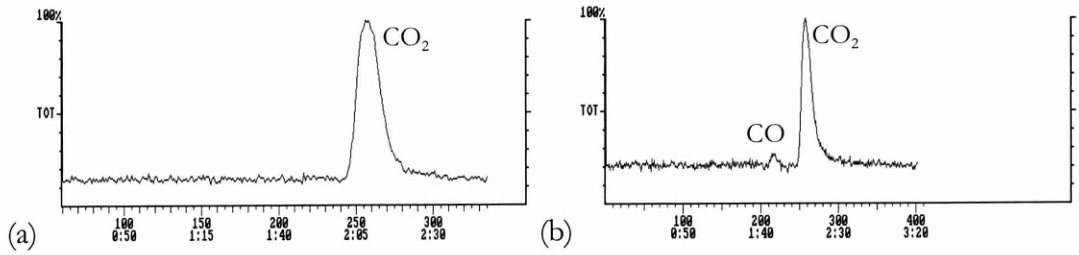

Figure 4.29 (a) CO injection over MnO_2 at 400°C showing complete combustion, (b) incomplete combustion of 17 nmol of CO at 200°C

4.5.6. Silver (I) Oxide

Although Pechanec (1973) has reported that silver metal has been used successfully in oxidation (with O_2 present), silver oxide is not known for this property. Silver metal has also been tested as the active metal on a support for CO oxidation (Gardner et al., 1991). NB oxidised silver wire was tested in section 4.4.6.

Silver (I) Oxide was supplied as powder by Aldrich, of which 0.081 g was used. It is known to decompose to Ag at temperatures above 150°C and up to 250°C (Cotton and Wilkinson, 1980). This would make it a potentially useful O_2 source on MODULUS, as little power would be needed compared to CuO which releases at 850°C. After installation, among the ions in the helium baseline was CO_2, the level of which decayed slowly. No TPD was performed due to the low decomposition temperature. Injecting CO over the oxide at 200°C resulted in good combustion. Large (35 nmol) samples of CO gave perfect conversion to CO_2 but peak shapes were quite asymmetrical – peak tailing of CO_2 resulted (Figure 4.30). O_2 release was only of a significant amount (60 counts/s) when the material was heated to 250°C

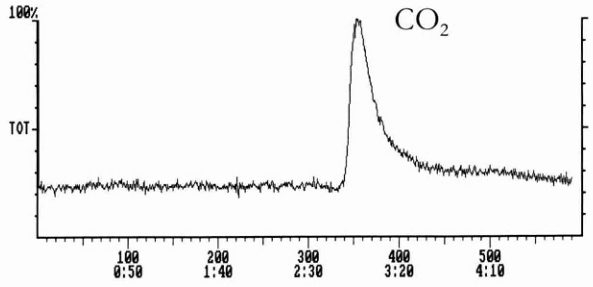

Figure 4.30 CO (20 nmol) injection over Ag_2O at 200°C showing complete conversion to CO_2

4.5.7. Platinised Copper Oxide

Copper oxide has been impregnated by an unknown method to produce a loading of 20% platinum (metals ratio), and used as supplied by Elemental Microanalysis Ltd. Particle size was of order 0.2-0.5 mm, which made loading the 0.068 g of material quite difficult in a 1 mm i.d. tube. This oxide had been marketed by the suppliers, to be used in combustion of organic compounds to CO_2 for $\delta^{13}C$ analysis.

On initial heating during TPD, a large amount of water was evolved, the flux of which decayed over time. CO injections were completely converted to CO_2 at 400°C. Lowering the temperature to 200°C gave incomplete combustion, but 250°C gave over 97% conversion of large samples (>25 nmol) (Figure 4.31 (a)). CH_4 was more demanding to convert. At 700°C, 10% conversion was seen, while at 800°C O_2 was evolved in large quantities. Approximately 65% combustion is seen from peak heights of CH_4 and CO_2 at 800°C (Figure 4.31 (b)).

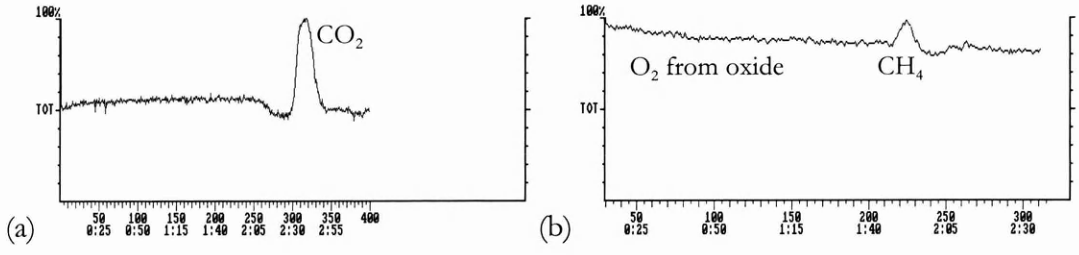

Figure 4.31 (a) CO complete conversion over CuO/Pt at 250°C, (b) TIC of CH_4 injection at 800°C showing O_2 emitted by oxide. CO_2 only visible in ion specific view, as it is lost in the baseline in the TIC

4.5.8. Titanium Dioxide

TiO_2 is not known for its oxidation ability. It has been used as a support for noble metals (Haruta et al., 1996) and has been tested for oxygen isotope exchange between CO_2 and bulk oxygen (Yanagisawa, 1995). TPD on TiO_2 (0.049 g used) showed a variety of evolved gases (Figure 4.32 (a)). Initially CO_2 and unusually (in TPD runs) CH_4 were released, then a large water release, followed by a small release of ions of m/z 43 and 57 (possibly $CH_3CH_2CH_2^+$ and $CH_3CH_2CH_2CH_2^+$). No combustion of CO was seen at 400°C. At 700°C conversion was less than 40% (Figure 4.32 (b)). Injecting CH_4 at this pressure resulted in conversion to CO_2 having 4% peak height of CH_4. This did not improve significantly at 900°C.

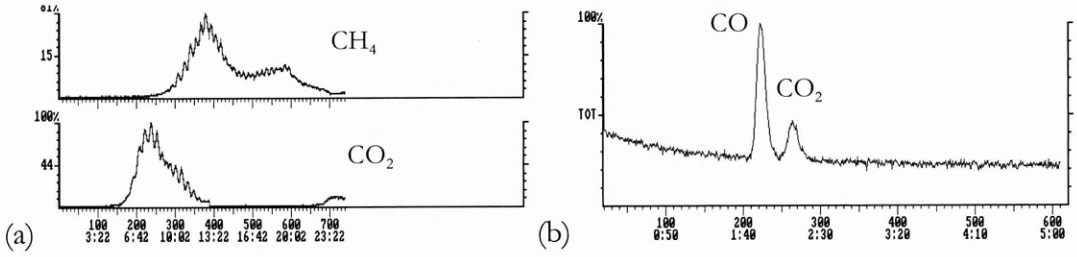

Figure 4.32 (a) TPD of TiO_2 showing CH_4 and CO_2 emission, (b) 17 nmol CO injection at 700°C showing incomplete conversion to CO_2

4.5.9. Gallium (III) Oxide

Pechanec (1973) classified Ga_2O_3 in the group capable of combusting CH_4 at 500-600°C in the presence of O_2. As gallium is a non-transition metal, any reduction-oxidation cycle with Ga_2O_3 would involve some of the material being reduced to metal. Ga_2O_3 released CO_2 and water in the TPD chromatogram (0.06 g used). Very little CO_2 was observed with methane combustion at 600°C. However, at 800°C there was little residual CH_4, and partial combustion was seen with equal peak heights for CO and CO_2 (Figure 4.33 (a)). Large amounts of CH_4 injected again showed partial combustion, but with some (<10%) CH_4 remaining. This also occurred at 1000°C (Figure 4.33 (b)). Conversion of CO was nil at 400°C.

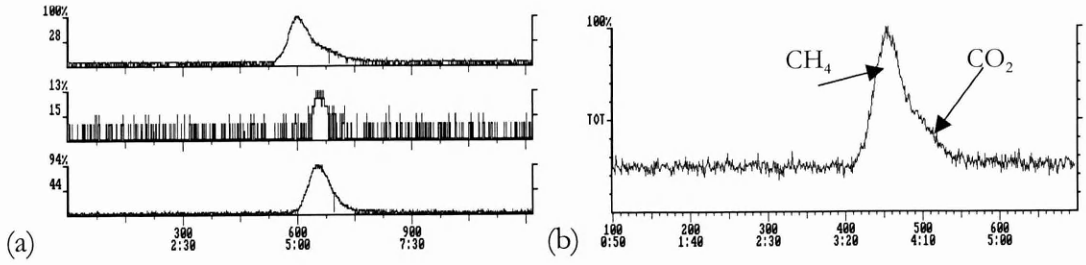

Figure 4.33 (a) Injection of CH_4 over Ga_2O_3 at 800°C showing incomplete combustion to CO and CO_2, (b) CH_4 oxidation at 1000°C

4.5.10. Bismuth (III) Oxide

Bi_2O_3 has previously been shown to be an efficient combustion catalyst as it was unselective in the partial conversion of methanol to its derivatives (Taylor et al., 1995). Methanol was almost exclusively converted to CO_2 at low temperatures (<350°C), while 30% conversion occurred at 235°C. Bi_2O_3 was not found to be as successful in the GC-ITD system testing CO and CH_4. TPD gave a large release of CO_2 only (0.23 g used). CO combustion was successful at 400°C or greater (Figure 4.34 (a)). CH_4 showed marginal combustion at 700°C (Figure 4.33 (b)). On removal, Bi_2O_3 had reacted to form some coloured powders and crystals, even though the melting point of 825°C was never reached.

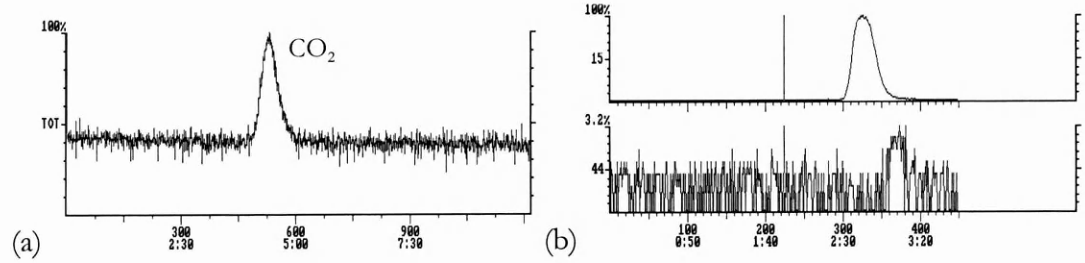

Figure 4.34 (a) complete combustion of 21 nmol of CO over Bi_2O_3 at 400°C, (b) marginal combustion of 17 nmol of CH_4 at 700°C

4.5.11. Iron-Nickel Oxide

The iron-nickel oxide mixture was a laboratory demonstration of the co-precipitation process, prior to making a number of other mixtures. No combustion data on mixtures of iron and nickel oxides are readily available in the literature. $FeNiO_x$ was prepared by co-precipitation of $FeCl_3$ and $NiCl_2$ with a 1:1 molar metals ratio (0.07 g used). Heating to 400°C gave a large

release of water. Carbon monoxide was completely converted to CO_2 at 400°C. The minimum combustion temperature for complete conversion was found to be 275°C (Figure 4.35 (a)). Methane conversion was also found to be complete at 800°C. At this temperature there was a small release of O_2. Increasing the temperature to 900°C gave a release rate of O_2 of five times that at 800°C. At the same time as the CO_2 (from combustion) peak eluted, a peak of mass 64 was detected (Figure 4.35 (b)). The compound responsible for this ion was not identified, but potentially could be CH_3CH_2Cl, or ClCHO as chlorine was used in the preparation of the compound.

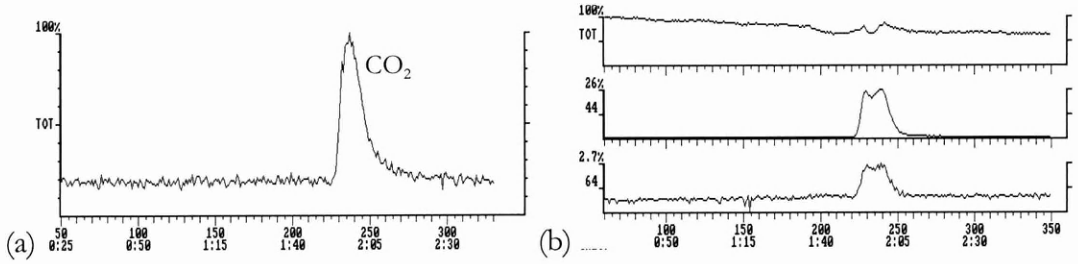

Figure 4.35 (a) CO (24 nmol) conversion over $FeNiO_x$ at 275°C, (b) CH_4 injection at 900°C showing O_2 emission and m/z 64 peak concurrent with CO_2 (possibly CH_3CH_2Cl but nothing was seen at m/z 66))

A second sample of smaller granule size $FeNiO_x$ (same preparation method) was prepared (0.07 g used). The first sample had a large granule size, such that filling the quartz tube was difficult. The second sample had additional grinding in a mortar and pestle before calcination. CO conversion was not complete at 275°C, but was at 350°C. Combustion of CH_4 was 100% at 700°C. At this temperature the pressure was at the maximum set by the helium tank regulator (4 bar), but the flow rate was only 0.42 sccm, giving greater contact time for the reaction. This may explain the increase in activity at this temperature. Surface area was also likely to have increased. No peak of mass 64 was observed, even though the compound was prepared in the same method as the first.

4.5.12. Palladium Oxide

A description of the activity of Palladium based oxides was given in section 4.5.1. This sample of PdO was used as supplied by Aldrich, at 99.99% purity (0.17 g used). Heating the palladium oxide to 450°C released CO_2 and also ions at mass 30, thought to be NO, the release of which decayed over time. This compound gave some of the best minimum combustion temperatures of any oxide. Carbon monoxide injections gave 100% combustion at 250°C (Figure 4.36 (a)), but with lower than expected peak areas. Methane was fully combusted at 350°C with no loss of expected peak area (Figure 4.36 (b)). The peak areas obtained from CO_2 produced by CH_4 injections are shown in Figure 4.36 (c). In comparison, complete conversion of CH_4 over the oxidised Pd sponge occurred at 450°C (section 4.5.1).

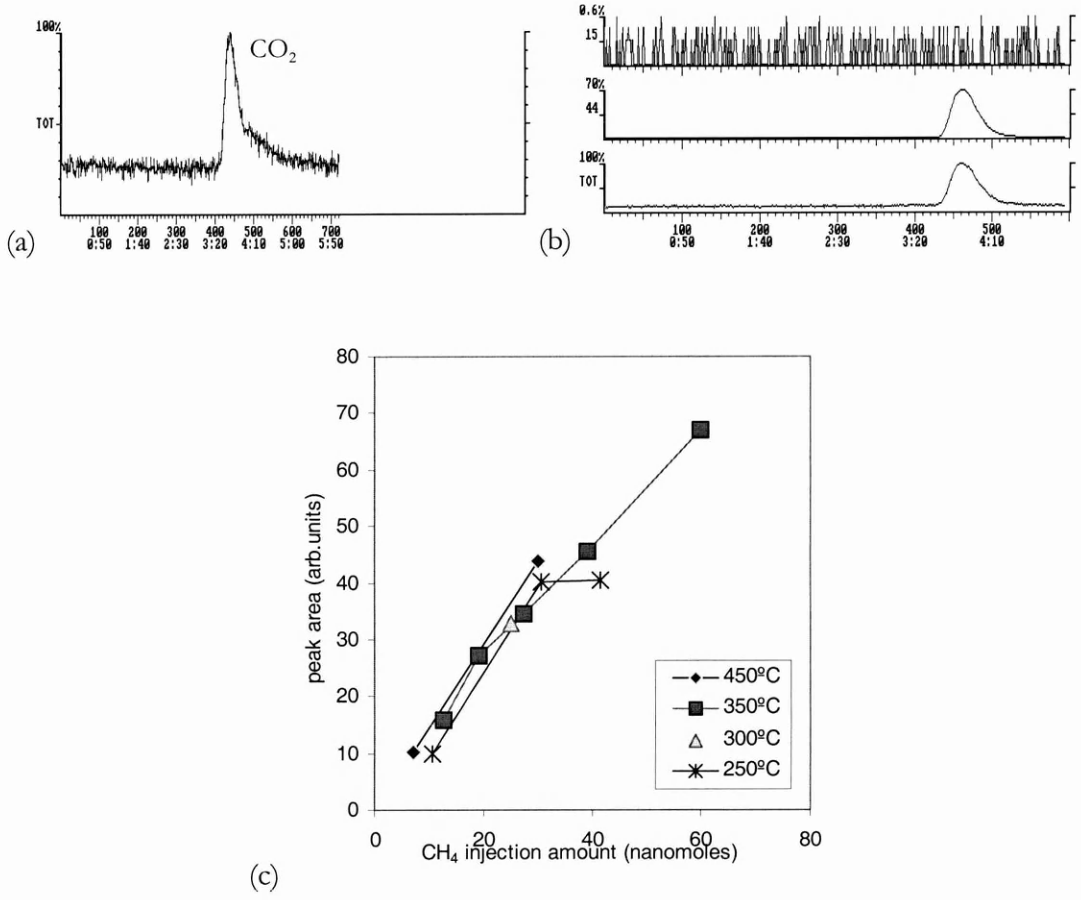

Figure 4.36 (a) complete CO conversion at 250°C over PdO, (b) complete conversion of CH_4 over PdO at 350°C, (c) injections of CH_4 at different temperatures over PdO

4.5.13. Antimony-Tin Oxides

Several studies of the activity of tin-antimony oxides have shown that they are active for the selective oxidation of propylene to acrolein (Berry, 1981). A series of antimony-tin oxides were created and tested. The first antimony-tin oxide was made with a 1:4 molar ratio of tin to antimony. 1.54g SnO_2 was mixed with 5.95g of Sb_2O_3. Both powders were ground together and fired at 1000°C in air for 12 hours, producing a mixture of stoichiometry Sb_4SnO_x.

Temperature ramping to 400°C showed moderate amounts of CO and CO_2 evolved (0.17 g used). Less than 40% carbon monoxide was converted at 500°C, and CO and CO_2 peaks were extremely wide (Figure 4.37 (a)). On attempting to combust methane at 700°C, only baseline was seen in the chromatograms (Figure 4.37 (b)).

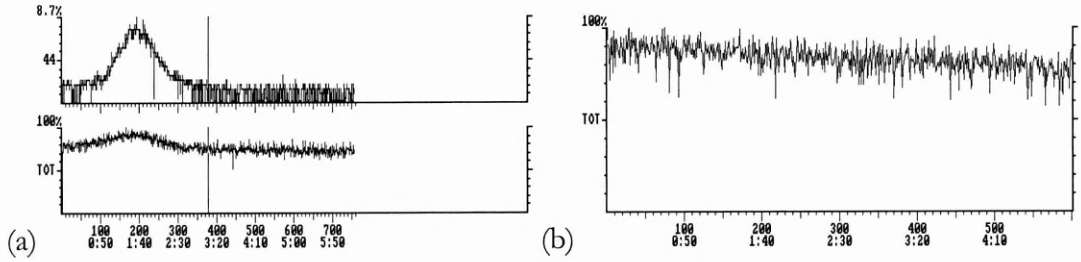

Figure 4.37 (a) CO injection over Sb_4SnO_x showing incomplete conversion, (b) CH_4 injection at 700°C, with no peaks of CH_4 or CO_2 present

A further mixture of the above oxide was produced containing tin and antimony in a 4:1 molar ratio. 5.98 g (2.53 ml) of $SbCl_5$ was diluted in excess water and 18.05 g $SnCl_2$ added. Concentrated ammonia was added to form the precipitate, which was filtered and dried to give $SbSn_4(OH)_x$. This compound was then heated in a furnace to 650°C for 12 hrs and then allowed to cool.

TPD showed CO_2 evolution with a concurrent large release of water (0.074 g used). At 400°C combustion of carbon monoxide was complete. The lowest temperature for 100% combustion was 300°C (Figure 4.38 (a)). A property of this catalyst was that CO_2 peak areas were very large

and peaks were perfectly symmetrical. Methane was 100% combusted at 600°C with similar symmetrical peak properties (Figure 4.38 (b)). Most CO_2 peaks from combustion over other oxides result in tailing. This is possibly due to the high pressure of the gas at the start of the column (59 psi absolute).

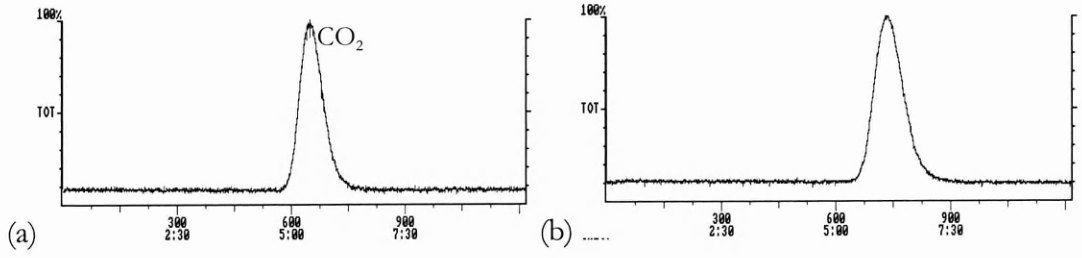

Figure 4.38 (a) CO injection at 400°C over $SbSn_4O_x$ showing complete conversion, (b) complete conversion of CH_4 at 600°C

A third preparation was made similarly to the second, but using a solution of $SnCl_4$ instead of $SnCl_2$ which should leave tin with a +4 oxidation state in the final compound (0.12 g used). On ramped heating, only water was seen to evolve. CO conversion was complete at 400°C. Methane combustion at this temperature was occurring at levels of around 1% (Figure 4.39 (a)). Increasing the temperature to 500°C released a large amount of H_2O and O_2 with a small amount of CO_2. Interestingly, evidence of the preparation was seen in the baseline of the chromatogram, as $H^{35}Cl^+$ and $H^{37}Cl^+$ (i.e. m/z 36 and 38) are shown in the individual mass spectra in the characteristic 3:1 ratio (Figure 4.39 (b)). A methane injection at 500°C produced more CO_2, but due to the amount of HCl in the ion trap, protonation was evident as CO_2 registered as m/z 45, from CO_2H^+. On increasing the temperature to 600°C, the $SbSn_4O_x$ evolved HCl and O_2, neither of which decayed significantly over time.

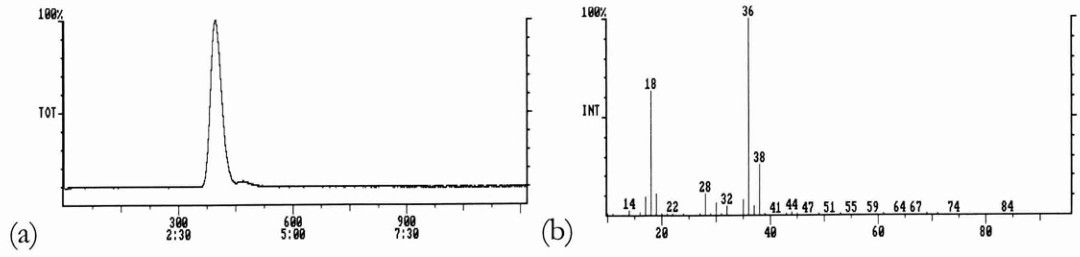

Figure 4.39 (a) partial methane combustion over $SbSn_4O_x$ at 400°C, (b) mass spectrum of background of presence of HCl

4.5.14. Hafnium Oxide

In study of Pechanec (1973), hafnium oxide was classified in the same group as gallium oxide and tin (IV) oxide; able to combust CH_4 between 500-600°C. After installation of HfO_2 (0.13 g used), the TPD showed two distinct peaks of CO_2, corresponding to two different release temperatures. At 400°C, only 17% combustion of CO was observed. Complete oxidation needed a temperature of 600°C (Figure 4.40 (a)). CH_4 conversion was complete at 800°C (Figure 4.40 (b)). At 700°C the m/z 15 peak indicated 80% conversion.

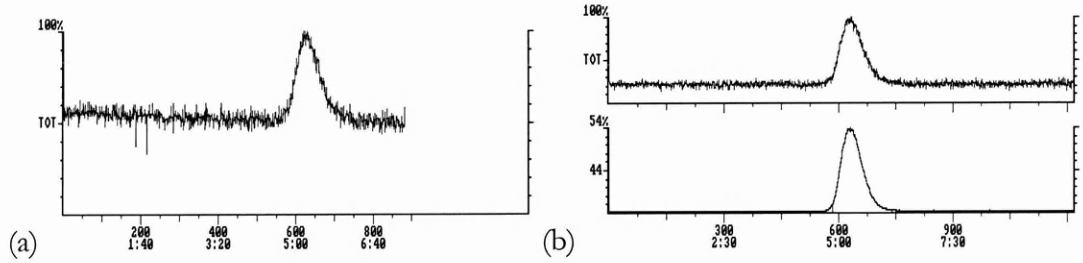

Figure 4.40 (a) complete conversion of CO over HfO_2 at 600°C, (b) complete conversion of CH_4 at 800°C

4.5.15. Silver Permanganate

Silver permanganate has been tested for use in elemental analysis (Korbl, 1956). Horacek (1960) found that the thermal decomposition product of $AgMnO_4$ would combust CH_4 at 487°C in the presence of O_2. TPD of $AgMnO_4$ (0.12 g used) resulted in a very large oxygen release, which was seen to be pure (Figure 4.41). No other compounds were detected At 400°C, O_2 release was measured to be around 1000 counts/s and very clean.

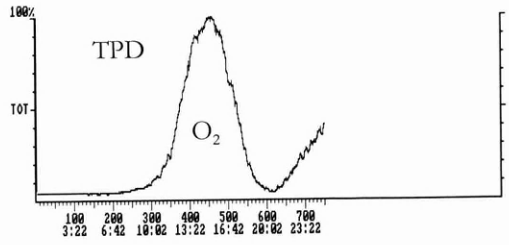

Figure 4.41 TPD of silver permanganate showing large oxygen release

At 150°C CO conversion was high. No CO remained but the CO_2 peak underwent heavy tailing (many minutes wide peak). At 100°C the same effect was observed, but the peak was smaller than expected for the size of injection, suggesting that permanent sorption of uncombusted CO or the product (CO_2) on the surface. At 350°C a trace amount (4%) of CH_4 was combusted to CO_2.

4.5.16. Ruthenium Oxide

Heating RuO_x (0.035 g used) from 100 to 400°C liberated CO_2. Combustion of CO at 400°C was complete but the CO_2 peak was wide and peak tailing was extreme (Figure 4.42 (a)). At 300°C a similar sized injection also showed peak problems – the peak was less than twice the height of the baseline (Figure 4.42 (b)). Lowering the temperature to 200°C gave a completely flat chromatogram showing neither reactant nor product. These effects would suggest that the physisorption of either uncombusted CO, or such an affinity for surface bound CO_2 that desorption is energetically unfavourable. Either of these effects negate the oxide from usability in oxidation catalysis.

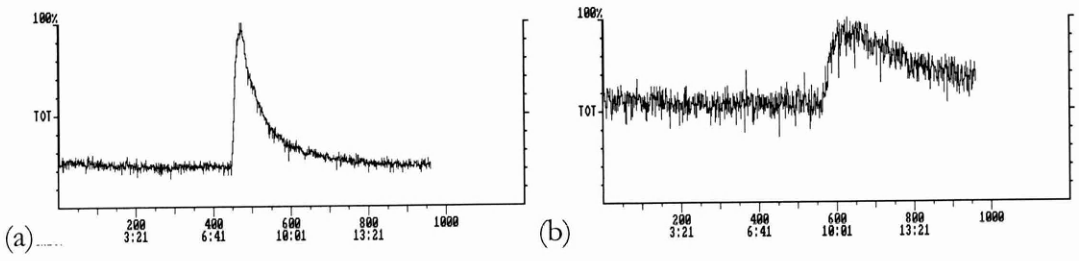

Figure 4.42 (a) carbon monoxide injection over Ru_2O_3 at 400°C showing peak tailing of CO_2, (b) CO injection at 300°C with greater tailing problems and a significant loss of material

4.5.17. Iron-Antimony Oxide

Iron-antimony oxides are not known for their combustion ability, but they have been used for fluid-bed ammoxidation (Sasaki, 2000). $FeSbO_x$ was made by mixing 2.0 g of Fe_2O_3 with 3.84 g of Sb_2O_4 in a mortar and pestle and directly heating the mixture to 800°C for 12hrs. The metal content in the product had a Sb/Fe ratio of 1.69. A typical CO_2 and water release was seen on the TPD experiment on 0.035 g of the compound. CO conversion was complete at 600°C. Methane was not completely combusted to CO_2 even at 800°C.

A second preparation was made from chlorides using co-precipitation, from 2.7 g $FeCl_3$ and 3.0 g $SbCl_5$ leading to a metals ratio of Sb/Fe of 1.31. TPD release (0.072 g used) was the same as the previous preparation, but CO conversion was complete at 300°C (Figure 4.43 (a)). There was a marked difference in methane combustion potency with the second catalyst, however. Perfect combustion was seen at 750°C (Figure 4.43 (b)). At this temperature, oxygen and water were liberated from $FeSbO_x$ and increased the baseline as seen in the chromatogram. Oxygen release was only apparent above 675°C.

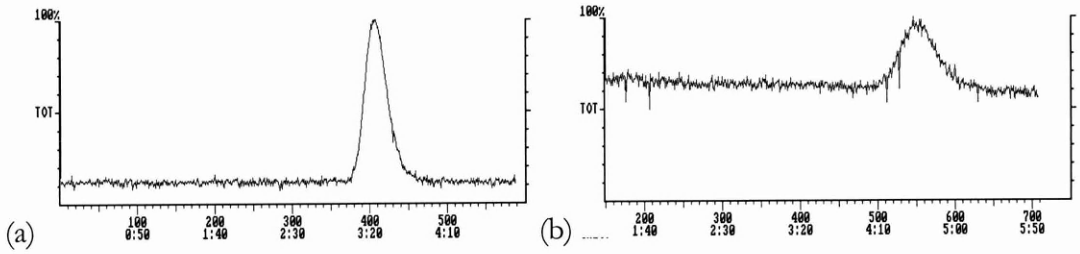

Figure 4.43 (a) complete oxidation of CO over $FeSbO_x$ (2nd preparation) at 300°C, (b) methane injection at 750°C with O_2 and H_2O enhanced background

4.5.18. Rhodium (III) Oxide

Rhodium (metal) is often used in oxidation catalysis when deposited on a ceramic support. Rhodium metal was reported by Pechanec (1973) to be active in CH_4 combustion (in O_2 gas, between 300-400°C). Rhodium is present in automobile three-way catalysts, because it is

relatively as active as Pt and Pd but at a lower cost (Heck and Farrauto, 1995). Using Rh_2O_3 itself as an oxidation agent is not well established.

The sample used was supplied by Engelhard Industries (Italy) as rhodium (III) oxide hydrate. To remove the bound water the compound was heated to 400°C overnight. The dried compound was then installed for use, of which 0.035g was used. A typical TPD trace was observed (from 100 to 400°C) showing CO_2 and water release. Conversion of CO was high at 400°C, giving 100% CO_2 for a 45 nmol injection. Adjusting the temperature to 300°C resulted in unusual CO_2 peak shapes, with a baseline dominated by a non-constant m/z 69 background (Figure 4.44 (a)). Ions appearing at m/z 69 are most often CF_3^+, formed by electron impact of either CF_4 gas or fluorinated hydrocarbons. The source of the CF_3^+ may be parts inside the Ion Trap as some contain PTFE, a polymer containing fluorine. On later injections this background served to cause problems with peak identification on the TIC. Increasing the temperature of Rh_2O_3 to 400°C and cooling to room temperature did not eliminate this ion. This effect was also seen on other occasions when no catalyst was present in the GC-ITD system, eliminating the catalyst as the source of the ion.

Injecting CH_4 over the oxide gave surprising results. At 300°C a large injection of CH_4 showed no remaining m/z 15 peak, and a large CO_2 peak. Lowering the temperature to 250°C and increasing the load to 43 nmol also gave 100% combustion (Figure 4.44 (b)). For carbon monoxide there was similarly active oxidation capability. Partial combustion was observed at room temperature for small injections (Figure 4.44 (c)). Increasing temperature to 100°C was sufficient for large samples.

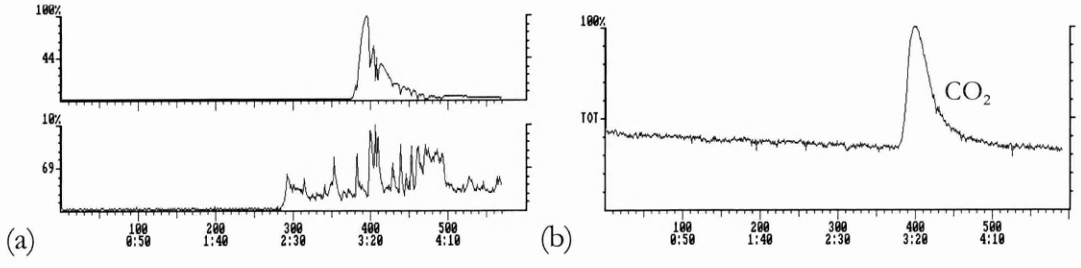

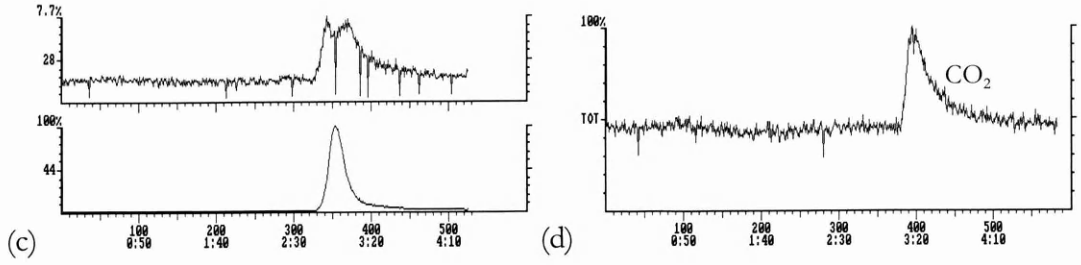

Figure 4.44 (a) CO injection over Rh_2O_3 with m/z 69 ions, (b) complete oxidation of CH_4 at 250°C, (c) carbon monoxide partial combustion at room temperature, (d) complete CO conversion at 300°C

On applying the same peak size and temperature analysis as per PdO (see section 4.5.12) there are problems, mainly due to the varying background of m/z 69 present in the chromatograms. Peak areas were calculated from the peaks appearing on the Total Ion Chromatogram, which integrates the quantities of all ions detected. As the mass 69 ion was constantly varying from second to second, this makes true area calculation difficult. The CO graph (Figure 4.45 (a) shows that 400°C gave the optimum combustion, although no residual reactant was detected on all combustions greater than 100°C. On examination of Figure 4.45 (b), the 300°C points are linear for CH_4 combustion. Although the 400° C points show greater peak areas, this could be due to the m/z 69 presence. Therefore no firm conclusions can be drawn from this analysis, as no uncombusted CH_4 was detected above 300°C. For the purposes of comparison with other materials, a conservative minimum complete combustion was taken as 400°C for both materials. Further investigation of the combustion properties were investigated in Chapter 5.

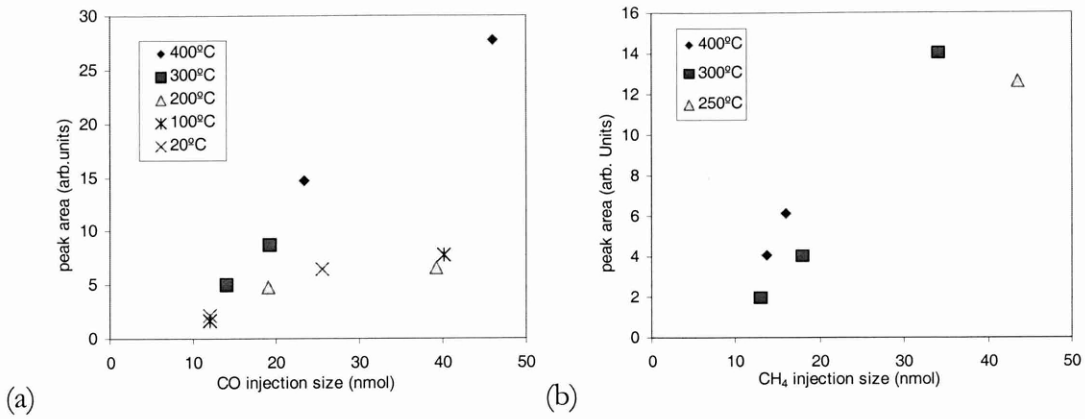

Figure 4.45 Peak areas versus injection size at various temperatures for (a) CO and (b) CH_4

4.5.19. Europium / Iron – Vanadate

V_2O_5 has been used extensively for oxidation chemistry. Pechanec (1973) found it to combust CH_4 at 600-700°C. Mars and van Krevelen (1954) studied the combustion reaction of V_2O_5 with aromatics to propose kinetics for redox reactions used by many investigators of oxidation catalysis. Although some iron vanadium compounds have been used, no europium based catalyst mixtures have been reported. An unknown loading of iron and europium on V_2O_5 was prepared by co-precipitation. Drying took place at 150°C followed by calcination at 250°C for 6 hrs. When heated to 400°C water was evolved in large quantities, as well as CO_2 and NO, possibly due to the lower than usual firing temperatures (0.05 g used). CO combustion was found to be good, but incomplete at 600°C, where 1% CO remained (Figure 4.46 (a)). Partial methane combustion (5% - from peak height) occurred at this temperature (Figure 4.46 (b)). No further injections were performed as more active reagents had already been tested.

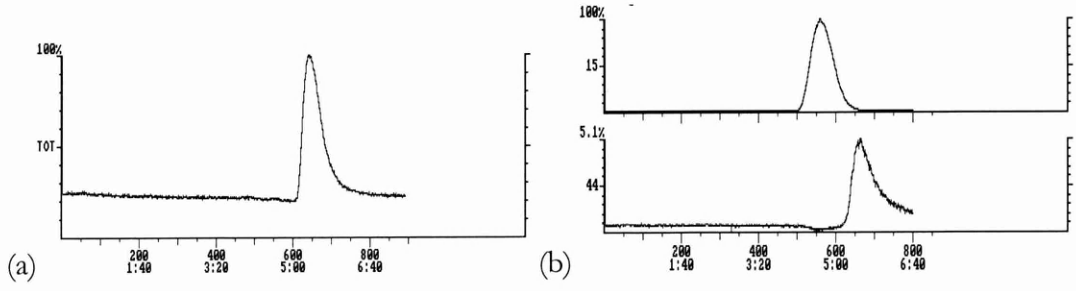

Figure 4.46 (a) 99% conversion of 8 nmol of CO at 600°C over V_2O_5/Fe/Eu, (b) partial methane conversion at 600°C

4.5.20. Cobalt-Chromium Oxides

Cobalt-chromium oxides are known to be active in complete oxidation of hydrocarbons. Oxidations of propylene and CO have shown high activity at low temperatures (Zwinkels et al., 1993). $CoCrO_x$ was made by heating a 1:1 (metals) molar ratio mixture of Cr_2O_3 and Co_3O_4 to 650°C for 2 hours. Ramped heating evolved CO_2 in large amounts (0.07 g used). CO combustion was 100% successful at 400°C, and was complete until the temperature was lowered to 100°C. At this temperature the CO_2 peak area was only half of expected amount and the peak showed tailing. Even at 50°C no residual CO was observed, and peak area was only 20% smaller than expected. At 500°C methane injections were 100% converted to CO_2 (Figure 4.47 (b). After raising the temperature to 600°C, the $CoCrO_x$ released a large amount of oxygen.

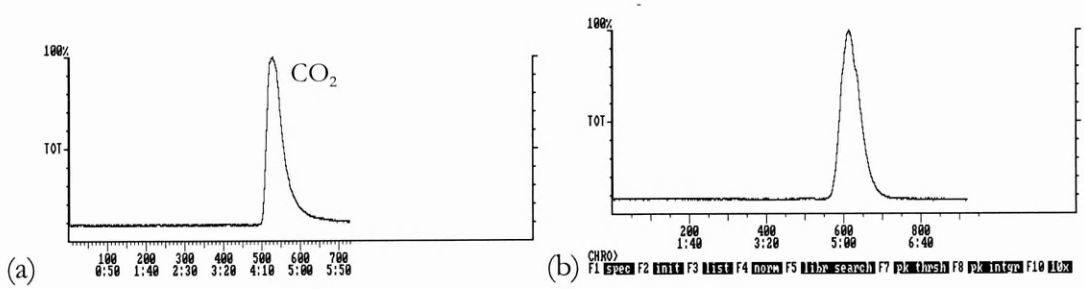

Figure 4.47 (a) complete conversion of 41 nmol of CO over the first preparation of $CoCrO_x$ at 200°C, (b) 100% methane conversion at 500°C

A second preparation of $CoCrO_x$ was made from co-precipitation of chromium (III) nitrate and cobalt (I) nitrate so that a 1:1 (metals) molar mixture was produced. On ramped heating a large amount of NO and O_2 was evolved from 0.07g of material (Figure 4.48). As this emission did not decay significantly when left at room temperature, the oxide was removed and no further studies were conducted.

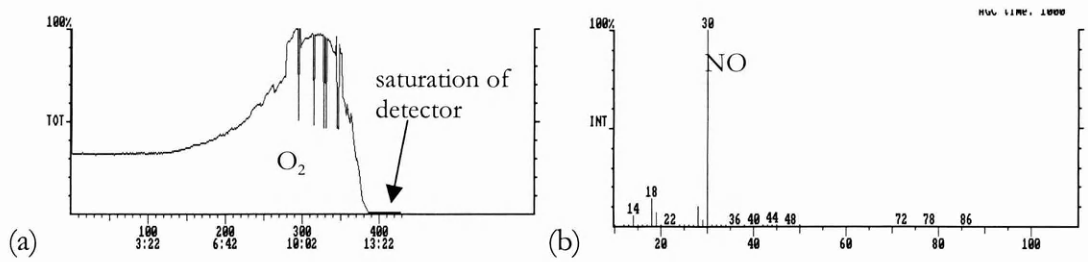

Figure 4.48 (a) O_2 evolution from the second preparation of $CoCrO_x$ saturating the ITD during TPD, (b) mass spectrum during run showing NO presence

4.5.21. Platinum / Palladium – Alumina

Some of the simplest preparations of oxidation/automobile catalysts can be made from noble metals supported on alumina ("The three way catalytic converter." Open University). Low loadings of Pt and Pd on alumina were prepared by wetness impregnation. A solution of 0.13 g $PtCl_4$ and 0.10 g $PdCl_2$ was washed onto α-Al_2O_3. The slurry was dried at 150°C and calcined at 600°C (ramping at 5°C/min) for 4 hours.

The TPD profile showed a large release of CO_2 (0.058 g used). The injection of CO at 400°C resulted in 100% conversion to CO_2. Minimum combustion temperature was found to be 250°C (Figure 4.49 (a)). On heating the compound to 600°C a large amount of H_2O and CO_2 was released, the flux of which decayed over time. Combustion of CH_4 was seen at 600°C (>50%), with the minimum temperature for complete conversion was 750°C (Figure 4.49 (b)).

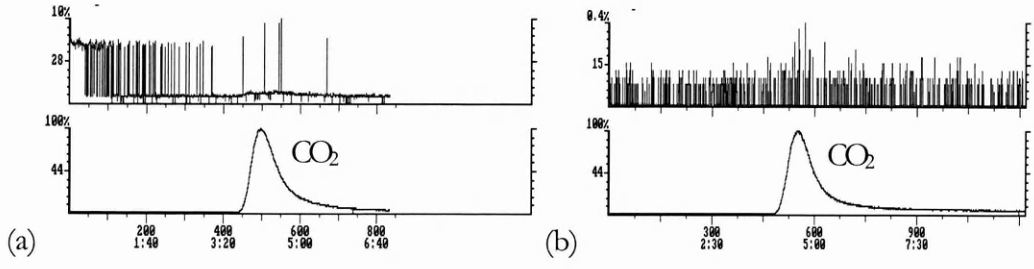

Figure 4.49 (a) complete oxidation of 27 nmol of CO on platinum/palladium/alumina at 250°C, (b) complete conversion of CH_4 at 750°C

4.5.22. Chromium-Copper Oxide

This oxide mixture has been investigated for potential within automobile catalysts, especially for the conversion of CO. Work done by Laine et al. (1987) has identified preparation conditions and pre-treatment required for maximum efficiency. A sample of $CrCuO_x$ was prepared by direct heating of the metal oxides, 1.52 g of Cr_2O_3 and 0.80 g CuO, corresponding to a Cu/Cr ratio of 1.25. The powders were ground together and heated to 600°C for 4 hours (after ramping at 5°C/hour). 0.04 g of material was used.

Performance under temperature ramping showed multiple releases of CO_2. As is common with most copper based oxides tested, carbon monoxide conversion was 100% at 400°C. Lowering the temperature did not affect combustion quality until below 100°C (Figure 4.50).

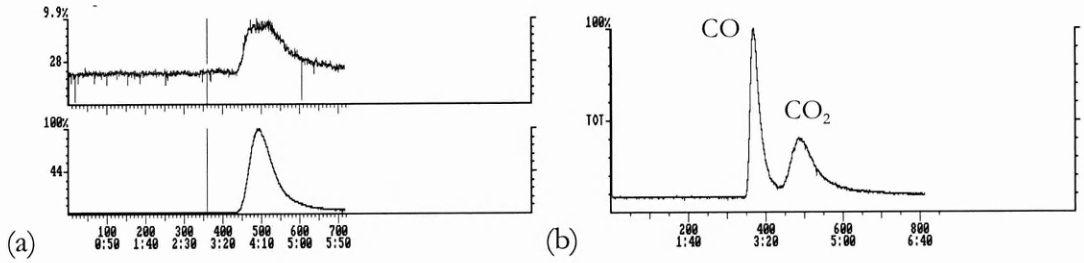

Figure 4.50 (a) complete conversion of 19 nmol CO on $CuCrO_x$ at 100°C, (b) partial oxidation of 30 nmol of CO at 50°C

Heating to 500°C gave partial methane conversion of 70% (Figure 4.51 (a)). Increasing the temperature to 600°C resulted in a large O_2 release which was present even after leaving for some hours. As the O_2 background was present after over 24 hours of high temperature exposure, it was very difficult to detect any other species (Figure 4.51 (b)).

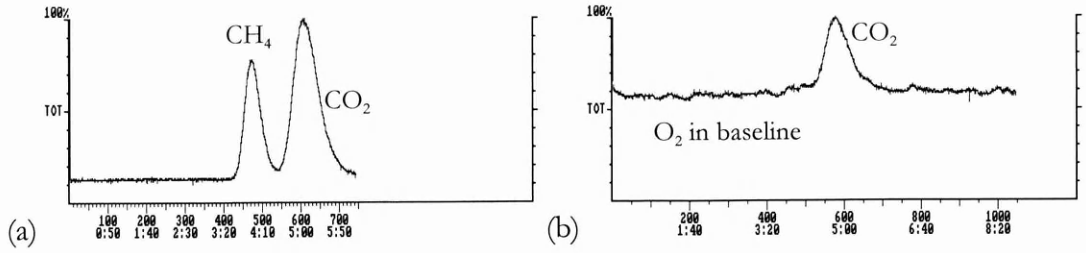

Figure 4.51 (a) partial methane conversion at 500°C on $CuCrO_x$, (b) methane injected at 600°C showing unknown proportion of conversion due to large O_2 background, although no CH_4 peak is obviously present

4.5.23. Palladium – Zinc Oxide

Zinc has been used as a support for noble metal catalysts (Hutchings et al., 1997). Palladium was tested as the active metal for oxidation. Pd was deposited on zinc Oxide via co-precipitation of 0.15 g $PdCl_2$ and 0.78 g ZnO. The precipitate was dried, and calcined at 650°C (ramping at 5°C/min) for 6 hours before cooling.

On ramped heating of 0.07g of Pd/ZnO, CO_2 was present as the major release with a minor amount of CO detected. CO combustion was complete at 400°C, and gave 100% conversion at 300°C and above (Figure 4.52 (a)). Heating to 550°C gave relatively efficient methane combustion of over 90%. Oxygen was present in the background of the scan. To decrease the O_2 level present at 600°C, Pd/ZnO was heated to 700°C for a few hours with the ITD filaments off, and then lowered to 600°C for combustion testing. Perfect combustion of CH_4 was seen with a 45 nmol injection at 600°C (Figure 4.52 (b)).

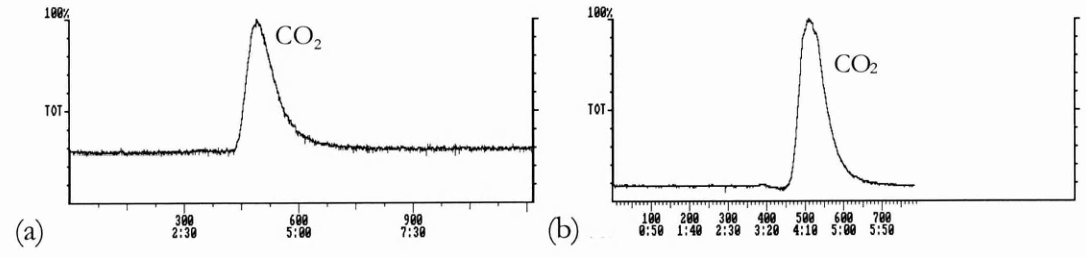

Figure 4.52 (a) 35 nmol of carbon monoxide injected over Pd/ZnO_2 at 300°C to form CO_2, (b) 45 nmol methane injection at 600°C giving 100% CO_2

4.5.24. Palladium / Platinum – Iron / Vanadium Oxide

Of all the oxides tested, this mixture had more individual metallic components than any other. iron (III) oxide (0.64 g) and V_2O_5 (0.30 g) were mixed with a slurry of $PdCl_2$ (0.30 g) and $PtCl_4$ (0.17 g) and dried, as per wetness impregnation. The mixture was calcined with the same conditions as the Pd/ZnO catalyst (650°C for 6 hours).

On installation of 0.07 g of the mixture, it was found that the pressure requirement was very low for 1 sccm, giving rise to a large air leak. Increasing the flow to 2 sccm increased the head pressure to 3 psi (above atmospheric pressure), enough to reduce the air background detected by the ion trap. CO_2 was the only detected species on ramped heating. At 450°C CO combustion was complete (Figure 4.53 (a)). Combustion of CH_4 at 600°C was minimal (<5%, Figure 4.53 (b)), while at this temperature the material was evolving O_2. At 700°C the O_2 release saturated the ITD.

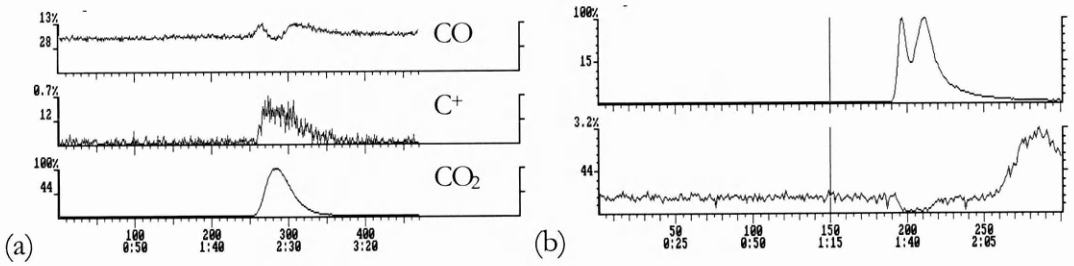

Figure 4.53 (a) complete conversion of 15 nmol CO over $Pd/Vd_2O_5/Pt/Fe$ mixture at 450°C, (b) minimal methane conversion (21 nmol) at 600°C, showing self-reaction of the CH_3^+ ion to $C_2H_5^+$ at time of highest concentration

4.5.25. Copper – Manganese Oxide

This oxide was created by co-precipitation of $CuCl_2 \cdot 2H_2O$ (0.31 g) and MnO_2 (0.54 g). The compound was dried, and calcined at 650°C for 4 hours. This led to a molar metals ratio in the compound of Mn/Cu = 3. Ramped heating of this compound evolved a large amount of CO_2. Injecting CO over the oxide at 500°C resulted in a 38% conversion to CO_2 (Figure 4.54), suggesting that CH_4 conversion would not reach 100% even at very high temperatures. As

other materials had already shown high combustion of both materials at this temperature, the next sample was tested.

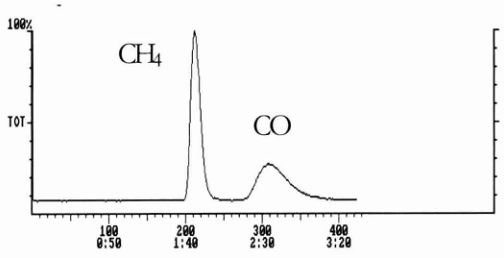

Figure 4.54 CO injection over $CuMnO_x$ showing partial conversion

4.5.26. Gold / Ferric Oxide

Previously thought to be less active than Pt group metals in oxidation reactions, gold has recently received a lot of attention (Thompson, 1998). Gold on various support oxides appears to have great ability for CO oxidation in the presence of O_2 (Haruta, 1993). Ferric oxide as a support for gold was shown to be the most active in such a reaction, at low temperatures with a loading of 5%, compared to CuO, ZrO_2, Sc_2O_3 and TiO_2. A loading of 3.2 % Au (metal) on α-Fe_2O_3 was prepared by co-precipitation and autoclaving. 0.35 g $HAuCl_4 \cdot 3H_2O$ was added to a solution of 15.18 g $Fe_2O_3 \cdot 9H_2O$ and dilute NH_3 was added to increase to pH 9-10. The mixture was then autoclaved at 200°C, at high pressure for 2 hours, before drying under an IR lamp.

0.06g of the material was installed. On heating, such a large release of CO_2 was present that mass 45 gave a greater ion count than mass 44 due to protonation from water. Combustion of carbon monoxide was complete at 350°C (Figure 4.55 (a)). Methane was also converted, with near perfect (>99%) combustion at 750°C (Figure 4.55 (b)).

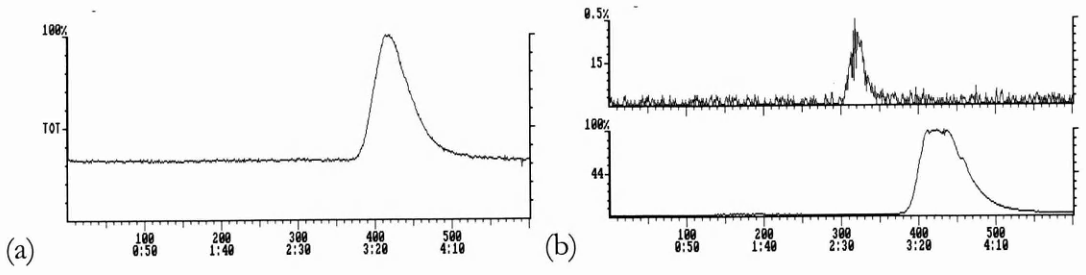

Figure 4.55 (a) complete conversion of 22 nmol CO over Au/Fe_2O_3 at 350°C, (b) near perfect combustion of 61 nmol methane at 750°C

4.5.27. Gold / Zinc Oxide

As with the previous sample, ZnO has also shown to be successful support for gold, from work undertaken by Haruta (1993). A loading of 5.2 % (metals) Au on ZnO was made by co-precipitation of 0.35 g $HAuCl_4 \cdot 3H_2O$ and 11.15 g $Zn(NO_3) \cdot 6H_2O$, by mixing at 80°C for an hour and precipitating at a pH<8 by using dilute NH_3. The filtrate was dried by IR and calcined at 600°C. The preparation is similar to a method described by Hutchings et al., (1997).

The TPD trace (0.08 g used) showed NO and CO_2 release, with a large amount of water. Testing the material at 400°C resulted in perfect combustion for small injections of CO, but for near complete combustion of large samples, >700°C was required (Figure 4.56 (a)). At 800°C, only 75% of methane was combusted (Figure 4.56 (b)). Higher temperature combustions were not performed.

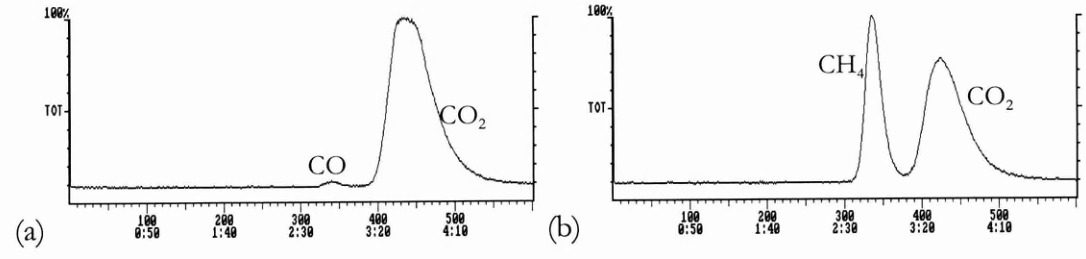

Figure 4.56 (a) incomplete combustion of CO over Au/ZnO at 700°C, (b) methane injection at 700°C

4.5.28. Silver Oxide + Gold / Ferric Oxide

This mixture of two powders already prepared was made by empirically mixing equal volumes of Ag_2O and Au/Fe_2O_3 and grinding in a mortar and pestle. The Ag_2O within the mixture could act as an oxygen source for the Au/Fe_2O_3 catalyst.

On installation of 0.093 g, the mixture was found to be wet, though heating overnight reduced the amount of H_2O detected. The complete CO oxidation was obtained at 400°C. Reducing the temperature to 300°C and injecting CO, resulted in no non-background ions being detected, leaving a flat chromatogram. Methane combustion at 500°C showed a complete CO_2 peak (Figure 4.57). In comparison to the constituent components, methane was combusted at lower temperature (than Au/Fe_2O_3), but CO required a similar temperature of the least efficient catalyst (Au/Fe_2O_3).

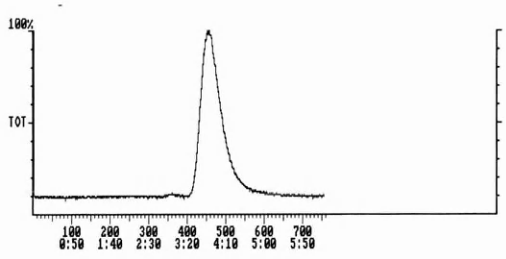

Figure 4.57 100% conversion of methane at 500°C over $Ag_2O/Au/Fe_2O_3$. Small peak is due to an air leak.

4.5.29. Rhodium / Palladium/ Cerium Oxide

This $Rh/Pd/CeO_2$ mixture was made by co-precipitation. In this instance, ceria would act as the support, and as the oxygen storage agent. Temperature ramping the 0.077 g of the powder resulted in release of water, CO_2 and oxygen. With initial injections, no combustion was seen with CO at 500°C. Unexpectedly, at 700°C methane was oxidised completely (Figure 4.58 (a). Lowering the temperature to 500°C left no uncombusted methane, but large CO_2 peak tailing was present. On this set of injections at 500°C, complete combustion with large tailing was observed with both CO and CH_4 injections (Figure 4.58 (b)). This may indicate affinity for the combustion products by the catalyst surface.

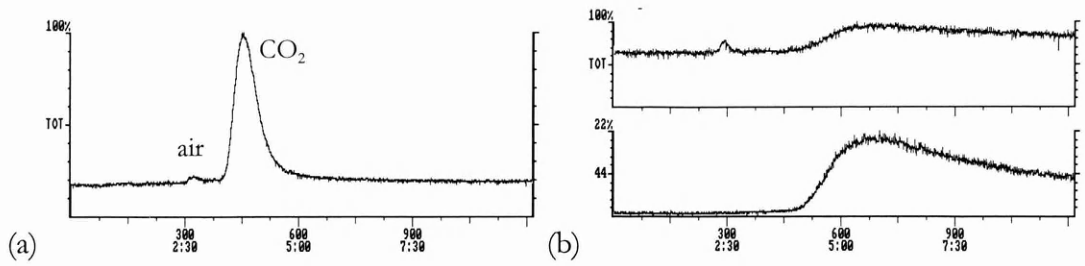

Figure 4.58 (a) perfect combustion of 16 nmol CH_4 over $Rh/Pd/CeO_2$ at 700°C – air present from leak in vacuum system, (b) 20.5 nmol CO injection at 500°C showing large peak tailing effect (and also an air peak)

4.5.30. Palladium / Potassium Chromate

A mixture of Pd/KCr_2O_7 was made by wetness impregnation of $PdCl_2$ and KCr_2O_7. Ramping the temperature (0.035 g used) at 20°C/min to 400°C resulted in very large O_2 releases. Lowering to 300°C stopped the O_2 flux, and CO combustion was attempted. Multiple CO injections were found to be completely converted to CO_2 at temperatures as low as 200°C. Some small sized injections of CO were completely converted at 100°C (Figure 4.59 (a)). Increasing the temperature of the mixture to 350°C liberated O_2 at 700 counts/s. CH_4 conversion at this temperature gave a combustion efficiency of 25 %. Increasing the temperature to 400°C resulted in a high O_2 flow, which saturated the Ion Trap. After leaving the compound at 400°C overnight, the O_2 emission was low enough to detect combustion. CH_4 was completely combusted at 500°C (Figure 4.59 (b)).

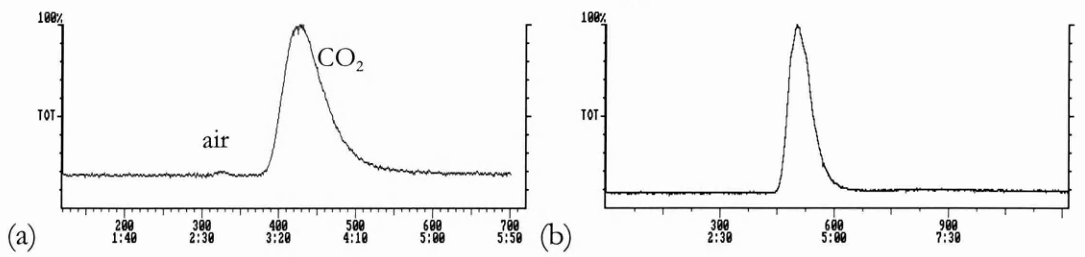

Figure 4.59 (a) successful oxidation of 15 nmol CO on Pd/KCr_2O_7 at 100°C, (b) complete combustion of 35 nmol CH_4 at 500°C after leaving overnight to reduce oxygen emission

4.5.31. Gold / Manganese Oxides

Gold supported on manganese oxide has received attention for the application of closed cycle CO_2 lasers (Upchurch et al., 1992). Any build up of CO in such a device may limit laser lifetime, so refilling the CO_2 chamber or reoxidation of CO to CO_2 at ambient temperatures is fundamental. Such closed cycle lasers are used in orbital satellites, where purging and refilling the CO_2 gas is impractical. Many mixtures have been tested for the oxidation reaction, the most studied are Pt/SnO_2, and Au/MnO_2 (Gardner et al., 1991). An attempt was made at making 5% metal loading of Au on MnO_x by co-precipitation, but the level of hydration of the manganese nitrate was unknown. 0.33 g of $HAuCl_4 \bullet 3H_2O$ was dissolved and added to a solution containing 4.5g $Mn(NO_3)_2 \bullet xH_2O$, which would result in Au 3.75% (metals) if the manganese nitrate was not hydrated. Concentrated ammonia was added until a black precipitate was formed, which was filtered. However, the addition of more ammonia resulted in a cream precipitate forming, which was also was filtered. After drying both precipitates, the cream compound turned brown, whereas the black compound retained its colour. A third mixture was made by adding some of both powders, and all three were calcined at 550°C (10°C/min ramp) for 12 hours.

The black compound was tested (0.038 g used). Ramped heating recorded two CO_2 emissions, the second release also containing O_2. At 400°C carbon monoxide was oxidised to CO_2 perfectly. The minimum combustion temperature was 150°C for CO conversion (Figure 4.60 (a)). Methane appeared to be combusted perfectly at 650°C (Figure 4.60 (b)).

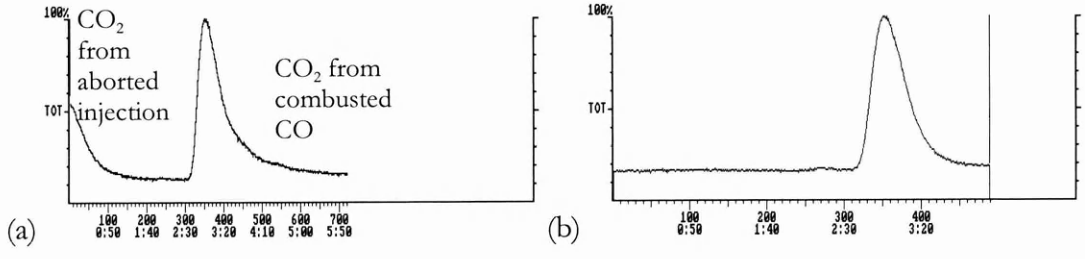

Figure 4.60 (a) CO conversion over Au/MnO_x at 150°C (first peak from an aborted injection), (b) complete conversion of 28 nmol CH_4 at 650°C

4.6. Powders - Inactive reagents

Many oxides tested showed no affinity for oxidation in this experimental arrangement, and are shown in Table 4.5. Many of those oxides were created by co-precipitation. As these compounds did not show promise for combustion efficiency, these compounds were not tested at every temperature step. The maximum temperature tested was generally 800-900°C. Specific combustion efficiencies were not measured unless peaks were easily visible on the chromatogram. The two Lanthanum compounds were prepared by Dr Robert Marshall and supplied by Dr Eleanor Crabb (OU Chemistry department).

Table 4.5 Oxides tested by the GC-ITD system that showed no sign on combustion ability. The column labelled volatiles lists the gases evolved during TPD and further temperature increases

Compound	Volatiles released on heating	Summarised combustion ability
Ca/SnO_x	CO & CO_2	3 % CO at 400°C, 12 % CH_4 at 800°C
MoO_3	CO_2, H_2O	no conversion to CO_2 for CO
Fe_2O_3	NO, HCl	no conversion to CO_2 for CO
5% Pt/Al_2O_3	O_2,	CO sorption by oxide
ZnO	2 CO_2 releases	10% CH_4, 5% CO at 900°C
La_2O_7	no TPD release	only baseline
SnO_3	sharp peaks	only baseline
WO_3	CO_2, H_2O	no conversion to CO_2 for CO
Nb_2O_5	CO, CO_2	no conversion to CO_2 for CO
Nd_2O_5	CO_2	no conversion to CO_2 for CO
Ta_2O_5	CO_2, H_2O	no conversion to CO_2 for CO or CH_4
PtO	NO, O_2 at 800°C	trace (<3 %) CO conversion
SbO_2	CO_2, H_2O	CO 100% at 600°C – bad peaks
4% Pd / $LaAl(NO_3)$	CO_2, H_2O	no conversion to CO_2 for CO
4% Pd / La_2O_3-Fe_2O_3	HCl	no conversion to CO_2 for CO
$Pd/KMnO_4$	CO_2, O_2	CO sorption by oxide

In addition to the above compounds, some preparations of the active reagents did not combust as well as others prepared under similar conditions. The details of these preparations are given in the descriptions of the active reagents in 4.5.

4.7. Conclusions from oxidised wire and powdered oxide tests

Many oxides showed promise with oxidation. Some oxides that were expected to perform under anoxic conditions did well, combusting CH_4 and CO at temperatures below expected. Other compounds reputed to be active in oxidation were far from active in this system. A summary of the ion trap tests is presented. Table 4.6 collates the minimum combustion temperature for CO and CH_4 for the greatest conversion to CO_2.

Table 4.6 Yield and temperature data for active oxides for CO and CH_4 combustion, showing maximum combustion efficiency and temperature (T) for the maximum efficiency.

Compound	section	max . CO conversion (%)	T for max. (CO) (°C)	Max. CH_4 conversion (%)	T for max. (CH_4) (°C)
Cu wire	4.4.1	100	420	95	1150
Mo/Pt wire	4.4.3	30	500		
Ni/Pt wire	4.4.4	100	500		
Cu/Pt wire	4.4.5	100	400	50	1000
Ag wire	4.4.6	50	700		
PdO (sponge)	4.5.1	100	200	100	450
NiO	4.5.2			60	700
CeO_2	4.5.3			100	900
Co_3O_4	4.5.4	100	400	99	750
MnO_2	4.5.5			50	500
Ag_2O	4.5.6	100	200		
Pt/CuO	4.5.7	97	250	65	800
TiO_2	4.5.8			40	900
Ga_2O_3	4.5.9			90 - partial	1000
Bi_2O_3	4.5.10	100	400		
$FeNiO_x$ (2^{nd})	4.5.11	100	350	100	700
PdO (Aldrich)	4.5.12	100	225	100	350
$SbSnO_x$	4.5.13	40	500	100	600
HfO_2	4.5.14	100	600	100	800
$AgMnO_4$	4.5.15	100	150		
Ru_2O_3	4.5.16	100	400		
$FeSbO_x$ (1^{st})	4.5.17	100	600		
$FeSbO_x$ (2^{nd})	4.5.17	100	300	100	750
Rh_2O_3	4.5.18	100	400	100	400
Eu/Fe on V_2O_5	4.5.19	99	600	5	600
$CoCrO_x$	4.5.20	100	200	100	500
Pd/Pt/α-Al_2O_3	4.5.21	100	250	100	750
$CrCuO_x$	4.5.22	100	100	70	500
Pd/ZnO	4.5.23	100	300	100	600
Pd/Pt/$FeVO_x$	4.5.24	100	450		
$CuMnO_x$	4.5.25	40	500		
Au/Fe_2O_3	4.5.26	100	350	>99	750
Au/ZnO	4.5.27	98	700	75	800
Ag_2O + Au/Fe_2O_3	4.5.28	100	400	100	500
Rh/Pd/CeO_2	4.5.29	0-100	500		
Pd/KCr_2O_7	4.5.30	100	200	100	500
$AuMnO_x$ (1)	4.5.31	100	150	100	650
ZnO	4.6	10	900		

Some of the oxides emitted volatile components in addition to the common release of water and CO_2 during the TPD process. In addition, some catalysts were created and prepared by co-precipitation or other methods (4.2.5). The details of all these factors are presented in Table 4.7.

Table 4.7 Combined volatile emission from oxides, preparation method & reagents, or supplier for each of the active oxides tested.

Compound	section	Volatiles released on heating	Method of production, or supplier	Reagents
Cu wire	4.4.1		Goodfellows	
Mo/Pt wire	4.4.3		Goodfellows	
Ni/Pt wire	4.4.4		Goodfellows	
Cu/Pt wire	4.4.5		Goodfellows	
Ag wire	4.4.6		Goodfellows	
PdO (sponge)	4.5.1	N_2 & O_2 released during TPD	heating	Pd sponge, air
NiO	4.5.2		Aldrich	
CeO_2	4.5.3	large quantities of CO_2 evolved after heating to 800°C	Aldrich	
Co_3O_4	4.5.4	O_2 evolution at 800°C	Aldrich	
MnO_2	4.5.5	O_2 release at 550°C	Aldrich	
Ag_2O	4.5.6	O_2 evolution from 250°C	Aldrich	
Pt/CuO	4.5.7	O_2 evolution at 800°C	Elemental Microanalysis	
TiO_2	4.5.8	CH_4 present in TPD	Aldrich	
Ga_2O_3	4.5.9		Aldrich	
Bi_2O_3	4.5.10		Aldrich	
$FeNiO_x$	4.5.11	peak m/z 64 concurrent with CO_2	co-precipitation	$FeCl_3$, $NiCl_3$
$FeNiO_x$ (2^{nd})	4.5.11		co-precipitation	$FeCl_3$, $NiCl_3$
PdO (Aldrich)	4.5.12		Aldrich	
$SbSnO_x$ (1)	4.5.13		heating	Fe_2O_3, Sb_2O_4
$SbSnO_x$ (2)			co-precipitation	$SbCl_5$, $SnCl_2$,
$SbSnO_x$ (3)		HCl evolved on heating to 500°C	co-precipitation	$SbCl_5$, $SnCl_4$,
HfO_2	4.5.14		Aldrich	
$AgMnO_4$	4.5.15	large O_2 release from 400°C	Aldrich	
Ru_2O_3	4.5.16		heating	Ru_2O_3•n(H_2O)
$FeSbO_x$ (1^{st})	4.5.17		heating	Fe_2O_3, Sb_2O_4
$FeSbO_x$ (2^{nd})	4.5.17	O_2 and H_2O released at 750°	co-precipitation	$FeCl_3$, $SbCl_5$
Rh_2O_3	4.5.18	m/z 69 peak released (probably from ITD)	heating	Rh_2O_3•n(H_2O)
Eu/Fe on V_2O_5	4.5.19	CO_2 and NO released at 400°C	co-precipitation	V_2O_5, Fe salt, Eu salt

Compound	section	Volatiles released on heating	Method of production, or supplier	Reagents
$CoCrO_x$	4.5.20	O_2 evolution at 600°C	heating	Cr_2O_3, Co_3O_4
$Pd/Pt/\alpha\text{-}Al_2O_3$	4.5.21		wetness impregnation	$PtCl_4$, $PdCl_2$, $\alpha\text{-}Al_2O_3$
$CrCuO_x$	4.5.22	O_2 evolution at 600°C	heating	Cr_2O_3, CuO
Pd/ZnO	4.5.23		co-precipitation	$PdCl_2$, ZnO
$Pd/Pt/FeVO_x$	4.5.24	O_2 evolution at 650°C	wetness impregnation	$PdCl_2$, $PtCl_4$, Fe_2O_3, V_2O_5
$CuMnO_x$	4.5.25		co-precipitation	$CuCl_2\bullet(H_2O)$, MnO_2
Au/Fe_2O_3	4.5.26		co-precipitation & autoclaving	$\alpha\text{-}Fe_2O_3\bullet 9H_2O$, $HAuCl_4\bullet 3H_2O$
Au/ZnO	4.5.27		co-precipitation	$HAuCl_4\bullet 3H_2O$, $Zn(NO_3)\bullet 6H_2O$
Ag_2O + Au/Fe_2O_3	4.5.28		Mixing	Ag_2O + Au/Fe_2O_3 (see above)
$Rh/Pd/CeO_2$	4.5.29		co-precipitation	unknown
Pd/KCr_2O_7	4.5.30	large O_2 release at 400°C	co-precipitation	KCr_2O_7, $PdCl_2$
$AuMnO_x$ (1)	4.5.31		co-precipitation	$HAuCl_4\bullet 3H_2O$, $Mn(NO_3)_2\bullet nH_2O$
ZnO	4.6		Aldrich	

The above two tables (Table 4.6 and Table 4.7) can be summarised to show only those materials producing low temperature complete combustion, in order of the combustion ability. By the combination of the data for volatile emission, CO and CH_4 combustion, a summary table can be created to show the most useful reagents for the MODULUS system.

Table 4.8 Combined CO and CH_4 combustion data for the highest activity catalysts

Compound	Minimum combustion temperature (°C)		Comments
	CO	CH_4	
PdO (Aldrich)	350°C	225°C	
Rh_2O_3	400°C	400°C	
PdO (sponge)	450°C	200°C	N_2 & O_2 on heating
$CoCrO_x$	500°C	200°C	O_2 evolved >600°C
Ag_2O + Au/Fe_2O_3	500°C	400°C	
Pd/KCr_2O_7	500°C	200°C	O_2 evolved >400°C
Pd/ZnO	600°C	300°C	
Au/MnO_x (1)	650°C	150°C	
$FeNiO_x$	700°C	350°C	

In general, good combustion was observed in almost all the copper based oxides, not surprising given the role CuO has played in oxidation in closed systems. Palladous compounds also show high activity in most oxide mixtures. Base oxides with gold added also improved the combustion efficiency for CO conversion.

4.7.1. Recommendations for MODULUS

From Table 4.8 it is evident that the oxidation unit for MODULUS can be any of the above compounds. For the greatest energy saving made with low temperature catalysis, the obvious choices are PdO, Rh_2O_3, and $CoCrO_x$. All these compounds were successful within the testing regime of CH_4 and CO combustion and associated flow conditions. All of these compounds were put forward for potential isotope ratio investigation.

5. ISOTOPIC INTEGRITY OF CARBON DURING COMBUSTION OF CARBON COMPOUNDS USING METAL OXIDES AS OXIDANTS

5.1. Introduction

For the complete isotopic analysis of cometary volatiles, MODULUS will have to perform chemical preparation on the samples. In order to make carbon isotopic measurements with no need to apply corrections, the compounds must be completely converted to CO_2 by the use of an oxidant. In principle, this process of oxidation could lead to undesirable changes in the carbon isotope ratio, resulting in CO_2 with a different $\delta^{13}C$ from that of the original compound. The choice of oxidant must be made to minimise, or if possible eliminate this fractionation effect (i.e. preserve the isotopic integrity of the carbon). In the previous chapter, a GC-ITD system was used to examine the activity of numerous metal oxides for combustion of CO and CH_4. This chapter takes the most efficient compounds and tests their ability to combust CO and CH_4 to produce CO_2 with minimum carbon isotopic fractionation. For this a standard continuous flow isotope ratio mass spectrometer was used.

The operational temperature of such an oxidant is also an important parameter. A low operating temperature reduces power consumption on the instrument, and therefore increases lifetime of the instrument. However, it will be shown that certain reagents require a minimum temperature below which fractionation can occur.

5.1.1. Sample testing using isotope ratio mass spectrometry - Experimental procedure

Based on the results obtained in Chapter 4, a series of metal oxides were considered for further evaluation. Each oxide was placed in a quartz tube (either 1mm or 5mm i.d.) and installed into the carrier gas stream. Methane or carbon monoxide was prepared for injection in a vacuum

system, and injected into the gas stream, using helium as a carrier gas. No GC was used in the experiments. Test gas (CO or CH_4) then passed over the heated metal oxide, and any CO_2 formed was trapped in a steel loop cooled to liquid N_2 temperatures; after sufficient time this was isolated, warmed to room temperature, and the evolved CO_2 admitted to an isotope mass spectrometer.

The above procedure was repeated for both test gases at different temperatures. Blanks of CO_2 from the oxides were also measured and minimised by leaving the materials under investigation to degas at over 300°C. Once CH_4 or CO was combusted, the $\delta^{13}C$ of CO_2 was noted and any anomaly in $\delta^{13}C$ investigated. CO_2 peak sizes (as calculated by the mass spectrometer software) were used to observe the percentage of CO or CH_4 combusted. Variations in $\delta^{18}O$ were also noted. At least two injections were performed at every temperature.

Both the sample testing on the oxides (on the GC-ITD) and the isotope ratio tests were carried out simultaneously. However, the development of the inlet system for the irMS took longer than the system for the GC-ITD. Due to this development, useful isotope ratio sample tests started later than one would have hoped. This led to a backlog of oxides to be tested on the irMS. Therefore, only a subset of the catalysts seen in Chapter 4 were investigated for isotopic integrity.

It should be noted that the operating conditions (including factors such as gas flow rate) on the irMS are different to that of the GC-ITD. Therefore systems that worked well in the irMS configuration would not necessarily work under the isotope investigation system. The operating conditions for the Ion Trap system are highly similar to the current MODULUS configuration.

As the initial ion trap tests gave favourable results for the NiO/Pt reactor tube, as well as its use in commercial systems (Brand, 1994), this material was the first to be investigated. The system used is shown and described in section 5.1.2.

5.1.2. Apparatus - irMS

The irMS consisted of the same vacuum system as used for the GC-ITD line, and can be seen in detail in Figure 5.1. A description of the complete vacuum system and gas injection system is given in Chapter 2. A series of T-pieces split the gas flow from the helium tank into three flows, one for the ITD, one to the interface unit of the Delta C, leaving one flow for the isotope sample introduction system. A 6-port Valco valve (⅛") was fitted with a 2 ml sample loop, and was linked to the main vacuum system. Gas was introduced here while the loop was in the load position, and once the valve had been switched to inject, gas then was forced along a path made from ⅛" stainless steel piping toward the reaction tube. The furnace and controller was of the same type as the GC-ITD system. Two three-way solenoid valves (24 V d.c., Precision Dynamics Inc.) were placed before and after the reactor, and a by-pass line was attached between them. This allowed gas to flow avoiding the reactor altogether, which was useful in blank testing and calibration of peak sizes with CO_2 injections. Downstream of the oxidiser unit, combusted and uncombusted products were swept towards another 6-port Valco valve, this time arranged such that a 10 ml sample loop could be immersed inside a liquid nitrogen dewar. At 77 K, CO_2 condensed, while CH_4 and CO were still volatile and were swept to vent by the helium stream.

After a suitable time period had elapsed for trapping CO_2, the valve was switched so that the loop was isolated from the reaction/preparation line, and now was in-line with the mass spectrometer system. Another helium stream flowed through the loop, with a different flow rate, passing over the condensed CO_2. The liquid N_2 was then removed from the loop, which was left to warm up to room temperature. While warming, CO_2 sublimed to the gaseous phase and was transported to the mass spectrometer inlet system, which consisted of a water remover (Nafion™ membrane) and a mechanical open-split interface (Finnigan Mat GC combustion interface II). A capillary then transported gas to the Finnigan Mat Delta C ion source.

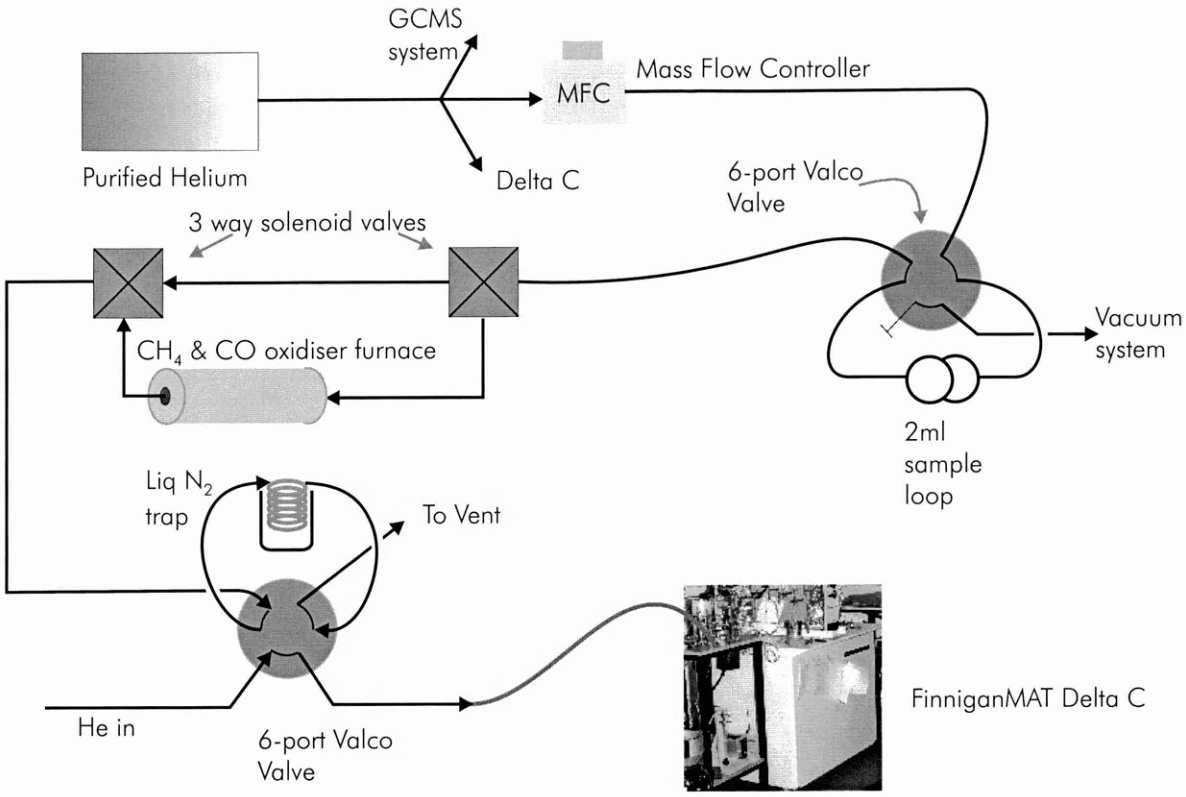

Figure 5.1 schematic diagram of the continuous flow system for measuring $\delta^{13}C$ of CO_2 from combusted CO or CH_4. The 3-way valves allow two possible paths for the gas, through or bypassing the reactor

The installation of a new sample tube into the irMS system involved the same process as the GC-ITD line (Chapter 4), requiring interruption of the helium stream. The consequences were nowhere near as dramatic – the Valco valve isolated the mass spectrometer interface from the combustion section. Once helium had flushed the contaminant air through the remaining pipework the sample was ready to be heated and tested. The 3-way (solenoid) valves were used for this purpose, diverting the helium flow through the by-pass while a reactor tube was changed.

5.1.3. irMS sample study & flow rate issues

The irMS system required more careful sample handling than the ion trap system. The 2 ml loop attached to the vacuum system, was filled with CO or CH_4 and isolated via a manual Nupro valve (NLV). Switching the Valco valve allowed the carrier gas to transport the test gas along a 5 metre length of 1/8" steel tubing towards the combustion tube. Experiments were

characterised in terms of timing of events. A typical injection consisted of the procedures in sequence as shown in Table 5.1.

Table 5.1 Event time sequence for the valve switching and liquid N_2 (cryotrap) removal following injection of test compounds over the catalysts. Trapping time is the time between sample injection and valve switching, in this case 6 minutes.

Time	Event
T=0 min	Liquid N_2 on trap; start data collection on mass spectrometer
T=1 min	Inject sample
T=7 min	Turn Valco valve on trap toward MS
T=8 min	Remove liq N_2 from loop, CO_2 sublimes after a few seconds
T=9+min	irMS analyses CO_2 peak, issues $\delta^{13}C$

The flow rate for this system was much higher than for the GC-ITD system, allowing less contact time for the gases to react with the oxide surface. The carrier gas flow rate was set in the range of 5 to 60 ml/min depending on oxide packing density. Setting the helium to the same flow rate as the ITD system (1 ml/min) would have been impractical. The trapping time for CO_2 under liquid nitrogen would have to have been increased, which would increase the proportion of contaminant CO_2 in the sample peak.

Similarly to the GC-ITD system, the flow rate of He over the irMS system catalyst was governed by the He pressure. However, instead of the mass flow controller, most all of the oxides tested in this chapter were tested with the presence of a Porter valve controlling pressure, allowing the requested helium head pressure to be set. Due to the sample requirements of isotopic analysis of carbon in atmospheric methane (Chapter 6), 300 ml air samples had to be injected. During the development of that system, it was found the mass flow controller hindered the ability of these samples to be flushed to the mass spectrometer. The Porter valve solved this issue, and was also used for the oxide isotope investigation system.

Some of the early oxide tests in this Chapter did not use the Porter valve; some regulated Helium flow by means of using two needle valves in series. Other tests used the mass flow controller before it's replacement by the Porter valve.

The non-porous nature of some powders often caused a restriction to gas flow, necessitating an increase of the He pressure to give an appropriate flow rate. Some oxides were so tightly packed so that only low (≤10 ml/min) flow rates were available, as limited by the regulator on the helium cylinder.

Sample sizes of the CO and CH_4 gases were measured with a Baratron (MKS) fitted to a 6-port Valco valve, with a sample loop of 2 ml volume. Downstream of the combustion unit, CO_2 was trapped under liquid N_2 in a 0.25 ml loop ($^1/_{16}$" stainless steel). On removal of the liquid N_2 the warming by ambient air defined the peak size detected by the mass spectrometer. As the warming was at a relatively constant rate, peak widths were very consistent. The maximum sample size that could be measured without overloading the detectors was approximately 100 nmoles, depending on peak width. At room temperature, 1.0 torr of ideal gas in the loop (2 ml volume) was equivalent to 107 nmol. Test gases were stored in aliquotters as detailed in Chapter 2. Repeated expansion of the test gas and splitting was required for the gas pressure to lie within the detectable range.

5.1.4. Format of Chromatogram from irMS

There was no direct connection from the combustion reactor to the mass spectrometer inlet. The detectors only measured species of m/z 44-46, which were either present in the sample loop as vapour, or volatile after removing the liquid nitrogen dewar from the loop. Therefore, the term chromatogram is not strictly accurate, as there was no continuous admission of different samples to the MS inlet to be measured against time. The recorded data shows detected voltages versus time, which appears very much like an ordinary GC trace. Mass 44 was usually displayed with another chromatogram showing the mass 45/44 ratio, which appears as the measured ratio of voltages and not the absolute ratio. There was also a positive bias voltage

applied so that no "divide by zero" effects occurred. The resistors on the three Faraday cups were not equal. The cup for mass 44 had a resistance of 3×10^8 Ω, mass 45 had 3×10^{10} Ω, and mass 46 had 1×10^{11} Ω. Due to Ohm's law, $V = IR$, the voltage measured by masses 44 and 45 were roughly equal as the ratio of the resistors is similar to the natural abundance ratio of ^{13}C to ^{12}C. The additional bias voltage left the background 45/44 ratio to be near 0.9. On passing reference gas, or a CO_2 sample into the system this ratio approached near 1.12.

If a GC column *is* used in such a system there is a time discrepancy between CO_2 molecules of masses 44, 45 and 46. Molecules of mass 45 arrive at the source earlier than mass 44 due to interactions of the compound with the stationary phase, and corrections have to be imposed (Ricci et al., 1994). The appearance of the 45/44 ratio trace shows a "swan" peak – an initial rise from baseline, then a sudden drop below the baseline, and rising to the baseline at the end of the "peak". On calculating the $\delta^{13}C$ values, algorithms in the software temporally shift the peak maxima of masses 44, 45 and 46 to be equal. Peak area ratios are then used and compared those from reference CO_2 before displaying the final $\delta^{13}C$ result.

Figure 5.2, shows a typical trace from the irMS system. Large and wide peaks at the start of the run are reference injections while the final peak is CO_2 that was trapped within the sample loop.

The data collection and analysis package for the Delta C was the ISODAT software set. This runs on a 486/20 Elonex PC, and under a partially-multitasking operating system named Concurrent DOS (Digital Research, now under Novell and licensed to IMS). Acquisition, data review, file management and all other processes operated within different modules within CDOS, which could control four tasks simultaneously. Unfortunately, inconsistencies within ISODAT hampered ease of use within the system. For instance, when calculating $\delta^{13}C$ and $\delta^{18}O$ results, $\delta^{13}C$ was always compared to the carbon standard PDB, while $\delta^{18}O$ was always compared to the reference gas. If sample $\delta^{18}O$ values are required, they must be calculated

externally. Throughout this thesis, all $\delta^{18}O$ values reported are with respect to the oxygen standard, V-SMOW.

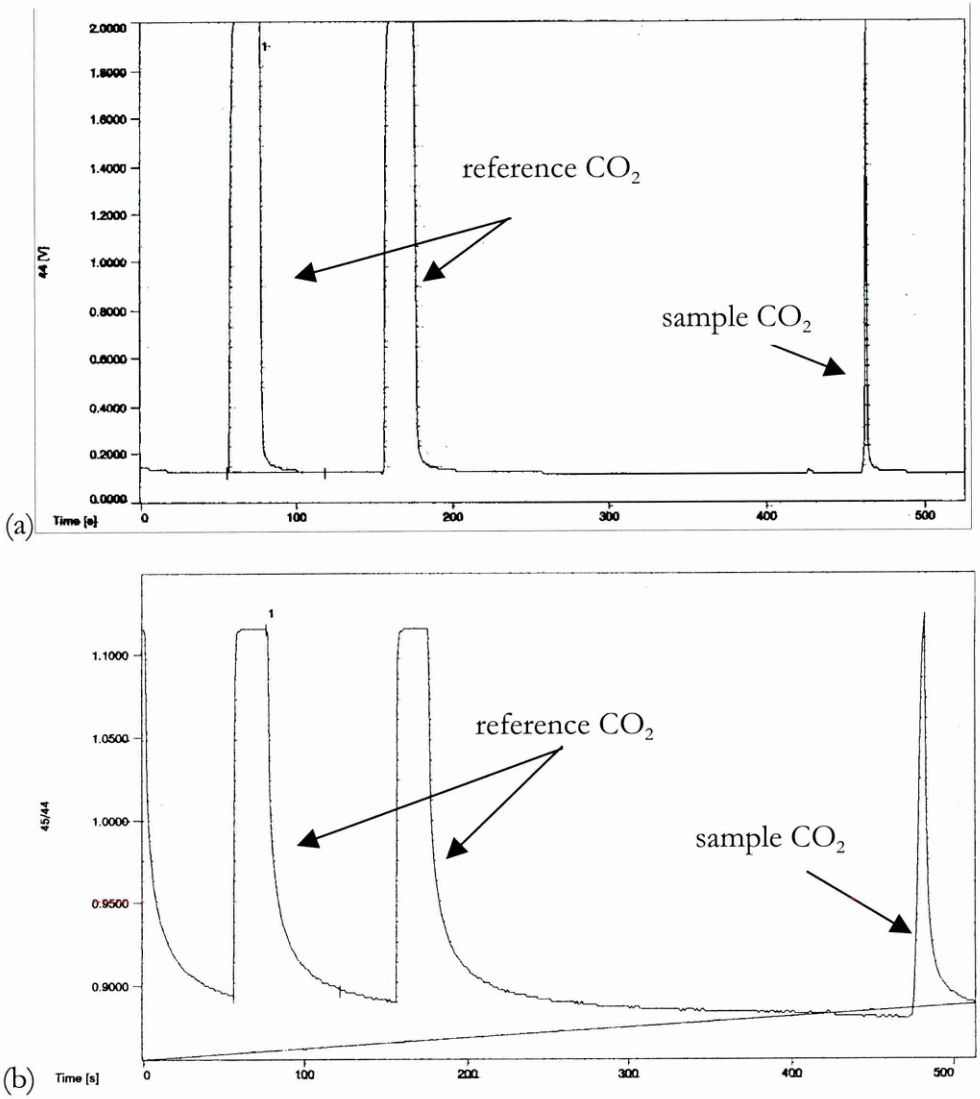

Figure 5.2 (a) sample chromatogram from the ISODAT software on a Finnigan MAT Delta C mass spectrometer, showing m/z 44 with time, and 2 reference peaks and one sample peak, (b) a chromatogram for similar injection, but with the m/z 45/44 ratio with time on display. The plot of 45/44 shows a diagonal line – this is only an artefact the software's printing.

For verification of the isotope values, the $\delta^{13}C$ and $\delta^{18}O$ of the reference gas must be measured against an international standard. This was done within the PSRI on a VG SIRA 24 dual inlet mass spectrometer using an internal standard, which has been validated back to NBS-19. Unfortunately, the carbon monoxide lecture bottle used in these experiments never had its oxygen isotope ratio verified by second system. The only oxygen isotope data available on the CO is from the combustion catalysts described in this chapter.

5.2. Results

5.2.1. Nickel Oxide / Platinum

The first experiments using NiO/Pt were used to check the combustion efficiency at various temperatures. 20 nickel wires (0.125 mm diam, 150 mm length) and two Pt wires (0.25 mm diam) were installed into a quartz tube (1 mm i.d.). Oxidation took place at 1150°C with O_2 flow. Combustion of CH_4 was tested at 700°C to 1000°C at 100°C steps. The flow rate of helium was set high, between 40 and 55 ml/min., by the use of two needle valves in series. Figure 5.3 shows the outcome of comparing peak area with injection size at different temperatures.

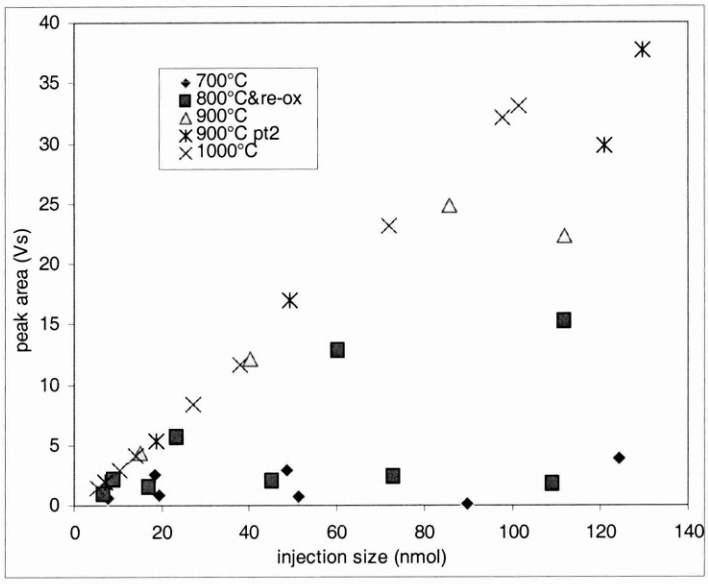

Figure 5.3 peak area of CO_2 from combustion of CH_4 to CO_2 over NiO/Pt over a temperature range of 700-1000°C compared to injection size of CH_4

It is evident from Figure 5.3, that only 1000°C shows a linear response to CH_4 combustion over the entire range of injection sizes. At 900°C linearity was not perfect, indicating less than 100% combustion at high injection loads. It is interesting to note that although the ion trap tests showed that 700°C was needed for complete combustion of CH_4 to occur, this has now increased to 1000°C once installed into the isotope ratio system. A higher flow rate resulting in lower contact time, coupled to the increase in the methane injection size probably caused this

effect. The detection limit of the Ion Trap Detector was an order of magnitude better (lower) than that of the irMS.

Two series of injections were undertaken at 700°C and 800°C with a flow rate of 54 ml/min flow rate. The first series showed very little combustion, so the NiO/Pt reactor was re-oxidised with O_2. The 700 & 800°C steps were repeated as part of the second series. The more active of the two series was seen after the re-oxidation. Two series were also performed at 900°C. The flow rate was lowered from 54 to 39 ml/min and another set of CH_4 injections were performed at 900°C and at 1000°C. Even the second injection series at 900°C gave high, but not perfect linearity. As can be seen from Table 5.2 the peak area is compared to that which is expected from the CO_2 calibration. For combustions at 1000°C the CO_2 peak is a few percent above the expected amount. The system blank at 1000°C had been tested previously and found to be insignificant.

Table 5.2 CH_4 combustions over NiO/Pt at different temperatures, showing expected CO_2 peak sizes compared to calibrations performed with CO_2

injection	He flow rate (ml/min)	Temperature (°C)	CH_4 injected amount (nmol)	CO_2 peak area (% expected)
1	54	700	19.3	16
2	54	700	7.7	38
3	54	800	72.8	11
4	54	800	109.3	6
5	54	800	45.3	16
6	54	800	17.2	34
7	54	800	6.7	70
Re-oxidation	of	Nickel-Platinum	reactor	
8	54	700	124.3	10
9	54	700	48.6	20
10	54	700	18.5	52
11	54	800	111.7	45
12	54	800	60.1	72
13	54	800	23.4	87
14	54	800	8.9	107
15	54	900	111.9	66
16	54	900	85.9	97
17	54	900	40.2	104

injection	He flow rate (ml/min)	Temperature (°C)	CH_4 injected amount (nmol)	CO_2 peak area (% expected)
18	54	900	15.0	112
19	39	900	120.7	82
20	39	900	129.6	96
21	39	900	49.2	118
22	39	900	18.8	106
23	39	900	7.1	127
24	39	1000	97.7	110
25	39	1000	71.9	108
26	39	1000	27.3	109
27	39	1000	10.5	114
28	39	1000	101.7	108
29	39	1000	37.7	107
30	39	1000	14.2	113
31	39	1000	5.4	157

It can be seen from Table 5.2 that at constant temperature, the percentage conversion depends on the injection size of CH_4. A smaller CH_4 injection is more likely to give a larger peak size, as can be seen in Figure 5.3. Other factors contributing to the peak area included contact time (flow rate) and the state of the oxide surface. Conversions over 100% can be attributed to a change in MS sensitivity, or a release of CO_2 from the oxide triggered by the combustion process.

Subsequent tests of the material were undertaken with the mass flow controller, which allowed the testing of the effect of flow rate on combustion properties. Two helium flow rates were used, 5 ml/min and 10 ml/min. Methane was injected in the normal manner (section 5.1.2), with liquid N_2 used to cool the sample loop to trap the CO_2. Trapping time was set to 4 minutes for 10 ml/min and 6 minutes for 5 ml/min. Peak areas, $\delta^{13}C$ and $\delta^{18}O$ measurements were noted and compared.

10 ml/min helium flow rate

Results from the combustion for the tests at 10 ml/min can be seen in Figs 5.4, 5.5 and 5.6. Figure 5.4 shows linear behaviour of peak area with injection size at lower temperatures than the

tests at higher flow rates. At 800°C the peak area response of CO_2 is as linear as at 1000°C, the temperature that 39 ml/min showed linearity.

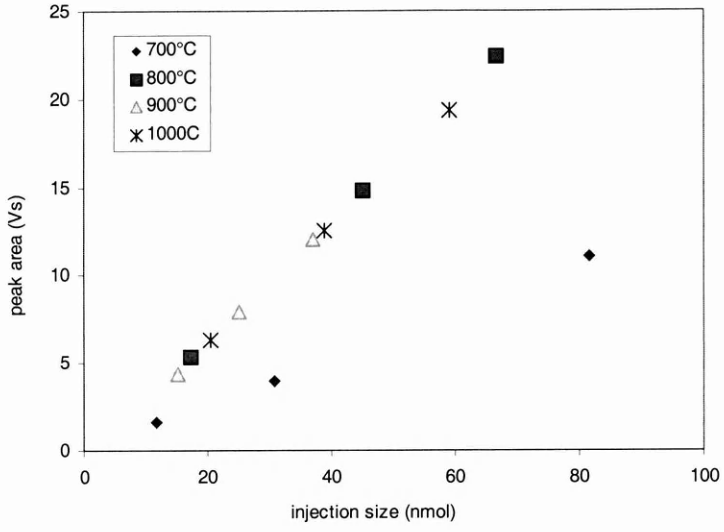

Figure 5.4 CO_2 peak area versus injection size from CH_4 injections over NiO/Pt at 10 sccm at different catalyst temperatures

The variation in the measured $\delta^{13}C$ of the combusted methane with temperature was also measured. As a fractionation indicator, $\delta^{18}O$ was also measured and any temperature effects noted in Figure 5.5 (b).

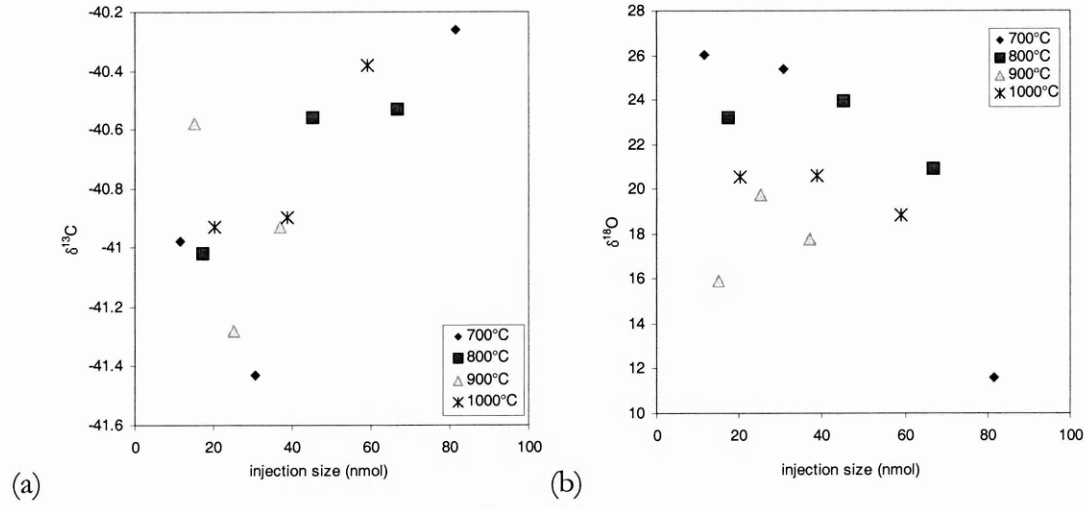

Figure 5.5 a) showing $\delta^{13}C$ of combusted CH_4 at various reactor temperatures, and (b) showing $\delta^{18}O$ of CO_2 from CH_4 combustion at various reactor temperatures (all at 10 sccm)

It can be seen from Figure 5.5 (a) that there was a significant amount of variation (total <2 ‰ over all temperatures) in the observed $\delta^{13}C$ isotope ratio at different temperatures. Recall that

the instrument precision was 0.10 ‰. The results can be re-plotted to show the variation in $\delta^{13}C/\delta^{18}O$ with the temperature of NiO/Pt which gives Figure 5.6.

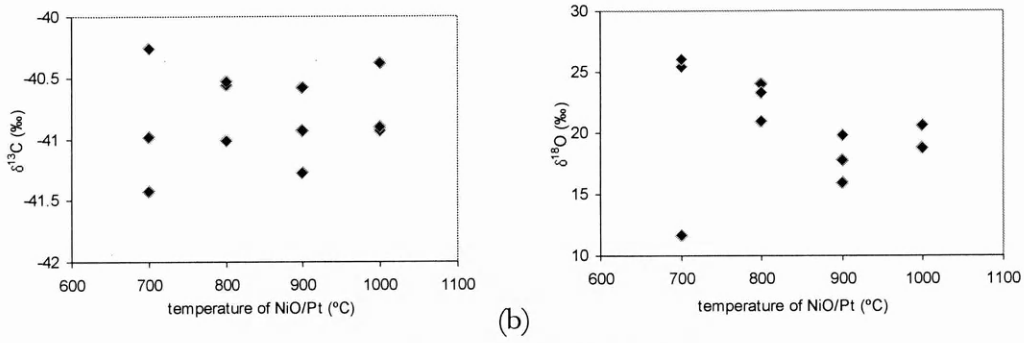

Figure 5.6 (a) showing range of $\delta^{13}C$ of CO_2 from CH_4 from combustion over NiO/Pt at different temperatures, and (b) showing $\delta^{18}O$ from the same combustions (all at 10 sccm)

From Figure 5.6 (a) showing $\delta^{13}C$ versus temperature, it is evident that there is little obvious change in the spread of the points or the mean $\delta^{13}C$ of the CO_2 with temperature. The spread of $\delta^{13}C$ results was temperature independent. The $\delta^{13}C$ means are displayed in Table 5.3.

Table 5.3 Mean and standard deviations of $\delta^{13}C$, $\delta^{18}O$ from combustions of CH_4 over NiO/Pt at temperatures 700-1000°C at 10 ml/min

Temperature (°C)	Mean $\delta^{13}C$	$\pm \sigma$, n=3, (‰)	Mean $\delta^{18}O$	$\pm \sigma$, n=3, (‰)
700	-40.9	0.6	+21.0	8.2
800	-40.7	0.3	+22.7	1.6
900	-40.9	0.4	+17.8	1.9
1000	-40.7	0.3	+20.0	1.0

From Table 5.3, the lowest recorded standard deviation was at 800°C, which also showed 100% combustion. There is no significant difference in $\delta^{13}C$ or standard deviation from 800 to 1000°C. According to these data there is no evidence to suspect that combustion at 800°C will not deliver untrustworthy $\delta^{13}C$ values.

The $\delta^{18}O$ values show an entirely different situation (Figure 5.6 (b)). The point at 700°C giving a $\delta^{18}O$ value of 11.6‰ is known to be spurious, as the peak size was on the saturation limit of the irMS detector. This still leaves a 10‰ shift in the values in $\delta^{18}O$. A temperature

dependence of $\delta^{18}O$ is observed, the lightest oxygen is produced at 900°C, while at 800°C $\delta^{18}O$ is heaviest.

5 ml/min helium flow rate

Repeating the test for the lower helium flow rate of 5 ml/min, produced a similar pattern for peak areas at the different temperatures. As the flow rate is slower, the contact time is greater, so therefore greater conversion at lower temperatures is expected.

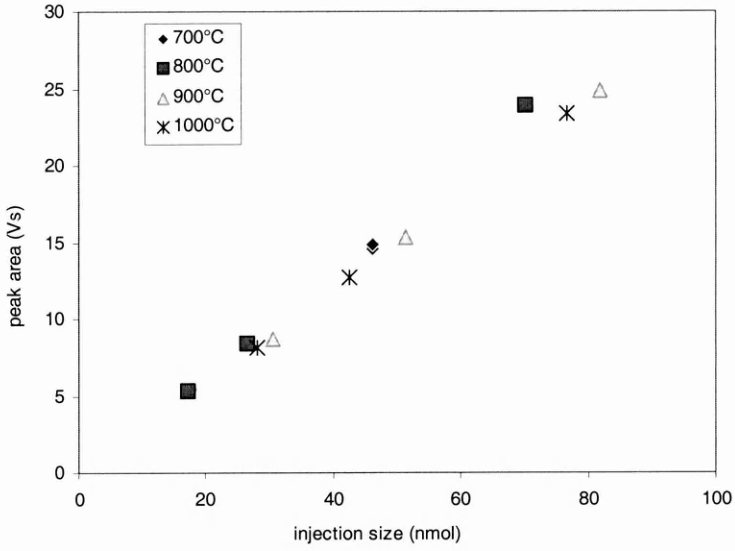

Figure 5.7 CO_2 peak area from CH_4 injections over NiO/Pt at 5 sccm at different catalyst temperatures

Figure 5.7 shows a problem with the linearity of the peak size. The regression lines from temperature series 700 and 800°C show a slightly higher gradient than points from 900 and 1000°C. This was assumed to be due to a time delay - the first two series of experiments were conducted over five days before the second series. During this period the sensitivity of the Delta C could have changed, and this is evident from this graph if the assumption is made that all combustions were 100%. The likelihood of combustion at 700°C being more efficient than at 1000°C was minimal. Although this graph's intention was to prove 100% combustion at certain temperatures, it has found combustion efficiency more invariant than the mass spectrometer detectors' sensitivity.

An examination of the isotopes of the CO_2 detected reveals similar patterns as the tests at the higher flow rate.

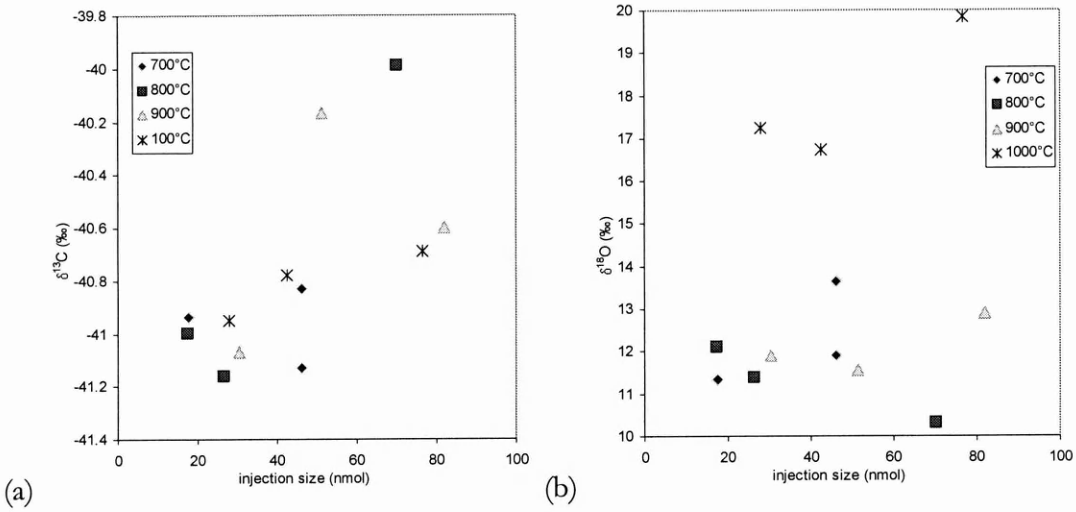

Figure 5.8 (a) showing $\delta^{13}C$ of combusted CH_4 at various reactor temperatures, and (b) showing $\delta^{18}O$ of CO_2 from CH_4 combustion at various reactor temperatures (all at 5 sccm)

Some injections of CH_4 produced $\delta^{13}C$ values over 0.6 ‰ away from the total bulk mean. Some values appear to err on the side of heavier $\delta^{13}C$ carbon ratios only (instead of an even spread about a central $\delta^{13}C$ mean), especially those with larger injection sizes. The values of $\delta^{18}O$ appear to show a surprising temperature effect. At 1000°C there was a 5‰ shift in $\delta^{18}O$ compared with lower temperatures. This can be seen easier in the Figure 5.9 (b).

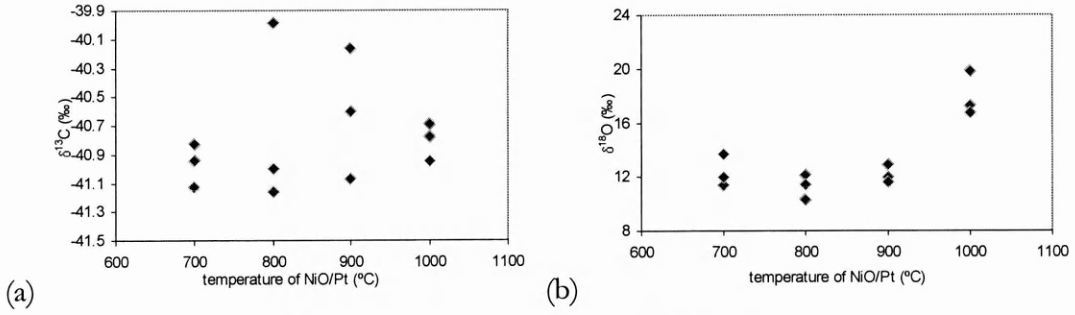

Figure 5.9 (a) showing range of $\delta^{13}C$ of CO_2 from CH_4 from combustion over NiO/Pt at different temperatures, and (b) showing $\delta^{18}O$ from the same combustions (all at 5 sccm)

The marked increase in $\delta^{18}O$ from the CO_2 had to be due to a temperature effect during combustion. Oxygen isotopic fractionation must have been occurring, or at least to a different extent than at lower temperatures. The only source of oxygen in the CO_2 (formed from CH_4

conversion) was the oxide, as the oxygen in the quartz tube has been proven not to interact or fractionate in this system. The nickel/platinum reactor was oxidised using O_2 of measured $\delta^{18}O$, with a value of +26.1‰ relative to SMOW. Therefore between 700-900°C the combustion process makes the $\delta^{18}O$ 15‰ less than the O_2 bottle, and at 1000°C it is 8‰ less. It is in contrast to the experiments at 10 ml/min the $\delta^{18}O$ minimum appears at 900°C. The $\delta^{13}C$ results of 5 ml/min are summarised in Table 5.4.

Table 5.4 Mean $\delta^{13}C$ and $\delta^{18}O$ from combustions of CH_4 over NiO/Pt at temperatures 700-100°C at 5 ml/min

Temperature (°C)	Mean $\delta^{13}C$ (‰)	$\pm \sigma$, n=3, (‰)	Mean $\delta^{18}O$	$\pm \sigma$, n=3, (‰)
700	-41.0	0.2	+12.3	1.2
800	-40.7	0.6	+13.0	0.9
900	-40.6	0.5	+12.1	0.7
1000	-40.8	0.1	+17.9	1.7

These data show that the $\delta^{13}C$ mean value for CO_2 from CH_4 combustion at all combustion temperatures show a spread of 0.35‰. With the limited number of points there are difficulties with using standard deviation as a measure of repeatability of the combined combustion-irMS system. However, it is seen that at 700°C there is no significant difference in consistency than at 1000°C at the 5 ml/min flow rate. There is no evidence that combustion of CH_4 at 700°C induced significant fractionation in carbon isotopes.

CO oxidation

The oxidation of carbon monoxide was also attempted using NiO/Pt catalyst to 600°C. The peak areas, carbon and oxygen isotope ratios are summarised in Figure 5.10.

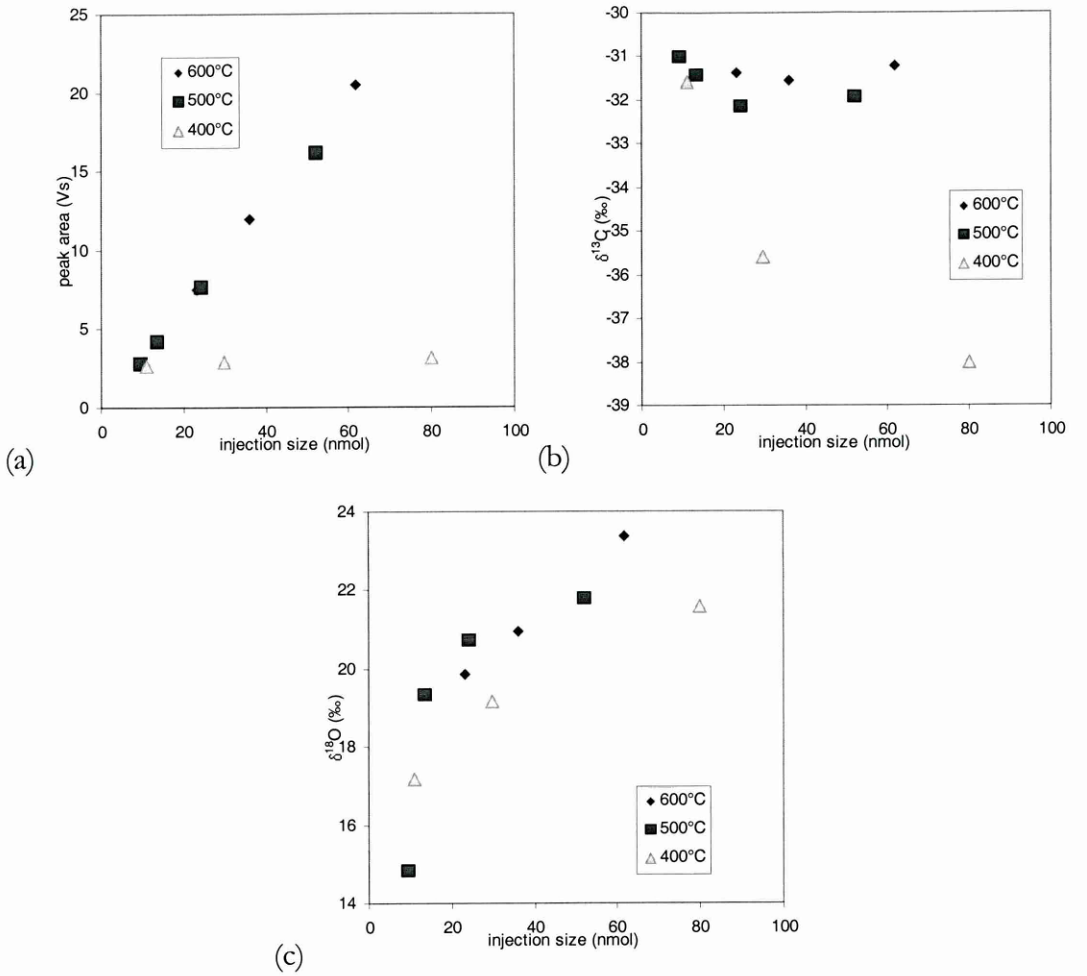

Figure 5.10 (a) peak areas of CO injection over NiO/Pt at 400-600°C, (b) $\delta^{13}C$ of CO injections in (a), (c) $\delta^{18}O$ of the injections in (a)

Table 5.5 Mean and standard deviation for combustion results of CO on NiO/Pt at various temperatures

Temperature (°C)	Mean $\delta^{13}C$ (‰)	$\pm \sigma$, (‰)	Mean $\delta^{18}O$ (‰)	$\pm \sigma$, (‰)
400	-35.1	3.2	+21.4	2.2
500	-31.6	0.5	+19.2	3.0
600	-31.4	0.2	+19.3	0.3

Data showing combustion of CO with temperature variation of NiO/Pt are represented graphically in Figure 5.10. Complete combustion can be seen with the oxidant at 500 and 600°C, whereas at 400°C combustion is minimal. It can be seen that the highest consistency carbon isotope values are with the NiO/Pt reactor set to 600°C. At 500°C consistency of $\delta^{13}C$ is lower. At 400°C fractionation is evident, making the carbon isotopically light on the larger injections, while on a 10 nmol injection the $\delta^{13}C$ is within 1‰ of the correct value. The oxygen

isotopes appear to show a relationship with CO injection size, at every temperature tested. Increasing injection size appeared to increase $\delta^{18}O$. Oxygen within CO is likely to exchange isotopically with oxygen bearing species on NiO.

Oxygen isotope exchange experiments with CO_2 and the oxide was performed and noted in Appendix C.

5.2.2. Iron-Nickel Oxide

A sample of iron-nickel oxide was installed into the irMS system and heated to 300°C to remove any contaminants. The blank produced by the compound was measured over a 4 minute trap time with a helium flow rate of 10 ml/min. The CO_2 peak area was found to be 0.018 Vs, which was deemed low enough for oxidation testing. Carbon monoxide injections at 300°C were attempted. No combustion was observed and so no testing of CH_4 was performed.

5.2.3. Silver Permanganate

The same sample tube containing $AgMnO_4$ as used in the ITD was installed into the irMS system. Helium flow rate was set to 7 ml/min, and the compound was heated to 150°C. The blank had a detected area of 0.128 Vs, low enough to show quantitative combustion effects. Combustion of CO was incomplete (<15%) at 150°C, and the compound even was less active at 200°C. On lowering the temperature down to 175°C there was still no significant increase in activity. Compared to the ITD system, this testing regime requires higher flow rate and greater test gas injection size, leading to greater temperatures required for complete combustion. Higher temperature would have yielded oxygen release. Therefore the contact time required for CO combustion is in excess of that provided by the flow rate.

5.2.4. Copper Chromium Oxide

The first preparation of this mixed oxide was used with a carrier gas flow rate of 2 to 3 ml/min, with the catalyst heated to 200°C. Blank levels were significant at 0.595 Vs for a trap time of 9 min. Increasing the temperature to 400°C, and after leaving for 30 minutes, the blank level was

measured to be 1.0 Vs. One carbon monoxide injection was made, with a peak area detected of 0.889 Vs, implying that no CO had been converted to CO_2.

A larger sample was produced, using 5 mm i.d. quartz tubing. This compound was examined for use in removing ambient CO for atmospheric methane analysis (Chapter 6). It was later tested for pure CO oxidation at a flow rate of 25 ml/min. Results are shown in Figure 5.11.

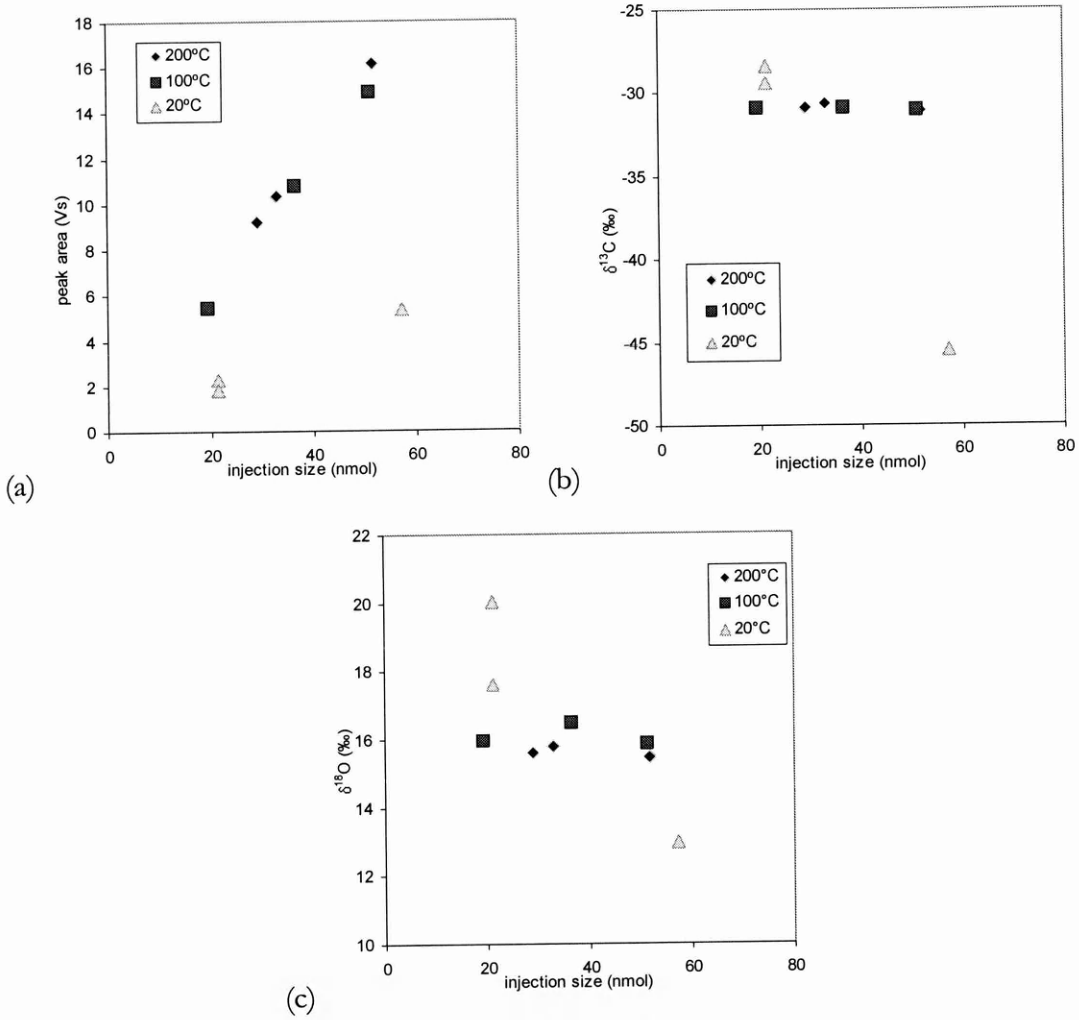

Figure 5.11 (a) peak sizes of CO_2 from CO injections over $CuCrO_x$ at 20-200°C, (b) $\delta^{13}C$ from injections shown in (a), (c) $\delta^{18}O$ from injections shown in (a)

Table 5.6 Mean $\delta^{13}C$ and $\delta^{18}O$ from $CuCrO_x$ CO combustions

Temperature (°C)	Mean $\delta^{13}C$ (‰)	$\pm \sigma$, (‰)	Mean $\delta^{18}O$ (‰)	$\pm \sigma$, (‰)
20	-34.4	9.6	+16.9	3.5
100	-30.9	0.1	+16.1	0.3
200	-30.9	0.2	+15.6	0.2

Examination of Figure 5.11 (a) reveals the lines formed by the 100 and 200°C points show near complete combustion occurring at those temperatures. It is clear however, that at 20°C combustion was minimal. Carbon isotope ratios of the converted CO were constant and the same at both 100°C and 200°C. The values of $\delta^{18}O$ at 100 and 200°C appear to be invariant of injection size and combustion temperature. Not surprisingly, partial combustion at 20°C did not produce any meaningful $\delta^{18}O$ or $\delta^{13}C$ values, as a spread of 9‰ and 15‰ respectively was detected.

5.2.5. Cobalt Chromium Oxide

A large reactor tube containing cobalt-chromium oxide was constructed. A quartz tube of 6 mm o.d., 5 mm i.d. was plugged using glass wool, and approx. 10 cm length of powder was loaded. With a 30 ml/min flow and 6 minute trap time, blank levels were low at 400°C. Using the same flow conditions carbon monoxide injections were undertaken. Combustion was found to be highly efficient at temperatures ranging between 200 to 400°C. Figure 5.12 show the peak areas, the carbon and oxygen isotopes.

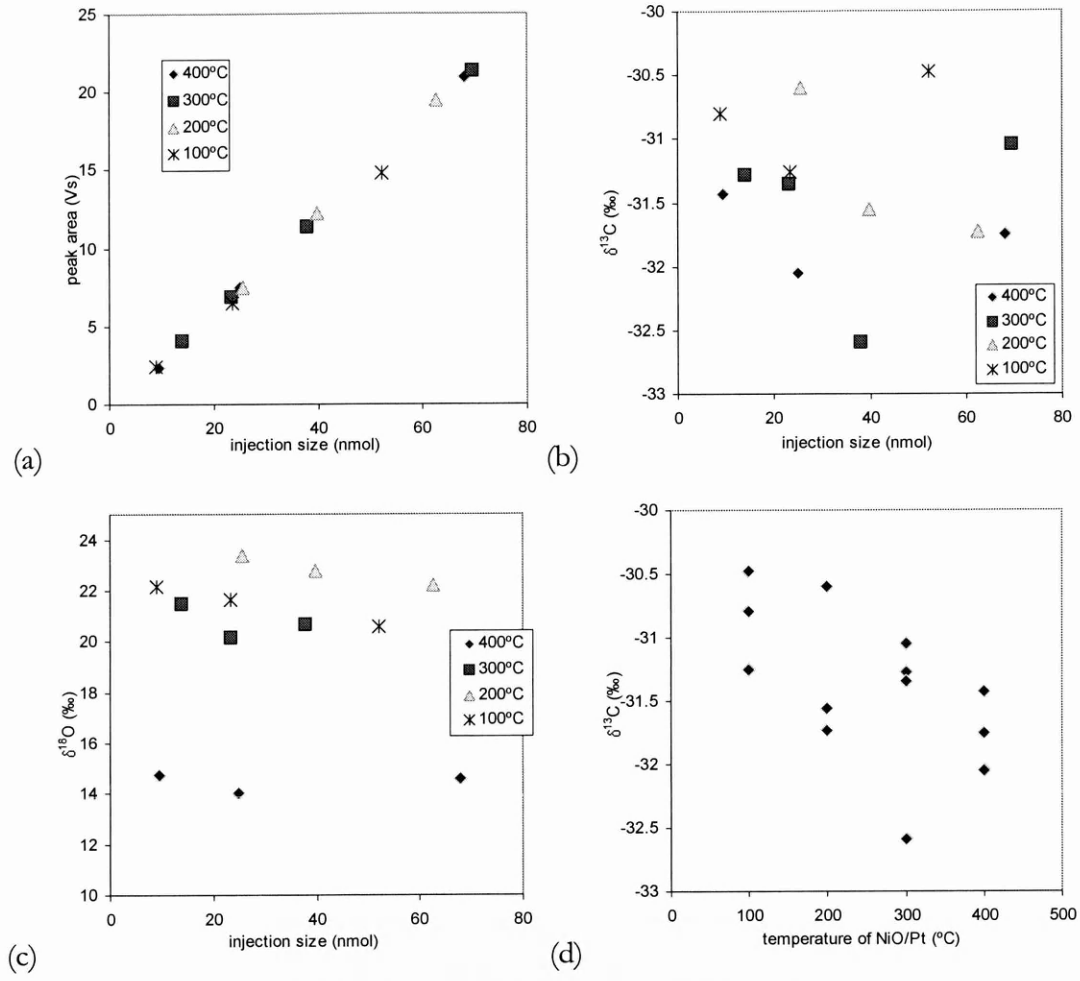

Figure 5.12 (a) peak areas of CO oxidation over $CoCrO_x$ at 100-400°C with injection size, (b) $\delta^{13}C$ of combusted CO with injection size, (c) $\delta^{18}O$ of combusted CO with injection size, (d) mean $\delta^{13}C$ of each temperature series, with 1σ std. dev. error

Figure 5.12 shows that the oxidation was complete (100 %) at temperatures of 100°C or above. Carbon isotope ratios show some dependence on temperature, with the lowest values were at the highest temperatures. $\delta^{13}C$ values are shown without injection size dependence in Figure 5.12 (d). Oxygen isotope data were highly temperature dependent. There was high repeatability in the $\delta^{18}O$ at different catalyst temperatures. A small dependence on injection size was present, where largest injection size lead to slightly lighter $\delta^{18}O$ values in the 100 & 200°C series. Two groups are seen to emerge, with one from the catalyst at 100, 200, and 300°C, while $\delta^{18}O$ at 400°C is prominent with a difference of –9 ‰ relative to the group from 100-300°C. Of the large group, 200°C shows perhaps the heaviest oxygen present. Attempts were made at CH_4

combustion up to 800°C but no conversion was observed. The results of the mean and standard deviation of both $\delta^{13}C$ and $\delta^{18}O$ are shown in Table 5.7.

Table 5.7 Mean $\delta^{13}C$ and $\delta^{18}O$ from CO conversions over $CoCrO_x$

Temperature (°C)	Mean $\delta^{13}C$ (‰)	± σ, (‰)	Mean $\delta^{18}O$ (‰)	± σ, (‰)
100	-30.9	0.4	+21.5	0.8
200	-31.3	0.6	+22.8	0.6
300	-31.6	0.2	+20.8	0.7
400	-31.7	0.3	+14.4	0.4

5.2.6. Cobalt (II,III) Oxide

A large (5 mm i.d.) combustion tube filled (6 cm depth) with Co_2O_3 was created for this experiment. The compound was heated to 300°C and left to degas. A high blank level (>1 Vs) only permitted testing of qualitative combustion efficiency. Very little combustion of CO was observed at 300°C. No CH_4 oxidations were attempted.

5.2.7. Rhodium (III) Oxide

Possibly contaminated Rh_2O_3 sample

As Rh_2O_3 was found to be the most active of all the oxides tested with the ion trap, it was expected to perform well under the irMS conditions. Two samples were prepared for analysis from the metal hydroxide. One was created under cleaner conditions than the other, as one was possibly contaminated by the insulation of the furnace used to heat the hydroxide. The quantity of oxide used in these tests was larger (approximately 2-3 x) than that used in the ion trap tests. Heating to 500°C was necessary to degas and reduce the blank CO_2 emission. Lowering the temperature to 300° produced negligible blanks. Carbon monoxide combustion was tested at various temperatures, and the results are shown in Figure 5.13, with mean and standard deviations shown in Table 5.8.

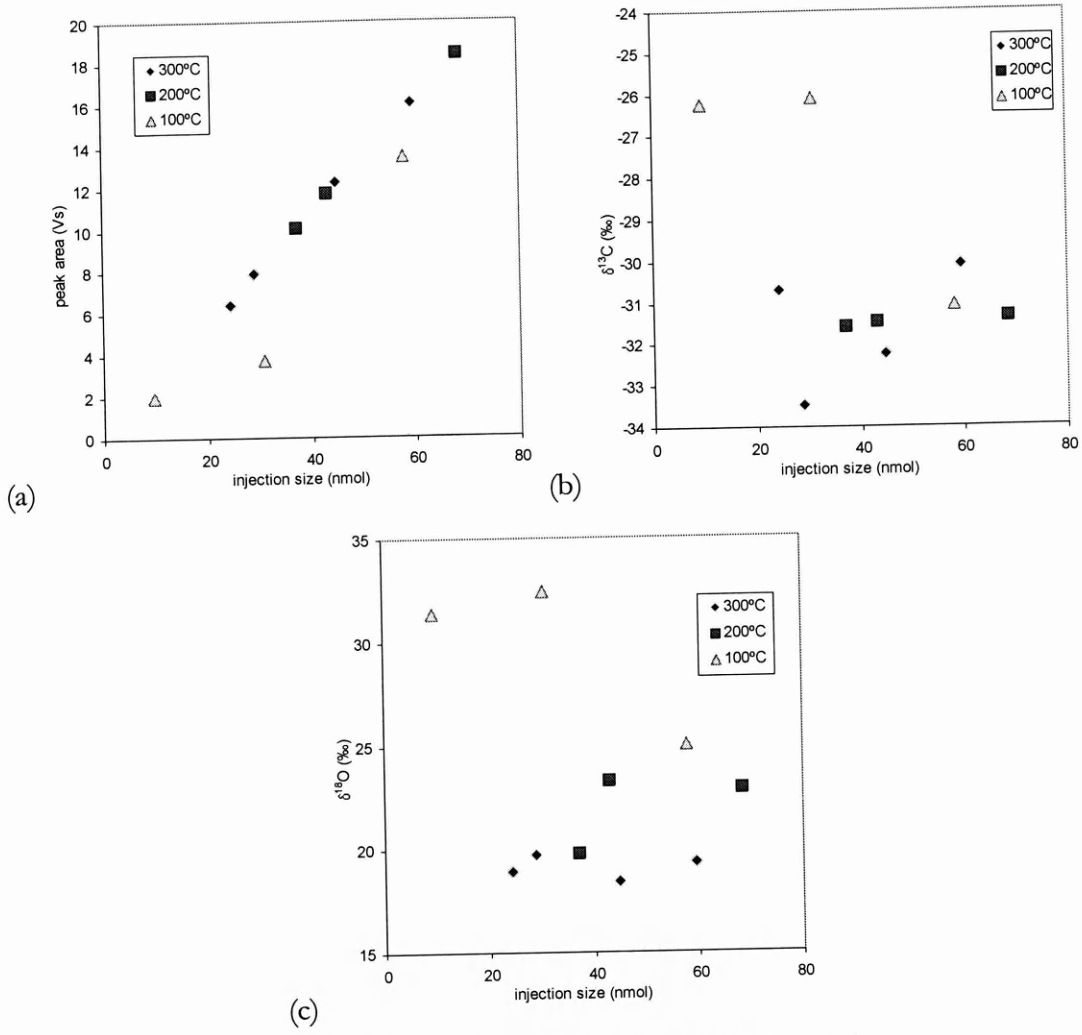

Figure 5.13 (a) CO_2 peak areas of combusted CO over Rh_2O_3 (low cleanliness) at 100-300°C, (b) $\delta^{13}C$ values of combusted CO with injection size, (c) $\delta^{18}O$ values of combusted CO with injection size

Table 5.8 Mean $\delta^{13}C$ and $\delta^{18}O$ for Rh_2O_3 (1st) CO combustions at 100-300°C

Temperature (°C)	Mean $\delta^{13}C$ (‰)	$\pm \sigma$, (‰)	Mean $\delta^{18}O$ (‰)	$\pm \sigma$, (‰)
100	-27.8	2.8	+29.6	4.0
200	-31.5	0.1	+22.0	1.9
300	-31.6	1.5	+19.1	0.6

From Figure 5.13 (a), it can be seen that the combustion was complete at 200°C and above. The carbon isotope ratios show highly reproducible values with combustion at 200°C. There is no difference (within experimental error) between $\delta^{13}C$ returned using the catalyst at either 200 or 300°C. Unexpectedly, results from combustions at 300°C resulted in greater standard deviation. In contrast, oxygen isotope ratios were more constant with combustions at 300°C.

Oxidation of CO was also carried out at higher temperatures and the results shown in Figure 5.14.

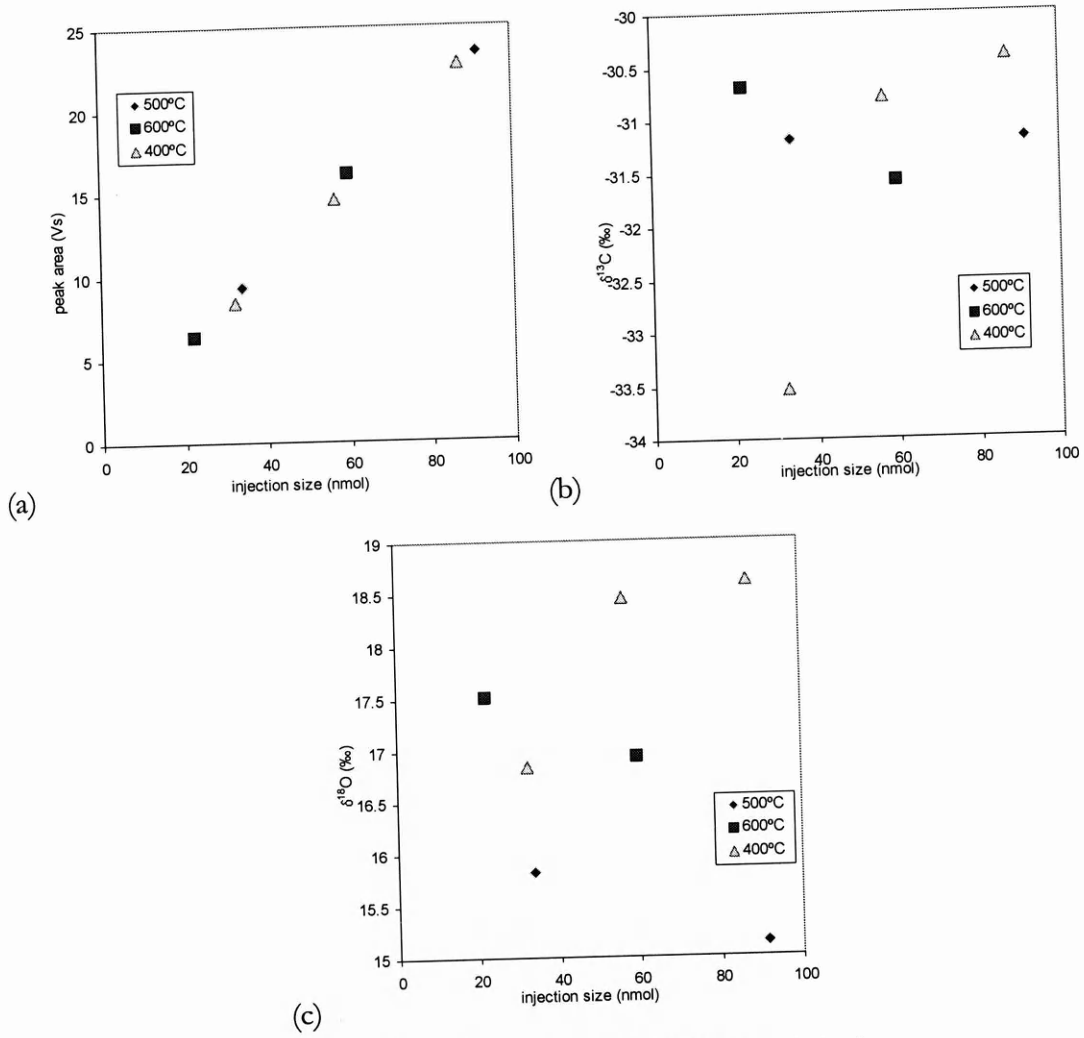

Figure 5.14 (a) CO_2 peak areas of combusted CO over Rh_2O_3 (low cleanliness) at 400-600°C, (b) $\delta^{13}C$ values of combusted CO with injection size, (c) $\delta^{18}O$ values of combusted CO with injection size

As would be expected, the combustion efficiencies at these temperatures were high (100 %). From Figure 5.14 (b), the carbon isotope ratio values showed lower consistency at 400°C than 500 and 600°C. The oxygen isotope ratio appeared constant to within 4‰ over the three temperatures tested.

Table 5.9 Mean $\delta^{13}C$ and $\delta^{18}O$ for Rh_2O_3 (1st sample) CO combustions at 400-600°C

Temperature (°C)	Mean $\delta^{13}C$ (‰)	$\pm \sigma$, (‰)	Mean $\delta^{18}O$ (‰)	$\pm \sigma$, (‰)
400	-31.9	1.7	+18.0	1.0
500	-31.2	0.0 (n=2)	+17.2	0.5
600	-31.1	0.6	+15.5	0.4

Methane combustion was also tested with Rh_2O_3. Within the ion trap system (Chapter 4), methane was completely combusted at 250°C or higher. This temperature was expected to be too low for the flow rate of over 30 ml/min. For these tests, the carrier gas flow rate was set to 24 ml/min.

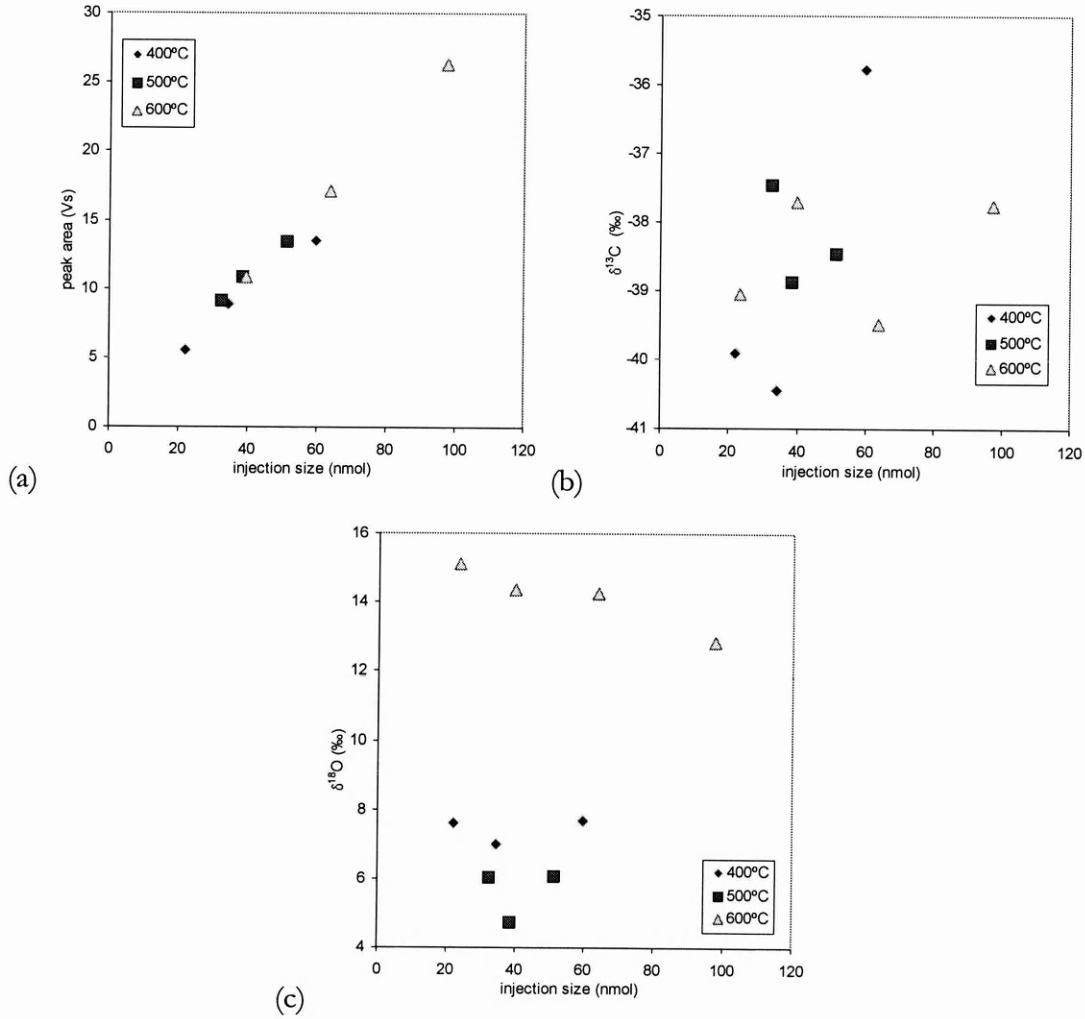

Figure 5.15 (a) CO_2 peak areas of combusted CH_4 over Rh_2O_3 (low cleanliness) at 400-600°C, (b) $\delta^{13}C$ values of combusted CH_4 with injection size, (c) $\delta^{18}O$ values of combusted CH_4 with injection size

From Figure 5.15 (a), combustion efficiency was 100% at 500°C and higher, while at 400°C efficiency was over 90%. The carbon isotope ratios showed poor (>1‰) consistency at all temperatures tested. No obvious temperature or injection size dependence is seen with $\delta^{13}C$ values. The $\delta^{18}O$ values show temperature dependence, and in the case of 600°C, sample size dependency. Higher temperature combustion resulted in heavier oxygen isotopes (Figure 5.15 (b)). At 600°C, increasing the injection size resulted in more negative $\delta^{18}O$ values. With CH_4 combustion, oxygen isotopes are more of an indicator of the fractionation in the combustion process. Potentially this shift could imply that ^{18}O ions are more labile in the oxygen lattice at this temperature than ^{16}O ions. Increasing the temperature to 700°C resulted in large CO_2 emission from the oxide. Summarised results of the combustions are seen in Table 5.10.

Table 5.10 Mean $\delta^{13}C$ and $\delta^{18}O$ for Rh_2O_3 (cleaner sample) CH_4 combustions at 400-600°C

Temperature (°C)	Mean $\delta^{13}C$ (‰)	$\pm \sigma$, (‰)	Mean $\delta^{18}O$ (‰)	$\pm \sigma$, (‰)
400	-38.7	2.6	+7.4	0.4
500	-38.3	0.7	+5.6	0.8
600	-38.5	0.9	+14.1	0.9

Cleaner Rh_2O_3 sample

The tests in the previous section were carried out on a sample of rhodium oxide possibly containing impurities introduced from placing the hydroxide into a drying furnace. A cleaner preparation of Rh_2O_3 was created from the hydroxide. Tests with CO and CH_4 combustion were repeated to see if the cleaner sample had improved combustion potential. Helium flow rates were set to between 40 and 50 ml/min. Results can be seen in Figure 5.16.

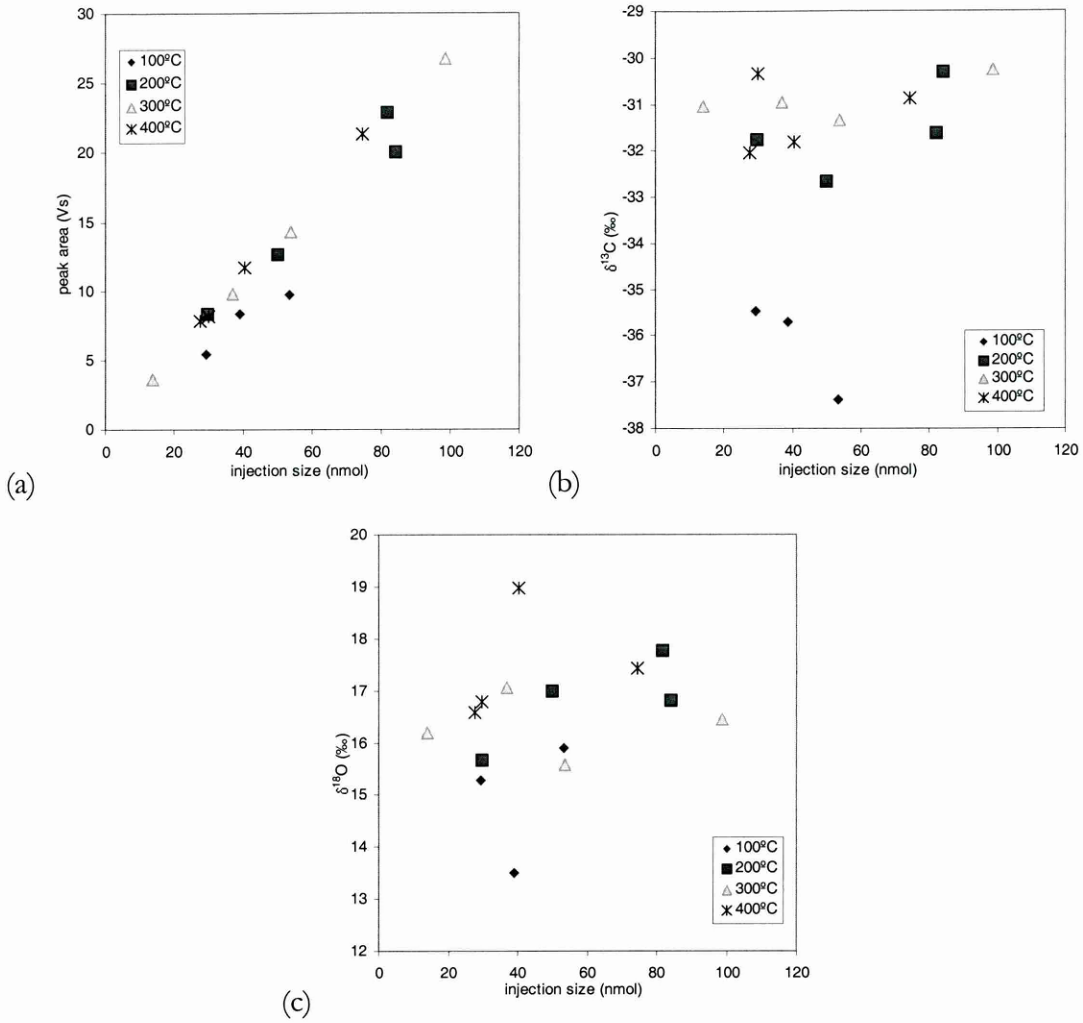

Figure 5.16 (a) peak sizes of CO_2 from CO combustion on Rh_2O_3 (clean) at 100-400°C, (b) $\delta^{13}C$ values of combusted CO with injection size, (c) $\delta^{18}O$ values of combusted CO with injection size

Figure 5.16 (a) gives details of the CO combustion at various temperatures, and mean data from the combustions can be seen in Table 5.11. Combustion efficiency was found to be greatest at 300°C or higher, as there seems to be a slight deviation from linearity at lower temperatures. Examination of the $\delta^{13}C$ values of the combusted CO (Figure 5.16 (b)) revealed greatest consistency was seen with combustion at 300°C. Only 100°C gave values showing obviously incorrect isotope ratios, with a 4‰ lighter shift from the expected value. Combustion at 200°C and 400°C resulted in a $\delta^{13}C$ mean similar to that at 300°C, but with greater variability. Oxygen isotope ratios were relatively constant (within 4‰), showing no dependence on temperature or injection size. Combustions at 200 and 300°C gave reproducible $\delta^{18}O$ ratios to within ±3‰.

Table 5.11 Mean $\delta^{13}C$ and $\delta^{18}O$ for Rh_2O_3 (cleaner sample) CO combustions between 100-400°C

Temperature (°C)	Mean $\delta^{13}C$ (‰)	± σ, (‰)	Mean $\delta^{18}O$ (‰)	± σ, (‰)
100	-36.2	1.0	+14.9	1.2
200	-31.6	1.0	+16.8	0.9
300	-30.9	0.5	+16.3	0.9
400	-31.3	0.8	+17.4	1.1

The oxidation of methane was also performed on the same sample. Results are shown in Figure 5.17 and in Table 5.12.

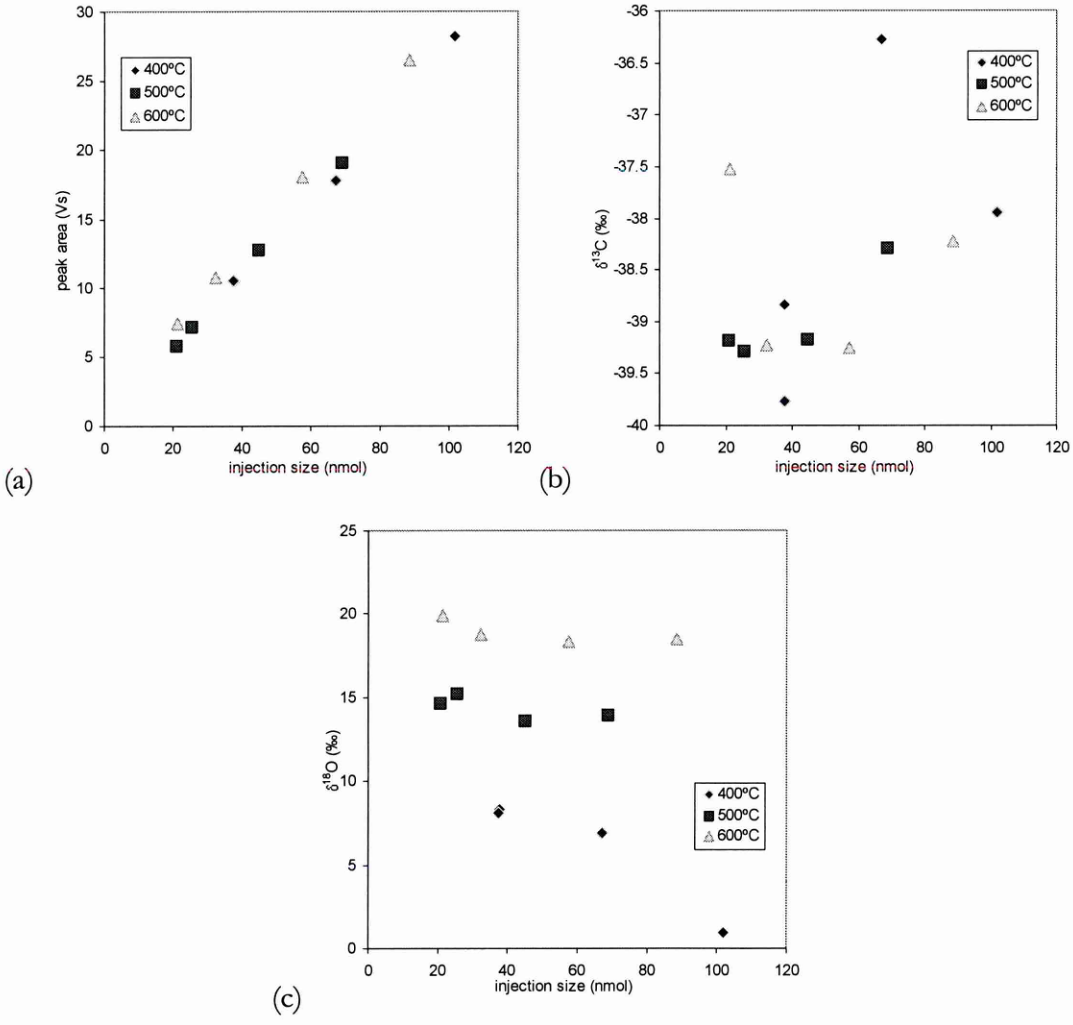

Figure 5.17 (a) peak sizes of CO_2 from CH_4 combustion on Rh_2O_3 (clean) at 400-600°C, (b) $\delta^{13}C$ values of combusted CH_4 with injection size, (c) $\delta^{18}O$ values of combusted CH_4 with injection size

Peak areas (Figure 5.17) gave an indication that combustion was complete at 500°C or higher. Carbon dioxide peak areas of 600°C combustions showed an offset (of about 1-2 Vs) of the line

derived from lower temperatures. This is likely to have been due to a blank from heating the Rh_2O_3 to 600°C, but the blank level at this temperature was not measured. Consistency of the measured carbon isotopes is not as high as other oxides tested. Only 500°C gave reproducible values, while at 600°C the spread in $\delta^{13}C$ was higher, supporting the evidence of a blank component. The spread in the values for all temperature ranges seemed to err in a heavier $\delta^{13}C$ direction compared to the median value. Oxygen isotopes show a dependence on combustion temperature. The low spread in $\delta^{18}O$ at each particular temperature even could identify a combustion temperature from a given $\delta^{18}O$ value. For each 100°C step increase, the $\delta^{18}O$ value increased by approx. 5‰. This temperature effect does correspond to that found by the CH_4 combustion on the previous Rh_2O_3 sample. This might be evidence for the possibility that ^{18}O ions are more labile at such temperatures than ^{16}O ions. A similar effect was seen with CO combustion with $CuCrO_x$ (5.2.4).

Table 5.12 Mean $\delta^{13}C$ and $\delta^{18}O$ for Rh_2O_3 (cleaner sample) CH_4 combustions between 100-400°C

Temperature (°C)	Mean $\delta^{13}C$ (‰)	± σ, (‰)	Mean $\delta^{18}O$ (‰)	± σ, (‰)
400	-38.2	1.5	+6.0	3.5
500	-39.0	0.5	+14.3	0.7
600	-38.6	0.8	+18.9	0.7

5.2.8. Cerium (IV) Oxide

Cerium (IV) oxide was heated in the presence of an O_2 flow of <10 ml/min and heated to 800°C. After leaving the oxide to degas under helium at 400°C its blank level was checked and found to be 1.9 Vs. This decreased to negligible amounts after leaving for over 12 hours. Carbon monoxide was injected, but no CO_2 was detected at 400°C, with flow rates at 40 ml/min. Combustion of CH_4 therefore also seemed unlikely, so the sample was removed

5.2.9. Palladium Oxide

The preliminary test of PdO (from sponge) within the irMS system used the same sample tube as used in the Ion Trap system. Combustions of CH_4 were attempted at 450 and 550°C, which was within the temperature range found to be successful on the ion trap system. Combustion was observed, but efficiency was at best only 30%. Carbon isotope values were comparable to those returned by NiO/Pt, even though the variability was high. The mean result was $\delta^{13}C = -39.0 \pm 1.8$ ‰. Flow rates were either 40 ml/min or 8 ml/min. Complete combustion of carbon monoxide was less efficient, with small peak areas measured at temperatures between 150°C and 400°C. Combustion efficiency was never greater than 25%.

Using the same PdO sample at higher flow rates (near 60 ml/min) resulted in highly efficient combustion of CH_4 at 450°C. The average result was $\delta^{13}C = -40.8 \pm 0.4$ ‰ (n=6). Consistency was also far greater than the combustions at lower flow rates reported in the previous paragraph. Under normal circumstances, one would expect that the combustion would be more efficient at lower flow rates.

After a new sample of PdO was created from Pd sponge, the same combustion properties were tested. Conversions to CO_2 on this sample had low efficiency, at flow rates from 5 to 20 ml/min and temperatures to 450°C. Using a sample of palladium oxide (as oxide, from Aldrich) also resulted in even lower combustion efficiency in the entire temperature range. Both carbon monoxide and methane never gave yields more than 15%. Flow rates used in this sample were between 10 and 1 ml/min. Using a flow rate this low required a cryogenic trapping time of up to 30 minutes, giving rise to a high blank component in the measured CO_2.

The use of the quartz tubes used in the ion trap tests (1 mm i.d.) was aborted as this was thought to be the cause of the non-uniformity within consecutive samples. A new sample of oxidised palladium sponge (5 mm i.d. tube) was created later in the study. Investigation of the ability to combust atmospheric CH_4 was also conducted and results can been seen in Chapter 6.

This sample was tested with pure CH_4 and CO and was generally successful (Figure 5.18), with helium flow rates between 40 and 60 ml/min.

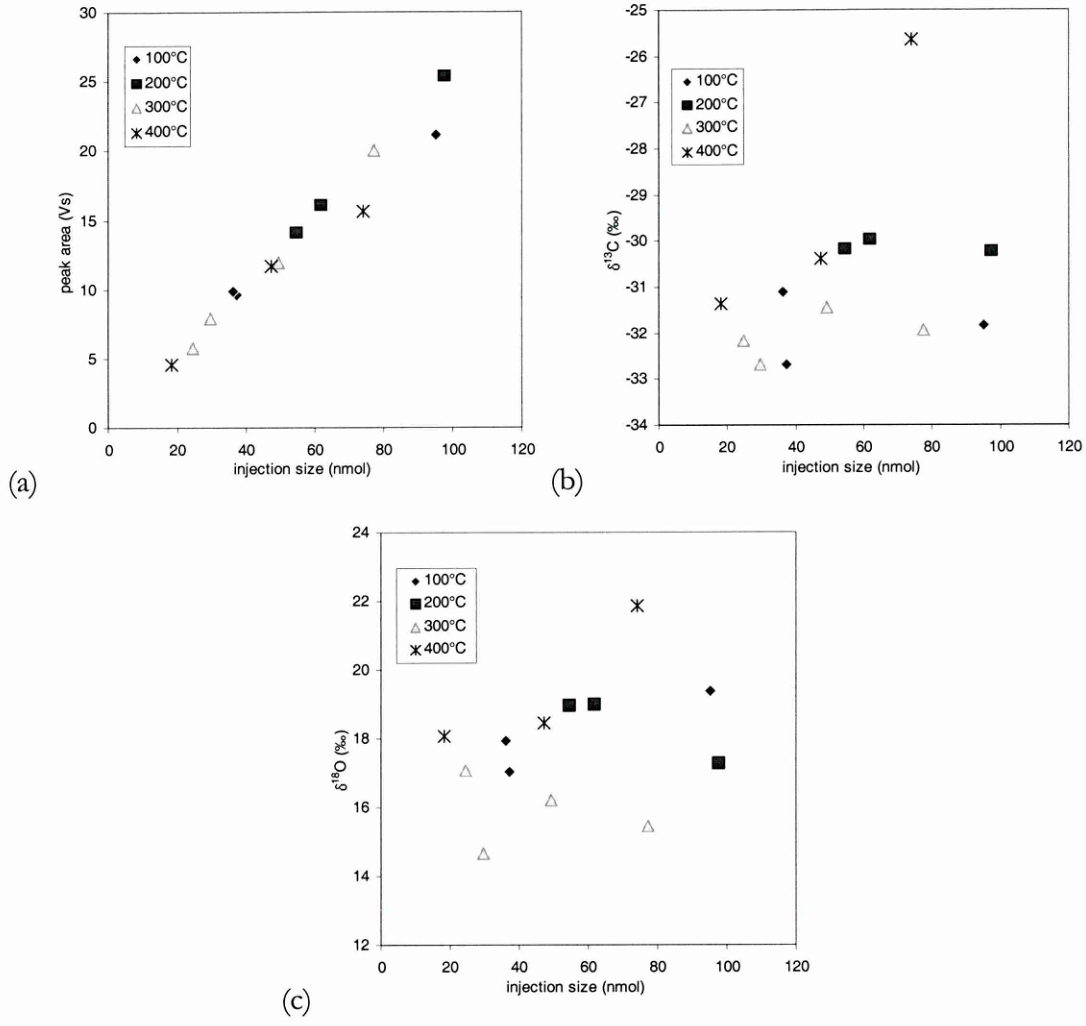

Figure 5.18 (a) peak sizes of CO_2 from CO combustion on PdO (sponge) at 100-400°C, (b) $\delta^{13}C$ values of combusted CO with injection size, (c) $\delta^{18}O$ values of combusted CO with injection size

Table 5.13 Mean $\delta^{13}C$ and $\delta^{18}O$ for the combustion of CO over PdO between 100-400°C

Temperature (°C)	Mean $\delta^{13}C$ (‰)	$\pm \sigma$, (‰)	Mean $\delta^{18}O$ (‰)	$\pm \sigma$, (‰)
100	-31.9	0.8	+18.1	1.2
200	-30.1	0.1	+18.4	1.0
300	-32.1	0.6	+15.8	1.0
400	-29.1	3.0	+19.4	2.0

From Figure 5.18 (b) showing CO combustion can be seen that values returned for the carbon isotope ratio were not as repeatable as other compounds such as $CuCrO_x$. Highest repeatability

was measured at 200°C ($\delta^{13}C$ = -30.1 ± 0.1 ‰), but this is 1‰ heavier from the expected value range (-31.5 ± 0.5 ‰). Carbon isotope ratios from combustions at 100°C and 300°C approached the expected range. Mean $\delta^{18}O$ values showed some variation with temperature (Figure 5.18 (c)). Each combustion temperature series gave a small range for its $\delta^{18}O$ results, (ignoring the spurious point at 400°C) but the ranges are not distinct.

Methane combustion on PdO also showed temperature dependence for carbon and oxygen isotope ratios (Figure 5.19 (b) and (c)). Mean $\delta^{13}C$ and $\delta^{18}O$ for the combustion series are shown in Table 5.14.

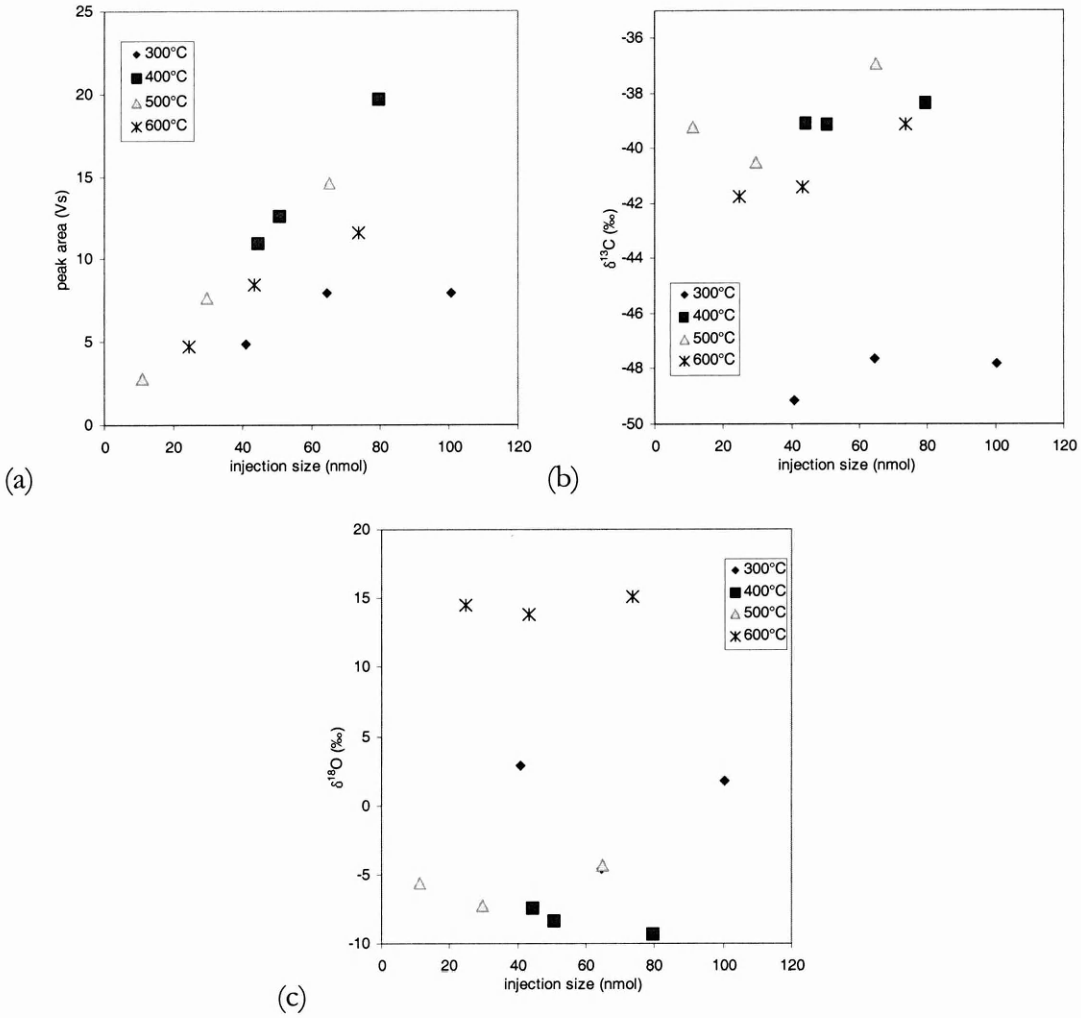

Figure 5.19 peak sizes of CO_2 from CH_4 combustion on PdO (sponge) at 300-600°C, (b) $\delta^{13}C$ values of combusted CH_4 with injection size, (c) $\delta^{18}O$ values of combusted CH_4 with injection size

Table 5.14 Mean $\delta^{13}C$ and $\delta^{18}O$ for the combustion of CH_4 over PdO between 300-600°C

Temperature (°C)	Mean $\delta^{13}C$ (‰)	± σ, (‰)	Mean $\delta^{18}O$ (‰)	± σ, (‰)
300	-48.2	0.8	0.0	4.0
400	-38.9	0.4	-8.4	0.9
500	-38.9	1.8	-5.7	1.5
600	-40.8	3.6	+14.5	0.7

At 300°C, methane was not completely combusted, while the same effect appeared unexpectedly at 600°C. This may have been due to a phase change within the oxide system, or that the oxide surface needed replenishing. Combustions at 400°C were seen to produce higher consistency than at 500°C, but very similar $\delta^{13}C$ mean (400°C: -38.9 ± 0.4 ‰; 500°C: -38.9 ± 1.8 ‰). Interestingly at 300°C CH_4 partial conversion favoured isotopically light carbon (-48‰). Oxygen isotopes of CO_2 from CH_4 also exhibited temperature dependence, with the 600°C partial combustion having higher (of the order of 15-20‰) $\delta^{18}O$ ratios than the complete combustions of 400 and 500°C, which show consistency between $\delta^{18}O$ values (–7 ± 2 ‰). This effect was also seen with both the Rh_2O_3 samples, possibly indicating increased ionic mobility for heavier ions in the lattice.

5.3. Summaries and Conclusions of Metal Oxide Isotope Ratio combustion testing

5.3.1. NiO/Pt

Initial tests at the flow rates of 40-55 ml/min showed complete CH_4 combustion required NiO/Pt temperatures of at least 1000°C. However, using a 10 ml/min flow rate required 800°C for perfect quantitative combustion, yet at 5 ml/min linearity appeared perfect at 700°C but instrumental problems put this into doubt. From the carbon isotope ratio data, the greatest consistency was observed at 1000°C with 5 ml/min - at lower temperatures, this flow rate gave results of greater irreproducibility. Using a flow rate of 10 ml/min appeared to give greater stability within different combustion temperatures, with very similar variability at 800 to 1000°C.

Mean oxygen isotope ratios showed different results according to the catalyst temperature. At 10 ml/min a small decrease of $\delta^{18}O$ with combustion temperature, was observed. At 5 ml/min there is no variation with temperature at 700-900°C, but at 1000°C $\delta^{18}O$ is 7‰ heavier.

Carbon monoxide conversion was found to be complete at temperatures in excess of 500°C at 30 ml/min. Carbon isotope ratios showed the highest precision at 600°C. Oxygen isotope values gave a linear correlation with CO injection size, at all temperatures tested. Increasing the injection size results in heavier $\delta^{18}O$ eluting.

Oxygen isotope exchange reactions were also present. Passing CO_2 over the catalyst provided insight into the amount of oxygen exchange occurring over the catalyst. At cold temperatures CO_2 was able to lose or swap with oxygen from the lattice, perhaps through a surface carbonate once adsorbed onto the NiO/Pt surface. At 800°C this process was less active. Carbon isotope ratios were shifted away from the expected value (measured bypassing the reactor path) by over +1.0‰ when the reactor was hot or cold. Oxygen isotope ratios indicated exchange with oxide ions on the NiO/Pt system *only* when the catalyst was at room temperature. Values for $\delta^{18}O$ were similar for the bypass set as for the NiO/Pt system held at 800°C, implying no exchange was taking place at this temperature.

5.3.2. $FeNiO_x$, $AgMnO_4$, Co_2O_3, and CeO_2

These oxides showed no useful combustion affinity when tested.

5.3.3. Copper-Chromium Oxide

Carbon monoxide combustions were investigated on $CuCrO_x$ at temperatures up to 200°C, with a 20 ml/min carrier gas flow. Complete combustion was seen at 200°C, but 100°C also showed high combustion, while at room temperature activity was low. Carbon isotope ratios showed very high consistency at 100 and 200°C., of which the lower temperature produced the best consistency, $\delta^{13}C = -30.9 \pm 0.08$ ‰, while the 200°C set produced $\delta^{13}C = -30.9 \pm 0.2$ ‰.

Oxygen isotope ratios for complete combustions were invariant with injection size, but a small temperature effect producing 0.5‰ lower $\delta^{18}O$ values were seen when the temperature increased to 200°C. No CH_4 injections were attempted

5.3.4. Cobalt-Chromium Oxide

Combustion of CO on $CoCrO_x$ was seen to be 100% at 200°C and above, with a helium flow rate of 30 ml/min. Carbon isotope ratio values were not as consistent as those for $CuCrO_x$. The lowest spread was observed at 300 and 400°C, and a temperature dependence of the $\delta^{13}C$ value was seen. Lower temperatures resulted in carbon isotopes being heavier by about 1‰. Oxygen isotopes showed dependence on sample size (slightly lighter with more gas) but large differences with temperature. Values for $\delta^{18}O$ at 400°C were 9‰ lighter than $\delta^{18}O$ from combustions at lower temperatures. No CH_4 injections were attempted

5.3.5. Rhodium Oxide

Two samples of Rh_2O_3 were tested. The first (possibly contaminated) was used for carbon monoxide conversion tests and complete combustion was found to occur at 200°C or above at a helium flow rate of 30 or 60 ml/min (depending on temperature). Carbon isotope ratios from CO conversion were highly repeatable at 200°C. Oxygen isotope ratios showed variation with temperature, with increasing temperature giving lower $\delta^{18}O$ values. The second series in the experiment concentrated on higher temperatures for CO combustion at 25-35 ml/min. Between 400 and 600°C the most consistent carbon isotope ratio was given by 500°C. Oxygen isotopes were constantly within a 4‰ window. Methane injections on this sample were also tested. Complete combustion for CH_4 was found to occur at 500°C. Consistency of $\delta^{13}C$ values was not as high as expected, with high σ values at all temperatures. Oxygen isotopes showed interesting results with discrete ranges for each temperature, showing different magnitudes of fractionation in the combustion process.

Both the CO and CH_4 tests were repeated with a second sample prepared from rhodium hydroxide. 300°C was necessary for the highest consistent results of CO combustion. Methane results showed greater consistency than the contaminated sample, but not as great as CO oxidation on either Rh_2O_3 sample. As with the first sample, setting the Rh_2O_3 at 500°C resulted in the lowest variability for measurement of $\delta^{13}C$ from CH_4 combustion. Oxygen isotope ratios also exhibited the same temperature dependence as the first sample.

5.3.6. Palladium Oxide

A variety of samples were tested from different sources, but the best results were seen from a large sized sample tube containing oxidised Pd sponge. Carbon monoxide combustion was tested and required 200°C or higher for complete combustion. Carbon isotope ratio consistency was not as high as other oxides, as there seemed to be a combustion temperature influence on $\delta^{13}C$ results. A 2‰ difference was observed in the mean values of $\delta^{13}C$ from 200 and 300°C. Oxygen isotope ratio showed variation with temperature but with no obvious pattern. Methane combustion was also tested in the 300-600°C temperature range. Quantitative combustion was seen to occur at 400 and 500°C only. Repeatability at 400°C was higher than at 500°C. Oxygen isotope ratios were also invariant for temperatures that provided complete combustion. Incomplete combustion resulted in fractionation to produce CO_2 with higher $\delta^{18}O$ values, compared to complete combustion.

5.3.7. Numerical summary

Table 5.15 Mean $\delta^{13}C$ and $\delta^{18}O$ values from CO and CH_4 conversions on various oxides at various temperatures. Oxides with poor combustion ability were omitted. Expected values of $\delta^{13}C$ for CH_4 was -40.7 ± 1.0 ‰ and for CO was -31.2 ± 1.0 ‰.

Oxide	Temperature (°C)	Flow rate (ml/min)	CH_4		CO	
			$\delta^{13}C$ mean (1σ)	$\delta^{18}O$ mean (1σ)	$\delta^{13}C$ mean (1σ)	$\delta^{18}O$ mean (1σ)
NiO/Pt	700	10	-40.9 ± 0.6	+21.0 ± 8.2		
	800	10	-40.7 ± 0.3	+22.7 ± 1.6		
	900	10	-40.9 ± 0.4	+17.8 ± 1.9		
	1000	10	-40.7 ± 0.3	+20.0 ± 1.0		
NiO/Pt	700	5	-41.0 ± 0.2	+12.3 ± 1.2		
	800	5	-40.7 ± 0.6	+13.0 ± 0.9		
	900	5	-40.6 ± 0.5	+12.1 ± 0.7		
	1000	5	-40.8 ± 0.1	+17.9 ± 1.7		
NiO/Pt	400	21			-35.1 ± 3.2	+21.4 ± 2.2
	500	30			-31.6 ± 0.5	+19.2 ± 3.0
	600	30			-31.4 ± 0.2	+19.3 ± 0.3
$CuCrO_x$	100	26			-31.0 ± 0.1	+16.1 ± 0.3
	200	20			-30.9 ± 0.2	+15.6 ± 0.2
$CoCrO_x$	100	45			-30.9 ± 0.4	+21.5 ± 0.8
	200	45			-31.3 ± 0.6	+22.8 ± 0.6
	300	33			-31.6 ± 0.2	+20.8 ± 0.7
	400	30			-31.7 ± 0.3	+14.4 ± 0.4
Rh_2O_3 (1)	100	62			-27.8 ± 2.8	+29.6 ± 4.0
	200	62			-31.5 ± 0.1	+22.0 ± 1.9
	300	33			-31.6 ± 1.5	+19.1 ± 0.6
	400	35			-31.9 ± 1.7	+18.0 ± 1.0
	500	35			-31.2 ± 0 (n=2)	+17.2 ± 0.5
	600	35			-31.1 ± 0.6	+15.5 ± 0.4
Rh_2O_3 (1)	400	24	-38.7 ± 2.6	+7.4 ± 0.4		
	500	25	-38.3 ± 0.7	+5.6 ± 0.8		
	600	25 & 35	-38.5 ± 0.9	+14.1 ± 0.9		
Rh_2O_3 (2)	100	50			-36.2 ± 1.0	+14.9 ± 1.2
	200	40			-31.6 ± 1.0	+16.8 ± 0.9
	300	40			-30.9 ± 0.5	+16.3 ± 0.9
	400	42			-31.3 ± 0.8	+17.4 ± 1.1
Rh_2O_3 (2)	400	45	-38.2 ± 1.5	+6.0 ± 3.5		
	500	45	-39.0 ± 0.5	+14.3 ± 0.7		
	600	45	-38.6 ± 0.8	+18.9 ± 0.7		
PdO (large)	100	40			-31.9 ± 0.8	+18.1 ± 1.2
	200	40			-30.1 ± 0.1	+18.4 ± 1.0

			CH_4		CO	
	300	40			-32.1 ± 0.6	+15.8 ± 1.0
	400	60			-29.1 ± 3.0	+19.4 ± 2.0
PdO (large)	300	40	-48.2 ± 0.8	0.0 ± 4.0		
	400	43	-38.9 ± 0.4	-8.4 ± 0.9		
	500	40	-38.9 ± 1.8	-5.7 ± 1.5		
	600	40	-40.8 ± 3.6	+14.5 ± 0.7		

5.4. Discussion

Table 5.1 lists the means of all the repeated injections of CO and CH_4. The purpose of this investigation was to be able to propose a suitable catalyst for oxidation of carbonaceous compounds within the MODULUS system. For the recommendation of the most useful in-line oxidation catalyst one has to assess the needs of the catalyst's role in the MODULUS system. In the simplest sense, the isotope requirement is such that the total system precision has to be limited by the mass spectrometer, not the chemistry. Currently the developed ion trap has a precision of between ±5 and ±10‰ for $\delta^{13}C$. In such an arrangement, any metal oxide at a set combustion temperature with associated variability less than that of the ion trap can be used. Matching the lowest temperature and the highest consistency should find the best reagent.

Methane

Results from the combustion of methane showed that Rh_2O_3 at 500°C, PdO at 400°C gave consistency high enough for this application. Using nickel oxide at 700°C would also achieve this level of repeatability, but complete combustion needed higher temperature than Rh or Pd oxides. A summary of the combustion data can be shown in Figure 5.20.

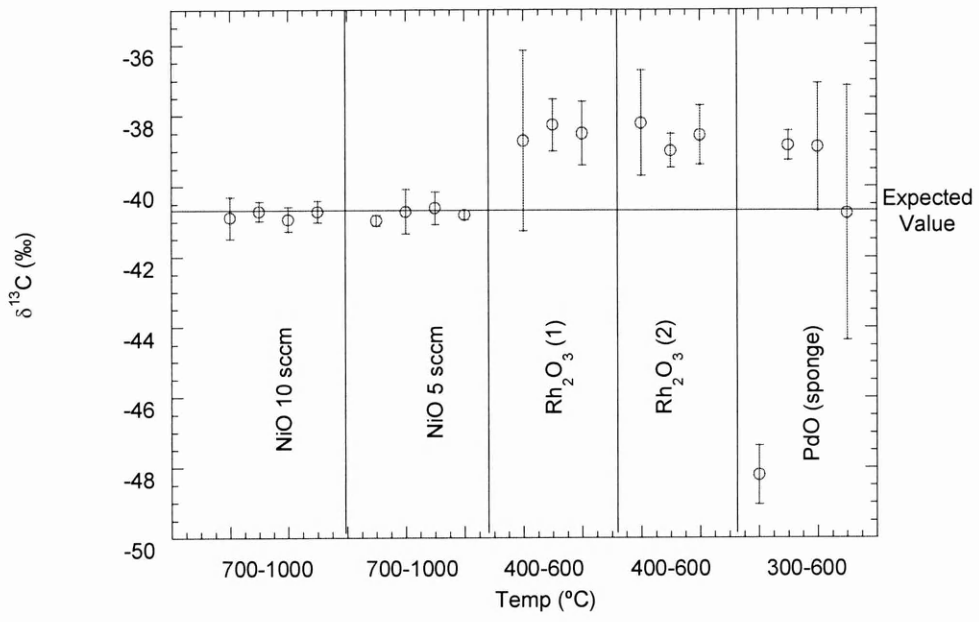

Figure 5.20 Mean $\delta^{13}C$ values of CO_2 from CH_4 combustion by various metal oxide catalysts at various temperature ranges

There is a notable difference between the $\delta^{13}C$ values returned by the NiO/Pt catalyst and that returned by the Rh and Pd Oxides of about 1.8‰. This is not thought to be due to the blank amount as this was found to be minimal. A fractionation process must be occurring on the Rh_2O_3 to cause this shift, assuming that the NiO/Pt (as the standard method) causes no fractionation. Apart from the incomplete combustion of CH_4 on PdO at 300°C, most deviation and hence fractionation, tends toward heavier carbon isotope values. The only viable temperature of the PdO tests (400°C) also shows the same (heavy) carbon isotope ratio. Another possibility for the difference is a change in the $\delta^{13}C$ of the CH_4 while in storage. An examination of the dates of the analyses suggests this is unlikely. It cannot be discounted that the fractionation effect seen may be due to the variation in flow rates between samples, although sample size, particle size & granularity also would have influence.

The difference in $\delta^{13}C$ rules out the use of these samples of Rh_2O_3 and PdO for high precision isotope ratio CH_4 analysis in terrestrial situations (for example $\delta^{13}C$ of atmospheric CH_4)

although both oxides are considered suitable for the specialised oxidations that MODULUS will perform. Within the mass spectrometer's precision the operating temperature can be lowered from 1150°C to 500°C (Rh) or 400°C (Pd).

Carbon Monoxide

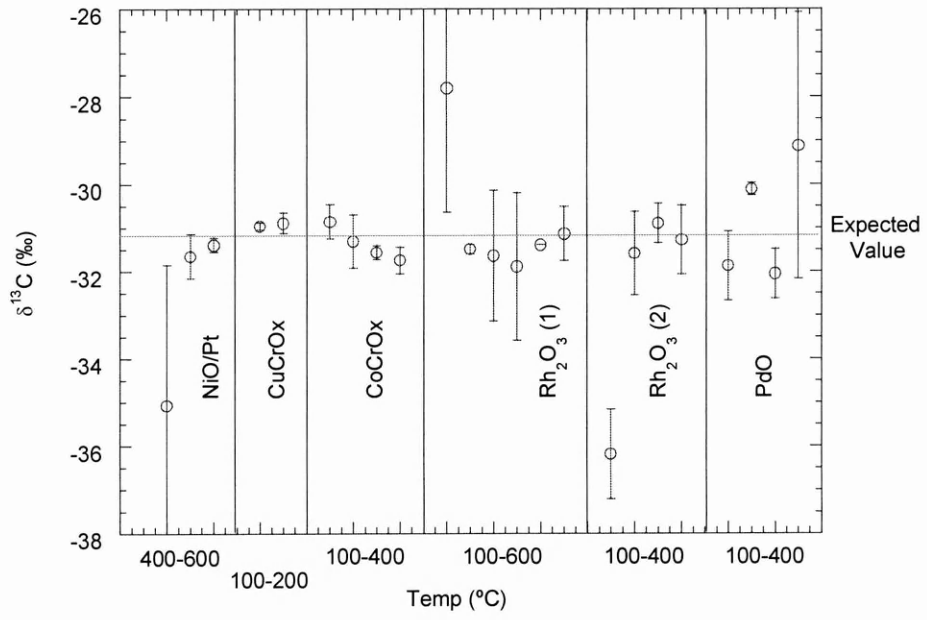

Figure 5.21 Mean $\delta^{13}C$ values of CO_2 from CO combustion by various metal oxide catalysts at various temperature ranges

The oxidised nickel/platinum wire was tested first, but this compound is not used as a standard method isotope ratio analysis of CO. For atmospheric trace CO analysis, combustion is performed by I_2O_5 (Brenninkmeijer, 1993). This compound is used as it does not exchange oxygen with CO, rather it adds oxygen of known $\delta^{18}O$ to form CO_2. This compound was not tested as its extreme oxidative properties make it unusable on MODULUS. Examination of Figure 5.21 shows variation in $\delta^{13}C$ from all the oxides. Cobalt-Chromium oxide displays its temperature dependence, which could possibly lead to mis-interpretation. This effect is also seen with PdO showing a 2‰ difference between 200 and 300°C $\delta^{13}C$ values (recall combustion

was incomplete at 100 and 400°C). High consistency is seen with $CuCrO_x$ at 100-200°C, Rh_2O_3 (1) at 200°C and (2) at 300°C, whereas using the NiO/Pt system would need 300°C higher for similar repeatability. At the time of analysis, no available system (within our department) was able to analyse the bottled CO to find the $\delta^{13}C$ and $\delta^{18}O$ without combustion.

For both CH_4 and CO combustion, MODULUS can use these low-temperature catalysts with no significant loss of science data returned. More of the successful oxides tested on the ITD system require testing on the ir-MS system. For a detailed investigation of the MODULUS system, a gas mixture needs to be created such that an entire collection of expected volatile species are transmitted at once through a GC column, then subjected to a combustion unit. Only in this configuration will it be obvious that the combustion unit will function as expected. This procedure should be attempted once a working model of MODULUS is constructed.

5.4.1. Entire recommendations to MODULUS

The column tests in Chapter 3 discovered that the J&W Scientific CarboPLOT column has the greatest separation ability for the carbon analysis channel on MODULUS. Oxidation tests in Chapter 4 showed that the most active oxidants as Rh_2O_3, PdO, $CuCrO_x$, and $CoCuO_x$. The isotopic integrity tests in this Chapter showed that $CuCrO_x$ has the best compromise of isotopic integrity versus operating temperature for CO oxidation. Similarly for CH_4 oxidation the best compromise was found in Rh_2O_3.

6. FAST MEASUREMENT OF CARBON ISOTOPE RATIOS OF ATMOSPHERIC METHANE WITHOUT CHROMATOGRAPHIC SEPARATION

The Rosetta mission will be launched in 2003. There will be no science data from the MODULUS system until the lander unit arrives on Wirtanen's nucleus, in 2011. Thus, the work of the previous chapters will have no applicable science result until that date. As a practical test for the work performed in Chapters 4 and 5, the results could be applied to a different application, with no such delay in result return. The new project chosen was the carbon isotope ratio analysis of atmospheric methane, for a variety of reasons:

- knowledge of the application within the PSRI
- combustion of CH_4 already performed in Chapters 4 & 5
- the availability of wetland air samples through PSRI contacts
- only minor modifications needed for adaptation of available instrumentation.

Therefore, the most active catalysts discovered for methane oxidation in the previous chapter were tested to replace the standard high-temperature catalyst. During the modifications for the system, other developments lead to a new analysis method.

6.1. Introduction

The rising concentration of atmospheric methane (IPCC, 1994) has caused concern in recent years. Atmospheric methane absorbs infrared radiation around 7.7μm, and as such has a significant effect on the energy balance of the Earth. Flux measurements have been used to constrain its sources and sinks. $\delta^{13}C$ and D/H measurements of the sources have also been used to examine the contribution of biogenic or non-biogenic processes in the formation of methane (e.g. Lowe et al., 1994). The analysis of $\delta^{13}C$ of ppm levels of a trace component of the atmosphere requires separation, combustion and occasionally pre-concentration (Merritt et al.,

1995b). This chapter summarises attempts to simplify the analysis of CH_4 by removing the need to isolate CH_4 via capillary chromatography, thus reducing the time period for sample analysis. The system developed was then applied to the measurements of $\delta^{13}C$ of samples of headspace air collected from peat cores containing methanogenic and methanotrophic bacteria, in order to investigate sulphate reduction by the bacteria.

6.1.1. Methane as a greenhouse gas

Human actions have contributed significantly to a change in atmospheric composition of trace gas species, ever since the widespread burning of fossil fuels. The atmospheric species with the most contribution to radiative forcing[10] are CO_2 and H_2O, while other species contribute to a lesser degree (CH_4, and N_2O). Infrared radiation emitted by the Earth's surface, can be reabsorbed by certain chemical species present in the atmosphere, causing re-distribution of energy otherwise destined for space. The net energy gain by the Earth system, relative to simple re-radiation to space, accounts for a 33°C rise in the average global temperature, assuming the earth to be a black body (IPCC, 1994). The naturally occurring chemical species responsible for the energy redistribution are termed *greenhouse* gases, whereas the contribution of trace gas of anthropogenic origin is termed the enhanced greenhouse effect.

Methane is estimated to contribute about 15% of the enhanced greenhouse effect although its atmospheric concentration is orders of magnitude lower than CO_2 (Hein et al., 1997). The current nominal concentration of CO_2 is near 350 ppm, while CH_4 is 1.7 ppm (IPCC, 1994). Both species are known to have increased in concentration due to human activity. Air bubbles trapped in ice cores record the atmosphere of past years, and can be extracted and analysed. The concentration of methane is known to have doubled in the past 300 years; in 1700 A.D. it is determined to be near 700 ppb. Pre-industrial concentration of CO_2 was 280 ppm.

[10]Radiative forcing is the change in net radiation at the tropopause caused by a change in solar or Earth's emitted infrared radiation.

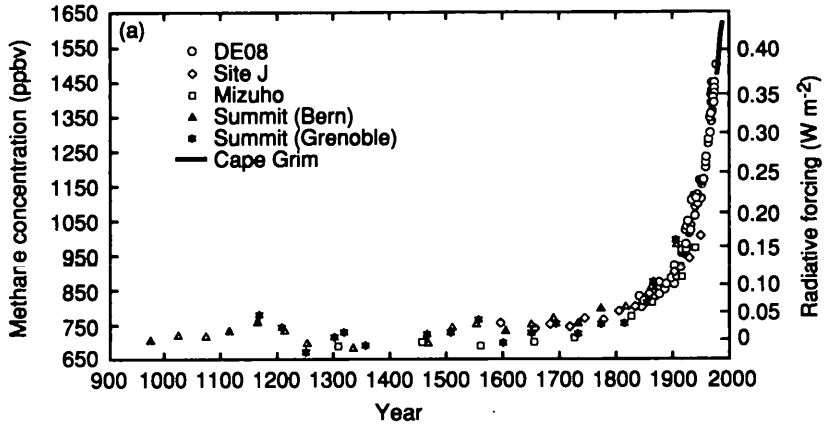

Figure 6.1 Concentration of atmospheric CH_4 over the past 1000 years from ice core/firn data and actual atmospheric monitoring (IPCC, 1994) and modern day analyses at Cape Grim, Tasmania

Various sources have been identified as major CH_4 emitters. Methanogenesis can occur in numerous biological systems, including those that follow the C_1 metabolic cycle, where CO_2 is converted to CH_4 through the action of various enzymes. Natural sources of CH_4 include wetlands (e.g. peat bogs), termite colonies and methane hydrates. Anthropogenic related sources include bacterial emissions from rice paddies, cattle and sheep, landfills and sewage. Utilisation of fossil carbon sources (natural gas and coal mines) are estimated to account for 20% of total emissions, while 70% of the total emissions result from human activity (IPCC, 1994).

The main sink of atmospheric CH_4 is the reaction with tropospheric hydroxyl radical (OH). Another of the sinks is the uptake by soil bacteria in upper soils, consuming the CH_4 from both the atmosphere and from generation in deeper soils (e.g. Waldron et al., 1999). Various models have been created to find the total source and sink flux influence on future trends of CH_4 emission.

6.1.2. Sulphate Reduction by bacteria

Certain strains of anaerobic bacteria play an important role in the sulphur cycle, as they gain energy from oxidising organic matter whilst reducing sulphur to H_2S. By using the example of acetate one may write the following; $SO_4^{2-} + 2CH_2O \rightarrow H_2S + 2HCO_3^-$ (Berner, 1985). This

equation should be regarded as an indicator of the carbon and sulphate pathway – this has not been demonstrated with methane to date.

Methanogenic bacteria can also co-exist in the same sediment or soil as the sulphate reducing bacteria, but sulphate reducing bacteria are dominant over methanogens until the supply of sulphates is consumed. Both bacteria groups can use the same organic substrate for their metabolism; one substrate is known to be acetate. [Acetate fermentation and CO_2 reduction are other ways that certain bacteria can produce methane] It is currently not known whether any CH_4 produced by methanogens is directly oxidised by the sulphate reducers, as in the equation above. Is it known, however that other bacterial groups can also oxidise CH_4 also within the same setting (Waldron et al., 1999).

6.1.3. Isotopes of CH_4 from different sources

As already stated, the determination of the $\delta^{13}C$ and δD of CH_4 has been used to understand the role of the sources and sinks within the methane cycle. By measuring samples of air, the increase from the ambient methane concentration and isotopic signature can be combined to estimate the flux of methane from a particular source. The $\delta^{13}C$ or D/H of the methane can then be compared to other sources, which can be combined to create a budget that is balanced isotopically. Models using isotope data may contain greater detail when compared to models that only use flux data. Different sources can give a range of $\delta^{13}C$ that can be distinct from other sources. This implies that samples of air can be analysed blind, and the $\delta^{13}C$ value can identify the origin of the air in certain circumstances.

Background atmospheric methane has been measured in various laboratories and is accepted to have $\delta^{13}C_{PDB} = -47.0 \pm 0.3‰$ (Stevens and Rust, 1982) but this value varies spatially, seasonally, and temporally. The variation in $\delta^{13}C$ with different sources can be demonstrated with Figure 6.2. Methane analysed as such has been found to range on the $\delta^{13}C_{PDB}$ scale from –80‰ to -40‰. The difference in the isotopes can be attributed to alternative formation pathways,

different source materials, and different physical processes occurring prior to the release to the atmosphere.

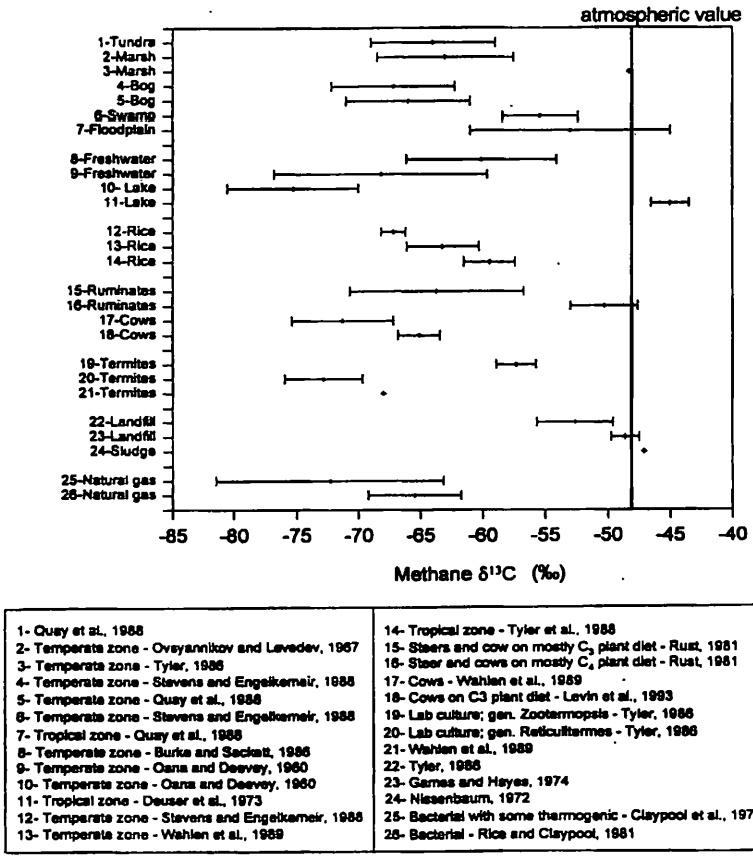

Figure 6.2 Extent of $\delta^{13}C$ variation for various bacterial sources of CH_4. 1σ dispersion is shown (Conny and Currie, 1996)

To constrain the atmospheric methane budget and to forecast future emissions, one needs data on flux and isotope ratio. Such data can be collected by the various laboratory methods to measure properties of atmospheric CH_4.

6.2. Methods for the analysis of atmospheric methane

6.2.1. Concentration measurements

The most common method for the measurement of the abundance of atmospheric CH_4 is via a GC-FID system. The atmospheric sample is separated into components via a GC column, and the FID quantifies the amount of each component present. The GC column used must be suited to the separation of volatiles; a packed column with a stationary phase such as PoraPLOT

Q is often used. Unless external drying agents are employed, the column must be able to survive the presence of water vapour within the sample. Temperature programming may also be necessary for the peak profile required by the detector. Such an analysis can be performed on 20 ml of air (at 1 bar), leading to a precision of ± 0.3 ppm on a system employed in the PSRI.

6.2.2. Techniques employed for the analysis of the isotopic composition of low concentrations of methane

The determination of the carbon and hydrogen isotope ratios of atmospheric methane has been more difficult to measure. Until recently high precision measurements involved large amounts of ambient air (1-50 l) with chemical separation of CH_4 and combustion off-line (Stevens and Rust, 1982).

One of the first analytical methods for carbon isotope analysis of CH_4 was developed by. Zeng et al., (1994). Samples of biomass burning effluent were expanded into a vacuum system, then transferred to a GC column (PoraPLOT Q) via a 6-way sampling valve. A combustion section (270 mm, 1 mm i.d. tube, with CuO particles at 750-800°C) was placed downstream of the column with a cryogenic (-100°C) trap to remove water from combustion. The combustion unit was tested with pure CH_4 and at 750°C was only 50% efficient. Increasing the temperature of CuO to 800°C resulted in 90% conversion. The limitation of the method was low sensitivity - 80 nanomoles (equivalent to 2.5 l of ambient air) were required, giving an precision of $\delta^{13}C$ of 0.5‰. No real air samples were measured.

The technique developed by Merritt et al. (1995b) uses a GC coupled to a dual inlet mass spectrometer with a combustion unit between the GC and the MS. 5 ml samples of air could be analysed in 15 minutes, returning a precision of ±0.2‰ of $\delta^{13}C$ in CH_4. This method uses a combination of two columns, a combustion reactor, a water separator and an open-split interface.

A pre-concentration column separates atmospheric components - N_2, O_2 and Ar from CH_4 and CO_2. The preparative column is cooled to -118°C to trap CH_4 and CO_2. These species are swept to the analytical column after warming. The first 1 m of this column is also cooled with liquid N_2 to -118°C and warmed after 4 minutes. The preparative column adsorbent was Hayesep D, and the analytical column was Porapak Q. A combustion reactor with NiO/Pt (for CH_4 to CO_2 conversion) is followed by a water separator and an open-split interface for CO_2 transmission to the ion source.

PreCon

A commercial interface known as the PreCon has been developed by Finnigan MAT for the analysis of CH_4 by dual inlet and continuous flow mass spectrometers. This unit is able to switch between two modes, one can analyse $\delta^{15}N$ of N_2O in air, while the other carries out $\delta^{13}C$ on CH_4 in air (Brand, 1994). For ambient concentrations of CH_4 the unit requires a 100 ml sample of air (see Figure 6.3). No vacuum system is present, the sample air is collected in a flow-through vessel which is flushed using helium. A helium backflush purges any ingressing contaminant air from the vessel installation. A trap containing NaOH and $Mg(ClO_4)_2$ removes CO_2 and water. A liquid nitrogen trap condenses any non-volatile species present. The remaining compounds (N_2, O_2, CO, CH_4, Ar) are flushed toward a micro combustion reactor. This reactor (NiO at 1000°C) combust both CO and CH_4 to CO_2 and water. The CO_2 is then trapped under liquid N_2 on a loop as part of a 6- port Valco valve. On warming, the CO_2 is transferred to a second sample loop, consistent with injection onto a PoraPLOT Q (25 m, 0.32 mm i.d.) capillary GC column for separation of CO_2 and N_2O generated from the oxidation of atmospheric N_2. The column elutes into a standard post column interface involving a water separator and an open-split.

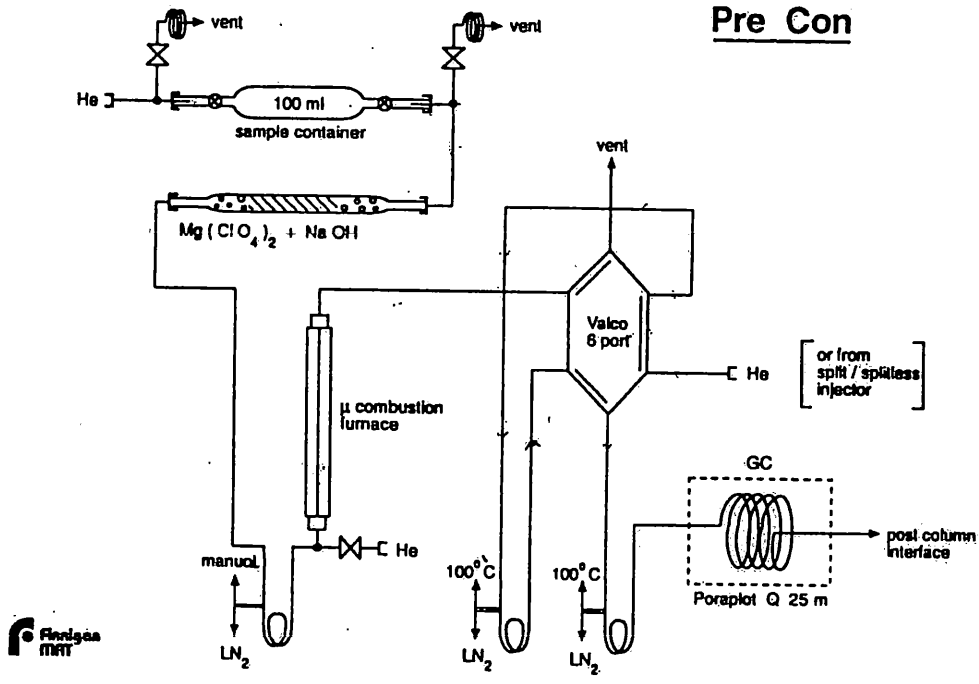

Figure 6.3 Schematic diagram of Finnigan MAT's PreCon system

GC/GC/C/irMS

Sugimoto et al. (1996) have recently developed an alternative method for the measurement of isotope ratio of CH_4 in air, and named the method GC/GC/C/irMS (Figure 6.4). The advantages over the Merritt et al. (1995b) system is that the chromatographic column at -118°C is avoided. The replacement uses two chromatographic columns for gas separation. A 92 ml air sample returned $\delta^{13}C$ values with a standard deviation of ±0.4‰. Concentration required for this precision was higher than ambient atmospheric, being 11ppm CH_4. No measurements were performed on air with ambient CH_4 concentration.

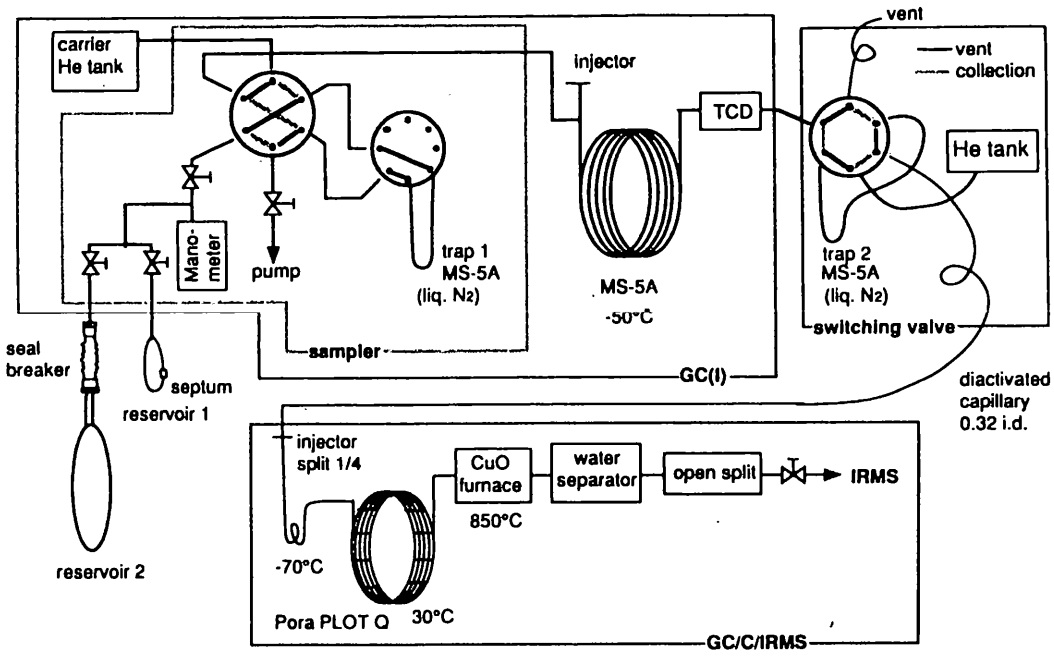

Figure 6.4 Schematic diagram of Sugimoto's GC/GC/C/irMS methane analysis system (Sugimoto, 1996)

The system requires the air sample to be trapped onto a sample loop filled with molecular sieve 5A held at liquid N_2 temperature. The sample is then passed through a 5A packed column. Cryogenic re-trapping then occurs after venting of atmospheric N_2, O_2, and CO_2. The remaining gases then passes through the PoraPLOT Q column and a CuO combustion section. Water is then removed and the CO_2 enters the mass spectrometer. The total time taken for analysis is 28 minutes. The gas sampler (region bounded in Figure 6.4) has an upper limit of 50 ml per injection, and hence any greater volume must be split, with the CH_4 trapped on the Molsieve between injections. Work done in our department finds the use of Molseive 5A questionable for ambient CH_4 trapping; only 30% or so of the CH_4 sample is trapped (Butterworth, 1999). This may be the cause of the limitation of the sample concentration in this system. Sugimoto et al. (1996) concluded that this system was unusable for samples of ambient concentration.

Combined isotope ratio analysis

The very low relative abundance of deuterium (D/H of SMOW = 6450) inevitably means measuring the ratio of D/H of CH_4 is more involved and difficult. For mass spectrometric

analysis the CH_4 is usually combusted to CO_2 and H_2O; the H_2O is subsequently reduced to H_2 using a Zn catalyst, and the H_2 is then analysed by the MS. An alternative method has been devised within the PSRI where methane itself is used as the analyte (Butterworth, 1997). The methane is separated via a GC system and trapped onto a molecular sieve, before being admitted to the inlet of a static mass spectrometer (MIRANDA). This instrument measures methane directly, comparing the m/z 17/16 ratio of CH_4. A new scale is produced ($\delta^{17}M$) which combines both the isotopic ratios of $^{13}C/^{12}C$ and D/H. On this reference scale many sources can still be distinguished. This technique can achieve precision of ±0.5‰, from a sample size of 300 picomole of CH_4 (≡ 10 ml of air). In addition, the D/H ratio can be measured indirectly by measuring the same sample for $\delta^{13}C$, thus giving D/H thereby allowing correction of $\delta^{17}M$.

Spectroscopic methods

Mass spectrometry is not the only method of analysis of atmospheric CH_4. Modern high-resolution spectroscopy can also be used to determine $\delta^{13}C$ and δD. Pairs of infrared absorption lines are measured using a tuneable diode laser as the light source. Currently the limiting factor is the concentration of CH_4 in air. $\delta^{13}C$ precision of ±0.4‰ (s.d) is seen from 50 ppm samples and δD precision of ±5.1‰ in samples of 2000 ppm (Bergamaschi et al., 1994). The advantages of this method are its portability, very little sample preparation is required, and the fact it is non-destructive.

Mass Spectrometry issues

The analysis time of the mass spectrometric methods is dependent on the flow through one or more cold gas chromatographic columns. Long analysis times lead to a limit in the amount of samples a laboratory can analyse per day. The separation, or removal, of atmospheric N_2, O_2, H_2O, CO, CO_2 and N_2O from CH_4, can be performed non-chromatographically, thus leading to a decrease in the total analysis time, leading to greater numbers of analyses per day. Production

of species that are isobaric to the combusted methane can be created by the combustion process. The creation of these species must be minimised or errors in isotopic composition can occur. Production can be minimised by the use of certain chemical techniques.

6.3. Development of a system for the analysis of $\delta^{13}C$ of methane: modifications to Delta C mass spectrometer inlet system used for catalyst investigations

The inlet system created for isotope studies on catalysts was the starting point for transformation into a system able to handle complex gas mixtures. Inevitably, the modifications to the existing combustion section did not yield results on the first attempt. Rather several modifications were necessary. These modifications were performed in parallel to catalyst investigation on the ITD system. Many issues had to be addressed, namely the transfer method for a large quantity of gas sample, making the sample reach the detector, removing contaminants from the sample, and perfecting the combustion unit. Using the concept of the commercial PreCon mass spectrometer inlet system, a system was developed for the analysis of $\delta^{13}C$ of CH_4 in air.

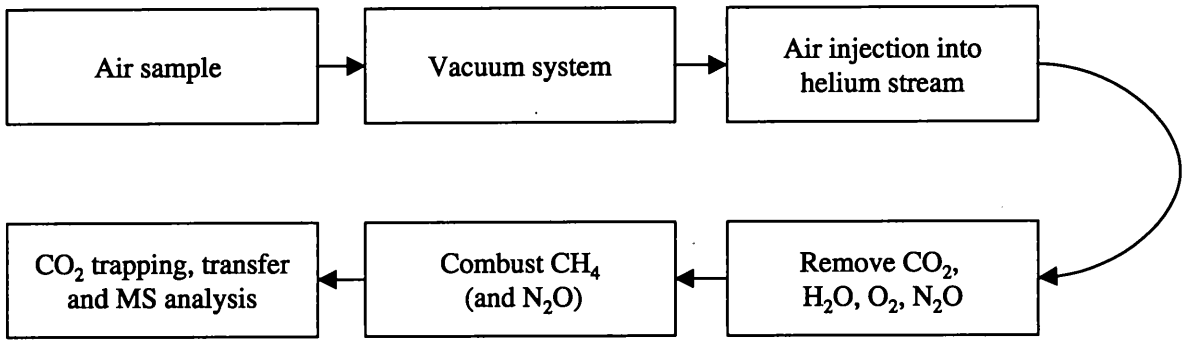

Figure 6.5 Flow chart showing protocol for the analysis of air samples. Each stage required development or adaptation of existing methods for successful analysis.

Firstly, the amount of analyte must be matched to the size range that the Delta C was able to analyse well. Then the undesired gases must be removed, trapped or diverted from the analyte. Finally, the analyte gas must be converted into a form suitable for analysis. The next sections catalogue the route taken to optimise the components.

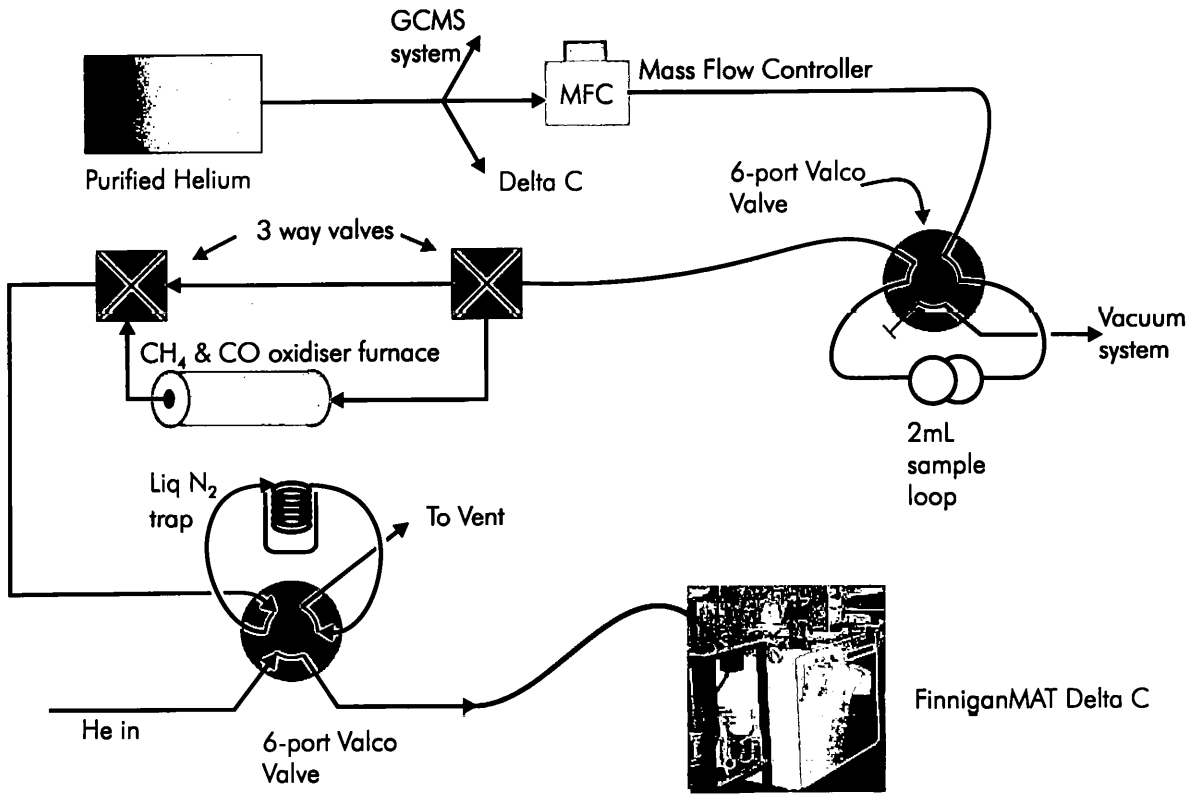

Figure 6.6 Schematic diagram of the system used to test the catalysts in Chapter 5. This system was the starting point for adaptation for use in atmospheric methane analysis

6.3.1. Optimisation of the sample loop

The primary aim of this study was to develop a system capable of determining the $\delta^{13}C$ of methane at ambient mixing ratios with sufficient precision to be meaningful. The sensitivity of the isotope ratio mass spectrometer available for the study determines the quantity of CH_4 to be admitted. From previous work with the mass spectrometer (Chapter 5) the detection range was found to be between 0.1 to 1.0 torr for a 2 ml volume of pure gas. Using the ideal gas law, this equated to between 10 and 100 nanomoles of pure gas. Assuming the concentration of CH_4 within ambient air to be 1.7 ppmv, then this would equate to between 150 and 1500 ml of ambient air.

Greater sample sizes gave larger peaks areas, and increased the reproducibility of the $\delta^{13}C$ values. A stainless steel vessel was found to be available, and was suitable as a flow through loop as both ends were fitted with Swagelok™ connectors. The volume of the vessel was 300 ml, which if filled with air, would contain 21 nanomoles of methane (assuming 20°C, 1.7ppmv

conc.). This size of vessel would be sufficient for peaks not to saturate, and still be large enough for reliable $\delta^{13}C$ values. It was known that samples of air to be tested would have *at least* this concentration, as air from any typical methane source (e.g. landfill, wetlands) would certainly have a higher concentration.

Once the size of the sample loop was determined, it had to be interfaced with the sample introduction system. The sample loop was attached to a 6-port Valco valve, which in turn was connected via a Nupro manual valve to the vacuum system used for catalyst testing (Figure 6.6). The 2 ml loop and the 300 ml loop used the same piping for transfer of He and sample to and from the irMS system. Therefore, only one of these loops could be connected at any one time. To fill the loop, the vessel containing the sample gas needed to be attached to the vacuum system. The loop was evacuated to 10^{-6} torr using a turbo pump. Due to the size of the loop (much larger than the combined vacuum system piping) this took at least 10 minutes. After shutting the valves to the pumps, the valve to the sample vessel was opened and gas was transferred to the sample loop. After the pressure had stabilised, the valves were shut and the 6-port valve could be switched to inject the air sample.

Once the sample pulse had reached the mass spectrometer, the Valco valve was switched back to the load position. The loop contained approximately 1 bar of helium, which needed to be evacuted. As the quantity of He was large, the pumping took some time, with the pressure still dropping after one hour. In practise, the loop did not need to be evacuated to such a degree. Adequate vacuum was achieved after approximately 10 minutes of pumping.

6.3.2. Injection of large quantities of gas

After attaching the 300 ml loop to a Valco valve some problems soon became apparent with injecting such a large amount of gas. The first test performed with the loop in place was a blank test. The volume was evacuated, and the Valco valve was set to "inject" this vacuum downstream for analysis. This blank test is useful to evaluate the size of any leaks within the system and the influence on $\delta^{13}C$ of any changes resulting from the leaks. Once the valve was

switched, a large amount of laboratory air was sucked back into the vent line. This was due to the fact that the pressure at the vent line exit dropped below ambient as the large evacuated volume was switched into the carrier gas. Helium flow was set to 50 ml/min, so re-filling the loop to 1 bar would take 6 minutes. The effect of the atmospheric back flow was that CO_2 from the atmosphere was trapped within the final (mass spectrometer transfer) Valco valve loop. This section deals with the various systematic approaches tried to overcome this problem.

The flow rate at the vent pipe exit was measured using a bubble flow meter. The flow was observed to slow after the Valco valve was switched, then stop, and then a reverse flow was seen for a short time. This backflow was present until the helium was able to fill the 300 ml vessel to above 1 bar (absolute), whereby the gas flow slowly recovered to the original set amount. The chromatogram collected by ISODAT returned a large amount of CO_2 over a wide time period not conforming to a normal peak shape. When the loop was filled to atmospheric pressure with laboratory air, on injection no CO_2 was detected.

The initial attempt at solving the backflow problem involved a large volume vessel was placed in the vent line, downstream of the final cryogenic loop. An Alltech hydrocarbon trap vessel, with the activated carbon removed, served as an empty flow-through vessel with a volume near to 170 ml. Its purpose was to act as a buffer containing helium at near atmospheric pressure (see Figure 6.7 (a)). The logic was that once the large sample loop was switched the reverse flow would preferentially purge helium over the final Valco loop, instead of laboratory air. The mass flow controller still provided He at the given rate, slowly increasing the helium pressure in the sample loop until positive flow was restored. On testing, air injections resulted in the detection of wide, flat peaks of CO_2 followed by multiple sharp peaks. The test was repeated at a lower pressure, enough to provide 20-100 nanomoles of CO_2 from 300 ml of air. Again, multiple peaks were present. The buffer volume was increased by adding another spent hydrocarbon trap, taking the total volume to over 300 ml. With this arrangement, injecting 1 bar of helium yielded a more realistic blank test than injecting an evacuated 300 ml vessel. The blank level was

low enough to indicate little atmospheric contamination of CO_2. There were still difficulties with the peak shapes of injected CO_2 when both volumes were present.

Helium buffering and backflow

In an attempt to overcome the problems of the peak shapes of the CO_2 entering the mass spectrometer, a liquid nitrogen trap was installed downstream of the final Valco valve, and upstream of the two buffer volumes (Figure 6.7 (b)). No CO_2 was detected once the sample loop was evacuated and injected. However, on injecting pure CO_2 the same chromatogram appeared. Additionally, when air was injected no sample peaks were seen either at low pressures or at 1 bar.

This configuration was not useful, and so changed. The next addition was a flow through vessel made from multiple 1 inch diameter steel pipes and flanges. Two of the ends were replaced with NW-25 to Swagelok™ converters for placement upstream of the sample (300 ml) loop attached to the vacuum line (Figure 6.7 (c)). The total volume was not measured, but estimated to be near 750 ml. With this in place, a 200 nmol injection of pure CO_2 gave a peak off-scale as expected, but the blank level (from leaks only – no injections) was also very high.

Although the performance of this configuration was good enough to provide usable peak shapes, blanks could not be tested, and so the buffer volumes on the vent line were removed. This was replaced by a helium feed controlled by a needle valve, with the supply split from a point downstream of the SAES Getter unit. A pipe was taken from the needle valve to the vent line and attached via a T-piece (Figure 6.7 (d)). This meant that measurement of the flow at the outlet of the vent line contained both the He flow through the sample loop, and now an auxiliary flow. Its purpose was again to provide helium preferentially rather than air, once the sample Valco valve was switched. As the flow measured by the bubble flow meter contained additive flows from both sources, the needle valve had to be closed to discover the carrier flow through the sample loop. The needle valve was then opened to set the auxiliary flow.

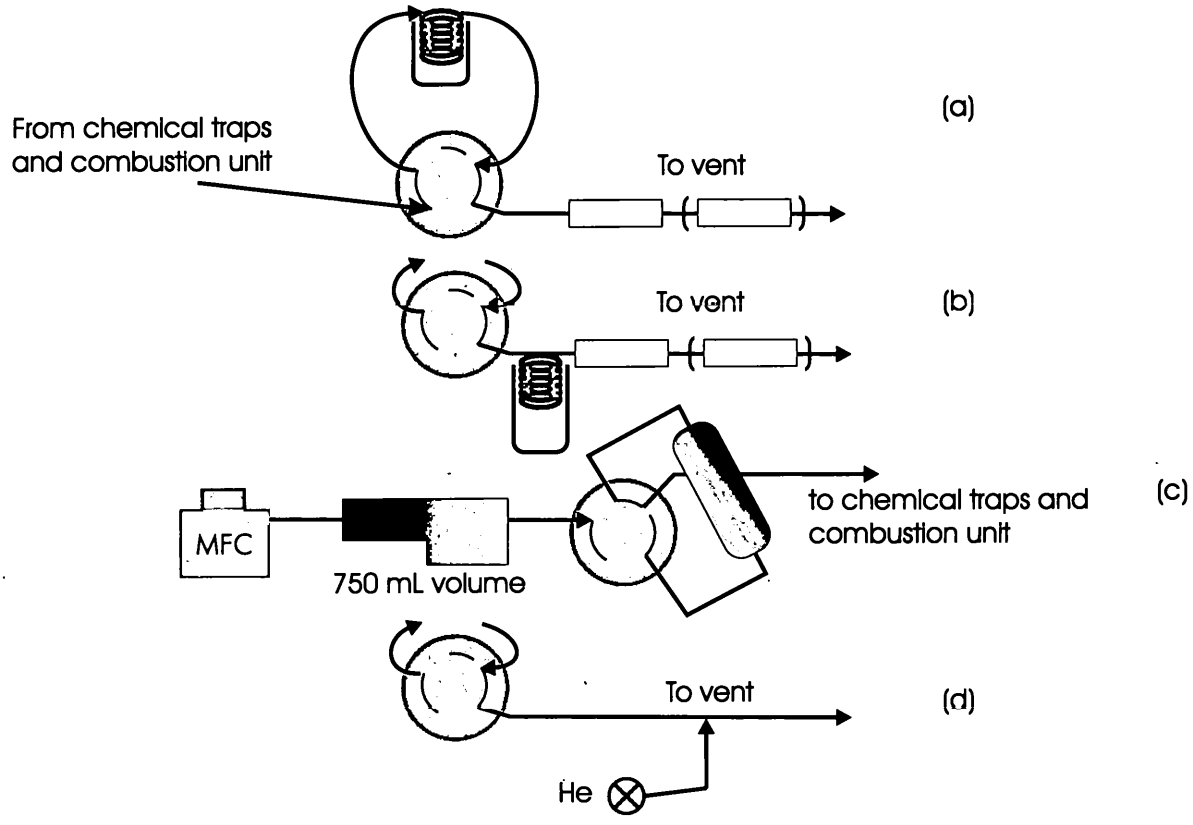

Figure 6.7 A survey of different methods tested to solve problems of contaminant air entering the inlet system; (a) empty volumes downstream of cryotrapping loop, (b) as in (a) but with additional cryotrap, (c) large volume upstream of sample injection loop, (d) helium backflow onto vent line downstream of the cryotrapping loop

Flow control

The carrier flow was set to 50 (sample path) and 50 (auxiliary) ml/min, measured as the total flow at the exit of the vent pipe. The blank level using this arrangement was found to be minimal. Injections of 97 ppm CO_2 in helium were found to show the $\delta^{13}C$ of the bottle used as –40.7 ± 1.8‰ (n=3). Another lecture bottle (Aldrich) containing 12ppm CO_2 in He was tested to have $\delta^{13}C$ = -36.8 ± 1.2‰ (n=3).

On further investigation it was deduced that the presence of the mass flow controller was thought to be hindering the recovery of the carrier flow. When the sample loop was in the load position, the MFC delivered helium such that the MFC outlet must be at above 1 bar absolute. As the sample loop was switched, the loop containing 1 bar of gas effectively dropped the pressure to just above 1 bar absolute. The difference in pressure between the inlet and outlet of

the mass flow controller was thus increased. Since flow rate is proportional to the pressure drop, this resulted in an increase in the flow through the analysis cell of the MFC. In an attempt to return the measured flow rate to the desired value, the MFC would attempt to *decrease* this flow rate, which was, course detrimental in this case. Replacing the MFC with a Porter valve (i.e. constant pressure) resulted in a quicker recovery of the flow rate. The Porter valve was found to be more dependable at giving a constant total flow rate. Blanks were found to be lower than any other configuration, and this was used for the air samples tested in this chapter.

Flash heating the cryogenic loop

Once the system was capable of successfully analysing $\delta^{13}C$ from CH_4 from air to a certain extent, improvements were made to the analysis process. After the combustion of CH_4 by means of the catalyst, CO_2 from combustion was trapped under liq. N_2, was warmed by removing the liq N_2 dewar from the loop. Within 20 seconds the CO_2 has been detected by the mass spectrometer. However, there was a problem with interference from small peaks that appeared within the major peak (Figure 6.19). These peaks were counted separately by the software, sometimes resulting in an erroneous background being selected for the major peak calibration.

One of the functions of the ISODAT software (Data Review II module) allows the manual selection of the background of the peaks. Unfortunately even calculating the multiple peaks as a single, the resultant $\delta^{13}C$ values were still incorrect. The problem was avoided by flash heating of the sample loop. Instead of allowing the laboratory air warming the loop to ambient, a cup of water at room temperature, was applied to the loop. The loop temperature rose to above -78°C (CO_2 sublimation temperature) within one or two seconds. The resulting peak was much narrower, had greater height, and produced less tailing. However, having these traits causes isotope ratio calculations to be less reliable. This method was used for all atmospheric analyses.

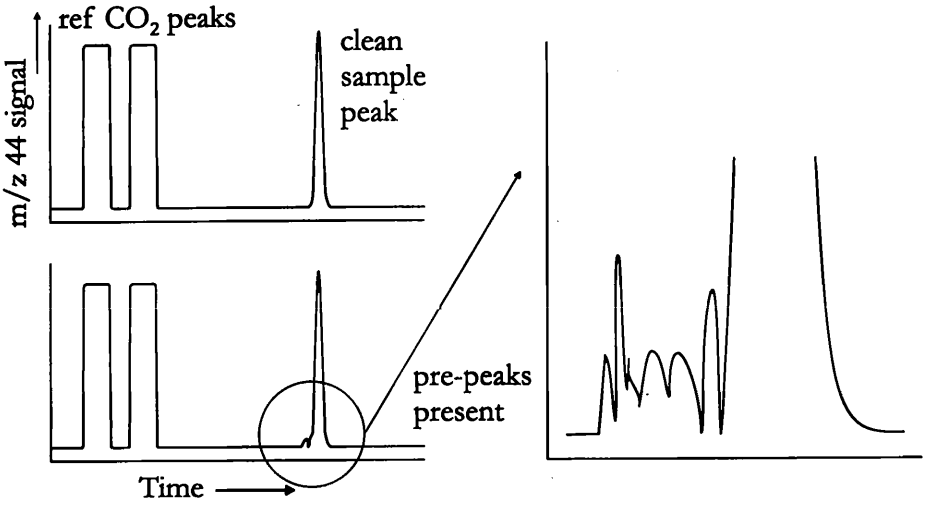

Figure 6.8 schematic chromatograms showing appearance of pre-peaks of CO_2 detected by the Delta C mass spectrometer under different injection methodologies

6.3.3. Atmospheric component removal

Atmospheric CO_2 was used as the primary test for the movement of gas from the sample injection loop to the mass spectrometer, therefore a CO_2 trap was not installed. However, if analyses of atmospheric methane were to be conducted then CO_2 present in the sample would need to be removed. The initial tests used a tube containing Molecular Sieve 3A for removing water vapour from the gas stream (Figure 6.9 (a)). Unless the study of the oxygen or hydrogen isotopes of water vapour is desired, its removal from the gas mixture is always beneficial for sample handling. Although the water trap was downstream from the sample loop, the high flow rate of dry He should have carried any water vapour that came in contact with stainless steel tubing walls into the trap.

Tests were carried out using a cryogenic trap upstream of the final irMS transfer loop (Figure 6.9 (b)). The condensable component of the gas mixture (air) was trapped whilst the sample methane passed over the combustion reactor. This loop was immersed in liquid N_2 for 5 minutes then allowed to reach room temperature once the final transfer loop had transferred CO_2 to the mass spectrometer. Chromatograms produced by this procedure had peaks appearing as part of the main peak, disrupting the isotope ratio calculations, therefore this additional cryogenic trap was not used.

H_2O/CO_2

To compare the system with others that analyse $\delta^{13}C$ from CH_4, the trapping agent was changed to material similar to that used in the Finnigan MAT PreCon system. Magnesium perchlorate was used as a water trap, and instead of sodium hydroxide, as used in the commercial unit, Carbosorb (PDZ Europa Ltd.) was used to trap CO_2. The container was arranged so that the water was removed first (Figure 6.9 (c)). Injection of a vacuum blank was found to show no peaks. An injection of 1 bar of laboratory air resulted in small peaks, implying that most of the CO_2 was trapped by the Carbosorb. One of these small peaks (large enough to calculate δ values) had a calculated $\delta^{18}O$ value of –474‰, implying that the peak was not CO_2. The peak area was too great for this isotope value to be due to a calculation error. The peak may have been due to the presence of atmospheric N_2O. It should be noted that the concentration of N_2O (310 ppbV), is approximately 20% of ambient CH_4.

Once this combined H_2O/CO_2 trap was installed, a combustion unit was placed downstream to convert CH_4 to CO_2. The initial tests showed a variety of isotope values with a 4‰ range, and the presence of N_2O was suspected. Incorporation of a liquid N_2 trap between the H_2O/CO_2 trap and the combustion reactor failed to effect any difference in peak shapes or isotopic composition.

N_2O

Traditionally, GC columns have been used to separate the components of air samples for isotope analysis. Separation of CO_2 from N_2O proved difficult using cryogenic or chemical traps. A PoraPLOT Q column was tested for functionality of CO_2/N_2O separation. This was installed in the GC Interface II downstream of the final sample loop and upstream of the Nafion™ water separator (Figure 6.9 (d)). It was connected in-line using Chrompak Universal Quick-seal column connectors. The effect of the GC column was not beneficial for isotope results. For air injections, two peaks (CO_2 from CH_4, N_2O) appeared separated by 4 minutes,

both had small amplitudes and areas, were asymmetrical, and thus rendered the isotope calculations useless.

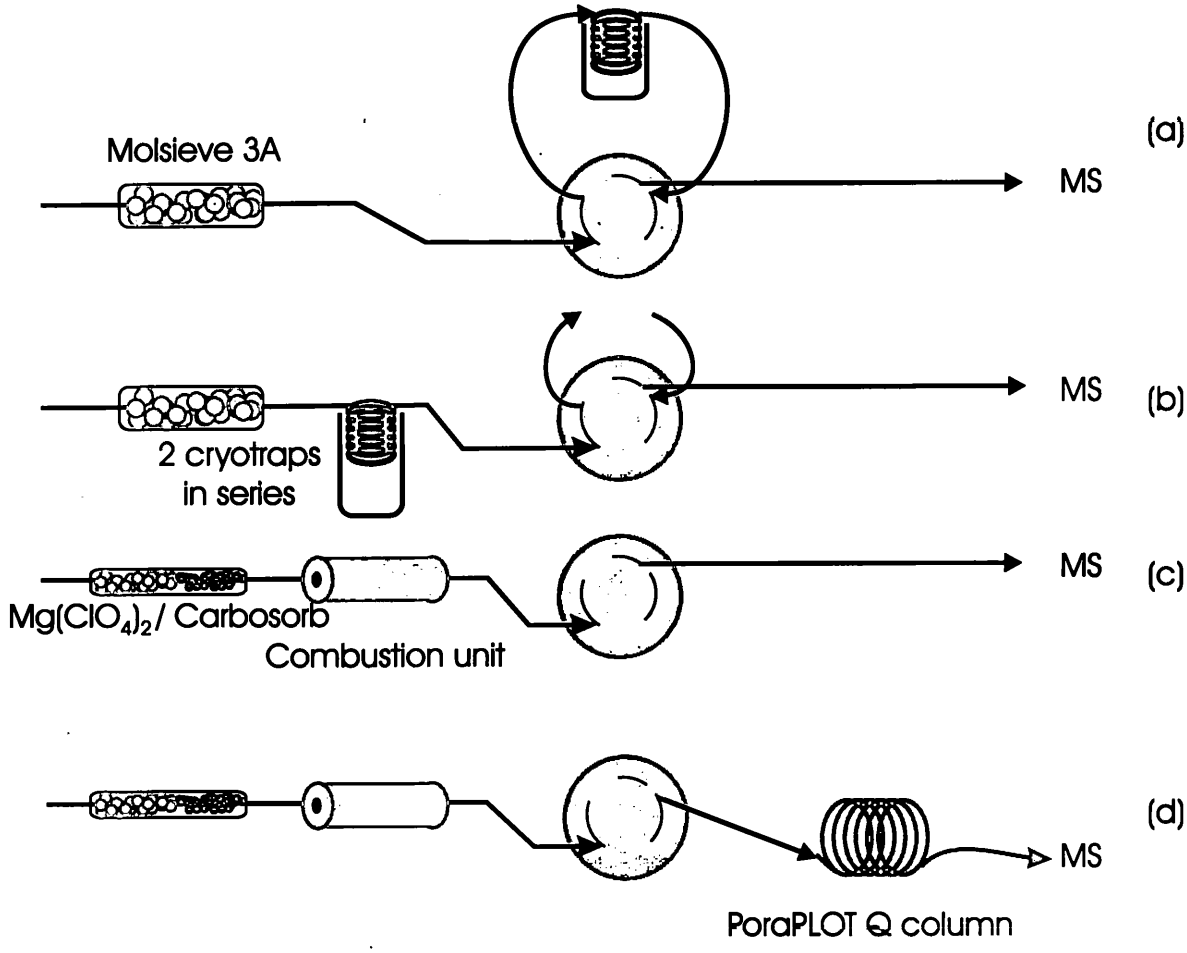

Figure 6.9 (a) Molsieve 3A upstream of cryotrapping loop, (b) as (a) with second CO_2 cryotrap upstream of trapping loop, (c) $Mg(ClO_4)_2$ and Carbosorb trap, with combustion unit upstream of trapping loop, (d) as (c) but with GC column installed in MS inlet

The influence of ambient N_2O upon the $\delta^{13}C$ of the CH_4 was investigated by placing a second water/carbon dioxide trap downstream of the combustion unit, to remove both components created from the combustion of methane (Figure 6.12 (a)). Thus, the remaining species at detectable mass ranges (m/z 44-46) could only be N_2O. Nitrous oxide has a boiling point of -88°C, which is 10°C lower than that of CO_2. Tests were performed using this system with the combustion unit at operating temperature and at room temperature. It was found that a larger 44 peak was seen when the reactor was cold. N_2O was obvious from the $\delta^{13}C$ returned

(-344‰). This implied that the hot reactor oxidised some N_2O to other oxides of nitrogen, not isobaric with CO_2 and therefore not a problem in this arrangement.

A custom gas mixture (5.6 ppmv N_2O, 10.2 ppmv CO_2, balance N_2) procured from Air Products Ltd was used for separation testing. Although this mixture is not a strict air analogue for these trace gases, it would show any problems with using standards at the parts per million concentration level. The gas mixture was injected along two possible paths, as seen in Figure 6.10.

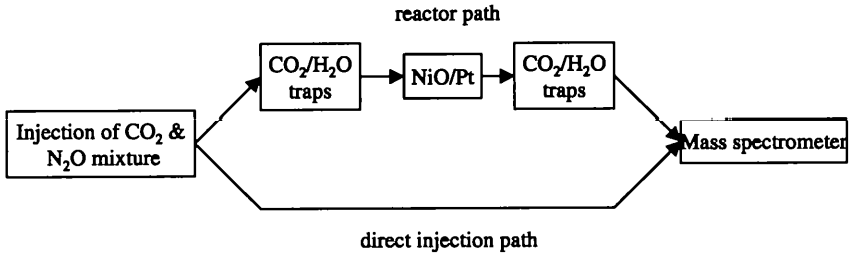

Figure 6.10 Schematic diagram showing 2 potential paths for N_2O/CO_2 gas mixture for N_2O abatement testing

One involved passing the mixture directly to the final transfer loop, while the other passed the gas through the 2 traps (H_2O/CO_2) with the combustion unit in the centre. On injecting this N_2O/CO_2 gas mixture through the direct injection path, a (single) peak was detected by the mass spectrometer. The peak was found to be very clean with no artefacts, and give a consistent $\delta^{13}C$ of -60.3 ± 0.6 ‰. Both compounds should be contributing to this detected peak.

Injecting the gas along the reactor path (in Figure 6.6) would remove all the CO_2, and leave only N_2O in the N_2 balance gas. The irMS traces observed two peaks, a major one, and a very small peak within the tail of the major peak. With the combustion reactor at room temperature, the total area of both peaks had only 5% of the area compared the direct injection path. The larger of the two peaks had $\delta^{13}C$ values of around –350‰, while the minor gave –58.5‰. Such a low value of $\delta^{13}C$ implies that this peak was not due to CO_2 – therefore only possible agent was

N_2O. The presence of the more realistic value of –58.5 ‰ on the small peak suggested some CO_2 was still present (either natural blank or untrapped mixture gas).

Increasing the temperature of the NiO/Pt reactor gave evidence of N_2O oxidation. At 700°C the N_2O peak was still present, but gradually as the temperature was increased to 1000°C, this peak was reduced, until at 1000°C it was small enough to be below the calculation threshold of the irMS software (Figure 6.11). The implication of this experiment is that a GC is not necessary for ambient N_2O/CO_2 separation for isotope analysis. The NiO/Pt combustion unit at 1000°C eradicated any nitrogen based compound from the m/z 44-46 window that would interfere with the analysis. It must be noted however that the gas mixture used had nitrogen as balance gas, not air. Different combustion characteristics may be present with O_2.

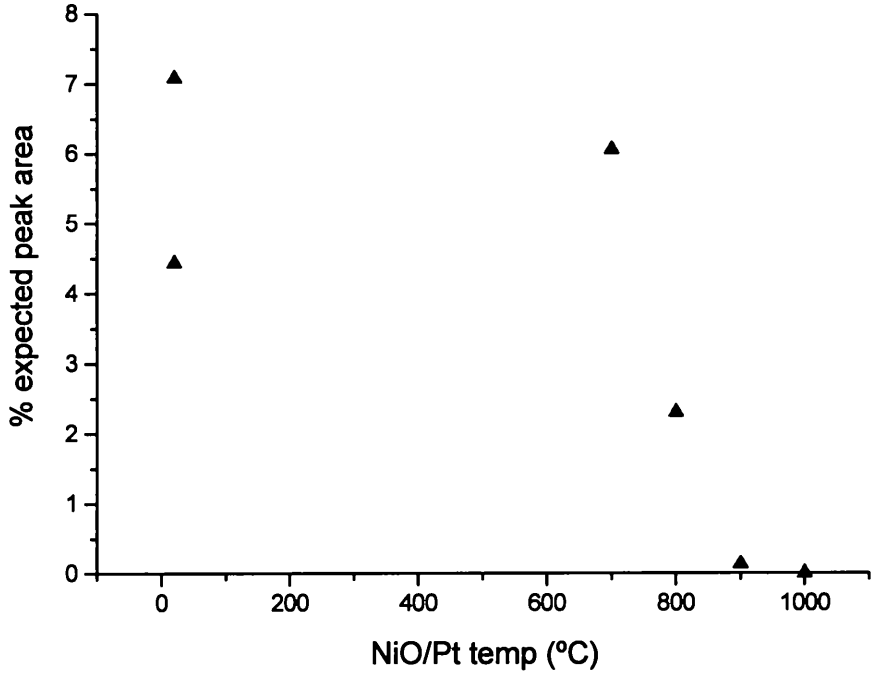

Figure 6.11 Atmospheric N_2O removal by NiO/Pt reactor at high temperatures. Expected peak area is the area that CO_2/N_2O mixture should have given were it not trapped. The injection at 1000°C resulted in no peak being detected by the MS. $\delta^{13}C$ of N_2O peaks were all between –300 and –350 ‰.

The final (permanent) addition to the system was the incorporation of a trap for O_2. A trap designed for carrier gas purification – Oxy-trap (Alltech) – consisted of <1 m of $^3/_8$" pipe coiled, filled with 13 % CuO and 87 % alumina, but it did not give details of preparation or substrate. The manufacturer claimed that one unit can remove 180 ml of O_2 (at STP), but warned against exposure to gases with ~1% O_2 as this damages the trap. No regeneration process was detailed, but in-house experiments on other systems has shown that the material can be regenerated by the addition of H_2 at elevated temperatures. 180 ml of O_2 is equivalent to 3 injections of 300 ml air. The oxy-trap was placed upstream of the water/carbon dioxide trap (Figure 6.12 (b)). After injecting 300 ml aliquots of air through the system with the secondary (post-combustion) CO_2 trap in place, no blank peaks were detected by the irMS (as would be expected). Once the secondary trap was removed so that CO_2 from CH_4 combustion could reach the irMS, $\delta^{13}C$ values from laboratory air had a precision of 0.5‰ (n=4, mean $\delta^{13}C$ = -48.1‰).

The manufacturers information suggested that large amounts of O_2 entering the trap may lead to the trap increasing in temperature. A K-type thermocouple was attached between the coils of the trap, and temperature rises of 1.8°C were seen after the first two injections. No rise was seen after subsequent air injections suggesting the trap had possibly come to its end of life. However, $\delta^{13}C$ from CH_4 showed higher repeatability with the spent trap in place, and no significant shift in isotopes of carbon.

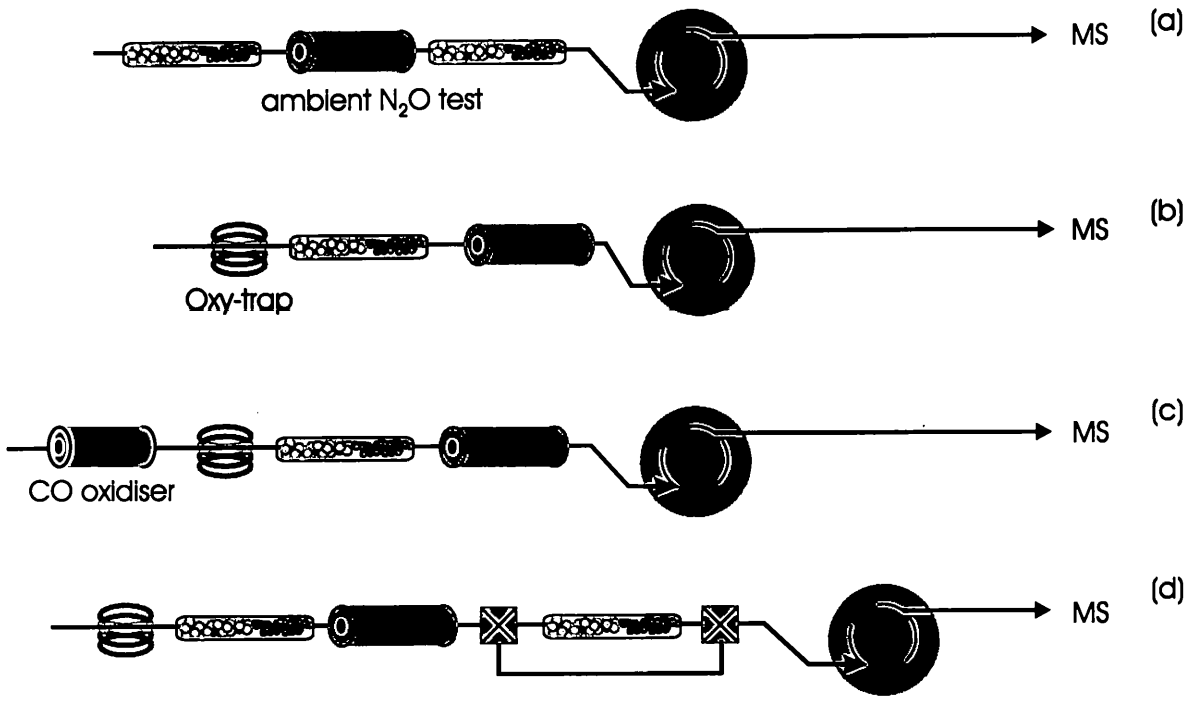

Figure 6.12 Atmospheric component removal (a) CO_2 removal arrangement for N_2O quantity test, (b) oxygen trap placed upstream of H_2O/CO_2 trap, (c) CO removal testing arrangement, d) switchable equivalent of (a) for occasional N_2O quantity test

CO

One concern left in place from examining the PreCon system was the presence of atmospheric carbon monoxide. Finnigan MAT recommend a correction be applied to $\delta^{13}C$ results obtained. The combustion reactor will convert both CO and CH_4 to CO_2, so the CO_2 measured by the mass spectrometer carries signals from both compounds. The correction assumes a CO mixing ratio of 70 ppb with a $\delta^{13}C_{PDB}$ of –28‰, compared to CH_4 with 1700 ppb (ambient concentration) and $\delta^{13}C_{PDB}$ of –47.2‰. Using two-component mixing with these values, a correction of –0.8‰ must be applied to the $\delta^{13}C$ value of the CH_4. This inevitably relies on the fact that one knows both the concentration and isotopic composition of both CO and CH_4.

A better method would be to remove the ambient CO from the air sample. Various oxides were tested for this purpose in Chapter 4. Among the oxides that showed complete combustion at low temperatures were $CuCrO_x$ and $CoCrO_x$. Cobalt-chromium oxide was examined for this purpose. A tube containing the oxide was placed upstream of the CO_2/H_2O trap (Figure 6.12

(c)). After temperature cycling to reduce any carbon blank, air was injected over the oxide at room temperature. No shift was observed in the $\delta^{13}C$ values measured (i.e. CH_4 reactor at 1000°C) . Heating the oxide to 200°C caused the $\delta^{13}C$ of the CH_4 to become 10‰ higher, while at 300°C the irMS measured $\delta^{13}C$ of CH_4 20‰ higher than with the $CoCrO_x$ at room temperature. This oxide was then replaced by copper-chromium oxide. Three repeated air injections were performed with the $CuCrO_x$ at room temperature, followed by injections with the oxide heated to 150°C. The first two injections showed that there was a significant shift in the $\delta^{13}C$ value more negative by approximately 1 ‰ (Figure 6.13 (b)). However, after these two injections, peak areas decreased dramatically, and $\delta^{13}C$ was inconsistent (Figure 6.13 (a)). Increasing the $CuCrO_x$ temperature to 200°C gave $\delta^{13}C$ with very low precision and thus the oxide was removed.

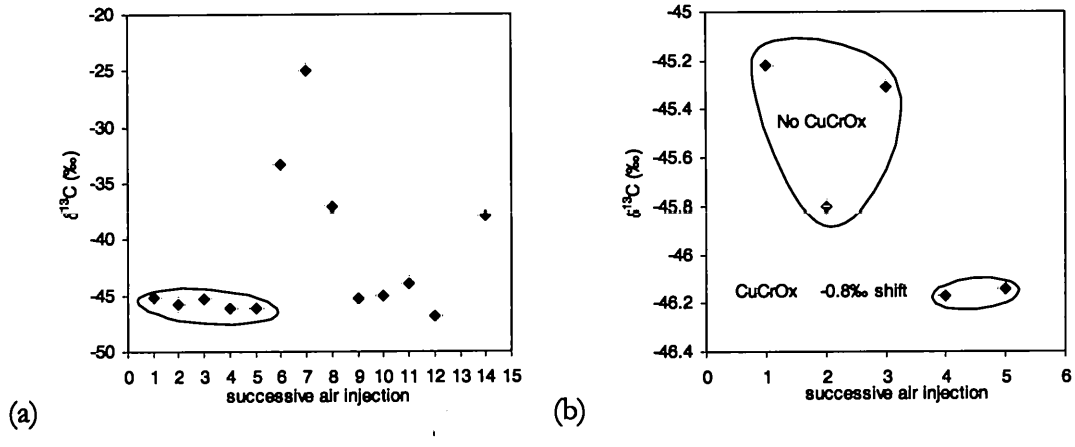

Figure 6.13 (a) $\delta^{13}C$ of CH_4 from successive air injections showing difference in $\delta^{13}C$ with and without $CuCrO_x$ catalyst removing atmospheric CO, (b) a close up of the elliptical area shown in (a)

Analyses of microbial CH_4 in this thesis were performed without oxidising CO for simplicity of analysis, but the $\delta^{13}C$ values were corrected for CO assuming 70 ppb at –28‰. The final configuration of the traps used for such analyses is shown in Figure 6.12 (d). A second CO_2/H_2O trap was installed in a path switchable by using 3-way valves (Precision Dynamics Inc). During air analyses, the path was set to bypass the trap. To test the efficiency of the combustion reactor to oxidise ambient N_2O, the path was changed to flow through second the

trap. This was used occasionally to confirm that no m/z 44-46 species entering the ion source were from N_2O.

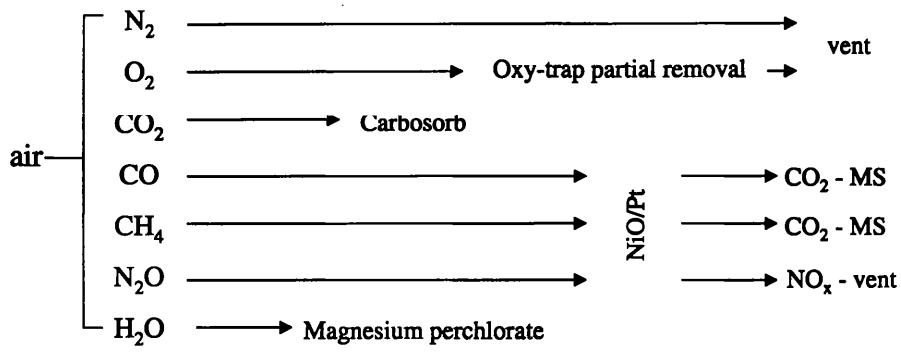

Figure 6.14 Summary of the removal agents for atmospheric contaminants

6.3.4. Combustion Unit – alternative catalysts

Some of the catalysts from Chapter 4 were placed in the system as shown in Figure 6.19, and then subjected to testing by repeatedly injecting air over the oxide at various temperatures. The oxides tested were $CuCrO_x$, PdO (sponge), PdO (Aldrich), and Rh_2O_3.

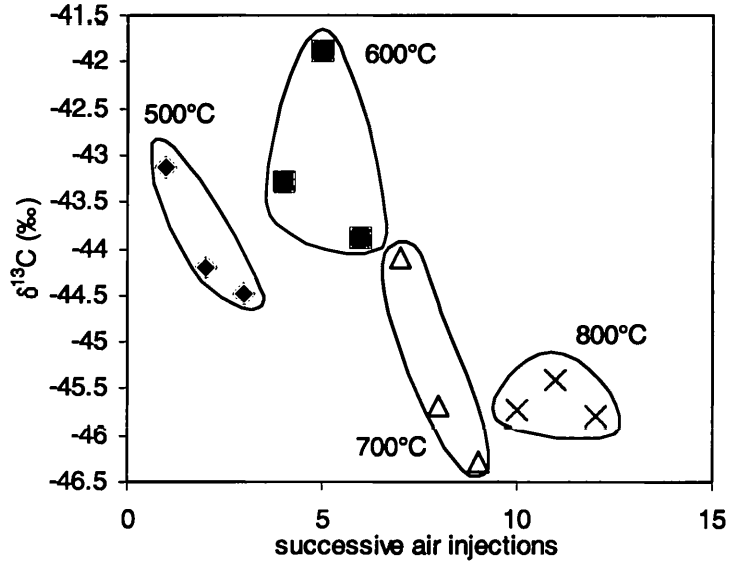

Figure 6.15 $\delta^{13}C$ from laboratory atmospheric methane by combustion over PdO from oxidised Pd sponge

Table 6.1 mean $\delta^{13}C$ from CH_4 combustion by PdO (sponge) as seen in Figure 6.15

Temperature (°C)	Mean $\delta^{13}C$ (‰)	std dev (σ)
500	-43.9	0.7
600	-43.0	1.0
700	-45.4	1.1
800	-45.6	0.2

Figure 6.15 shows the most promising of all the tests, with oxidised Pd sponge used as the oxidation reagent. Low reproducibility was seen at temperatures of 500 to 700°C. At 800°C the consistency was high, suggesting that this material has the potential to oxidise CH_4 as well as NiO/Pt. By examination of the mean $\delta^{13}C$ from injections at 800°C, there is also a shift from the value produced by the NiO/Pt reactor of approximately -3‰.

The injections were repeated using PdO from Aldrich Chemicals. Figure 6.16 shows the results with a large deviation in $\delta^{13}C$ at all the temperatures tested. Peak sizes were far in excess of expected sizes at 600°C, suggesting a blank component released on combustion at this temperature. The amount of the standard blank at this temperature was relatively low. The variability, and the offset from the believed true value of the $\delta^{13}C$ at all the temperatures tested, discounted that sample of PdO from methane oxidation.

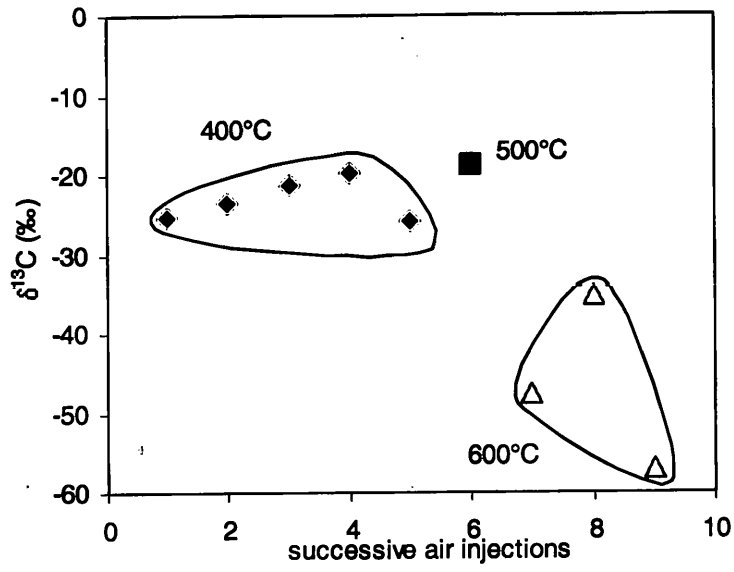

Figure 6.16 $\delta^{13}C$ from atmospheric methane by combustion over PdO from powder, supplied by Aldrich

Table 6.2 mean $\delta^{13}C$ from CH_4 combustion by PdO (sponge) as seen in Figure 6.16

Temperature (°C)	Mean $\delta^{13}C$ (‰)	std dev (σ)
400	-23.2	2.6
500	-25.8	n/a
600	-46.6	10.3

Rhodium oxide was also tested in this arrangement. Blank levels were found to be low at 400°C, but peak areas from the injection of 1 bar, 300 ml of air produced so much CO_2 that the mass spectrometer became saturated. The interaction of air with the compound is not straightforward. This pattern continued with temperatures up to 700°C, whereupon the oxide was removed. Attempts at using the $CuCrO_x$ as used in CO oxidation (section 5.3.3.) also produced very large amounts of CO_2 evolved from a single injection. One of the injections on-scale produced $\delta^{13}C$ values of –74‰, some 30‰ lower than the known value.

As the purpose of this small trial was to examine potential CH_4 oxidation alternatives, the number of injections was small. However it can be seen from Figure 6.16 that oxidised Pd sponge at 800°C offers the greatest potential. Other successful oxides from Chapter 4 may also

show potential for this application. As more effort would be needed to evaluate the ability of PdO relative to NiO/Pt, the latter was used as the oxidation component for the air analysis.

6.3.5. Combustion Unit – standard catalsyt

It has been shown in Chapters 4, 5, and 6, numerous potential methods exist to oxidise CH_4 to CO_2 for isotope analysis. Chapter 5 also showed isotope integrity tests of various metal oxides. Although total oxidation occurred with other materials at lower temperatures than the standard catalyst (NiO/Pt), the $\delta^{13}C$ precision was not as high, and deviation from the expected value was observed. The NiO/Pt was used at 1000°C for reasons shown in the pure CH_4 tests, but this was also assumed to be needed for CH_4 in air (Merritt et al., 1995a). Repeated tests were performed on NiO/Pt on laboratory air to find reproducibility within the system. Variation in $\delta^{13}C$ with successive injections was found, but this was expected as the effect was also seen by the manufacturers of the PreCon system (Figure 6.17), a commercial inlet system for $\delta^{13}C$ and $\delta^{15}N$ analysis of ambient CH_4 and N_2O.

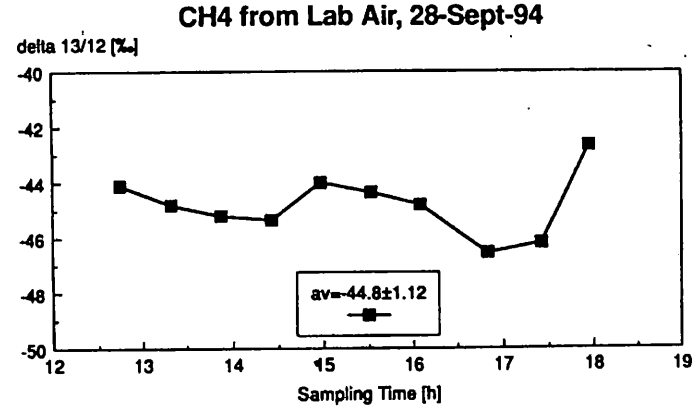

Figure 6.17 $\delta^{13}C$ from injections of atmospheric CH_4 using the PreCon system with a Finnigan MAT irMS system. Source: PreCon Manual

The reproducibility of the system with the NiO/Pt reactor was tested at various times during the system development and during air sample analyses. Before the system was in its final configuration, repeated injections of laboratory air were performed with NiO/Pt at 1000°C.

This can be seen in Figure 6.18, in the first column. The configuration during these tests were that both oxygen, carbon dioxide and water traps were present in the same configuration as in Figure 6.19, but the switchable secondary CO_2 and H_2O traps were not present. The cryogenic loop was allowed to be warmed (by removal of liquid N_2) with no additional heating.

The second column in Figure 6.18, shows tests that were also performed using ambient warming of the cryogenic loop, after the testing of some CO removal catalysts. The configuration is the same as the first series. Pre-peaks were present on the CO_2 traces during this series, leading to large uncertainties in $\delta^{13}C$ values (as explained in Figure 6.8).

Data in the third column were taken as the method switched to using flash heating of the cryogenic loop. The configuration now includes the switchable flow path containing the secondary traps, although these traps were bypassed. The fourth column contains injections using the same method as the third series, performed before the preliminary sulphate sample measurement (section 6.5.2). The fifth column contains measurements taken (using the same method and configuration) during the main sample analysis series (section 6.5.4). During the series of injections, the NiO/Pt reactor was replaced with fresh oxidised Ni&Pt wire, due to suspect $\delta^{13}C$ values from one sample. The reactor temperature was increased to 1050°C, near the maximum attainable, to see if an increase in temperature would effect any change in the reproducibility of the $\delta^{13}C$ values.

The sixth column shows another series of air injections again taken during the main sample analysis series. These injections were also performed with the oxide at 1050°C. The mean and standard deviations for each injection series are shown in Table 6.3.

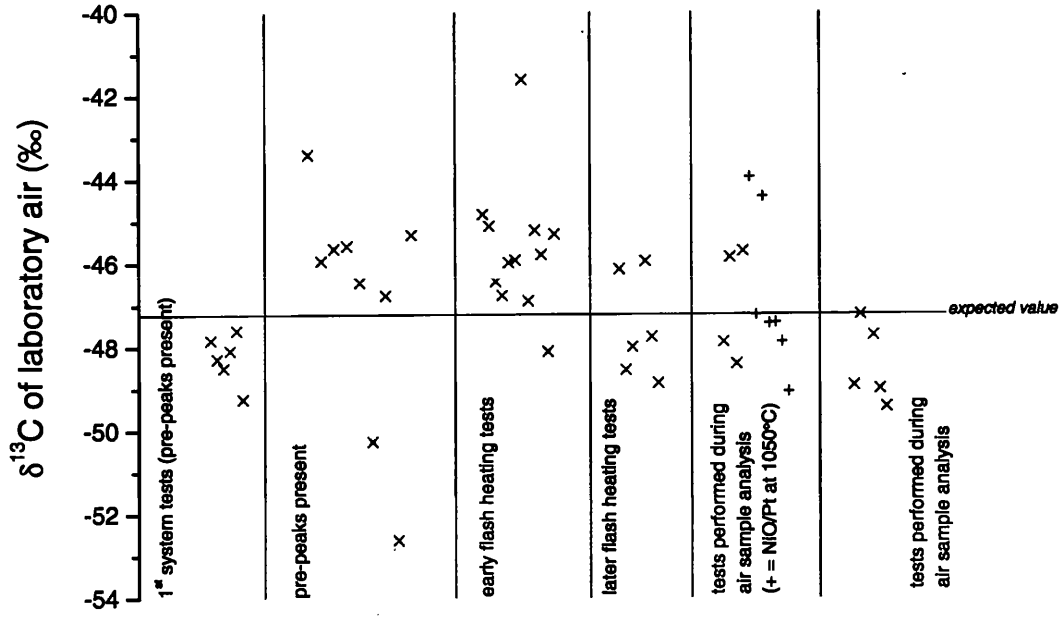

Figure 6.18 $\delta^{13}C$ of methane from injections of air under 6 different test regimes

Table 6.3 tabulated form of data shown in Figure 6.18, giving standard deviation of each series

Column	Configuration	$\delta^{13}C$	$\pm\sigma$	n
1	H_2O/CO_2 traps, no flash heating, no secondary path	-48.6	0.6	6
2	H_2O/CO_2 traps, no flash heating, no secondary path	-46.9	2.8	9
3	H_2O/CO_2 traps, flash heating, secondary path	-45.7	1.6	11
4	H_2O/CO_2 traps, flash heating, secondary path	-47.6	1.2	6
5	H_2O/CO_2 traps, flash heating, secondary path	-46.9	1.6	11
6	H_2O/CO_2 traps, flash heating, secondary path	-48.5	0.9	5

6.3.6. Final system for 300 ml air sample analysis

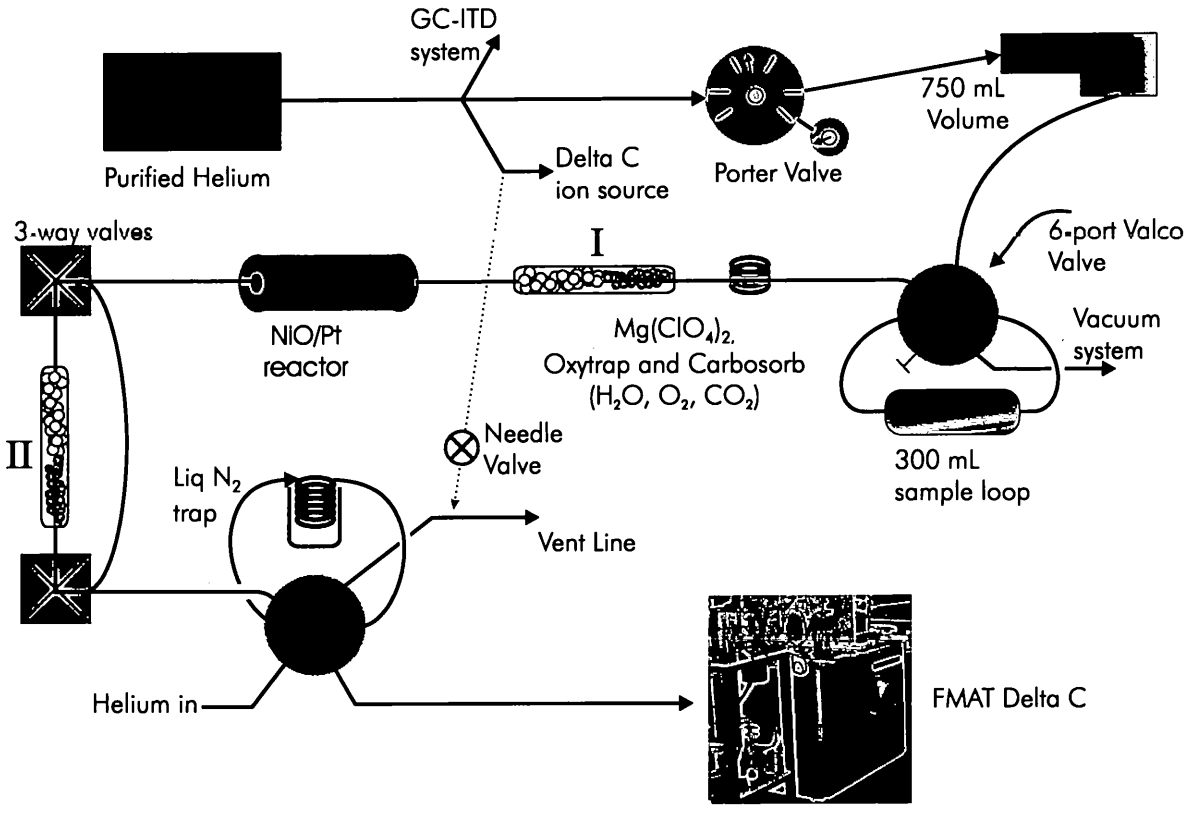

Figure 6.19 Schematic diagram of final system used for isotope analysis of atmospheric methane

The system shown in Figure 6.19 is the configuration that has been used to analyse all the non-laboratory air samples performed in this chapter. The switchable path (with 2nd trap, labelled as II) allowed testing for the presence of ambient or produced N_2O (using the same method as shown on page 220). Not shown is another pair of 3 way valves that bypass the entire trap system, providing a path that starts just before the oxygen trap and ends downstream of the valve downstream of the 2nd H_2O/CO_2 trap. Its purpose was to create a path for the direct analysis of CO_2 at low concentrations, providing the ability to check any fractionation occurring within gas transfer.

6.4. Application of the fast method to the analysis of $\delta^{13}C$ of CH_4 from air samples collected from a Finnish peat bog

The first non-laboratory air samples to be analysed by the configuration as shown in Figure 6.19, were supplied by Dr. Sarah Jackson (PSRI). These samples were collected during a fieldwork

season for analysis on MIRANDA (Jackson et al., 1999), the operation of which was described earlier. This static mass spectrometer requires only 8 nanograms of CH_4 for analysis (<10 ml ambient air), making replicated measurements of the isotopic composition of CH_4 emissions from various sources feasible.

The field site chosen was Jänkäjärvi, 10 km NNE of Kaamanen, northern Finland. The surface was peat, containing a core of permafrost. The aim of the sample analysis was to use $\delta^{17}M$ measurements to allow a comparison between CH_4 budget estimated from meteorological measurements and those extrapolated from headspace chamber measurements.

Samples were collected in 100 ml evacuated flasks, which at ambient concentrations, would correspond to a total of 7 nmol of CH_4. Although this is lower than the target 20 nmol, the measurements can still be made and provide $\delta^{13}C$ with reasonable precision. Concentrations of the samples had been measured using a GC-FID system, so a portion of each sample had been used in the analysis. The estimated pressure remaining in the vessel was 850 mbar. The majority of the samples had concentrations considerably above ambient, as may be seen in Table 6.4.

Table 6.4 Collated data from analysis of CH_4 from Finnish bog air samples

Sample	CH_4 conc (ppm)	Peak area (Vs)	$\delta^{13}C$ (‰)
ambient air	1.7	0.46	-45.2
1	10.9	2.11	-79.6
2	9.6	1.73	-80.5
3	7.0	1.18	-76.9

6.4.1. Isotope Dilution Plots

The sampling method for the above samples involved a static chamber (30 cm height and diameter) adapted for the attachment of glass bottles. This was placed over the ground while the air was sampled at various time intervals. The more time for collection, the more CH_4 from

the soil enters the air in the chamber. Therefore the methane in the samples contains a mixture of the background air, and the bacterial methane emitted by methanogens in the soil. To find the actual $\delta^{13}C$ of the emitted CH_4, the influence of the ambient air within the sample must be corrected for. This can be done by resolving the two components such that:

$$\delta_{sample} \cdot c_{sample} = \delta_{ambient} \cdot c_{ambient} + \delta_{emitted} \cdot c_{emitted} \qquad (6.1)$$

where δ is isotopic composition, and c is concentration. Following from the assumptions 1) of constant background concentration and isotopes and 2) of conservation of methane within the closed system, i.e.

$$c_{sample} = c_{ambient} + c_{emitted}\ , \qquad (6.2)$$

then the equation (6.1) can be re-arranged so that the isotopic ratio is proportional to the inverse of the concentration:

$$\delta_{sample} = \frac{(\delta_{ambient} \cdot c_{ambient} - \delta_{emitted} \cdot c_{ambient})}{c_{sample}} + \delta_{emitted} \qquad (6.3)$$

As can be seen from the above equation, as $c_{sample} \rightarrow \infty$ then $\delta_{sample} = \delta_{emitted}$. Hence if the δ_{sample} is plotted against $(c_s)^{-1}$, the δ-intercept gives the isotopic composition of the source (Thom et al., 1993). Real samples should show a linear trend, and extrapolation of a regression line gives the intercept. A plot created by this method is termed an isotope dilution plot. It should be noted that equation (6.1) is only an approximation, most valid for small differences in delta values for the two sources. For a true relationship one needs to use absolute isotope ratios, not delta values.

6.4.2. Isotope Dilution of Finnish air samples

The data shown in Table 6.4 can be displayed in the manner described above (Figure 6.20).

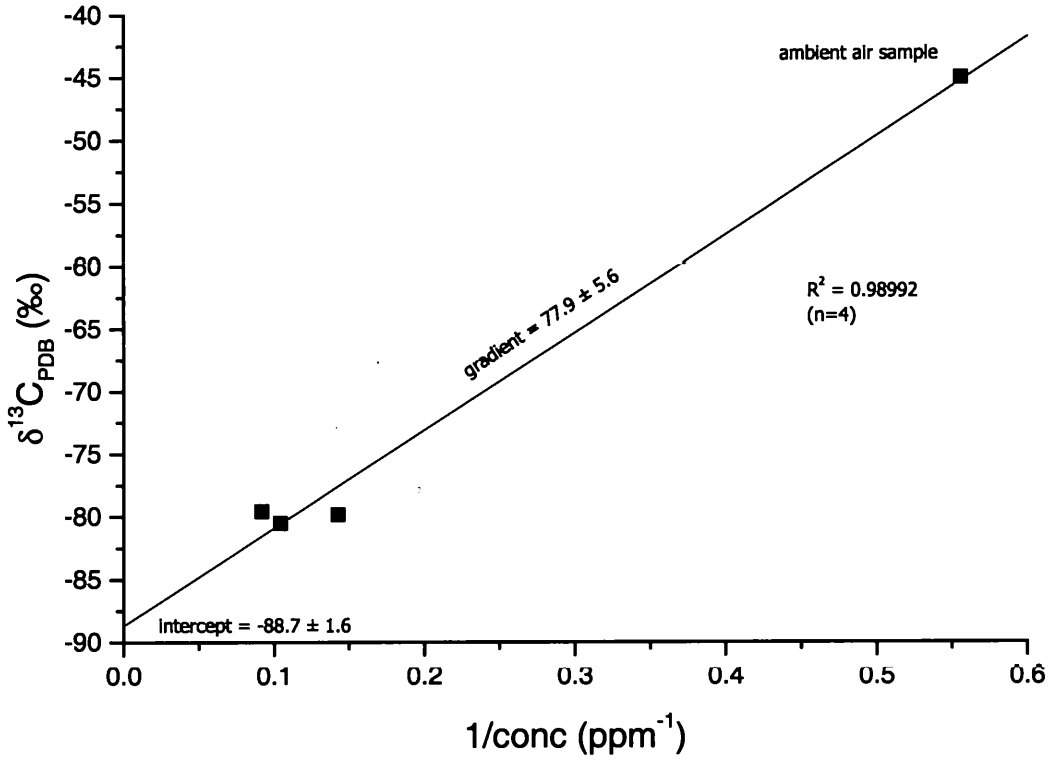

Figure 6.20 Isotope dilution plot of results from Finnish air samples

Figure 6.20 shows that the series of samples gave $\delta^{13}C_{PDB}$ = -88.7 ± 1.6‰. This value may be among the lowest measured methane $\delta^{13}C$ from similar terrain. A recent study (Waldron et al., 1999) sampled methane from Scottish bogs and marshes at various depths and found $\delta^{13}C(CH_4)$ of between –83 to –60‰ (mean of all samples from wetlands; individual samples reached to -86‰). Another compiled study (Conny, 1996) showed that $\delta^{13}C$ ranges from bogs were from -73 to –60‰. Only such sources as natural gas and lakes produced $\delta^{13}C$ approach this (-83 to -63‰). Other samples collected at the same time and place by Dr. Sarah Jackson have been analysed on MIRANDA. If such a sample was split, a portion could be run on MIRANDA, and another portion in the system as described in this chapter. The combined $\delta^{13}C$ and δD could then be produced.

The $\delta^{13}C$ value produced from the analysis gives indication of the pathway of methane formation. Along with acetate fermentation, another process leading to methanogenesis is CO_2 reduction. Jackson et al., (1999) speculated that the active mechanism of CH_4 production is CO_2

reduction. It has been reported that $\delta^{13}C$ values of CH_4 from CO_2 reduction lie in the range -110 to -60 ‰ while $\delta^{13}C$ values from acetate fermentation lie in the range -65 to -50 ‰ (Whiticar et al., 1986). Therefore, the low $\delta^{13}C$ values from this study agree with the CO_2 reduction pathway. This is consistent with Dr. Sarah Jackson's conclusions from $\delta^{17}M$ data.

6.5. Analysis of $\delta^{13}C$ of CH_4 from peat cores

Almost all of the air samples examined in this chapter are the result of a collaboration with Vincent Gauci (Dept. of Earth Sciences, OU/Institute of Terrestrial Ecology, Edinburgh). Peat cores were obtained from a bog located in Caithness, Scotland and were stored in a laboratory in ITE under controlled conditions of humidity and temperature. Air samples were taken using a headspace chamber and methane flux measured using GC-FID concentration measurements.

The addition of sulphate to the soil has been found to decrease the CH_4 flux (V. Gauci, *pers. Comm 1998*). A preliminary test was proposed to discover if $\delta^{13}C$ of emitted CH_4 was fractionated on the addition of sulphate. A more detailed test examining temperature variations on $\delta^{13}C$ would follow if successful.

6.5.1. Sample handling and analysis procedure

Samples of air were collected in a different manner than for the Finland samples. Peat cores were equlibrated for a day at each specific temperature. Headspace chambers were installed on different peat cores, and left for 40 minutes, until the air was sampled. Air sample collection was not performed by evacuated 100 ml glass flasks (as in the Finland samples), but by using 1 litre plastic gas bags (SKC Inc). As they are not fixed volume containers, air had to be pumped into them by gas tight syringes. This process may cause isotopic fractionation, but was not tested. No tests were performed on isotope integrity of sample with long storage times. Fitting the bags to the vacuum line required the use of $\frac{3}{8}$ to $\frac{1}{4}$ inch Swagelok™ converters. Leak testing was accomplished by pumping the bags to 10^{-3} mbar as measured by a Penning gauge in place near the pumps, and then switching a valve so the bag and volume were isolated. The

Baratron on the vacuum system then measured the rise in pressure over time with the bag valve open, and closed. Pumping using rotary and turbomolecular pumps resulted in the measured pressure of the bag was no lower than 10^{-3} mbar. The size of the bags allowed a maximum of three injections per bag, two filling the sample loop to 1 bar, with the final injection filling the loop to a variable amount between 300-900 mbar.

Previous work by Jackson (1999) has shown that the $\delta^{17}M$ of CH_4 emitted from different areas of a peatbog, under the same environmental conditions (temperature/water table depth) is very reproducible. Whilst the flux may vary significantly between cores, this would indicate that the chemical processes occurring are very similar. However, the relative properties of the microbial communities may differ.

The system used for analysis is shown in Figure 6.19. The oxidation unit was a fresh NiO/Pt wire reactor, which was used at 1000°C at first. During the full scale experiment, the temperature was increased to 1075°C when the precision of $\delta^{13}C$ values were not as high as expected. Flow rates of helium were set to 70 ml/min through the Porter regulator and 130 ml/min total including the backflush flow. The timeline (in minutes) for analysis was as such:

T=0 liquid N_2 was applied to the final trapping loop and the trace started.
T=1 the air sample loop was set to inject.
T=7 the cryotrapping loop was set to inject.
T=8 liquid N_2 was removed from the trapping loop, and cold water was applied to the loop for rapid heating for CO_2 sublimation.

6.5.2. Preliminary study

Nine cores were kept at constant temperature (10°C) in a constant environment (temperature/humidity). One set of three cores were untreated (no sulphate added). A second set of three cores had an equivalent of 50 kg/ha of sulphate applied to them in one dose. Another three had the same total dose applied over regular intervals.

Three samples were collected for each core treatment (control, single dose, and continuous dose) and two samples of ambient air. The eleven samples were injected and the $\delta^{13}C$ values collected by using NiO/Pt as the oxidation unit. The size of the bags allowed multiple injections (3) from each sample. System blanks were measured before the injections and found to be small (<0.2 Vs).

6.5.3. Results from preliminary experiments

The compiled results from the samples collected can be seen Table 6.5.

Table 6.5 Collated data from analysis of air samples from headspace chambers in the preliminary experiment. The column headed 'bag' identifies the gas bag label with the suffix indicating the injection from the bag. Those runs with shaded backgrounds have such a large peak height that the major peak may have saturated the mass spectrometer, and are excluded from plots.

Dose (kg.ha)	rate	bag	press (mbar)	peak height (V)	peak area (Vs)	$\delta^{13}C$ (‰)	$\delta^{18}O$ (‰)
50	continuous	503.1	atm	5.92	4.865	-55.0	+22.2
50	continuous	503.2	atm	6.272	4.501	-54.6	+22.8
50	continuous	503.3	atm	error			
50	continuous	535.1	atm	8.43	5.089	-56.7	+22.6
50	continuous	535.2	atm	7.1796	4.632	-58.6	+23.3
50	continuous	535.3	750	6.777	3.893	-55.0	+21.8
50	continuous	514.1	atm	3.268	7.582	-59.0	+28.7
50	continuous	514.2	atm	11.797	7.649	-60.2	-9.7
50	continuous	514.3	741	6.896	4.217	-59.4	+27.4
50	single	515.1	atm	7.477	5.333	-59.2	+21.8
50	single	515.2	atm	6.375	4.927	-59.3	+23.1
50	single	427.1	atm	5.322	4.204	-50.2	+25.7
50	single	427.2	atm	7.735	5.148	-51.7	+23.2
50	single	427.3	363	3.085	2.207	-47.4	+26.6
50	single	432.1	atm	9.597	7.698	-21.9	+6.51
50	single	432.2	atm	9.32	6.18	-58.9	+22.9
50	single	432.3	662	7.475	4.664	-57.0	+26.3
ambient		429.1	atm	5.588	3.574	-50.4	+20.5
ambient		429.2	atm	6.206	3.801	-51.6	+18.4
ambient		429.3	548	4.269	2.605	-49.5	+21.0
ambient		420.1	atm	5.923	3.793	-44.0	+27.1
ambient		420.2	atm	9.625	5.656	-48.7	+18.4
ambient		420.3	502	4.417	2.852	-46.0	+24.2
control		507.1	atm	6.955	4.636	-58.0	+23.8
control		507.2	atm	7.271	4.583	-58.4	+24.2
control		507.3	898	6.562	4.388	-58.0	+23.1
control		428.1	atm	11.451	7.605	-60.6	-9.1
control		428.2	900	11.098	7.396	-57.6	-1.0
control		428.3	639	8.147	5.733	-61.9	+23.7
control		473.1	atm	7.447	4.919	-55.0	+24.4
control		473.2	atm	7.735	4.749	-55.3	+24.5

Dose (kg.ha)	rate	bag	press (mbar)	peak height (V)	peak area (Vs)	$\delta^{13}C$ (‰)	$\delta^{18}O$ (‰)
control		473.3	585	3.606	2.532	-52.4	+27.5

Observation of $\delta^{18}O$ values showed that low values correspond to high peak heights. This is an indication of the peak being above or near the detector's 10V saturation. In these situations, the peak's area would not be calculated correctly and hence the ratio of peak areas would lead to false $\delta^{13}C$. These values had to be removed when calculating the mean of the $\delta^{13}C$ values for each sample. Figure 6.21 shows a plot of $\delta^{18}O$ versus peak height.

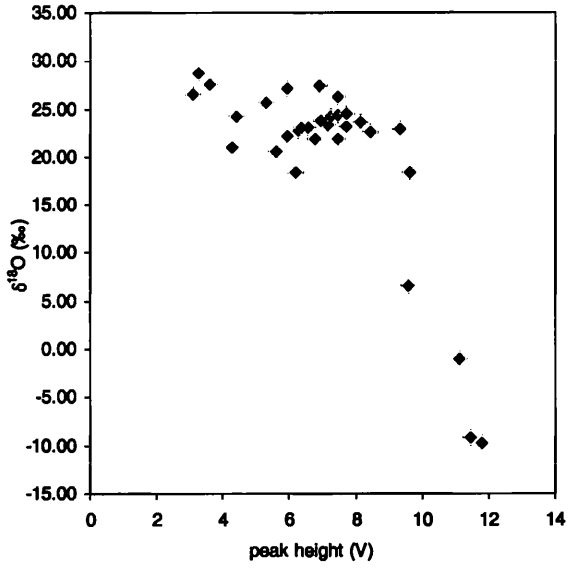

Figure 6.21 plot of $\delta^{18}O$ versus the peak height of CO_2 to find peaks over the saturation of the detector

Some samples (e.g. bag 420) showed low reproducibility on repeat injections. Some bas returned 2 $\delta^{13}C$ results within error, and a third distant by few ‰, for example bags 507 and 427. Means of all usable $\delta^{13}C$ values were compared to the CH_4 concentration measured by GC-FID (Table 6.6). Isotope dilution plots were generated and results are shown in Figure 6.22.

Table 6.6 Summary of data from Table 6.5, showing mean and standard deviation of $\delta^{13}C$ values

bag	Dose (kg/ha)	CH_4 conc. (ppb)	mean $\delta^{13}C$ (‰)	std dev σ
503	50 continuous	2514	-54.8	0.3
514	50 continuous	3733	-59.4	n/a
535	50 continuous	2707	-56.8	1.4
515	50 single	3012	-59.3	0.05
432	50 single	3368	-58.0	1.4
427	50 single	2203	-51.0	2.2
420	Ambient	2000	-46.2	2.4
429	Ambient	2014	-50.5	1.1
473	control	2386	-54.2	1.6
507	control	2744	-58.1	0.2
428	control	4424	-61.9	n/a

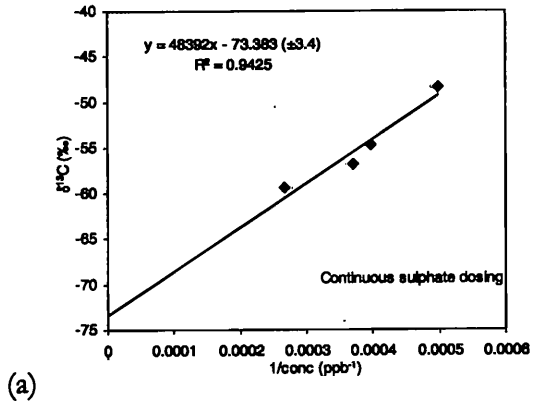

(a)

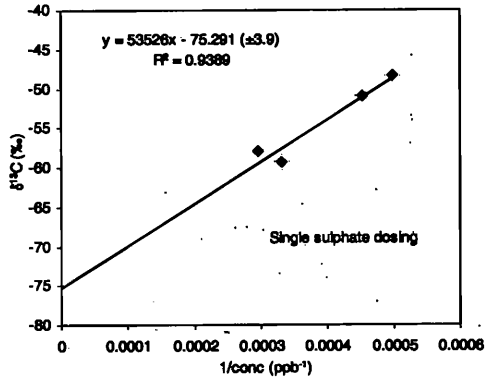

(b)

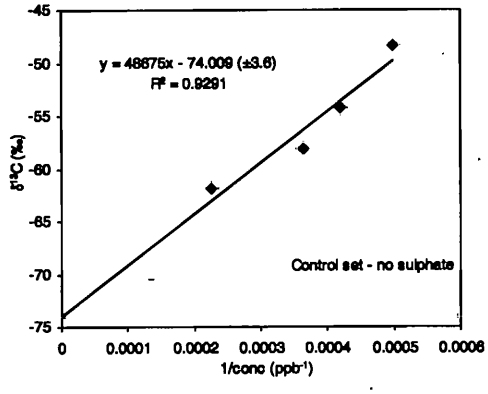

(c)

Figure 6.22 Isotope dilution plots of each sample set taken in the preliminary study (a) continuous sulphate dosing set, (b) single dose set, (c) control set. The intercept error is one standard error

Table 6.7 Methane isotopes emitted by methanogens under three different sulphate addition environments.

Sample set	$\delta^{13}C_{PDB}$ of CH_4 (‰)
Control set	-74.0 ± 3.6
Single dose	-73.4 ± 3.4
Continuous dose	-75.3 ± 3.9

The graphs show that there is no significant difference in $\delta^{13}C$ of CH_4 by adding sulphate to the peat cores. The correlation coefficients are high, giving the impression of good linearity with the different cores. Any difference is within the error returned by the linear extrapolation. Data in Figure 6.22, suggest that no difference in the isotopic composition of the methane emitted was observed when sulphate reducers have more of substrate compared to the control.

The option was open to pursue the study, to a larger scale, combining CH_4 isotope measurements with cores kept at different temperatures, with and without sulphate addition. Although pursuing the full scale investigation may not have yielded any more isotope shifting effects, it involved three different temperatures, and different $\delta^{13}C$ values may be expected, resulting from varying reaction pathways.

The decision was taken to proceed with the full analysis of the cores, using principally the same method as used during the preliminary study.

6.5.4. Full scale analysis with examination of temperature effects on $\delta^{13}C$ of CH_4

In this experiment series, the same core samples had previously been used to investigate the effects of temperature on $\delta^{13}C$ (CH_4) and examine any variation from sulphate addition. As shown in the previous section, no significant $\delta^{13}C$ change with sulphate addition was found at 10°C. However, this study aims to investigate if temperature may show some fractionation differences. 24 cores were separated into 3 groups, which were stored at either 5, 15, or 20°C. Each of the groups were further separated into two sub-groups, with one set of four cores receiving a single dose of sulphate while the other four were left as the control. Four samples of

ambient air were also taken. All the samples were transported to PSRI for analysis using the same SKC plastic bags as in the preliminary study.

6.5.5. Results from major sample collection

The results of $\delta^{13}C$ analysis of CH_4 are displayed in Table 6.8. The resultant mean $\delta^{13}C$ was filtered for obviously spurious results. Observing the results from this sample series it was seen that some sample bags provided two coinciding $\delta^{13}C$ values, with a third value 3 to 5‰ distant. These values were removed from mean measurements. The use of low $\delta^{18}O$ values as an indicator of errors within peak area calculations was not as effective for this sample series. In some cases $\delta^{13}C$ values that were out (compared to other values from the same bag) by over 3 ‰ were accompanied by acceptable $\delta^{18}O$ values. In other cases, another injection from the same sample yielded acceptable $\delta^{13}C$ but unacceptable $\delta^{18}O$. For this reason, more emphasis was placed on $\delta^{13}C$ reproducibility for data filtering.

Table 6.8 Collated data from analysis of air samples from headspace chambers in the full-scale experiment. Individual $\delta^{13}C$ measurements not shown. [CH_4] indicates concentration of CH_4 in the samples

Temperature (°C)	Treatment (kg/ha)	Bag#	[CH4] ppb	$\delta^{13}C$ filtered mean (‰)	$\sigma_{(n-1)}$
5	0	429	2225	-54.1	0.7
5	0	473	2071	-49.6	0.1
5	0	503	2435	-54.1	0.7
5	0	515	2519	-58.5	0.4
5	50	427	2396	-58.0	1.5
5	50	507	2291	-55.0	0.6
5	50	514	2041	-50.4	0.7
5	50	535	2766	-56.3	1.1
15	0	219	2386	-57.0	0.6
15	0	479	3786	-59.8	0.6
15	0	482	2391	-54.6	0.2
15	0	536	2238	-57.3	0.2
15	50	423	2300	-57.3	0.8
15	50	432	2452	-59.2	0.1
15	50	561	3101	-58.8	1.0
15	50	564	2059	-52.4	0.2
20	0	107	5449	-66.3	n/a
20	0	203	3363	-62.4	0.1
20	0	462	4138	-65.6	0.2
20	0	467	3160	-65.4	0.2
20	50	422	4385	Error in injection	
20	50	436	3821	-66.4	n/a
20	50	448	2554	-56.0	n/a
20	50	474	4465	-65.7	0.7
mean ambient		4 bags	1982	-50.1	1.4

Using the results in Table 6.8, isotope dilution plots can be created for the six differing sample sources. In addition, by combining the data for the treated and untreated cores, general trends of variation of $\delta^{13}C$ with temperature can be observed. The error shown in the intercept value is the 1σ standard error.

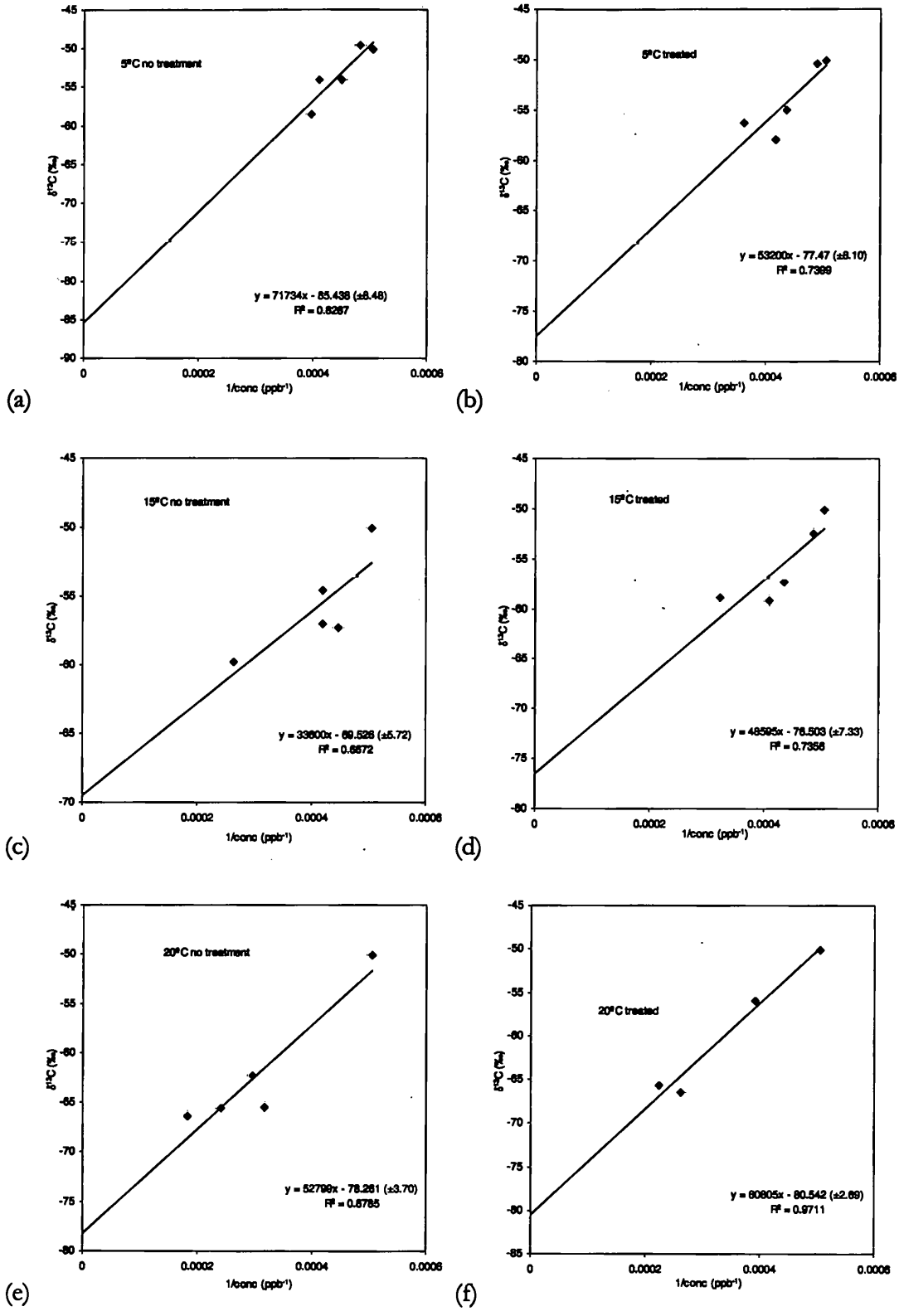

Figure 6.23 Isotope dilution plots of each sample set taken in the full scale study (a) core at 5°C – no sulphate, (b) core at 5°C – sulphate added, (c) core at 15°C – no sulphate, (d) core at 15°C – sulphate added, (e) core at 20°C – no sulphate, (f) core at 20°C – sulphate added. The intercept error is one standard error

All of the plots in Figure 6.23 show a linear trend of $\delta^{13}C$ with the reciprocal of concentration, which suggests the additional methane in the samples is from the same bacterial source. Increasing core temperature generally leads to greater concentrations of CH_4 in the collected air samples. The correlation coefficient displayed gives an indication of the fit of the data to a line. The correlation coefficient values from the preliminary experiments (R^2=0.92-0.94) are higher than most of the lines in this series, indicating a larger spread (in reciprocal concentration) of points, which is probably due to the smaller concentrations of CH_4 in these samples. A summary of the $\delta^{13}C$ of the methane emitted is shown in Table 6.9.

Table 6.9 Carbon isotopes from methane emitted by methanogens under six different sulphate addition conditions

Sample set	Intercept $\delta^{13}C$ (‰)	1σ Standard error in intercept $\delta^{13}C$ (‰)	R^2 correlation coefficient
5°C control	-85.4	8.5	0.83
5°C treated	-77.5	8.1	0.74
15°C control	-69.5	5.7	0.67
15°C treated	-76.5	7.3	0.74
20°C control	-78.3	3.7	0.88
20°C treated	-80.5	2.7	0.97

The most obvious trend in Table 6.9 is that the standard error decreases with increasing temperature. Methane flux is generally proportional to core temperature, thus more CH_4 was present in the atmosphere over the samples held at 20°C, leading to larger peaks, and hence higher precision. A plot of the temperature dependence of this error is shown in Figure 6.24.

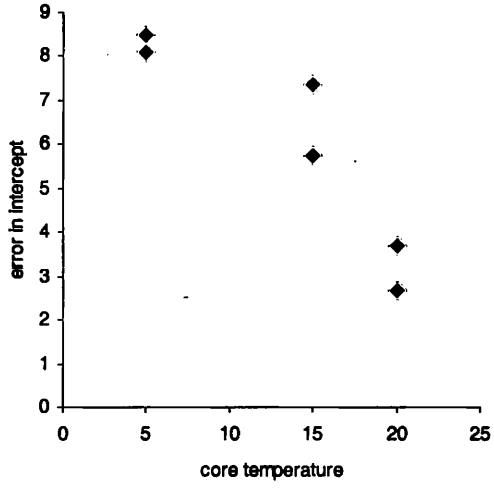

Figure 6.24 Plot of error of intercept in isotope dilution plot versus core temperature

The source of error is likely to be the difficulty in measuring a small amount of emitted CH_4 on top of the large ambient background. By examination of Table 6.8, it can be seen that only the 20°C samples produced CH_4 concentrations that are double in size to that of ambient samples. The total spread of $\delta^{13}C$ intercepts give a range of 16‰. However, on closer examination one sample set (15°C control) has a $\delta^{13}C$ value 7‰ higher than the next nearest value. The five other intercept $\delta^{13}C$ values appear to lie within the range of the largest standard error. The Finnish samples contained much higher concentrations of CH_4, and hence the standard error on the intercept of the isotope dilution plot is much lower.

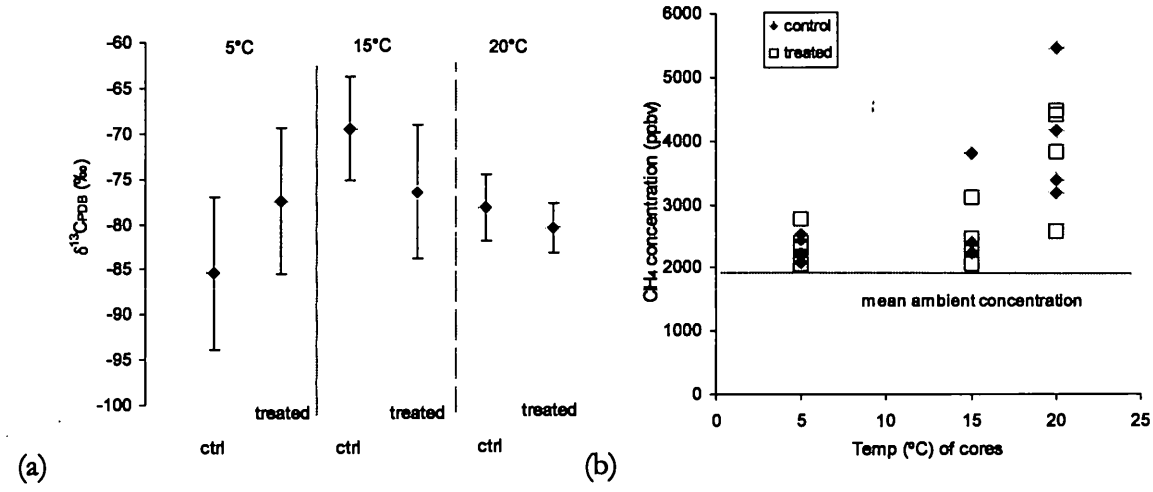

Figure 6.25 (a) $\delta^{13}C$ of methane from the six peat core regimes with associated errors, (b) variation of methane concentration of control and treated samples with storage temperature

The large errors of the $\delta^{13}C$ values spoil the validity of the data. Even the highest temperature samples show relatively large errors in the $\delta^{13}C$ intercepts (Figure 6.25 (a)). No pattern is evident between differences in control and sulphate treated cores. The lightest carbon isotope measurement is from the lowest temperature, with the possibility of lower reaction rates producing this shift in carbon isotope ratios. The heaviest carbon isotope ratio measured was present in the control sample kept at 15°C (-69.5 ‰) which is significantly different from the treated one at that temperature, as well as the other samples. The difference between concentration of mean control and treated samples may give an indication of an alternative favoured pathway.

Analysis by GC-FID by V. Gauci at ITE, Edinburgh, showed that methane concentration within the samples increased with temperature. It can be shown that the addition of sulphate to the cores results in reduced emission of CH_4 but the degree of inhibition is temperature dependent. At 5°C mean inhibition is negligible, but at 15°C the mean treated sample CH_4 concentration is 8 % lower than the control and at 20°C it is 5 % (Figure 6.25 (b)). The effect on temperature on methane inhibition via sulphate has been discovered and studied in detail through a major sampling campaign performed by V. Gauci (*pers. comm,1998*). He found a

strong relationship between temperature and inhibition, suggesting that it is unlikely that the concentration dip at 15°C is reproducible and significant.

The highest temperature samples show the lowest spread in $\delta^{13}C$ measurement. The difference between the control and treated results at 20°C is within the deduced experimental (standard) error of both intercept points. Therefore little conclusions can be drawn from this difference in $\delta^{13}C$. The large errors in $\delta^{13}C$ measurements of the 5°C samples also make the $\delta^{13}C$ intercepts difficult to interpret. The isotope dilution plots can be redisplayed for comparison of all three temperature sets (Figure 6.26), and also to show each of the six individual groups (Figure 6.27).

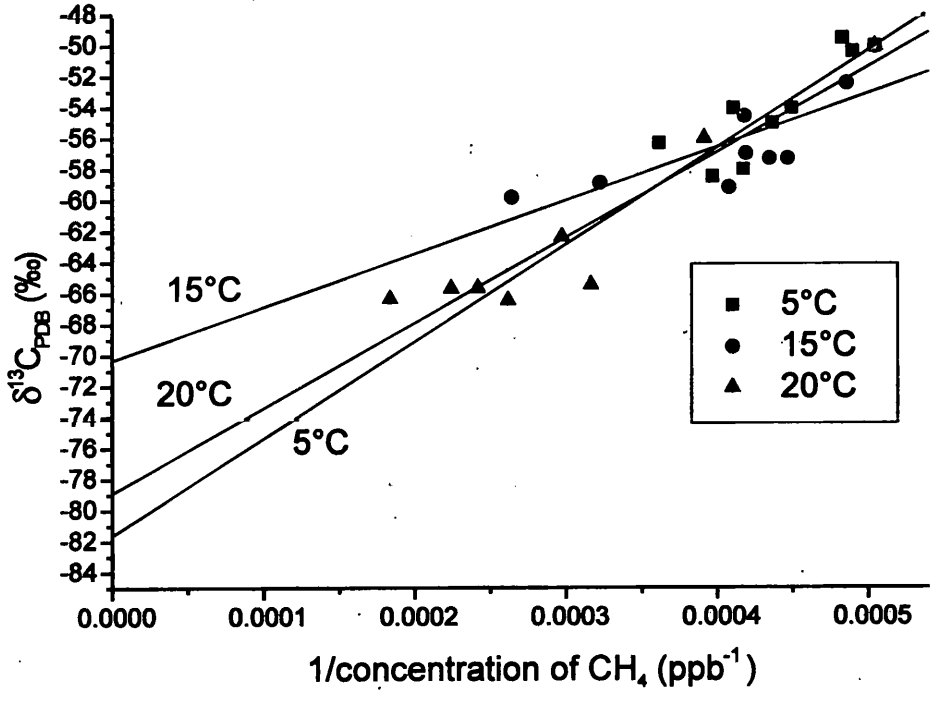

Figure 6.26 Isotope dilution plots for combined results of treated and untreated samples at different temperatures

By examination of Figure 6.26 the sources of the standard error of the intercept become visible. The 5°C samples have a low spread of concentration, which causes the large standard error in the intercept. On the 15°C series it is evident that the two highest concentration measurements influence the intercept most. However there is a definite shift in $\delta^{13}C$ from the 20°C samples at similar concentrations. The measurements from 20°C core samples have the largest range of

CH_4 concentrations, which directs the low standard error for the extrapolated intercept. From visual examination of the graph, the difference in the intercept of the 15°C and 20°C samples appears to be significant, and the values are shown in Table 6.10.

Table 6.10 mean $\delta^{13}C$ from combined treated and untreated air samples from three temperature sets

Sample set	Intercept $\delta^{13}C$ (‰)	1σ Standard error in intercept $\delta^{13}C$ (‰)	R^2 correlation coefficient
5°C combined	-80.7	6.1	0.73
15°C combined	-70.3	4.2	0.62
20°C combined	-78.9	2.6	0.88

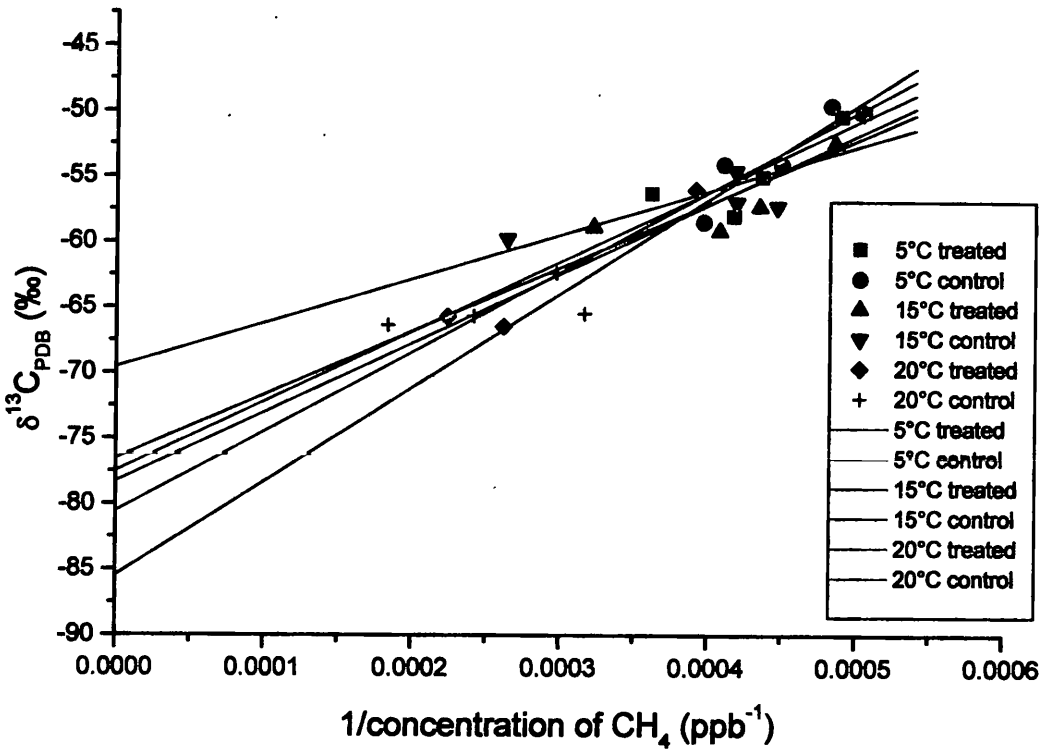

Figure 6.27 Isotope dilution plot for all six treated and untreated sample sets with regression lines for each set (Figure 6.23 combined plots)

Figure 6.27 shows the linear fits of all the individual plots from Figure 6.23 onto one graph. It shows the variation in concentration from the individual test regimes, and also serves as a tool to discover the source of errors on the intercepts from linear regression. One must note that the lowest concentration point (highest value on the reciprocal concentration scale) is the mean

ambient air analysis, and is present in all the linear fits. The intercepts of four of the lines fall into a 4‰ window, leaving two outliers, the 5°C control and the 15°C control samples. By examination of the 15°C control sample points the intercept seems to be defined by the $\delta^{13}C$ of the highest concentration sample (3.8 ppmv), whereas the points at the lower concentrations (2.3 ppmv), still show a spread in $\delta^{13}C$ values.

6.5.6. Summaries of both methane experiments

As far as is known, these are the first $\delta^{13}C$ data of CH_4 from experiments involving sulphate addition to soil. To gain detailed information of the processes in the methanogen/sulphate reduction system, more samples would have to be analysed, preferably by using samples collected over a time period on the same core. The primary improvement to the technique would be to ensure that much higher concentrations of methane are present in the samples. No repeatable pattern was present between $\delta^{13}C$ values of treated and untreated samples. If the behaviour at 15°C is truly unusual, then high-resolution temperature experiments must be performed. The preliminary study gave indication that no difference in the carbon isotopic composition of the emitted methane was present (at the 3‰ level) between treated and untreated samples. If this condition is applied to a further study, the combined treated and untreated samples can be analysed as pooled, as is shown in Figure 6.26. Although the standard errors on the intercept are large, the peculiarity of the $\delta^{13}C$ intercept result 15°C appears to be worthy of further investigation.

6.6. Summary and Conclusions

This chapter described the development of a new inlet system for $\delta^{13}C$ measurement of atmospheric methane. Instead of using a GC to separate the atmospheric components, a series of chemical traps and oxidation units were used, making the analysis faster, from 15 minutes to 8 minutes. Many configurations were tested to provide the ability of dealing with large gas samples. A backflush addition of helium eliminated any atmospheric leakage within the system,

while a large volume of He was placed upstream of the sample loop to eliminate the introduction of contaminant air.

Carbosorb and magnesium perchlorate were used to remove CO_2 and water respectively from the air sample. NiO/Pt at 1000°C was chosen for use as the oxidant for methane. Testing with N_2O showed that the oxidant was able to oxidise atmospheric N_2O to other nitrogen oxides, thereby negating the need for chromatographic separation of the components with interfering mass. The partial removal of O_2 using a chemical O_2 trap prevented the formation of N_2O from N_2 oxidation. A switchable trap was installed for instant evaluation of the N_2O reaching the mass spectrometer. The reagents tested for CO oxidation did not perform well when exposed to 300 ml of air. The potential of PdO (sponge) to be used as an alternative to NiO/Pt was demonstrated but not fully investigated.

The system was demonstrated with samples from wetlands in Finland. By use of isotope dilution plots a correction was performed for background air. The $\delta^{13}C_{PDB}$ of the CH_4 collected was found to be -88.7 ± 1.6 ‰.

An experiment has been carried out to measure $\delta^{13}C$ changes in CH_4 emitted from peat cores. A small scale trial was started in which the peat cores were kept under similar conditions, but with three different treatments applied. Analysis of the methane collected showed no difference (within experimental error) in $\delta^{13}C$ from CH_4 from the three sets.

The further experiment involved comparing an the effect of the addition of sulphate onto the $\delta^{13}C$ of bacterially emitted methane within soil core samples with control at different temperatures. The collected air samples containing methane was analysed and found to have $\delta^{13}C$ with a large error when corrected for background air. This error was due to the relatively low concentration of CH_4 in the samples. No pattern was evident in $\delta^{13}C$ between treated and untreated samples. The highest $\delta^{13}C$ values were seen from methane from cores at 15°C, while the lightest $\delta^{13}C$ was observed from samples kept at 5°C and untreated. However, the $\delta^{13}C$

values returned from each sample series have such large uncertainties that comparisons with other data may be invalid.

In any future application of the technique to other air samples, the concentration of CH_4 within such samples should be as high as the experiment allows. With such samples true fast and precise $\delta^{13}C$ analysis can be performed.

7. CONCLUSIONS

7.1. Technical Summary

This thesis describes work undertaken for the development of sections of the MODULUS instrument on Rosetta. Before the start of the project, the many potential chromatographic columns to be used on MODULUS remained untested for the application. In addition, the temperatures required for sample pre-treatment were beyond the heating ability of the power sources. As an immediate application for the technique investigated for MODULUS, novel methods for analysing the $\delta^{13}C$ of atmospheric CH_4 were investigated, whose complicated inlet systems and/or long analysis times had been used previously.

The construction of a gas transfer system was necessary to enable testing of catalysts and GC columns. This consisted of a steel vacuum manifold and vacuum pumps, and 6-port valves for the interface between vacuum and helium carrier gas. Both ion trap and isotope ratio mass spectrometers were interfaced to the same vacuum system, allowing qualitative analytical identification and isotope ratio measurement of an individual sample. The manifold also allowed the storage of test gases used in the project.

Four gas chromatographic columns were evaluated for the separation of volatile compounds, namely N_2, O_2, CO, CO_2, CH_4 and H_2. The separation ability of the columns was tested from ambient temperatures to -30°C. Vibration testing was performed on the columns for Rosetta spacecraft qualification. The separation ability of all the columns was unchanged following the vibration test after reconditioning, in contrast to conventional expectations of PLOT columns. The two columns that were recommended for use in MODULUS were J&W Scientific's CarbonPLOT for best CH_4-CO_2 separation, and Restek Corporation's Molecular Sieve 5Å for separation of all the stated compounds but with permanent retention of CO_2.

Downstream of the GC columns on MODULUS lie combustion reactors for the conversion of organic compounds to CO_2 for $\delta^{13}C$ analysis. Low temperature equivalents of the oxidants CuO and NiO were sought to fulfil the MODULUS experimental conditions. Approximately 60 reagents were tested for combustion ability of CO and CH_4 at low temperatures. The temperature of quantitative combustion was measured and the lowest combustion temperatures were observed in Rh_2O_3, PdO, Au/MnO_x, $CoCrO_x$, and the mixture $Ag_2O + Au/Fe_2O_3$.

Quantitative combustion does not imply absence of isotopic fractionation. Stable carbon isotopes of combusted CO and CH_4 were measured using a Finnigan MAT Delta C mass spectrometer at various temperatures. The inaccuracy in $\delta^{13}C$ caused by the combustion process must be lower than the precision of the mass spectrometer on MODULUS. Using Rh_2O_3 or PdO between 400-500°C to combust CH_4 would preserve adequate isotopic integrity. The power saving of using either of these oxides instead of the proposed NiO at 1150°C would allow MODULUS to analyse more cometary samples. The combustion behaviour of CO was evaluated both for its own sake, but also to simulate easily oxidised hydrocarbons, with $CuCrO_x$ and Rh_2O_3 giving adequate isotopic integrity between 100 and 300°C. This contrasts to the MODULUS's original proposed method of using CuO at 600°C. No catalyst preserved the isotopic integrity of the original CH_4 sample better than the standard laboratory method (NiO at 1150°C for CH_4).

Using an inlet system developed for experiments relevant to MODULUS, a novel faster method was developed to analyse methane at ambient concentrations. Samples were stored and transferred using the vacuum system explained in Chapter 2. By isolating combusted methane from the rest of the atmospheric gases, the need for gas chromatography was eliminated. This approach reduces duration of analysis. The method was tested by examining methane produced by soil bacteria. Isotope dilution plots were used to correct for mixing of bacterial methane with atmospheric methane. One experiment showed no perceptible change in the $\delta^{13}C$ value

produced by methanogens once sulphates were added to the soil. Another experiment examined temperature variations in methane $\delta^{13}C$ when sulphate was added. An anomaly was found where soil kept at 15°C produced methane with $\delta^{13}C$ of 6‰ greater than cores kept at 5°C and 20°C. However, this could be attributed to uncertainty in the atmospheric calibration process.

7.1.1. Further Work

The most obvious enhancement to the work conducted in this thesis would be to use a lab model of MODULUS for GC testing. Testing of suitable chromatographic columns would be advantageous if performed within in the developed mass spectrometer. This should be conducted in an evacuated chamber, as the MODULUS instrument does not have an active pump (instead the ion trap will be directly open to the vacuum of space). This approach would allow any artefacts from MODULUS' novel injection system to be investigated.

The list of metal oxides tested for combustion is by no means exhaustive. Small changes in the preparation methods for any oxide can cause great changes in their surface properties, which influence combustion ability. In a further study, one could examine all different preparation methods of the viable reagents and find the most active compound. Other volatile compounds would be tested, especially species commonly detected in comets. A catalyst must also be created to ensure minimal damage of the active surface by poisoning agents, as there is a possibility of catalyst poisoning by halides or sulphides.

Only a few of the viable catalysts were tested for isotopic shifts during combustion. Others may introduce less uncertainty than the materials tested in Chapter 5. A greater number of combustions of CH_4 and CO would constrain the uncertainty more accurately. Effect of flow rate and impure samples on isotopic integrity could also be analysed. It was hoped that one of the catalysts tested would offer similar performance to NiO at 1150°C but at a lower temperature. The replacement could then be used in laboratories analysing $\delta^{13}C$ of atmospheric

methane as in Chapter 6. Other, as yet uncategorised catalysts may still fulfil this role. Both test gases used, CO and CH_4, should have their isotope ratios measured by a different laboratory. The reagent commonly used to convert ambient CO to CO_2, (I_2O_5) should also be tested under the same protocol.

The analysis method developed in Chapter 5 does not currently produce very high precision results. More testing could improve the precision delivered by slight modifications to the inlet system. Calibration of the system using a CH_4 carbon isotope standard would also verify the $\delta^{13}C$ values produced during analysis. The new method must be further validated before air samples from other laboratories can be obtained and analysed. For the greatest precision of $\delta^{13}C$ measurements, samples must contain at least twice the ambient concentration of CH_4 in air.

The laboratory housing the Finnigan MAT Delta C mass spectrometer also contains the static mass spectrometer that measures dual isotope ratios of methane. Splitting an air sample could be easily performed via a capillary, linking both machines to analyse the same sample. Combining the isotope ratios from both instruments would allow both $\delta^{13}C$ and D/H to be returned from each air sample.

Results from the sulphate reduction experiment displayed a lack of a range of methane concentrations. This could be addressed by changing the sampling method, so that multiple air samples can be withdrawn from the same core at set time intervals. Samples collected after many hours should contain a greater concentration of methane with the same isotope ratio. Measurements from multiple samples would allow greater accuracy in determination of the true $\delta^{13}C$ of the emitted methane (via isotope dilution plots).

LIST OF SUPPLIERS AND MANUFACTURERS

Aalborg, Ltd
Cole-Parmer Instrument Company (UK), Unit 3, River Brent Business Park, Trumpers Way, Hanwell, London W7 2QA

Air Products Plc
Weston Road, Crewe, Cheshire, CW1 1BT

Aldrich Chemical Company
The Old Brickyard, New Road, Gillingham, Dorset, SP8 4XT

Alltech Associates Applied Science Ltd
Units 6-7, Kellet Road Industrial Estate, Kellet Road, Carnforth, Lancashire, LA5 9XP

Bambi Air Compressors Ltd
Bradbourne Drive, Tilbrook, Milton Keynes, Bucks, MK7 8AZ

Edwards High Vacuum International
Manor Royal, Crawley, West Sussex, RH10 2LW

Elemental Microanalysis Ltd
Okehampton Business Park, Okehampton, Devon, United Kingdom, EX20 1UB

Engelhard – Clal, Italy
Via Ronchi, 17, 20134 MILANO

Europa Scientific
Europa House, Electra Way, Crewe Business Park, CW1 1ZA

Eurotherm Controls Ltd Head Office (Controls)
Faraday Close, Durrington, Worthing, West Sussex, BN13 3PL

Finnigan MAT
Paradise, Hemel Hempstead, HP2 4TG

Agilent / Hewlett-Packard Ltd
Chemical Analysis Group, Heathside Park Road, Cheadle Heath Stockport, Cheshire, SK3 0RB

J&W Scientific Incorporated,
91 Blue Ravine Road, Folsom, California, 95630-4714 USA

MKS Instruments (Scotland) Ltd.,
Delta House, Carmondean Centre South, Livingston, West Lothian EH54 8PT

Multi Lab
High St. Newburn, Newcastle on Tyne, NE15 8LN, Newcastle

North London Valve and Fitting Co. Ltd
34 Capitol Way, Capitol Industrial Park, London, NW9 0EQ

Precision Dynamics, Inc.
c/o All Air Incorporated, 175 Clearbrook Road, Elmsford, NY 10523, USA

RS Components Ltd
PO Box 99, Corby, Northants, NN17 9RS

SAES Getters (GB) Ltd
5 Southern Court, South Street, Reading, Berkshire, RG1 4QS

Scientific Glassware Engineering (UK) Ltd (SGE)
1 Potters Lane, Kiln Farm, Milton Keynes, Bucks, MK8 0AN

SMC Pneumatics (UK) Ltd
Vincent Avenue, Crownhill, Milton Keynes, Bucks, MK8 0AN

Thames Restek UK Ltd
Fairacres Industrial Centre, Dedworth Road, Windsor, England, Berkshire SL4 4LE

Varian Associates Ltd
28 Manor Road, Walton-on-Thames, Surrey KT12 2QF

Varian Chrompack International (UK) Ltd
Unit 4, Indescon Court, Millharbour, London, E14 9TN

LIST OF ACRONYMS AND ABBREVIATIONS

AGC	Automatic Gain Control
a.m.u.	atomic mass unit
CDOS	Concurrent DOS
CF-irMS	Continuous Flow – isotope ratio – Mass Spectrometry
CHON	Carbonaceous particles containing carbon, hydrogen, oxygen and nitrogen
d.c.	Direct current
E.C.D.	Electron Capture Detector
EI	Electron Impact
F.I.D	Flame Ionisation Detector
GC	Gas Chromatography
GC/C/irMS	Gas Chromatography – Combustion – isotope ratio Mass Spectrometry
GCirMS	Gas Chromatography isotope ratio Mass Spectrometry
GC-ITD	Gas Chromatograph – Ion Trap Detector
GirMS	Gas isotope ratio Mass Spectrometry

IPCC	Intergovernmental Panel on Climate Change
i.d.	Internal diameter
irMS	isotope ratio Mass Spectrometry
ITD	Ion Trap Detector
ITE	Institute of Terrestrial Ecology
MFC	Mass Flow Controller
MODULUS	Methods Of Determining and Understanding Light-elements from Unequivocal Stable isotope compositions
NASA	National Aeronautical and Space Administration (USA)
NBS	National Bureau of Standards(USA)
NIST	National Institute of Standards and Technology (USA)
NLV	North London Valve and Fitting Co. Ltd
o.d.	Outside diameter
OU	The Open University
OSC	Oxygen Storage Component
PLOT	Porous Layer Open Tubular
ppbv	parts per billion by volume
ppmv	parts per million by volume

PSRI	Planetary Science Research Institute, The Open University
PSSRI	Planetary and Space Sciences Research Institute, The Open University
sccm	standard cubic centimetres per minute
TDL	Tuneable Diode Laser
TDLAS	Tuneable Diode Laser Spectroscopy
V-PDB (or PDB)	(Vienna-) PeeDee Belemnite
V-SMOW (or SMOW)	(Vienna-) Standard Mean Ocean Water
WCOT	Wall Coated Open Tubular

OXYGEN ISOTOPE EXCHANGE OF CO_2 OVER NOBLE METAL / CERIA AND NICKEL OXIDE / PLATINUM CATALYSTS

Introduction

Metal oxides can provide a substrate for the chemisorption of volatile compounds. Some metal oxides have high affinity for compounds that are chemisorbed, and react with the surface at high rates. The affinity of such compounds with the surface can be examined by the use of isotope tracers – volatile compounds with higher than normal rare isotopes. For example, the surface properties of Molybdenum oxide can be measured by the oxidation of $^{12}C^{18}O$, via the detection of the combustion products ($^{12}C^{18}O_2$, and $^{12}C^{16}O^{18}O$) (Iizuka, 1994). Passing labelled O_2 over multiples of oxides has been used to examine the kinetics of the exchange reaction (Winter, 1958) and surface ion mobility (Duprez, 1997). Labelled oxygen in CO, H_2O, CO_2 and O_2 have all been used. By the use of isotope ratio mass spectrometry, the use of expensive labelled volatiles can be avoided. As long as the isotope ratio of oxygen in the oxide and volatile compound are different, then irMS can detect exchange properties.

During the course of the project, there were opportunities of testing CO_2 oxygen exchange with two oxides, Rh/Pd doped Ceria, and NiO/Pt. The latter was investigated in-between some other samples, hence this sample was not investigated to the same extreme as the ceria compound.

Experimental – Ceria catalyst

A sample of Ceria containing Rh and Pd was prepared by Mr. Paul Wynn. The compound had been previously tested for combustion ability in 4.1.29. A few grams of the compound was loaded into a 5 mm i.d. sample tube, and installed into the same catalyst test system as described in Chapter 5. Once installed, the catalyst was heated in the presence of an O_2 flow of 6 ml/min,

between 250 to 750°C. The O_2 cylinder provided gas with isotope ratio of $\delta^{18}O_{SMOW}$ = +26.1‰. In terms of the CO_2 reference gas (working standard) on the Delta C mass spectrometer, the cylinder gas was calibrated to $\delta^{18}O_{WS}$ = +14.6‰.

After some hours the compound was left to cool and the O_2 flow was replaced with the standard helium flow of 60 ml/min. The CeO_2/Pd/Rh compound was heated to 400°C and left to degas until CO_2 blanks were low. Repeated aliquots of CO_2 were measured injected into the mass spectrometer bypassing the ceria compound. The 3-way valves were arranged so that the helium flow from the vacuum system to the mass spectrometer was bypassing the reaction tube.

After multiple measurements of the CO_2's carbon and oxygen isotope ratios, CO_2 from the same aliquotter device was admitted so that it flowed over the CeO_2/Pd/Rh. This was repeated at different catalyst temperatures.

Results – Ceria catalyst

At room temperature, the CeO_2/Pd/Rh permanently adsorbed all the CO_2 that was injected. At elevated temperatures, the affinity for adsorption decayed. At 400°C over 90% of the CO_2 was adsorbed. However, at 600°C and greater permanent CO_2 adsorption was minimal. The carbon and oxygen isotope ratios of the desorbed CO_2 were measured.

Carbon

The bypass carbon isotope ratio was measured to be $\delta^{13}C$ = -39.93 ± 1.06 ‰. The $\delta^{13}C$ of the exchanged CO_2 is shown in Figure c.1.

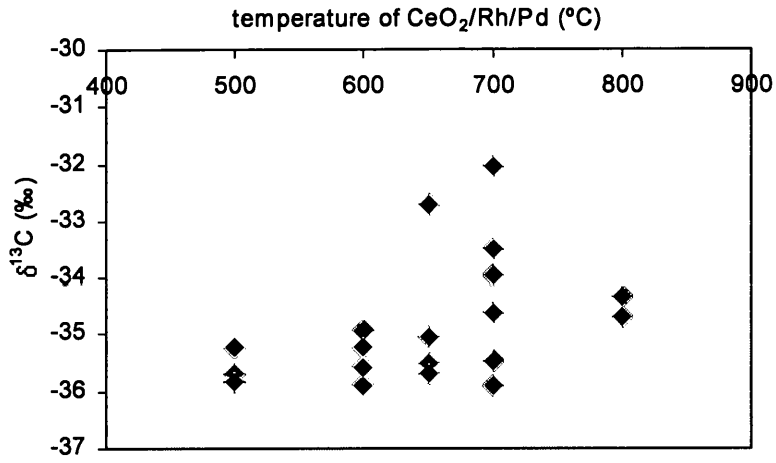

Figure c.1 Carbon isotope ratio of CO_2 exchanged with Ceria/Rh/Pd catalyst

It appears that the carbon does not fractionate appreciably via the exchange process. Values of $\delta^{13}C$ from exchanges at 500 and 600°C are within the error of measurement of the unexchanged CO_2. At 650, 700 and 800°C there seems to be an effect that CO_2 becomes isotopically heavier after exchange. However, these measurements may be an artefact of the presence of pre-peaks seen on the trace (see Chapter 6).

Oxygen

The bypass oxygen isotope ratio was measured to be $\delta^{18}O_{WS} = -0.43 \pm 0.48$ ‰. The $\delta^{18}O$ of the exchanged CO_2 is shown in Figure c.2.

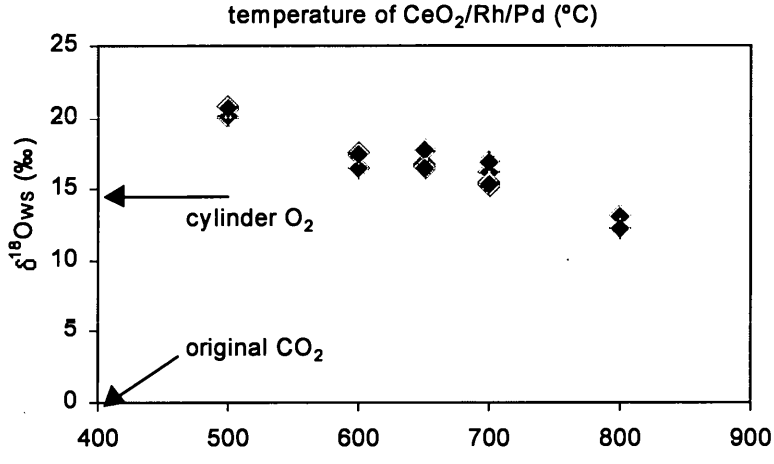

Figure c.2 oxygen isotope ratio of CO_2 exchanged with Ceria/Rh/Pd catalyst

Temperature dependent fractionation of oxygen in CO_2 is obvious from Figure c.2. The $\delta^{18}O$ of the O_2 from the cylinder was +14.6‰. This oxygen probably saturated the available sites of the oxide, covering the sites with oxygen of a specific $\delta^{18}O$. From Figure c.2, fractionation (or possibly oxygen exchange) may have been occurring in both lighter and heavier directions, during the adsorption-desorption process, depending on temperature.

Conclusions – Ceria catalyst

Although some of the CO_2 injections suffered from peak problems when the CO_2 pulse arrived at the mass spectrometer, this does not negate the temperature dependent oxygen fractionation effect detected. The fractionation appears to be linear with temperature. The mechanism of adsorption-exchange-desorption appears to work in both directions. The $\delta^{18}O$ of the CO_2 exchanged with the oxygen from the O_2 cylinder, at higher temperatures the $\delta^{18}O$ of CO_2 was lower than cylinder O_2, but at lower temperatures, the $\delta^{18}O$ was higher than cylinder O_2. Thus, at temperatures lower than 800°C, the lighter oxygen atoms remained on the surface (or desorbed as CO or O_2 which were undetectable). At 800°C the $\delta^{18}O$ shows that the exchanged oxygen fractionated so that lighter CO_2 was desorbed, or that mixing between surface oxygen and oxygen from the original CO_2 occurred.

The order of the CO_2 injection series may have had an influence. First the CeO_2/Rh/Pd was set to 600°C, then 800°C, 700°C, 650°C, and finally 500°C. The compound did not have an O_2 flow re-applied between each temperature series.

Experimental – Nickel Oxide / Platinum catalyst

The method of the exchange of CO_2 was the same as that for the ceria catalyst. Aliquots of CO_2 were passed over the NiO/Pt catalyst, and then bypassed the reactor. Only a few measurements were taken with CO_2 exposure, at 20°C and 800°C. The sample was the same as that used in 5.2.1.

Results – Nickel Oxide / Platinum

The carbon, oxygen isotopes, and CO_2 peak areas can be seen in Figure c.3.

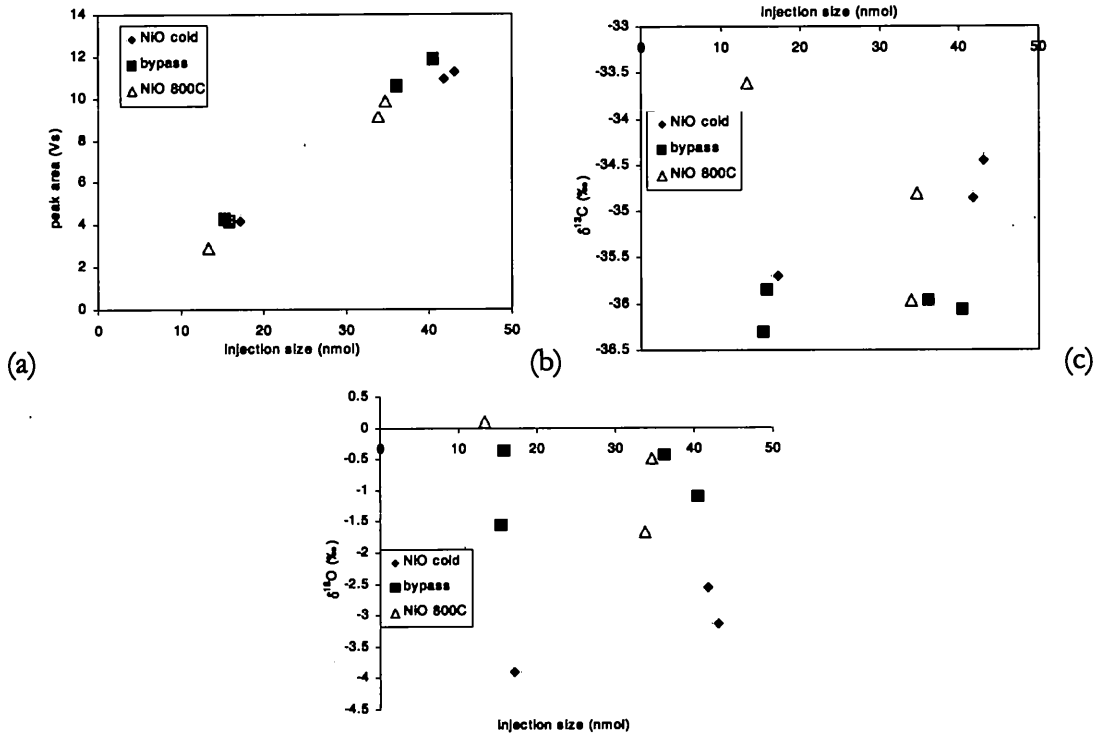

Figure c.3 (a) Peak size of CO_2 injection over/bypassing NiO/Pt and (b) $\delta^{13}C$ of CO_2 recorded in the same run, (c) $\delta^{18}O$ of CO_2 recorded over the same injections

Passing CO_2 over a cold NiO reactor appeared to let CO_2 adsorb onto the oxide surface. There was a marked drop in the peak area expected from the size of injection. Examination of Figure c.3 (b) show that CO_2 bypassing the NiO/Pt gave the most consistent $\delta^{13}C$ values. When the reactor path was selected (via 3-way valves) for the carrier gas then the interaction between the oxide and the CO_2 distorted the carbon isotope ratio, which appeared to get heavier. Oxygen isotope ratios were also seen to be affected by the interaction with NiO/Pt. Figure c.3 (c) shows the variation in observed $\delta^{18}O$ with injection size under different conditions.

Conclusions – Nickel Oxide / Platinum catalyst

Some (<10%) CO_2 was sorbed by the oxide when at room temperature, but not when at 800°C. Repeatability of $\delta^{13}C$ was not high when CO_2 was passed over the catalyst at either temperature. Oxygen isotope exchange only occurred at room temperature.

REFERENCES

Altwegg, K., Balsiger, H., and Geiss, J. (1999). Composition of the volatile material in Halley's coma from in situ measurements. *Space Science Reviews*, **90** (1-2), 3-18.

Arrendale, R. F., Severson, R. F., and Chortyk, O. T. (1984). Open split interface for capillary gas-chromatography mass-spectrometry. *Analytical Chemistry*, **56** (8), 1533-1537.

Aston, F.W. (1919). The possibility of separating isotopes. *The London, Edinburgh and Dublin Philosophical Magazine*, **37**, 523-534.

Attendorn, H. G., and Bowen, R. N. C. (1997). *Radioactive and Stable Isotope Geology*, Chapman & Hall, London.

Baker, L. (1997). *pers comm.* Open split positioning problems, The Open University, Milton Keynes, UK.

Barber, S. J. (1998). Development of a quadrupole ion trap mass spectrometer for the determination of stable isotope ratios: Application to a space flight opportunity. PhD thesis, The Open University, Milton Keynes, UK.

Barrie, A., Bricout, J., and Koziet, J. (1984). Gas chromatography-stable isotope ratio analysis at natural abundance levels. *Biomedical Mass spectrometry*, **11** (11), 583-588.

Becker, R. H., and Pepin, R. O. (1984). The case for a martian origin of the shergottites - nitrogen and noble-gases in EETA-79001. *Earth and Planetary Science Letters*, **69** (2), 225-242.

Becker, R. H., Glavin, D. P., and Bada, J. L. (1997) Polycyclic aromatic hydrocarbons (PAHs) in Antarctic Martian meteorites, carbonaceous chondrites, and polar ice. *Geochimica et Cosmochimica Acta* **61** (2), 475-481.

Behm, R. J., and Brundle, C. R. (1991). On the formation and bonding of a surface carbonate on Ni(100). *Surface Science*, **225** , 327-343.

Bergamaschi, P., Schupp, M., and Harris, G. W. (1994). High precision direct measurements of $^{13}CH_4/^{12}CH_4$ and $^{12}CH_3D/^{12}CH_4$ in atmospheric methane sources by means of a long path tunable doide laser absorption spectrometer. *Applied Optics*, **33** (33), 7704-7716.

Berner, R.A (1985). Sulphate Reduction, organic matter decomposition and pyrite formation. *Philosophical Transactions of the Royal Society of London A*, **A315**, 25-38.

Berry, F. J. (1981). Tin - Antimony Oxide Catalysts. *Advances in Catalysis*, **30**, 97-131.

Biemann, K., Oro, J., and Toulmin, P., Orgel, E., Nier, A. O., Anderson, D. M., Simmonds, P. G., Flory, D., Diaz, A. V., Rushneck, D. R., Biller, J. E. and LaFleur, A. L. (1977). The search for Organic substances and inorganic volatile compounds in the surface of Mars. *Journal of Geophysical Research*, **82** (28), 4641-4657.

Binzel, R. P., Xu, S., Bus, S. J., and Bowell, E. (1992). Origins for the near-earth asteroids. *Science*, **257** (5071), 779-782.

Bogard D. D. and Johnson P. (1983) Martian gases in an Antarctic meteorite. *Science*, **221**, 651-654.

Boice, D., and Huebner, W. (1997). "Comets." in "*Encylcopedia of Planetary Sciences*", Chapman-Hall, London. 115-119.

Bourne, S., and Croasmun, W. R. (1988). Cross-bore open-split interface for gas-chromatography coupled with mass-spectrometry and infrared spectrometry. *Analytical Chemistry*, **60** (19), 2172-2174.

Brand, W. A. (1994). *GC Combustion Interface II manual*, Finnigan Mat, Bremen.

Brenna, J. T., Corso, T. N., Tobias, H. J., and Caimi, R. J. (1997). High-precision continuous-flow isotope ratio mass spectrometry. *Mass Spectrometry Reviews*, **16** (5), 227-258.

Brenninkmeijer, C. A. M. (1993). Measurement of the Abundance of ^{14}CO in the Atmosphere and the $^{13}C/^{12}C$ and $^{18}O/^{16}O$ ratio of atmospheric CO with applications in New-Zealand and Antarctica. *Journal of Geophysical Research-Atmospheres*, **98** (D6), 10595-10614.

Butterworth, A. L. (1997). Determination of the combined isotopic composition of atmospheric methane, PhD thesis, The Open University, Milton Keynes.

Butterworth, A. L. (1999). *pers. comm.* Molsieve 5Å trapping efficiency of CH_4. The Open University, Milton Keynes, UK.

Chang, Y. F., and McCarty, J. G. (1996). Novel oxygen storage components for advanced catalysts for emission control in natural gas fuelled vehicles. *Catalysis Today* **30** (1-3), 163-170.

Conny, J. M., and Currie, L. A. (1996). The isotopic characterization of methane, non-methane hydrocarbons and formaldehyde in the troposphere. *Atmospheric Environment*, **30** (4), 621-638.

Cotton, F., and Wilkinson, G. (1980). *Advanced Inorganic Chemistry - A comprehensive text*, J. Wiley and Sons.

Craig, H. (1957). Isotopic standards for carbon and oxygen and correction factors for mass spectrometric analyses of carbon dioxide. *Geochimica et Cosmochimica Acta*, **12** , 135-149.

Cuif, J. P., Blanchard, G., Touret, O., Seigneurin, A., Marcizi, M., and Quemere, E. (1997). (Ce, Zr)O_2 solid solutions for 3 way catalysts. *Report number 970463*, Rhone-Poulenc.

Dansgaard, W. (1964). Stable isotopes in precipitation. *Tellus*, **XVI** (4), 437-468.

Duprez, D. (1997). Study of surface mobility by isotopic exchange: recent developments and perspectives. *Studies in Surface Science and Catalysis*, **112** , 13-28 .

Ebel, S. (1973). CHN Analysis: principles, possibilities and automation. *Fresenius Zeitschrift für Analytische Chemie*, **16** , 264.

Engel, T., and Ertl, G. (1982). "Oxidation of carbon monoxide." in: "*The chemical physics of solid surfaces and heterogenous catalysis*", King and Woodruff eds., Elsevier, Amsterdam, 73-93.

Farrauto, R. J., Hobson, M. C., Kennelly, T., and Waterman, E. M. (1992). Catalytic chemistry of supported palladium for combustion of methane. *Applied Catalysis A-General*, **81** (2), 227-237.

Gardner, S. D., Hoflund, G. B., Schryer, D. R., Schryer, J., Upchurch, B. T., and Kielin, E. J. (1991). Catalytic behavior of noble-metal reducible oxide materials for low-temperature CO oxidation. 1. Comparison of catalyst performance. *Langmuir*, **7** (10), 2135-2139.

Gauci, V. (1998). *pers. comm.* Inhibition of CH_4 flux from methanogens due to sulphate addition to soil. The Open Univeristy, Milton Keynes, UK.

Gelman, B. G., Zolotukhin, V. G., Mukhin, L. M., Lamonov, N. I., Levchuk, B. V., Lipataov, A. N., Nenarokov, D. F., Rotin, V. A., and Okhotnikov, B. P. (1980). Gas chromatograph analysis of the chemical composition of the Venus atmosphere. *Space Research*, **20**, 219-221.

Gevrey, S., Luna, A., Taphanel, M. H., Tortajada, J., and Morizur, J. P. (2000). Experimental and theoretical studies of the gas-phase reactivity of the $(HO)_2P{=}O^+$ phosphonium ions towards methanol. *International Journal of Mass Spectrometry*, **196** (SISI), 545-563.

Haneda, M., T., M., Kakuta, N., and Ueno, A. (1994). Catalytic and thermal behaviour of cerium oxide supported on SiO_2 and Al_2O_3 for methane combustion. *Bulletin of the chemical society of Japan*, **67**, 2617-2620.

Haruta, M., Ueda, A., Tsubota, S., and Sanchez, R. M. T. (1996). Low-temperature catalytic combustion of methanol and its decomposed derivatives over supported gold catalysts. *Catalysis Today*, **29** (1-4), 443-447.

Haruta, M. T., Kobayashi, S., Kageyama, T., Genet, H., Delmon, M. B. (1993). Low-temperature oxidation of CO over gold supported on TiO_2, α-Fe2O_3, and Co_3O_4. *Journal of Catalysis*, **144** (1), 175-192.

Heck, R. M., and Farrauto, R. J. (1995). *Catalytic Air Pollution Control - Commercial Technology* . John Wiley and Sons, Chichester.

Hein, R., Crutzen, P. J., and Heimann, M. (1997). An inverse modelling approach to investigate the global atmospheric methane cycle. *Global Biogeochemical Cycles*, **11** (1), 43-76.

Hinshaw, J. V., Ettre, L. S. (1994). *Introduction to open-tubular column gas chromatography.* Advanstar Communications, Cleveland, OH.

Hinshaw, J. V., Ettre, L. S. (1993). *Basic relationships of gas chromatography.* Advanstar Communications, Cleveland, OH.

Hoefs, J. (1987). *Stable Isotope Geochemistry*, Springer - Verlag, London.

Hoffman, J. H., and Hodges, R. R, Donahue, T. M and McElroy, M. B. (1980). Composition of Venus lower atmosphere from the Pioneer Venus mass spectrometer. *Journal of Geophysical Research*, **85** (A13), 7882-7890.

Hoflund, G. B., Gardner, S. D., Schryer, D. R., Upchurch, B. T., and Kielin, E. J. (1995). Au/MnO_x catalytic performance-characteristics for low-temperature carbon monoxide oxidation. *Applied Catalysis B-Environmental*, **6** (2), 117-126.

Horacek, J. K., Körbl, J., Pechanec V. (1960). Bestimmung von Kohlenstoff und Wasserstoff in organischen Verbindungen. Wirksamkeit von Verbrennungskatalysatoren II. *Mikrochimica Acta*, 294-298.

Hoyle, F., and Wickramasinghe, N. C. (1986). The case for life as a cosmic phenomenon. *Nature*, **322** (6079), 509-511.

Huebner, W. F. (1990). *Physics and Chemistry of Comets*, Springer-Verlag, London.

Hutchings, G. J., Mirzaei, A. A., Joyner, R. W., Siddiqui, M. R. H., and Taylor, S. H. (1998). Effect of preparation conditions on the catalytic performance of copper manganese oxide catalysts for CO oxidation. *Applied Catalysis A-General*, **166** (1), 143-152.

Hutchings, G. J., Siddiqui, M. R. H., Burrows, A., Kiely, C. J., and Whyman, R. (1997). High-activity Au/CuO-ZnO catalysts for the oxidation of carbon monoxide at ambient temperatures. *Journal of the Chemical Society-Faraday Transactions*, **93** (1), 187-188.

Iizuka, Y. (1994). ^{18}O Tracer Studies of CO Oxidation With O_2 on MoO_3. 1. Diffusion of ^{18}O atoms from active sites during the catalysis and the determination of the number of active-sites. *Journal of the Chemical Society-Faraday Transactions*, **90** (9), 1301-1306.

IPCC. (1994). Climate Change - radiative forcing of climate change., Intergovermental Panel on Climate Change.

Jackson, S. M. (1998). An investigation of the combined stable isotopic composition of methane emissions from northern wetlands, PhD thesis, The Open University, Milton Keynes, UK.

Kainz, G., and Horwatitsch, H. (1960). Über sehr wirksame Rohrfüllungen zur C-H-Bestimmung. *Fresenius Zeitschrift für Analytische Chemie*, **177** , 321-327.

Kainz, G., and Horwatitsch, H. (1962). Über die unterschiedliche Wirksamkeit oxydischer und metallischer Katalysatoren bei der C-H- und N-Analyse. *Mikrochimica Acta*, **1-2**, 7-15.

Keller, H. U. (1990). "The Nucleus." in "*Physics and Chemistry of Comets*", W. F. Huebner ed., Springer Verlag, London, 13-68.

Keller, H. U., Delamere, W. A., Huebner, W. F., Reitsema, H. J., Schmidt, H. U., Whipple, F. L., Wilhelm, K., Curdt, W., Kramm, R., Thomas, N. (1987). Comet P/Halley's nucleus and its activity. *Astronomy and Astrophysics*, **187**, 807-823.

Kissel, J., and Krueger, F. R. (1987). The organic-component in dust from comet Halley as measured by the PUMA mass-spectrometer on board VEGA-1. *Nature*, **326** (6115), 755-760.

Körbl, J. (1956). Verwendung des thermischen Zersetzungsproduktes von Silberpermanganat in der organischen elementaranalyse. *Mikrochimica Acta*, **11**, 1705-1721.

Kührt, E., Knollenberg, J., and Keller, H. U. (1997). Physical risks of landing on a cometary nucleus. *Planetary and Space Science*, **45** (6), 665-680.

Laine, J., Albornoz, A., Brito, J., Carias, O., Castro, G., Severino, F., and Valera, D. (1987). "Development of a copper chromite catalyst for carbon monoxide automobile emission control." in "*Catalysis and automotive pollution control*", A. Crucq and A. Frennet, eds., Elsevier, Amsterdam, 387-393.

Langmuir, I. (1922). The mechanism of the catalytic action of platinum in the reactions 2CO + O_2 = $2CO_2$ and $2H_2$ + O_2 = $2H_2O$. *Transactions of the Faraday Society*, **17**, 621-675.

Leckrone, K. J., and Hayes, J. M. (1998). Water-induced errors in continuous-flow carbon isotope ratio mass spectrometry. *Analytical Chemistry*, **70** (13), 2737-2744.

Ligon, W. V., and Grade, H. (1991). Adjustable open-split interface for gas-chromatography mass-spectrometry providing solvent diversion and invariant ion-Source pressure. *Analytical Chemistry*, **63** (20), 2386-2390.

Lowe, D. C., Brenninkmeijer, C. A. M., Brailsford, G. W., Lassey, K. R., Gomez, A. J., and Nisbet, E. G. (1994). Concentration and ^{13}C records of atmospheric methane in New-Zealand and Antarctica - evidence for changes in methane sources. *Journal of Geophysical Research-Atmospheres*, **99** (D8), 16913-16925.

Ma, T. S., and Gutterson, M. (1976). Organic Elemental Analysis. *Analytical Chemistry*, **48** (5), 101R.

Mars, P., and van Krevelen, D. W. (1954). Oxidations carried out by means of Vanadium oxide catalysts. *Special Supp Chem. Eng. Sci*, **3**, 41-59.

Matthews, D. E., and Hayes, J. M. (1978). Isotope ratio monitoring gas chromatography-mass spectrometry. *Analytical Chemistry*, **50** (11), 1465.

McKay, D. S., Gibson, E. K., ThomasKeprta, K. L., Vali, H., Romanek, C. S., Clemett, S. J., Chillier, X. D. F., Maechling, C. R., and Zare, R. N. (1996). Search for past life on Mars: Possible relic biogenic activity in Martian meteorite ALH84001. *Science*, **273** (5277), 924-930.

McKinney, C. R., McCrea, J. M., Epstein, S., Allen, H. A., and Urey, H. C. (1950). Improvements in mass spectrometers for the measurement of small differences in isotope abundance ratios. *Reveiws of Scientific Instrumentation*, **21**, 724-730.

Merritt, D. A., Freeman, K. H., Ricci, M. P., Studley, S. A., and Hayes, J. M. (1995a). Performance and optimisation of a combustion interface for isotope ratio monitoring Gas-Chromatography Mass-Spectrometry. *Analytical Chemistry*, **67** (14), 2461-2473.

Merritt, D. A., Hayes, J. M., and Marais, D. J. D. (1995b). Carbon isotopic analysis of atmospheric methane by isotope-ratio-monitoring Gas-Chromatography Mass-Spectrometry. *Journal of Geophysical Research-Atmospheres*, **100** (D1), 1317-1326.

Mook, W. G., Grootes P.M. (1973). The measuring procedure and corrections for the high precision mass spectrometric analysis of abundance ratios, especially referring to carbon, oxygen and nitrogen. *International Journal of Mass Spectrometry & Ion Physics*, **12** , 273-298.

Mukhin, D. F., Nenarokov, D. F., Porschnev, N. V., Bondarev, V. B., Gelman, B. G., Israel, G., Raulin, F., Runavot, J., and Thomas, R. (1987). Preliminary calibration results of Vega1 and 2 GC. *Advances in Space Research*, **7** (12), 329-335.

Murray, J. B. (1999). Arguments for the presence of a distant large undiscovered Solar System planet. *Monthly Notices of the Royal Astronomical Society*, **309** (1), 31-34.

Newburn, R. L., Neugebauer, M., and Rahe, J. (1991). *Comets in the post-Halley era*, Kluwer Academic Press, Dordrecht.

Nier, A. O. (1947). A mass spectrometer for isotope and gas analysis. *Review of Scientific Instruments*, **18** (6), 398-410.

Oort, J. H. (1950). The structure of the cloud of comets surrounding the Solar System, and a hypothesis concerning its origin. *Bulletin of the Astronomical institutes of the Netherlands*, **11** (408), 91-110.

Oro, J. (1961). Comets and the formation of biochemical compounds on the primitive earth. *Nature*, **190** (4774), 389-390.

Open University. "The three way catalytic converter." in course S342, Principles of chemical change.

Owen, T., Biemann, K., Rushneck, D. R., Biller, J.E., Howarth, D.W., and LaFleur, A.L. (1977). The composition of the atmosphere at the surface of Mars. *Journal of Geophysical Research*, **82** (28), 4635-9.

Oyama, V. I., and Berdhal, B. J. (1977). The Viking gas exchange experiment results from Chryse and Utopia surface samples. *Journal of Geophysical Research*, **82** (28), 4669-4680.

Oyama, V. I., Carle, G. C., and Woeller, F., Pollack, J. B., Reynolds, R. T., and Craig, R. A. (1980). Pioneer Venus gas chromatography of the lower atmosphere of Venus. *Journal of Geophysical Research*, **85** (A13), 7891-7902.

Paul, W., and Steinwedel, H. (1956). Verfahren zur Trennung bzw. zum getrennten Nachweis von ionen verschiedener spezifischer Ladung. Deutsches Patentamt, Germany.

Pechanec, V. (1973). Verbrennungskatalysatoren in der Organischen Elementaranalyse 1. Katalytische Verbrennungsaktivität von Metallen und Metalloxiden. *Collection Czechoslov Chem. Communication*, **38** , 2917-2925.

Pillinger, C. (1997). Comets: history in the sky. *Physics World*, **10** (10), 41-44.

Platzner, I. T. (1997). Modern isotope ratio mass spectrometry. Chemical analysis, J. D. Winefordner, ed., John Wiley and Sons, Chichester.

Prasad, R., Kennedy, L. A., and Ruckenstein, E. (1984). Catalytic combustion. *Catalysis Reviews-Science and Engineering*, **26** (1), 1-58.

Ramdasi, S. S., Kulkarni, S. Y., Gokarn, A. N., and Pande, A. R. (1993). Simple method for the simultaneous evaluation of combustion and selective oxidation catalysts. *Journal of Chemical Technology and Biotechnology*, **57** (2), 109-112.

Raulin, F., Sternberg, R., Coscia, D., VidalMadjar, C., Millot, M. C., Sebille, B., and Israel, G. (1999). Chromatographic instrumentation in space: Past, present and future developments for exobiological studies. *Advances in Space Research*, **23** (2), 361-366.

Ricci, M. P., Merritt, D. A., Freeman, K. H., and Hayes, J. M. (1994). Acquisition and processing of data for isotope-ratio-monitoring mass-spectrometry. *Organic Geochemistry*, **21** (6-7), 561-571.

Sagan, C., and Druyan, A. (1997). *Comet*, Headline Press, Chatham, Kent.

Sano, M., Yotsui, Y., Abe, H., and Sasaki, S. (1976). A new technique for the detection of metabolites labelled by the isotope ^{13}C using Mass fragmentography. *Biomedial Mass Specrometry*, **3**, 1-3.

Santrock, J., Studley, S.A., Hayes,. J. (1985). Isotopic analyses based on the mass-spectrum of carbon dioxide. *Analytical Chemistry*, **57**, (7), 1444-1448.

Sasaki, Y. (2000). Preparation and performance of iron antimonate catalysts for fluid-bed ammoxidation. *Applied Catalysis A-General*, **194** (SISI), 497-505.

Schoeller, D. A., and Klein, P. D. (1978). A Simplified Technique for collecting breath CO_2 for isotope ratio mass spectrometry. *Biomedical Mass Spectrometry*, **5** (1), 29-31.

Shariff, S. M., Robson, M. M., Bartle, K. D., Myers, P., and Clifford, A. A. (1996) Use of liquid chromatography packings in high pressure gas chromatography. *Journal of High Resolution Chromatography* **19**, 527-529.

Sternberg, R., Szopa, C., Coscia, D., Zubrzycki, S., Raulin, F., VidalMadjar, C., Niemann, H., and Israel, G. (1999). Gas chromatography in space exploration - capillary and micropacked columns for in situ analysis of Titan's atmosphere. *Journal of Chromatography A*, **846** (1-2), 307-315.

Stevens, C. M., and Rust, F. E. (1982). The carbon isotopic composition of atmospheric methane. *Journal of Geophyscical Research*, **87** (C7), 4879-4882.

Sugimoto, A. (1996). GC/GC/C/IRMS system for carbon isotope measurement of low level methane concentration. *Geochemical Journal*, **30** (3), 195-200.

Taylor, S. H., Hargreaves, J. S. J., Hutchings, G. J., and Joyner, R. W. (1995). An initial strategy for the design of improved catalysts for methane partial oxidation. *Applied Catalysis A-General*, **126** (2), 287-296.

Terribile, D., Llorca, J., Boaro, M., deLeitenburg, C., Dolcetti, G., and Trovarelli, A. (1998). Fast oxygen uptake/release over a new CeO_x phase. *Chemical Communications* (**17**), 1897-1898.

Thom, M., Bosinger, R., Schmidt, M., and Levin, I. (1993). The regional budget of atmospheric methane of a highly populated area. *Chemosphere*, **26** (1-4), 143-160.

Thompson, J.J. (1912) New method of chemical analysis, *Science Progress*, **7**, 48-65.

Thompson, D. (1998). New advances in gold catalysis. *Gold Bulletin*, **31**, (4), 111-118.

Tsubota, S., Ueda, A., Sakurai, H., Kobayashi, T., and Haruta, M. (1993). "Application of supported gold catalysts in environmental problems." in "*Environmental Catalysis*", John Wiley and Sons, 420-427.

Toliver, W.H. and Morris, M.L. (1966) Chemical analysis of permanent and organic gases in a 30-day manned experiment. *Aerospace Medicine* **37**, 233-238.

Upchurch, B. T., Schryer, D.R., Davis, P. P., and Brown, K. G. (1992) CO_2 catalyst development and testing at LARC. *3rd international DRA/NASA conference on long life laser technology*, 90-104.

Urey, H.C. (1948) Oxygen isotopes in nature and the laboratory. *Science,* **108**, 489-496.

Vandeputte, K., Moens, L., and Dams, R. (1996). Improved sealed-tube combustion of organic samples to CO_2 for stable carbon isotope analysis, radiocarbon dating and percent carbon determinations. *Analytical Letters*, **29** (15), 2761-2773 .

Vanysek, V. (1991). "Isotope ratios in Comets." in "*Comets in the post-Halley era*", R. L. Newburn, M. Neugebauer, and J. Rahe eds., Kluwer Academic Press, Dordrecht.

Verdant, M., and Schwehm, G. H. (1998). The International Rosetta Mission. *Esa Bulletin-European Space Agency*, **93**, 39-50.

Waldron, S., Hall, A. J., and Fallick, A. E. (1999). Enigmatic stable isotope dynamics of deep peat methane. *Global Biogeochemical Cycles*, **13** (1), 93-100.

Whipple, F. (1950). A Comet model. I The acceleration of Comet Encke. *Astrophysical Journal*, **111**, 375-394.

Whiticar, M.J, Faber E., and Schoell, M. (1986). Biogenic methane formation in marine and freshwater environments: CO_2 reduction vs. acetate fermentation - Isotope evidence. *Geochimica et Cosmochimica Acta*, **50**, 693-709.

Winter, E. (1958). The reactivity of oxide surfaces. *Advances in catalysis* , **10**, 196-241.

Wright, I. P., McNaughton, N. J., Fallick, A. E., Gardiner, L. R., and Pillinger, C. T. (1983). A high-precision mass spectrometer for stable carbon isotope analysis at the nanogram level. *Journal of Physics E-Scientific Instruments*, **16** (6), 497-504.

Wright, I. P., and Pillinger, C. T. (1998). MODULUS - An experiment to measure precise stable isotope ratios on cometary materials. *Advances in Space Research*, **21** (11), 1537-1545.

Yanagisawa, Y. (1995). Oxygen exchange between CO_2 and metal (Zn and Ti) oxide powders. *Energy Conversion and Management*, **36** (6-9), 443-446.

Yao, Y. Y. (1984). The oxidation of CO and hydrocarbons over noble metal catalysts. *Journal of Catalysis*, **87**, 152-162.

Yost, R. A., McClennen, W., and Snyder, A. P. (1987). Picogram to microgram analysis by gas chromatography/ion trap mass spectrometry. *35th ASMS Conference on Mass spectrometry and allied topics*, Denver, 789-790.

Zeng, Y. Q., Mukai, H., Bandow, H., and Nojiri, Y. (1994). Application of gas-chromatography combustion-isotope ratio mass-spectrometry to carbon isotopic analysis of methane and carbon-monoxide in environmental-samples. *Analytica Chimica Acta*, **289** (2), 195-204.

Zwinkels, M. F. M., Jaras, S. G., Menon, P. G., and Griffin, T. A. (1993). Catalytic materials for high-temperature combustion. *Catalysis Reviews-Science and Engineering*, **35** (3), 319-358.